PROPERTIES OF JTA GRAPHITE

Seymour A. Bortz

IIT Research Institute

FOREWORD

This is Report No. IITRI-G6001 and AFML-TR-68-178, entitled "Properties of JTA Graphite." The report is the Final Technical Report of IITRI Project G6001, conducted from May 1965 through December 1967 under Contract No. AF33(615)-3028, Task No. 738106, and Project No. 7381 by IIT Research Institute, 10 West 35th Street, Chicago, Illinois 60616 for the Air Force Materials Laboratory, Air Force Systems Command, Wright-Patterson Air Force Base, Ohio 45433. The report was submitted for review in May 1968.

The Air Force program monitor for this program was Mr. Marvin Knight, MAAE. In addition to the author, the following IITRI personnel contributed to the work reported: C. L. Connors, T. B. Wade, F. Sadlon, P. Janson, E. Mazanek, and C. Levesque.

Publication of this report does not constitute Air Force approval of the report's findings or conclusions. It is published only for the exchange and stimulation of ideas.

This technical report has been reviewed and is approved.

A. OLEVITCH
Chief, Materials Engineering Branch
Materials Support Division
Air Force Materials Laboratory

ABSTRACT

The purpose of this program was to attempt to test a material that forms its own oxidation resistant protection and to characterize the physical and the mechanical properties of Union Carbide Corporation's JTA graphite in order to determine its usefulness for aerospace applications. Two 7-in.-diameter, 6.5-in.-long and two 14-in.-diameter, 7-in.-long JTA billets were examined. They had no gross flaws or density differences and were acceptable within the limitations of the procurement specifications. Their densities were >3.00 g/cc, and they contained graphite, zirconium diboride, and beta-silicon carbide, the distribution of which varied only slightly among the four billets. The zirconium diboride and beta-silicon carbide content at the edge of the billets was less than that in the center. The oxidation resistance varied with temperature and oxygen pressure. Maximal oxidation resistance under ambient conditions occurred at 2750°F. The strength was retained at low pressures ($<10^{-1}$ torr) and at temperatures as high as 3650°F. Oxidation at temperatures of >1750°F produced a protective zirconium coating. Sonic modulus measurements were not sensitive enough to differentiate between flaw distributions of the with- and the across-grain orientations. JTA graphite is anisotropic, and its with-grain orientation is about twice as strong as its across-grain orientation. A minimal 1/4-in. cross section was adequate for determining average mechanical properties. Its strength did not vary between strain rates of 0.02 and 20 in./min. The ratio of the tensile strength to the flexural strength to the compressive strength is 1:1.45:2.5 for the with-grain orientation (tensile strength, 12,140 psi) and 1:1.23:5.2 for the across-grain orientation (tensile strength, 6300 psi). Under ambient atmospheric conditions and all temperatures tested, strength loss due to oxidation was about one-third to one-half the measured strength. The strength of the interior of oxidized JTA was the same as that of the virgin material. The mechanical properties peaked at 3150°F, at which the strength was higher than at ambient temperatures. The thermal properties, except for thermal expansion, were the same for all four billets. The variability of the mechanical data was within limits generally noted for ceramic materials but greater than that desired by designers of brittle materials. The batch-to-batch differences, primarily due to raw-material impurities and processing variations (e.g., hot-pressing-temperature variation), must be reduced.

CONTENTS

Section		Page
I.	Introduction	1
II.	Summary	2
III.	Materials Characterization	6
	1. Powder X-Ray Diffractometry	6
	2. Chemical Analysis	17
	3. Metallographic Analysis	19
	4. Electron-Microprobe Analysis	19
	5. Density and Porosity Measurements	25
	6. Dynamic-Modulus Studies	27
	7. Permeability Experiments	34
	8. Oxidation Studies	34
IV.	Mechanical Properties	57
	1. Size	57
	2. Strain Rate	72
	3. Tension	72
	a. Ambient-Environment Tests	77
	b. High-Temperature Inert-Atmosphere Tests	77
	c. High-Temperature Air-Atmosphere Tests	87
	4. Flexure	105
	a. High-Temperature Inert-Atmosphere Tests	105
	b. Air-Atmosphere Tests	110
	5. Compression	128
	a. Ambient-Environment Tests	128
	b. High-Temperature Inert-Atmosphere Tests	134
	c. High-Temperature Ambient-Atmosphere Tests	134
	6. Torsion	134
	7. Elasticity	154
	8. Creep Resistance	160
V.	Thermal Properties	175
	1. Thermal Expansion	175
	2. Thermal Conductivity	175
	3. Specific Heat	182
	4. Normal Emittance	189
VI.	Conclusions and Recommendations	194
	References	195
	Appendix I: JTA Specifications	197
	Appendix II: Chemical Analysis	199
	Appendix III: Analysis of Variance of Flexural Strength for 7-F-12, 7-F-14, and 14-G-1	204
	Distribution List	209
	DD Form 1473: Document Control Data - R&D	

TABLES

Table		Page
I	Previous Mechanical Data on JTA Graphite	4
II	New Mechanical Data on JTA Graphite	5
III	X-Ray Characterization of JTA Graphite	16
IV	Semiquantitative Analyses of JTA Graphite	18
V	Densities Samples Through Center of JTA Graphite Billets	26
VI	Experimental Conditions of Oxidation Tests of JTA Graphite	38
VII	Results of X-Ray Analysis of Protective JTA Coating Formed at 3100°F in Air	41
VIII	JTA Graphite Specimens used for Determination of Size Effect by Flexural Testing at Room Temperature	58
IX	Effect of Size of Billet 7-F-12	59
X	Effect of Size of Billet 7-F-14	60
XI	Effect of Size of Billet 14-G-1	61
XII	Combined Size-Effect Data for Billets 7-F-12, 7-F-14, and 14-G-1	66
XIII	Results of Tensile Tests under Ambient Conditions	79
XIV	Results of Tensile Tests in Inert Atmosphere	88
XV	Results of Tensile Tests in Air Atmosphere	102
XVI	Results of Flexural Tests in Various Atmospheres	108
XVII	Flexural Data for JTA Graphite	127
XVIII	Results of Compression Oxidation Tests	135
XIX	Compression of JTA Graphite in an Inert Environment	150
XX	Room-Temperature Elastic Properties of JTA Graphite	159

Table		Page
XXI	Poisson's Ratios Obtained by Ring-and-Disc Method	161
XXII	Thermal Conductivity of JTA Graphite	181
XXIII	Enthalpy Values for JTA Graphite	183
XXIV	Enthalpy Values for JTA Graphite	184
XXV	Enthalpy Values for JTA Graphite	185
XXVI	Specific Heat of JTA Graphites	187
XXVII	Emittance of Virgin and Oxidized JTA Graphite	193

ILLUSTRATIONS

Figure		Page
1	Sectioning of JTA Billets for Radiographic Analysis	7
2	Radiographs of Billet 7-F-12 (Side 1)	8
3	Radiographs of Billet 7-F-12 (Side 2)	9
4	Radiographs of Billet 7-F-14 (Side 1)	10
5	Radiographs of Billet 7-F-14 (Side 2)	11
6	Radiographs of Billet 14-G-1	12
7	Radiographs of Billet 14-G-3	13
8	Section of 7-in.-Diameter, 6.5-in.-Long Billet for Radiographic Examination Indicating Locations from Which specimens for Microprobe, X-ray, and Metallographic Analyses were Obtained	14
9	Section of 14-in.-Diameter, 7-in.-Long Billet for Radiographic Examination Indicating Locations from Which Specimens for Microprobe, X-ray, and Metallographic Analyses were Obtained	15
10	Photomicrographs of JTA Billet 7-F-12	20
11	Photomicrographs of JTA Billet 7-F-14	21
12	Photomicrographs of JTA Billet 14-G-1	22
13	Photomicrographs of JTA Billet 14-G-3	23
14	Microprobe Analysis of Section 3A of Billet 7-F-12	24
15	Flexural Strength vs Sonic Modulus for Billets 7-F-12, 7-F-14, and 14-G-1	29
16	Flexural Strength vs Sonic Modulus for Billet 14-G-3	30
17	Flexural Strength vs Sonic Modulus for Billets 7-F-12, 7-F-14, and 14-G-1	31
18	Flexural Strength vs Sonic Modulus for Billet 14-G-3	32

Figure		Page
19	Sonic Modulus vs Density for Billet 14-G-3	33
20	Schematic Diagram of Permeability Measuring System	35
21	View of Specimen Holder	36
22	Permeability Apparatus	37
23	Appearance of Flexural Specimens After 60-min Soak and Testing in Air	39
24	Development of Oxide Coating on JTA Samples Due to Exposure to Air at 3100°F	40
25	Metallograph of Edge of JTA After Exposure to Air at 1832°F for 60-min	42
26	Metallograph of Edge of JTA After Exposure to Air at 2732°F for 60-min	43
27	Metallograph of Edge of JTA After Exposure to Air at 3100°F for 20-min	44
28	Metallograph of Edge of JTA After Exposure to Air at 3100°F for 40-min	46
29	Metallograph of Edge of JTA After Exposure to Air at 3100°F for 60-min	47
30	Weight Loss of JTA Graphite at 1800°F, in Static Air	48
31	Weight Loss of JTA Graphite at 1800°F, in an Air Atmosphere	49
32	Weight Loss of JTA Graphite at 3100°F, in an Air Atmosphere	50
33	Weight Loss of JTA Graphite at 3600°F, in Static Air	51
34	Weight Loss of JTA Graphite at 3600°F, in an Air Atmosphere	52
35	Strength of JTA Graphite at 1800°F, in an Air Atmosphere	53
36	Strength of JTA Graphite at 3100°F, in an Air Atmosphere	54
37	Strength of JTA Graphite at 3600°F, in an Air Atmosphere	55

Figure		Page
38	Effect of Specimen Size on Flexure Strength	62
39	Flexural-Strength Distribution of With-Grain Orientation	64
40	Flexural-Strength Distribution of Across-Grain Orientation	65
41	Effect of Size on Tensile Strength	67
42	Possible Results of Model Scaling	68
43	Combined Flexural Strength Distribution Curve	70
44	Combined Flexural Strength Distribution Curve	71
45	Strain Rate Effect on Tensile Strength of JTA Graphite	73
46	Tensile Grips Developed at IITRI and Used with Collet Samples	74
47	Dumbbell Tensile Specimen with and Without Typical Fractures	75
48	Burst Test Failures	76
49	Internal Pressure Burst Test	78
50	Distribution Curve for Room Temperature Across Grain Tension Tests	80
51	Distribution Curve for Room Temperature Across Grain Burst Tension Tests	81
52	Distribution Curve for Room Temperature With Grain Tension Tests	82
53	Distribution Curve for Room Temperature With Grain Burst Tension Tests	83
54	Weibull Plot for JTA Tested in Tension	84
55	Weibull Plot for JTA Tested in Tension	85
56	High-Temperature Extensometer	86
57	Typical Stress-Strain Curve of JTA in Tension at 1830°F	89

Figure		Page
58	Typical Stress-Strain Curve of JTA in Tension at 2750°F	90
59	Typical Stress-Strain Curve of JTA in Tension at 3100°F	91
60	Typical Stress-Strain Curve of JTA in Tension at 3600°F	92
61	Distribution Curve in With Grain Tension at 1832°F	93
62	Distribution Curve in With Grain Tension at 2732°F	94
63	Distribution Curve in With Grain Tension at 3182°F	95
64	Distribution Curve in With Grain Tension at 3632°F	96
65	Distribution Curve in Across Grain Tension at 1832°F	97
66	Distribution Curve in Across Grain Tension at 2732°F	98
67	Distribution Curve in Across Grain Tension at 3182°F	99
68	Distribution Curve in Across Grain Tension at 3632°F	100
69	Tension Test Fixture for Air Testing of JTA Graphite Showing Induction Coils Heating Sample During Soak Period	101
70	% Loss of JTA Graphite in Relation to Temperature and Time	103
71	Material Loss of JTA Graphite in Relation to Temperature	104
72	Effect of Temperature on Tensile Strength of JTA in Inert and Air Atmospheres	106
73	Flexural Test Fixture for Air Testing JTA Graphite, Showing Induction Coils Heating Sample During Soak Period	107

Figure		Page
74	Flexural Strength of JTA Graphite	109
75	Room-Temperature Flexural Stress vs Deflection of JTA Graphite	111
76	Flexural Stress vs Deflection Curve of JTA Graphite at 1800°F	112
77	Flexural Stress vs Deflection Curve of JTA Graphite at 2750°F	113
78	Flexural Stress vs Deflection Curve of JTA Graphite at 3200°F	114
79	Flexural Stress vs Deflection Curve of JTA Graphite at 3600°F	115
80	Flexural Stress vs Deflection Curve of JTA Graphite at 4000°F	116
81	Distribution Curve for With Grain Flexural Strength in an Inert Atmosphere at 1832°F	117
82	Distribution Curve for With Grain Flexural Strength in an Inert Atmosphere at 2732°F	118
83	Distribution Curve for With Grain Flexural Strength in an Inert Atmosphere at 3182°F	119
84	Distribution Curve for With Grain Flexural Strength in an Inert Atmosphere at 3632°F	120
85	Distribution Curve for With Grain Flexural Strength in an Inert Atmosphere at 3992°F	121
86	Distribution Curve for Across Grain Flexural Strength in an Inert Atmosphere at 1832°F	122
87	Distribution Curve for Across Grain Flexural Strength in an Inert Atmosphere at 2732°F	123
88	Distribution Curve for Across Grain Flexural Strength in an Inert Atmosphere at 3182°F	124
89	Distribution Curve for Across Grain Flexural Strength in an Inert Atmosphere at 3632°F	125
90	Distribution Curve for Across Grain Flexural Strength in an Inert Atmosphere at 3992°F	126

Figure		Page
91	Effect of Atmosphere on Flexural Strength With Grain Orientation of JTA	129
92	Effect of Atmosphere on Flexural Strength of Across Grain Orientation of JTA	130
93	Compression Deflectometer for High-Temperature Tests	131
94	Distribution Curve for JTA Tested in Compression	132
95	Distribution Curve for JTA Tested in Compression	133
96	Distribution Curve for JTA Tested in Compression	136
97	Distribution Curve for JTA Tested in Compression	137
98	Distribution Curve for JTA Tested in Compression	138
99	Distribution Curve for JTA Tested in Compression	139
100	Distribution Curve for JTA Tested in Compression	140
101	Distribution Curve for JTA Tested in Compression	141
102	Weibull Plot for JTA Tested in Compression	142
103	Weibull Plot for JTA Tested in Compression	143
104	Weibull Plot for JTA Tested in Compression	144
105	Weibull Plot for JTA Tested in Compression	145
106	Weibull Plot for JTA Tested in Compression	146
107	Weibull Plot for JTA Tested in Compression	147
108	Weibull Plot for JTA Tested in Compression	148
109	Weibull Plot for JTA Tested in Compression	149
110	Effect of Atmosphere on High-Temperature Compressive Strength of Across Grain Orientation of JTA	151
111	Effect of Atmosphere on High-Temperature Compressive Strength of With Grain Orientation of JTA	152

Figure		Page
112	Typical Failure of JTA Torsion Samples	153
113	Horizontal and Vertical Deflections in Ring and Disk	157
114	Typical Creep Curve	163
115	Short Term Flexural Creep for JTA	164
116	Short Term Flexural Creep for JTA	165
117	Short Term Flexural Creep for JTA	166
118	Short Term Flexural Creep for JTA	167
119	Short Term Flexural Creep for JTA	168
120	Short Term Flexural Creep for JTA	169
121	Long Term Flexural Creep for JTA	170
122	Long Term Flexural Creep for JTA	171
123	Long Term Flexural Creep for JTA	172
124	Log-Log of Summarized Creep Data	174
125	Average Thermal Expansion Coefficient of With Grain JTA Graphite	176
126	Average Thermal Expansion Coefficient of Across Grain JTA Graphite	177
127	Schematic Diagram of Apparatus for Measuring Specific Heat	179
128	Thermal Diffusivity Apparatus and Associated Systems	180
129	Enthalpy of JTA Graphites	186
130	Specific Heat of JTA Graphites	188
131	JTA Graphite Before and After Heating During Emittance Measurements	190
132	Total Normal Emittance of Virgin and Oxidized JTA Graphite	192

SECTION I

INTRODUCTION

The extreme environments of nose cones, rocket nozzles, and leading edges require materials capable of withstanding severe thermal and mechanical conditions. Attention was focused on refractory composite materials because of their high strength at elevated temperatures, thermal protection, and oxidation resistance. However, in structures required to resist extreme environments, these materials often exhibit a wide variability in properties. This experimental program was designed to determine the physical and the mechanical properties of one such composite refractory oxidation-resistant material, JTA graphite.

Considerable emphasis was placed on determining the uniformity of properties among JTA graphite billets having the same and different dimensions. Data were obtained for two 7-in.-diameter, 6.5-in.-long billets and two 14-in.-diameter, 7-in.-long billets.

SECTION II

SUMMARY

Information developed during this program is summarized below.

1. JTA graphite consists of graphite, zirconium diboride (ZrB_2), and beta-silicon carbide (β-SiC).

2. No gross flaws or density differences were observed in the billets studied.

3. No compositional and only slight microstructural variability was observed.

4. Densities were higher than the specified 3.00 g/cc and appeared to be uniform throughout the bulk material.

5. Chemical and x-ray analyses indicated batch-to-batch differences, primarily due to raw-material impurities and processing-temperature variations.

6. Microprobe analysis did not provide additional significant microstructural information.

7. Sonic modulus determinations were not sensitive enough to distinguish flaws affecting strength of with- and across-grain orientations.

8. Maximum oxidation resistance under static conditions was exhibited at as high as 2750°F. At pressures lower than 10^{-1} torr, little oxidation occurred at as high as 3650°F with 1-hr exposures.

9. Mechanical data for the four billets did not differ statistically.

10. A 1/4-in. cross sectional dimension was adequate for determining mechanical properties.

11. Statistical scaling laws, such as the Weibull size-effect equation, were used to conservatively estimate mechanical properties for scaled-up prototypes.

12. No measurable strain-rate effects on strength between strain rates of 0.02 and 20 in./min were observed.

13. The ratio of anisotropic behavior for JTA was 2:1 for with- and across-grain orientation.

14. The ratio of tensile strength to flexural strength to compressive strength was 1:1.45:2.5 for the with-grain orientation (tensile strength, 12,140 psi) and 1:1.23:5.2 for the across-grain orientation (tensile strength, 6300 psi).

15. Indirect methods of torsion measurements of Poisson's ratio and shear modulus were not satisfactory because of JTA's anisotropy.

16. After a 1-hr exposure to oxidizing conditions and temperatures as high as 3650°F, strengths were from one-third to one-half lower than those in an inert environment.

17. Thermal properties (excluding thermal expansion) did not differ among the billets.

18. The test techniques used to obtain properties appear to be adequate for all the measurements made except for obtaining shear strength, shear modulus, and Poisson's ratio. A comparison of various techniques used for testing brittle materials is described in a report, "Analysis and Review of Mechanical Testing Procedures for Brittle Materials."(1) Additional data is required before recommendations can be made to obtain shear strength, shear modulus and Poisson's ratio. The techniques for making high temperature mechanical property measurements of graphite under oxidizing conditions appear to be adequate as described in this report.

Thermal properties appeared to be more consistent than mechanical properties. However, the JTA graphite measurement variability among and within billets appeared to be similar to that generally observed for brittle ceramics. Table I provides a summary of prior-existing JTA-property data, and Table II provides similar data, obtained during this program.

Table I. PREVIOUS MECHANICAL DATA ON JTA GRAPHITE(2)
(Room temperature, 14-in.-diameter billets)

Property	With grain				Across grain			
	Number of tests	Value Avg.	Error (ν), %	Billet no.	Number of tests	Value Avg.	Error (ν), %	Billet no.
Bulk density, g/cc	22	2.966	23	1	8	3.028	1.1	1
	21	2.854	3.5	2				
Coefficient of expansion, in./in. °F								
<2732°F	2	5.6		1,2	2	6.0		1
2732-3632°F	2	5.6		1,2	2	11.0		1
Tensile								
Strength, psi	4	10,010	7.0	1				
Elastic modulus (2), 10^6 psi		5.6				3.6		
Flexure								
Strength, psi	5	17,750	4.7	1	5	9,592	5.2	1
	5	12,784	5.6	2				
Elastic modulus, 10^6 psi	5	9.1		1	5	4.95		1
	5	7.1		2				
Compression								
Strength, psi	3	15,330	2.6	1	5	22,160	8.7	1
	5	12,592	11.2	2				
Elastic modulus, 10^6 psi	5	2.9		1	5	3.6		1

Table II. NEW MECHANICAL DATA ON JTA GRAPHITE

Property	With grain			Across grain		
	Number of tests	Value		Number of tests	Value	
		Avg.	Error (ν), %		Avg.	Error (ν), %
Bulk density, g/cc						
Billet 7-F-12	30	3.065	1.48			
Billet 7-F-14	30	3.077	0.76			
Billet 14-G-1	30	3.091	0.68			
Billet 14-G-3	30	3.054	0.90			
Tensile, psi						
Strength	30	12,140	9.398	30	6,300	6.708
Elastic modulus	30	10.65	6.474	30	3.74	9.880
Flexure, psi						
Strength	30	17,520	14.8	30	7.945	9.7
Elastic modulus	30	11.80	21.14	30	4.32	26.06
Compression, psi						
Strength	30	33,100	5.86	30	30,330	8.61
Elastic modulus	30	3.67	10.08	30	2.31	17.75
Thermal properties						
Expansion, in./in. °F x 10^6	5	3.0-3.75		5	2.9-4.1	
Conductivity, Btu/hr ft °F	3	72-40.5		3	37-20	
Poisson's ratio	6	0.3[a] 0.1[b]		6	0.1[a] 0.3[b]	

[a]Flat.

[b]Edge.

SECTION III

MATERIALS CHARACTERIZATION

JTA graphite is manufactured by the Carbon Products Division of Union Carbide Corporation. This grade is a multiphase composite material(3) containing 48 wt. % carbon, 35 wt. % zirconium, 8 wt. % boron, and 9 wt. % silicon and formed by hot pressing. The material is reported to have good oxidation resistance and mechanical strength at high temperatures. To characterize JTA graphite IITRI used metallographic, electron-microprobe, chemical and X-ray analyses. Metallographic, X-ray and chemical analyses provided the most useful data.

Four billets were employed in this study. They were produced to meet specific JTA graphite specifications (Appendix I). The billets were sectioned and radiographed by UCC for cracks and voids larger than 0.03 in. before being sent to IITRI. The billets were coded as follows: 7-F-12, 7-F-14, 14-G-1, and 14-G-3. The first numeral indicates the diameter (in inches) of the billet, the letter denotes the pressing series, and the end numeral indicates the pressing number of that particular series. The 7-in.-diameter billets were 6.5 in. long, and the 14-in.-diameter billets were 7 in. long.

Figure 1 shows the sectioning of the billets for radiographic examination. Each piece was given three exposures: 4 min at 265 kv, 3.5 min at 24 kv, and 2.5 min at 200 kv. A medium-speed film, type AA, was used. The exposures are shown in Figures 2 through 7. Examination of these negatives revealed that the billets were a heterogeneous mixture of the various compounds that make up JTA graphite -- ZrB_2, SiC and graphite. No major flaw areas or large differences in density were detected.

Representative samples were cut from the billets for metallographic, microprobe and X-ray analyses. Figures 8 and 9 show the areas from which the samples were cut.

1. POWDER X-RAY DIFFRACTOMETRY

Powder X-ray patterns were obtained for all four billets. The results from an analysis of these patterns are listed in Table III. The major constituents were graphite, ZrB_2 and β-SiC; traces of alpha-silicon carbide (α-SiC) were detected in billet 7-F-14. Carbon Products(3) reports that graphite, ZrB_2 and α-SiC should be present in JTA graphite. The difference in the SiC structure is probably due to changes in procedures of fabrication of the early experimental material and the material evaluated during this program. The β-SiC is the low-temperature cubic phase of this compound; it begins to convert to the hexagonal phase at 3900°F. If the raw material consists of powders of carbon, ZrB_2

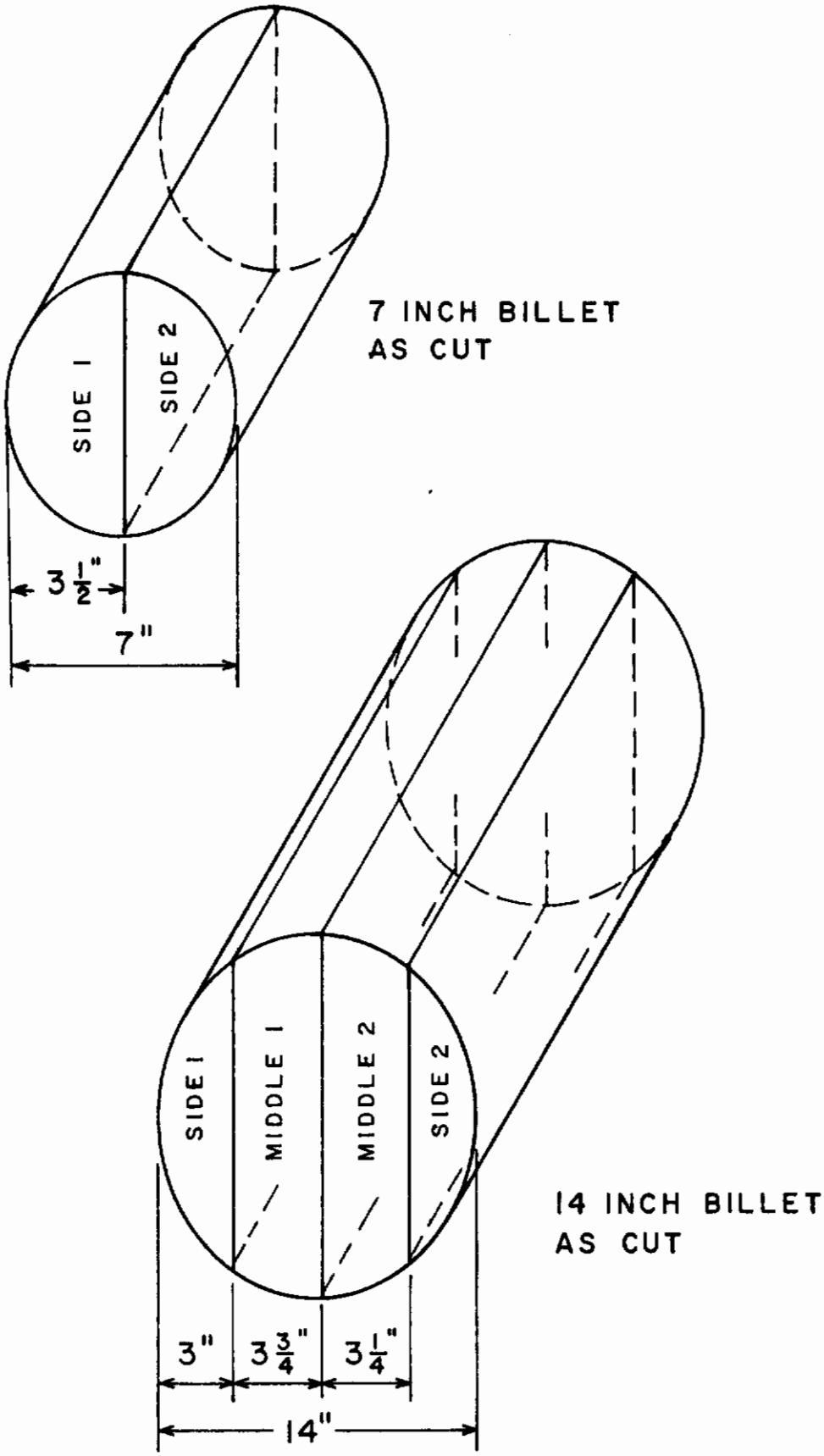

Figure 1. SECTIONING OF JTA BILLETS FOR RADIOGRAPHIC ANALYSIS

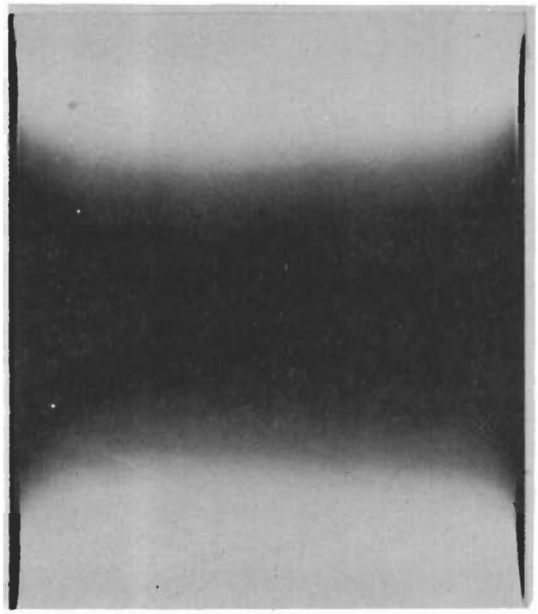

4-MIN, 265-KV EXPOSURE

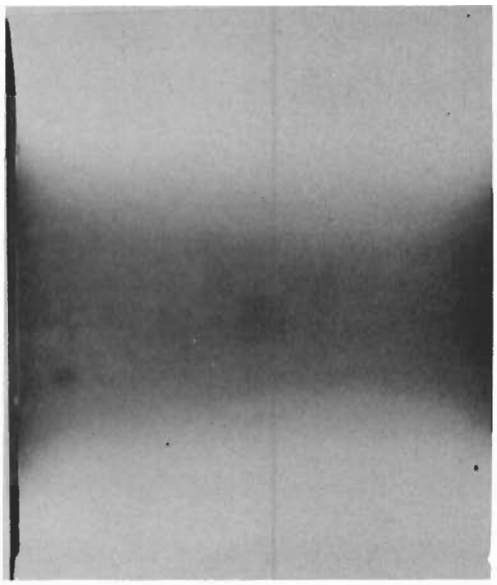

3.5-MIN, 240-KV EXPO

2.5-MIN, 200-KV EXPOSURE

Figure 2. RADIOGRAPHS OF BILLET 7-F-12 (SIDE 1)

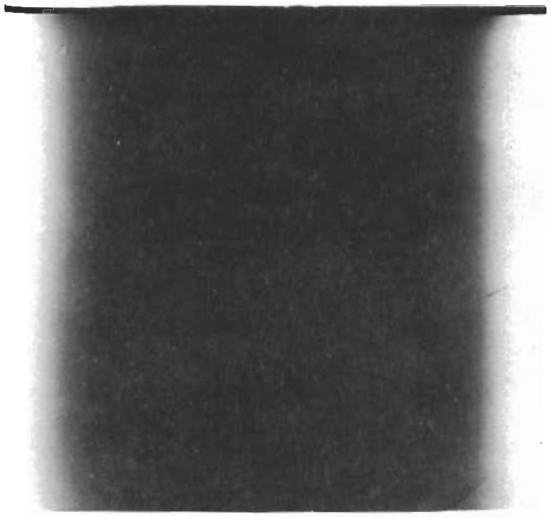

4-MIN, 265-KV EXPOSURE

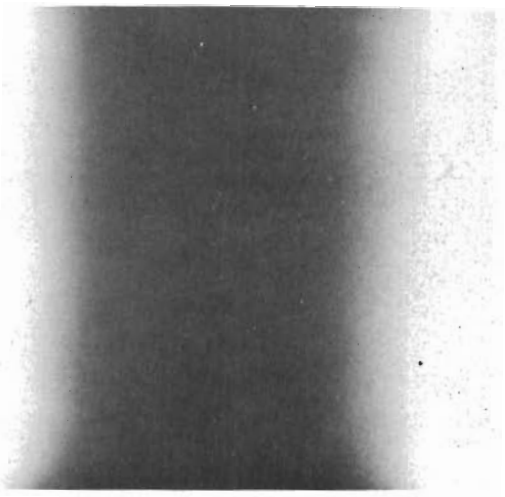

3.5-MIN, 240-KV EXPOSURE

2.5-MIN, 200-KV EXPOSURE

Figure 3. RADIOGRAPHS OF BILLET 7-F-12 (SIDE 2)

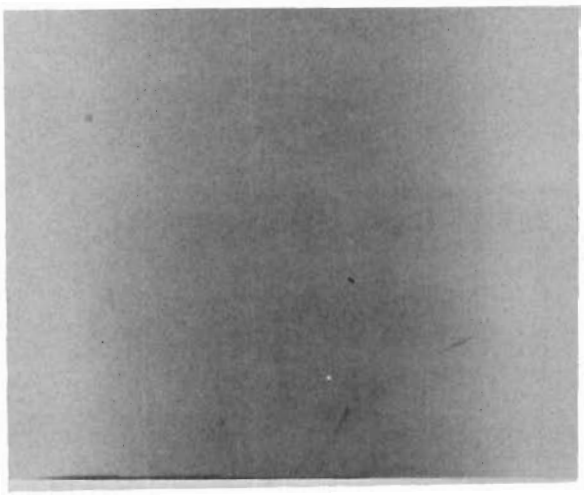

4-MIN, 265-KV EXPOSURE

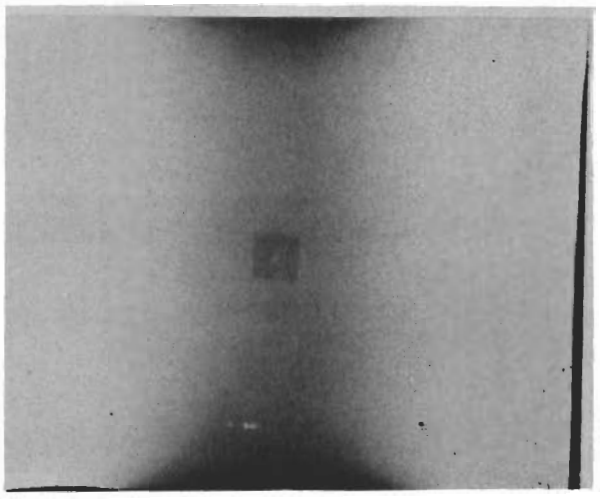

3.5-MIN, 240-KV EXPOSURE

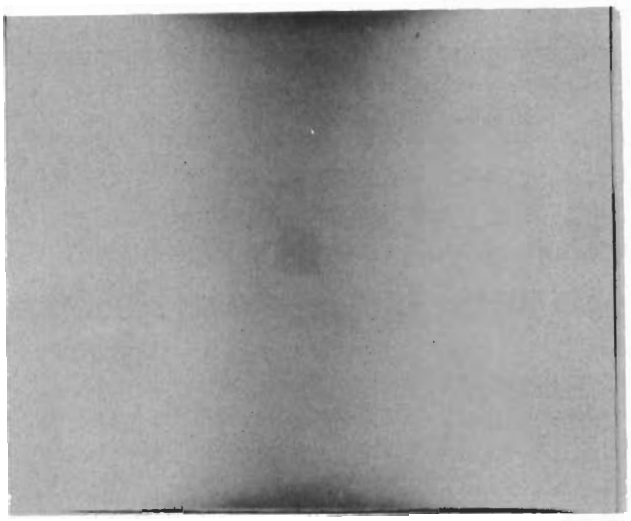

2.5-MIN, 200-KV EXPOSURE

Figure 4. RADIOGRAPHS OF BILLET 7-F-14 (SIDE 1)

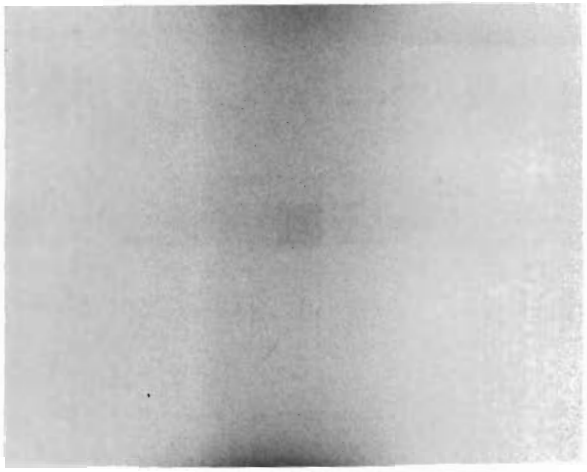

4-MIN, 265-KV EXPOSURE

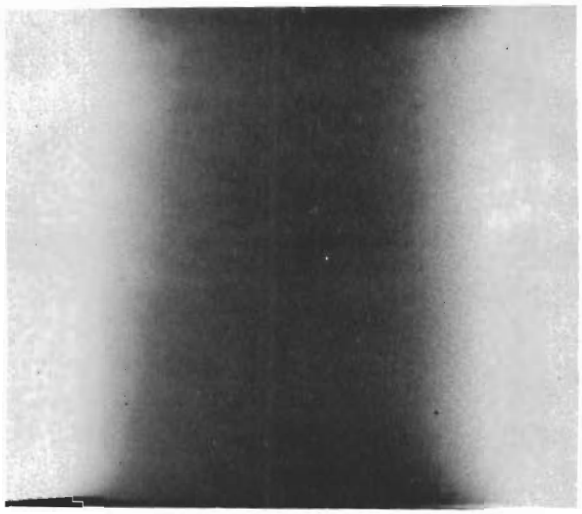

3.5-MIN, 240-KV EXPOSURE

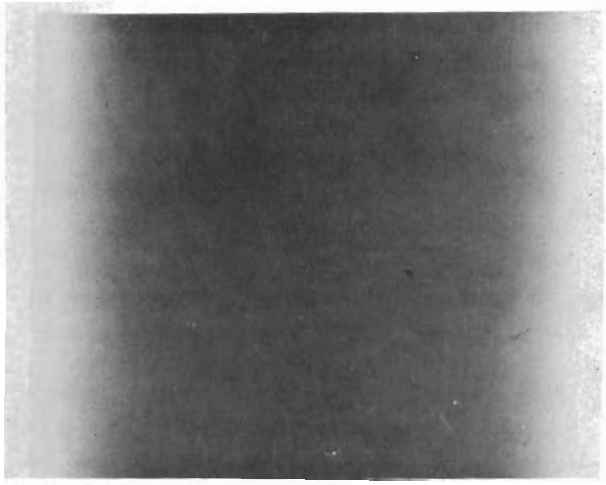

2.5-MIN, 200-KV EXPOSURE

Figure 5. RADIOGRAPHS OF BILLET 7-F-14 (SIDE 2)

4-MIN, 265-KV EXPOSURE

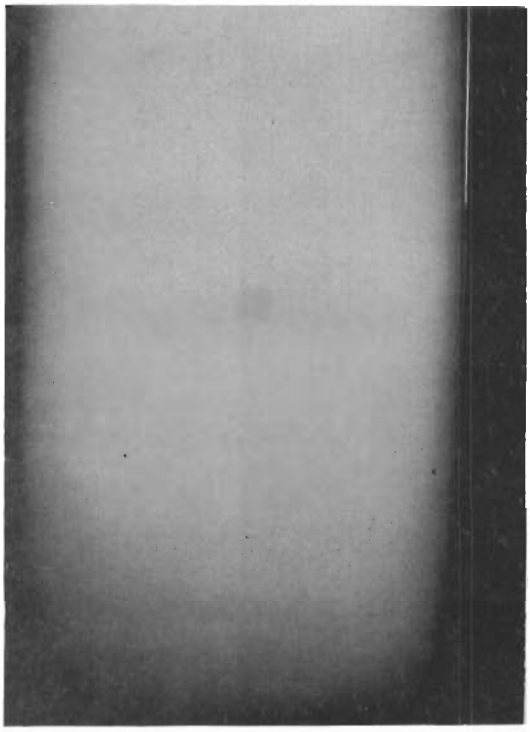

3.5-MIN, 240-KV EXPOSURE

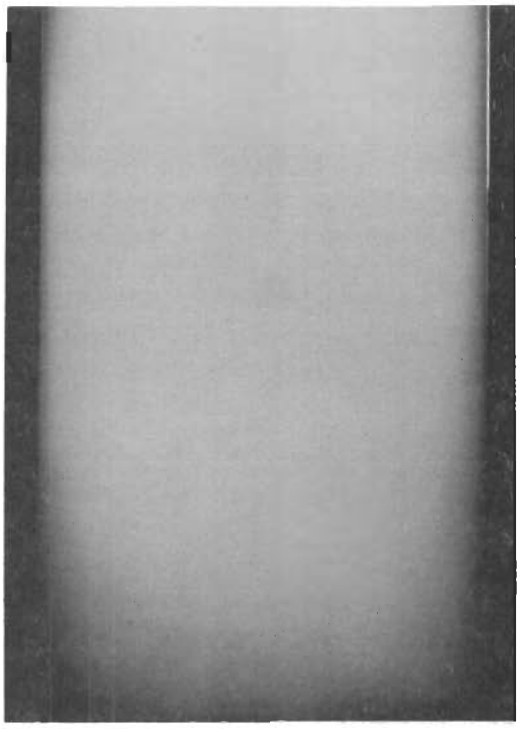

2.5-MIN, 200-KV EXPOSURE

Figure 6. RADIOGRAPHS OF BILLET 14-G-1

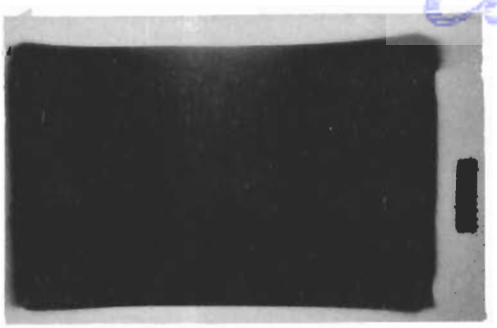

4-MIN, 265-KV EXPOSURE

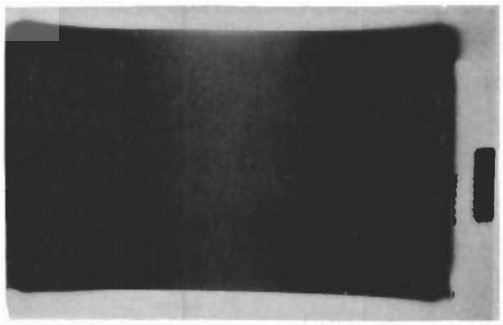

4-MIN, 265-KV EXPOSURE

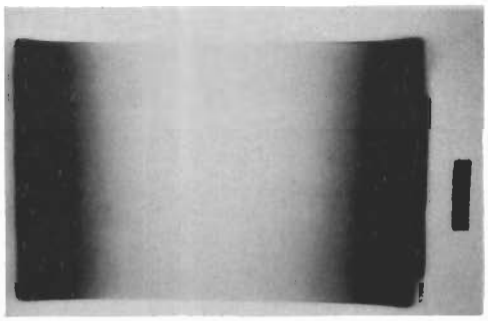

3.5-MIN, 240-KV EXPOSURE

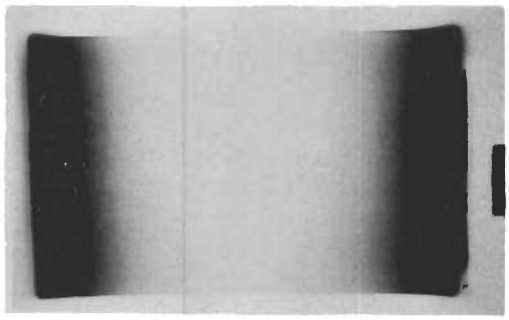

3.5-MIN, 240-KV EXPOSURE

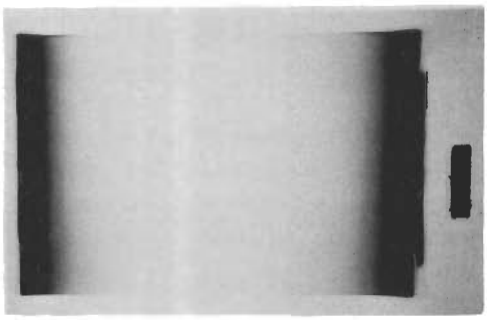

2.5-MIN, 240-KV EXPOSURE

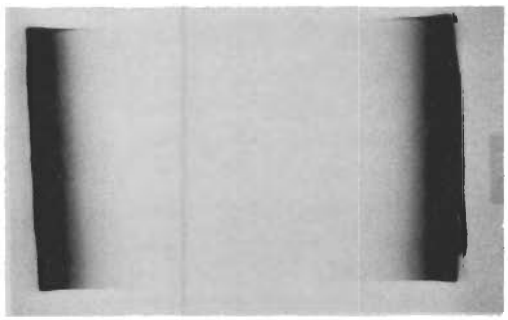

2.5-MIN, 240-KV EXPOSURE

SIDE 1

SIDE 2

Figure 7. RADIOGRAPHS OF BILLET 14-G-3

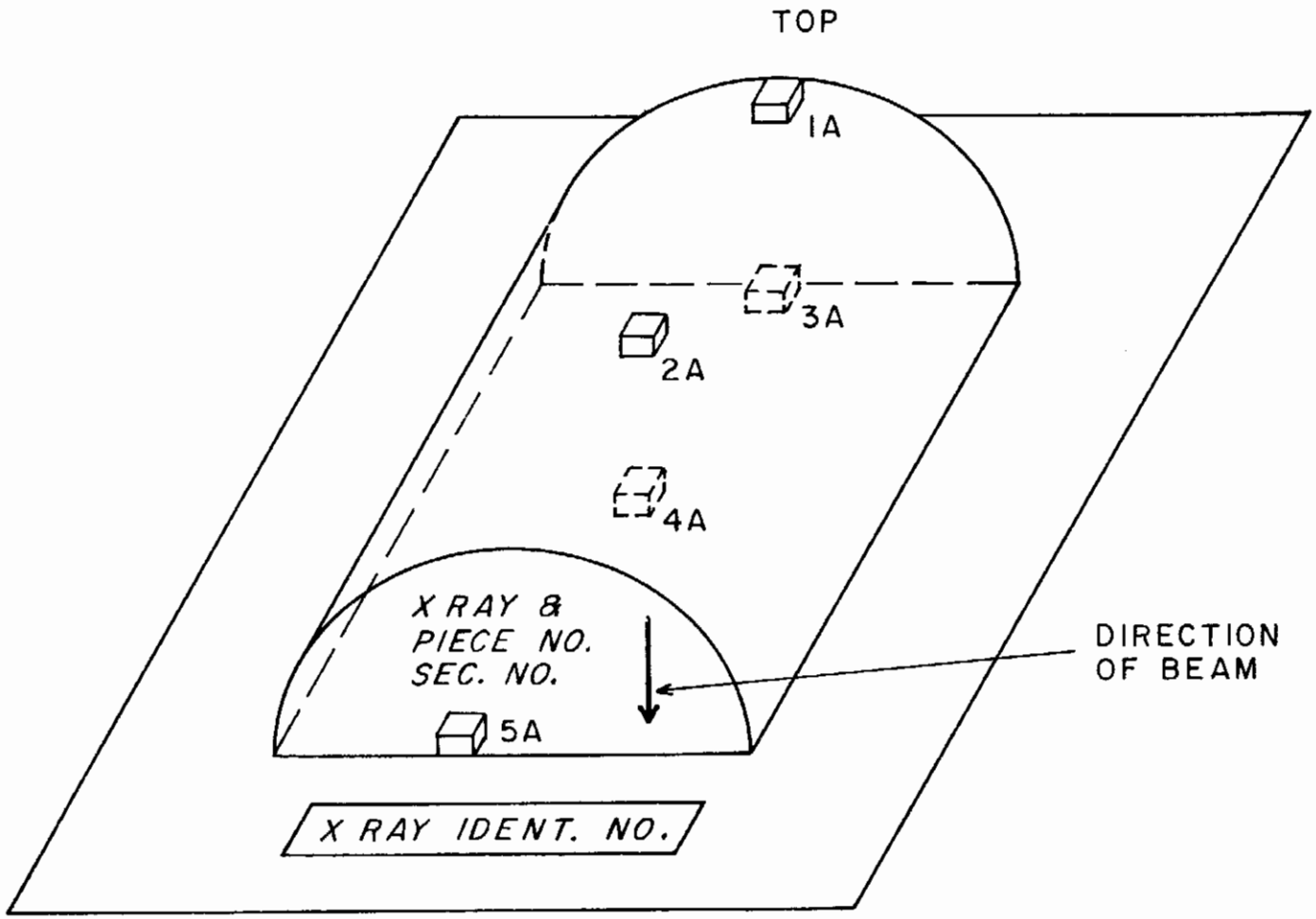

Figure 8. SECTION OF 7-IN.-DIAMETER, 6.5-IN.-LONG BILLET FOR RADIOGRAPHIC EXAMINATION INDICATING LOCATIONS FROM WHICH SPECIMENS FOR MICROPROBE, X-RAY, AND METALLOGRAPHIC ANALYSES WERE OBTAINED

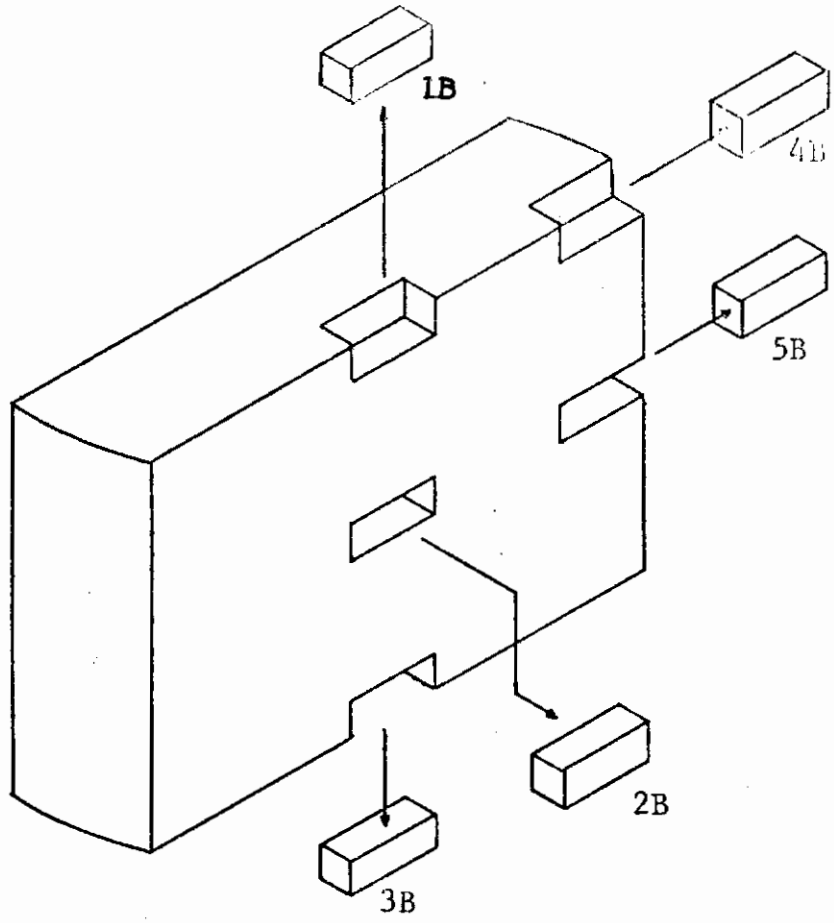

Figure 9. SECTION OF 14-IN.-DIAMETER, 7-IN.-LONG BILLET FOR RADIOGRAPHIC EXAMINATION INDICATING LOCATIONS FROM WHICH SPECIMENS FOR MICROPROBE, X-RAY, AND METALLOGRAPHIC ANALYSES WERE OBTAINED

Table III. X-RAY CHARACTERIZATION OF JTA GRAPHITE

Billet no.	Section	Composition
7-F-12	1A	Graphite + ZrB_2 + SiC
	2A	Graphite + ZrB_2 + SiC (trace)
	3A	Graphite + ZrB_2 + SiC (trace)
	4A	Graphite + ZrB_2 + SiC
	5A	Graphite + ZrB_2 + SiC
7-F-14	1A	Graphite + ZrB_2 + β-SiC + α-SiC (trace)
	2A	Graphite + ZrB_2 + β-SiC + α-SiC (trace)
	3A	Graphite + ZrB_2 + β-SiC + α-SiC (trace)
	4A	Graphite + ZrB_2 + β-SiC + α-SiC (trace)
	5A	Graphite + ZrB_2 + β-SiC + α-SiC (trace)
14-G-1	1	Graphite + ZrB_2 + β-SiC
	2	Graphite + ZrB_2 + β-SiC
	3	Graphite + ZrB_2 + β-SiC
	4	Graphite + ZrB_2 + β-SiC
	5	Graphite + ZrB_2 + β-SiC
14-G-3	1B	Graphite + ZrB_2 + β-SiC
	2B	Graphite + ZrB_2 + β-SiC
	3B	Graphite + ZrB_2 + β-SiC
	4B	Graphite + ZrB_2 + β-SiC
	5B	Graphite + ZrB_2 + β-SiC

and silicon, α-SiC begins to form at temperatures above 3900°F and is completely transformed to α-SiC between 3900°F and 4170°F(4). If the material is cooled very slowly from 4170°F to room temperature, α-SiC reverts back to β-SiC. However, this process usually does not occur under normal cooling procedures. The inference is that the JTA graphite examined was hot pressed at temperatures at or below 3900°F because of the presence of α-SiC determined from X-ray analysis.

2. CHEMICAL ANALYSIS

X-ray analysis provided a general classification of the composition of the JTA graphite billets but did not provide an analysis of quantitative composition, which was obtained from a chemical analysis of the billets. X-ray identification is effective only to approximately a 5% composition; impurities constituting less than 5% of the total content were determined through a spectrographic analysis performed by Charles C. Kamin Company and Chicago Spectro-Service Laboratory, Inc.

Chemical analysis by Carbon Products Company indicated that JTA graphite consists approximately of 35.90 ± 0.75% zirconium, 8.78 ± 0.6% silicon, 46.30 ± 2.30% carbon, and 9.30 ± 1.00% boron. A comparison of these values with results of a chemical analysis performed at Bell Aerosystems Company(5) reveals that differences in composition do exist (Appendix II). These differences probably account for the variances in the physical and the mechanical properties of JTA graphite.

The results of spectrographic analyses of the four billets are listed in Table IV. There were considerable Al, Fe, Mo, V, Mn, and Cr impurity variations among billets 7-F-12, 7-F-14 and 14-G-1. These billets were received during the first phase of the program and were presumably made from the same batch of raw material. Billet 14-G-3 was received approximately one year later and was fabricated from another batch of raw material. This difference probably explains why the impurity content of billet 14-G-3 was so different from that of the other three billets. Since the variability in raw materials and materials processing probably account for the spread in properties observed in JTA graphite, material characterization is very important in an assessment of material properties. The maximal amount of impurities was less than the 1.5% limit in the material specifications (Appendix I).

The spectrographic analysis assumes that the impurities were volatilized even though the base material was not. This assumption was true for only Al, Fe, Ba, Cu, Co, Mn, and Ca and was probably not true for Ti, Mo, V, and Cr. Therefore, the analysis holds for the lighter elements and those that do not form refractory carbides.

Table IV. SEMIQUANTITATIVE ANALYSES OF JTA GRAPHITE

Element	Element content, wt. % Billet no. 7-F-12	7-F-14	14-G-1	14-G-3
Zirconium	a	a	a	
Boron	a	a	a	
Silicon	a	a	a	
Aluminum	0.05	0.2	0.2	0.01
Iron	0.2	0.08	0.05	0.5
Titanium	0.1	0.1	0.1	0.001
Molybdenum	0.1	<0.01[b]	<0.01[b]	---
Barium	0.03	0.03	0.03	---
Copper	0.02	0.03	0.03	0.05
Vanadium	0.02	0.005	0.005	0.001
Cobalt	0.01	0.01	0.01	0.50
Manganese	0.01	0.005	0.005	0.001
Chromium	0.01	0.001	0.002	0.01
Calcium	0.005	0.005	0.005	0.0005
Magnesium	0.0002	0.0004	0.0002	0.005
Tin				0.001
Nickel				0.10
Zinc				0.10
Lead				0.01
Cadmium				0.001

[a]Trace.

[b]The major portion of the base material in this sample was not volatilized in the dc-arc discharge; therefore no quantitative results can be given for the principal element. The value shown is based on the assumption that the impurity was volatilized even though the base material was not.

3. METALLOGRAPHIC ANALYSIS

Figures 10 through 13 show the structure of the JTA graphite billets. The light areas are ZrB_2, the dark-gray areas are graphite, and the light-gray areas are SiC. In general, the graphite was uniformly distributed in the billets, while the amount of ZrB_2 and SiC varied. The quantity of the constituent materials and the size of the grains differed slightly between the interior of the billets and their outside edges. The average size of the graphite grain appeared to be 120 ± 30 μ x 70 ± 15 μ; the size of the ZrB_2 varied from about 100 to <1 μ, and the SiC varied from 50 to <1 μ.

There were minor differences between the 7- and the 14-in.-diameter billets. The 7-in.-diameter billets (7-F-12 and 7-F-14) were similar in structure; the various phases of material in the center of the billets were randomly distributed, while the edge material appeared to have a higher concentration of small grains of ZrB_2, and SiC predominated at the graphite grain boundaries. Also, there appears to be somewhat less ZrB_2 in the edge material. Other work[6] with hot-pressed graphite-carbide composites has shown that low-melting phases are squeezed out of the structure and diffuse into the mold during hot pressing, and the remaining material concentrates along the grain boundaries. The 14-in.-diameter billets (14-G-1 and 14-G-3) exhibited much more structural homogeneity than the 7-in.-diameter billets. However, the trend toward grain boundary segregation of small grains of second- and third-phase materials was present.

The billets are hot pressed in the form of truncated cones and machined to a cylindrical shape. Since the larger billets probably have more material cut away than the smaller billets, the evidence of edge segregation would be less for the larger billets.

Close examination of the samples under the microscope at about 1000x magnification showed microcracks in the ZrB_2. Once located, they could be seen at the lower magnification (320x) of the photomicrographs shown in the figures. These cracks have also been reported by L. Marcus in a study at Bell Aerosystems Company.[5]

4. ELECTRON-MICROPROBE ANALYSIS

Figure 14 presents the results of a microprobe analysis taken at position 3A of billet 7-F-12. The IITRI equipment can detect >5 wt. % amount of material with an error of +5 wt. %. The penetration depth is 5 μ for carbon, silicon and boron, and 1 μ for zirconium.

While the microprobe confirmed the x-ray and chemical result that graphite, zirconium, boron, and silicon were present, the

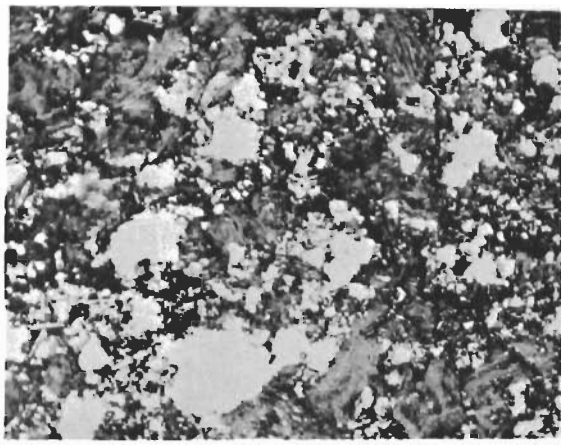

1A Location

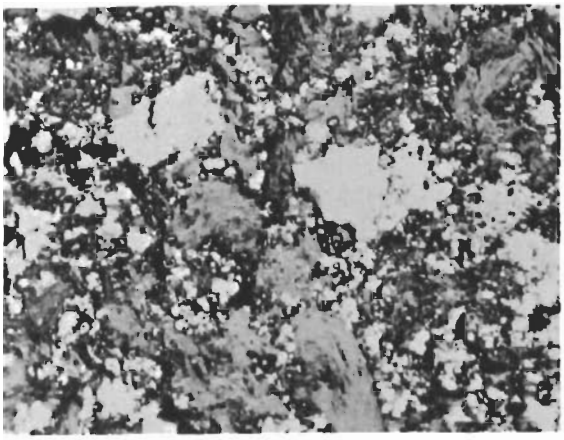

2A Location

50μ

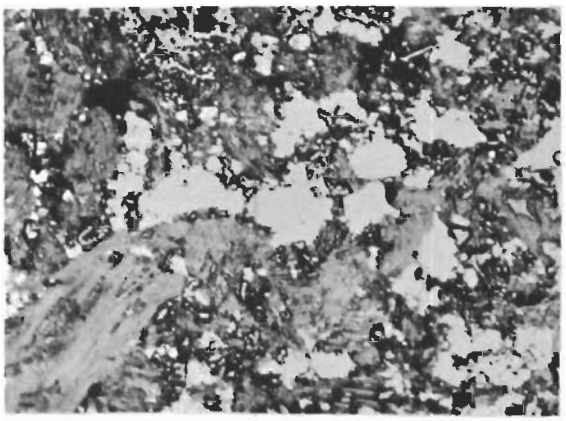

3A Location

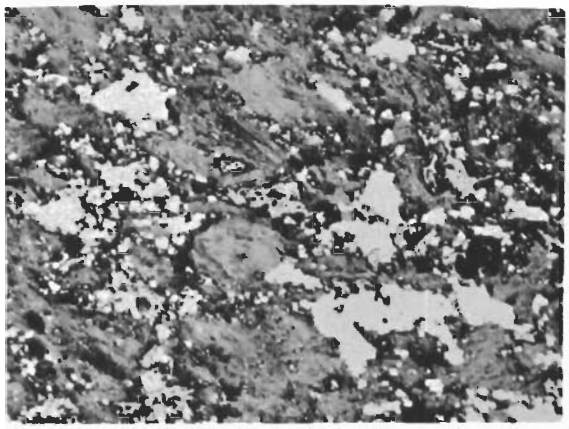

4A Location

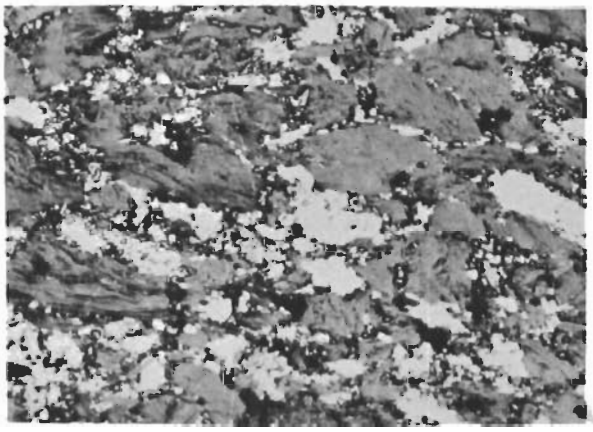

5A Location

Figure 10. PHOTOMICROGRAPHS OF JTA BILLET 7-F-12

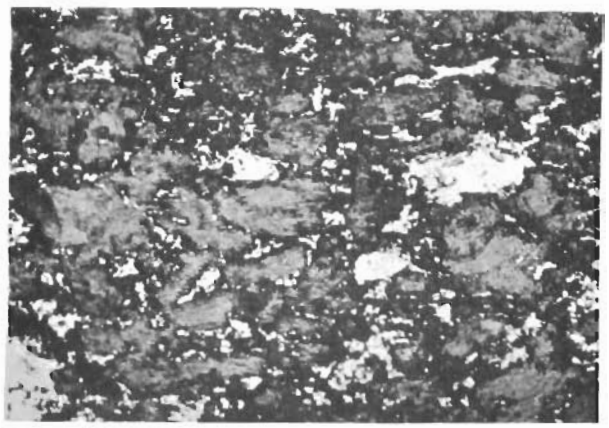

1A Location

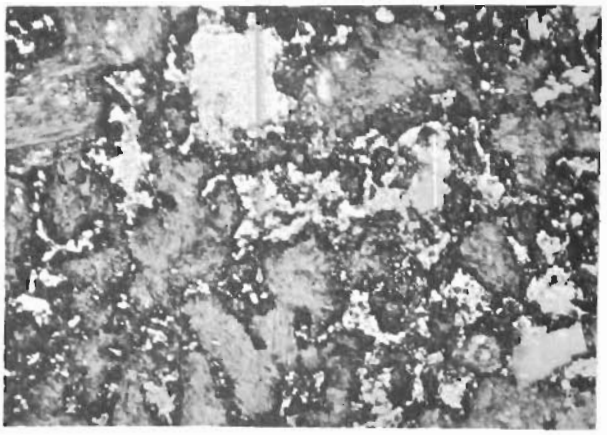

3A Location

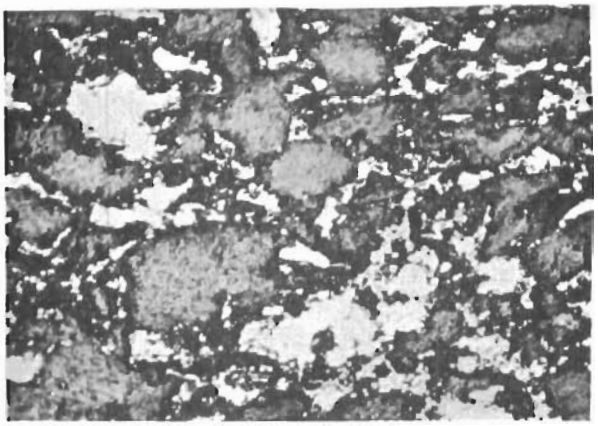

2A Location

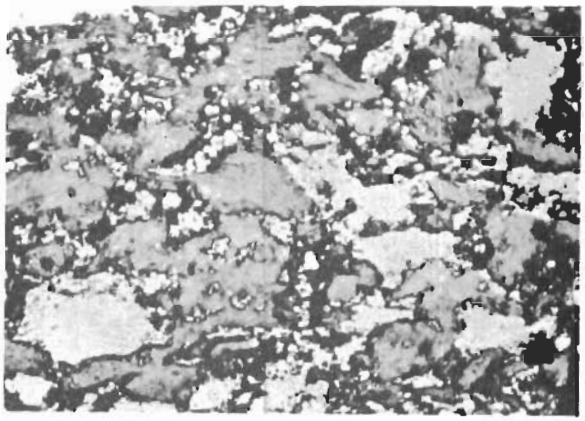

4A Location

50μ

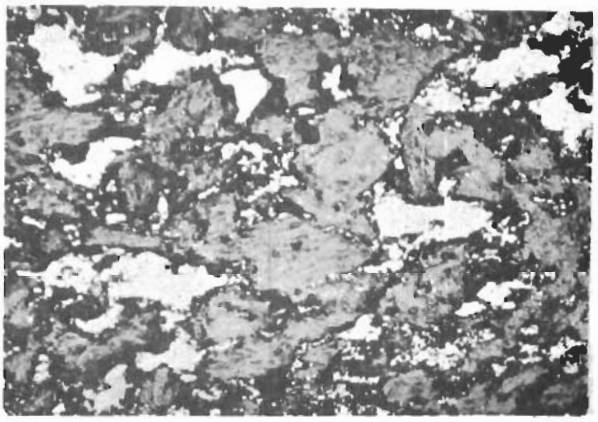

5A Location

Figure 11. PHOTOMICROGRAPHS OF JTA BILLET 7-F-14

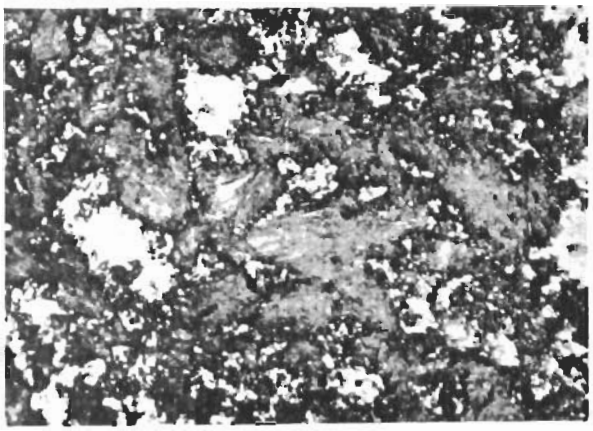

1A Location

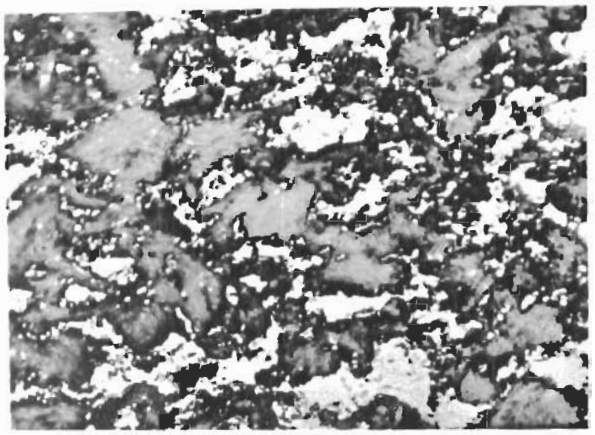

2A Location

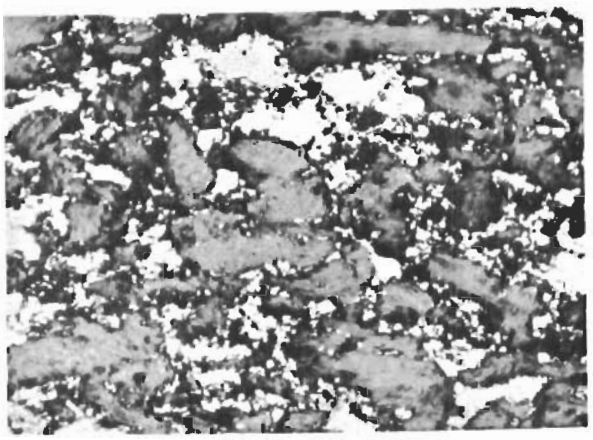

3A Location

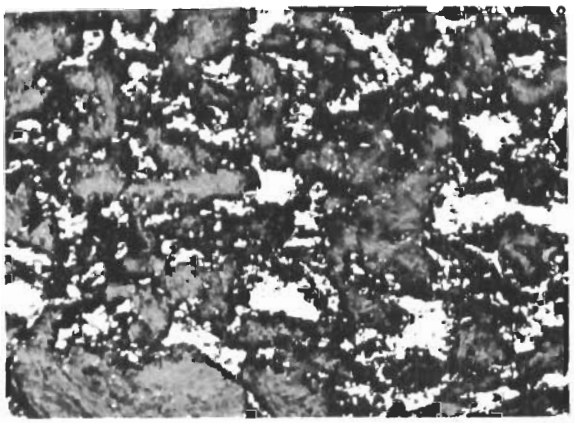

4A Location

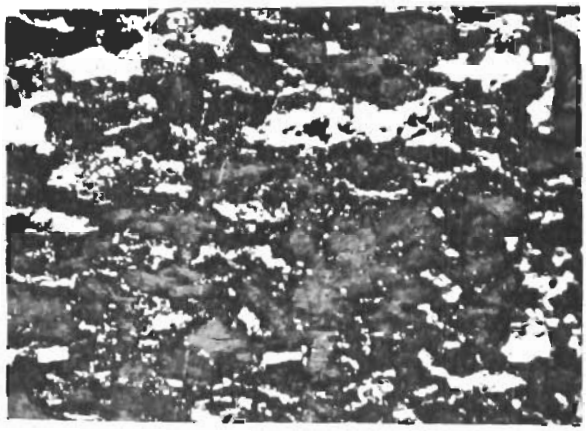

5A Location

50μ

Figure 12. PHOTOMICROGRAPHS OF JTA BILLET 14-G-1

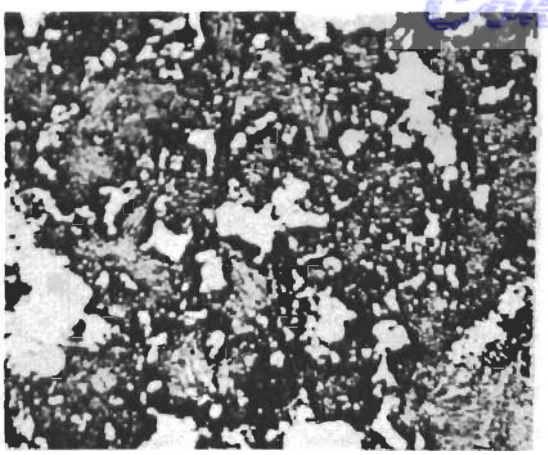

1B Location

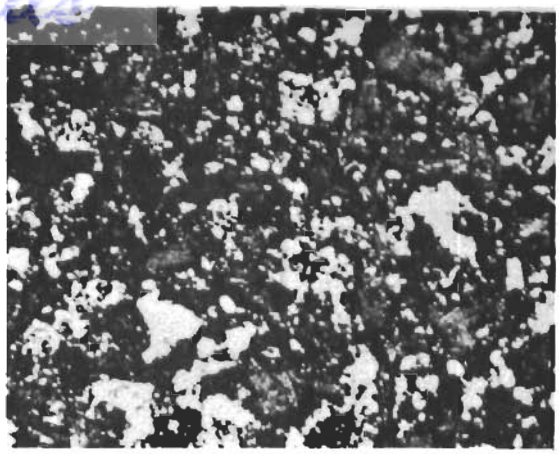

3B Location

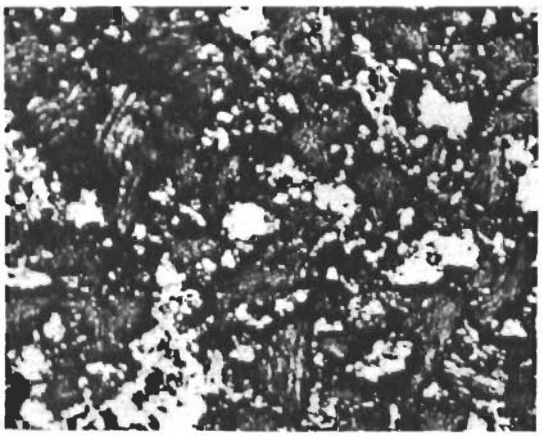

2B Location

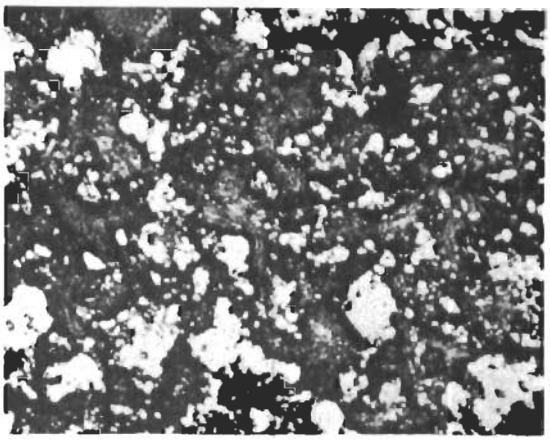

4B Location

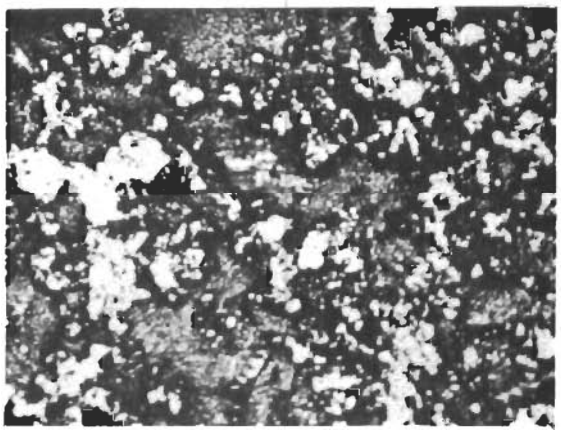

5B Location

50u

Figure 13. PHOTOMICROGRAPHS OF JTA BILLET 14-G-3

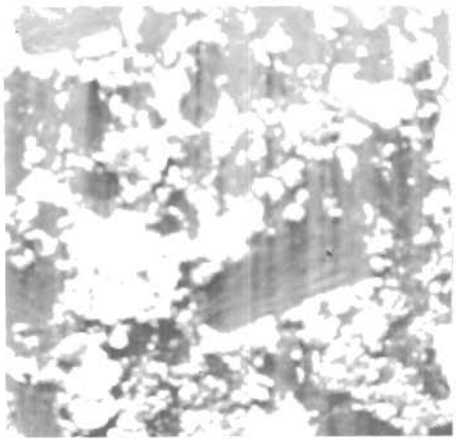

BEAM SCAN

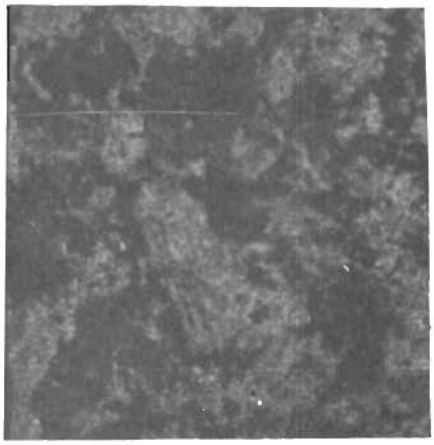

CARBON

ZIRCONIUM

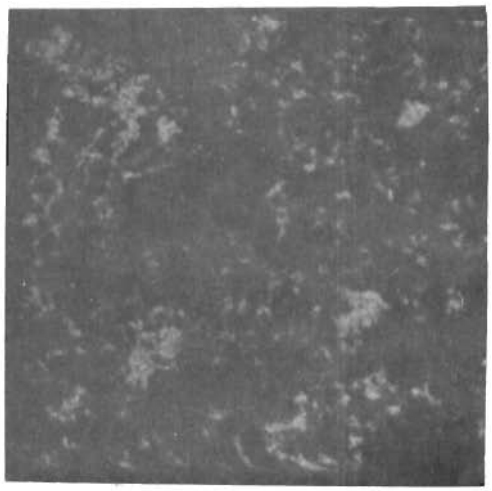

SILICON

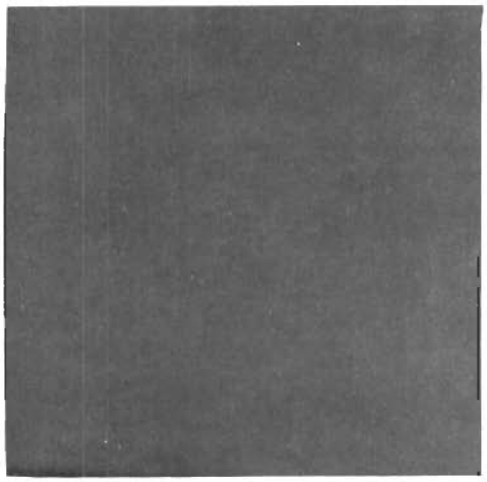

BORON

Figure 14. MICROPROBE ANALYSIS OF SECTION 3A OF BILLET 7-F-12

microprobe results concerning the amount and the location of these elements were inconclusive when compared with other analytical results and those in the literature. Preliminary examination of material from billet 7-F-14 produced results similar to those obtained for the 7-F-12 billet, and this method of analysis was dropped.

Theoretically, the zirconium-rich area should contain 81 wt. % zirconium and 19 wt. % boron and the silicon-rich area should contain 70 wt. % silicon and 30 wt. % carbon. Actual analytical results did not conform with these theoretical results; in the carbon-rich area <5 wt. % silicon, zirconium, and boron were present, and in the zirconium-rich area 46 wt. % zirconium, 22 wt. % boron, and <5 wt. % carbon, zirconium and boron were present.

The data indicate that free silicon and little SiC were present, a very unlikely conclusion. If the literature values (43 wt. % ZrB_2, 13 wt. % SiC, and 44 wt. % C), are assumed to be correct chemical and x-ray analyses are better methods of characterizing the lighter elements (Zr, Si, B) in JTA graphite than electron-microprobe analysis. With further improvement in microprobe equipment, this method of material characterization can take its place along-side x-ray diffraction, chemical, and spectrographic analyses.

5. DENSITY AND POROSITY MEASUREMENTS

Specification requirements are that the bulk density of the JTA graphite be greater than 3.00 g/cc. Bulk-density measurements confirmed the structural uniformity shown by the radiographic and metallographic analyses. Measurements of 20 samples from each billet (Table V) showed very little density variation through the billets (<1.5%) and among the billets (<1%).

Porosity (p), which includes the difficult-to-measure closed-pore volume, can be calculated from the measured bulk density (ρ) and the calculated theoretical maximum density (ρ_m):

$$p = 1 - \frac{\rho}{\rho_m} \qquad (1)$$

A method for calculating the porosity of JTA graphite is given in a recent report(7). Use is made of the fact that JTA graphite is 48.1 wt. % carbon, 42.4 wt. % ZrB_2, and 9.5 wt. % silicon. The calculated theoretical maximum density is given by the relationship:

$$\rho_m = \frac{\rho_{carbon}}{1 - (0.5905)C} \qquad (2)$$

where C ($0 < C < 1$) is the mass function of zirconium, boron, and silicon, the metallic elements of the fabricated composite. From the following assumptions, the theoretical maximum density can be

Table V. DENSITIES SAMPLES THROUGH CENTER OF JTA GRAPHITE BILLETS

Sample no.		Density, g/cc Billet no. 14-G-1	7-F-14	7-F-12	14-G-1
1		3.093	3.040	3.082	3.025
2		3.065	3.071	3.112	3.061
3		3.067	3.118	3.082	3.071
4		3.103	3.052	3.082	3.052
5		3.102	3.063	3.082	3.087
6		3.073	3.048	3.107	2.994
7		3.116	3.053	3.112	3.071
8		3.088	3.042	3.076	3.050
9		3.141	3.103	3.082	3.083
10		3.114	3.085	3.132	3.049
11		3.074	3.101	2.982	3.043
12		3.067	3.072	3.032	2.982
13		3.116	3.103	3.047	3.074
14		3.083	3.083	3.077	3.060
15		3.086	3.115	2.954	3.075
16		3.072	3.085	2.984	3.037
17		3.091	3.057	3.041	3.070
18		3.065	3.068	3.087	3.060
19		3.117	3.095	3.079	3.097
20		3.088	3.082	3.090	3.050
	Avg.	3.091	3.077	3.065	3.054
	Std. Dev.	±0.021	±0.023	±0.049	±0.027
	Variance	0.676%	0.760%	1.484%	0.900%

calculated from C and the x-ray density of each phase in the composite material: the mass ratio of ZrB_2 to silicon is 42.4:9.5; all silicon is in the form of α- and β-SiC; and the x-ray densities are 2.267 g/cc for pure carbon, 6.10 g/cc for ZrB_2, and 3.216 g/cc for SiC. The value of C for this composition of JTA graphite is 42.4% (ZrB_2) plus 9.5% (silicon), or 51.9% (metallic additives). Therefore:

$$\rho_m = \frac{2.267 \text{ g/cc}}{1 - (0.5905)(0.519)} = \frac{2.267 \text{ g/cc}}{1 - 0.3} = \frac{2.267 \text{ g/cc}}{0.7}$$

$$= 3.23 \text{ g/cc} \qquad (3)$$

The average bulk density of the JTA used during this program was 3.072 g/cc, and the average porosity was:

$$p = 1 - \left(\frac{3.072 \text{ g/cc}}{3.23 \text{ g/cc}}\right) 100 = 5\% \qquad (4)$$

At low porosities, the error can be relatively large; however, if used consistently, these equations can be used to predict changes in mechanical and physical properties.

6. DYNAMIC-MODULUS STUDIES

Attempts were made to characterize mechanical properties by obtaining the dynamic modulus of the specimens used to determine whether the material in the billets exhibited significantly different flexural strengths. The studies consisted of correlating the dynamic, or the sonic, modulus of the samples with their flexural strength. This technique is different from ultrasonic techniques in that the test piece is made to vibrate in one of its natural frequencies rather than at that of a high-frequency beam of energy passed through the material. For most applications, the natural frequencies are within the audible range (10,000 to 20,000 cps); therefore dynamic-modulus testing is often referred to as sonic testing.

The natural frequency of a rod or a rectangular bar can be related to its properties in the equation:

$$f = \frac{m^2}{2\pi L^2} \qquad \frac{EI_g}{Ad} \qquad (5)$$

where

f is the frequency of vibration (cps)
m is the vibration constant
L is length (in.)
E is Young's elastic modulus
I is the moment of inertia
g is the acceleration due to gravity
A is the cross sectional area
d is the density of the material.

Equation 5 states that the resonant frequency (f) is proportional to both the radius of gyration (r - I/A) and the square root of Young's elastic modulus (E) and is inversely proportional to the square of the length of the bar ($1/L^2$). Therefore if a flaw reduces the moment of inertia or if the elasticity of the material is impaired, the resonant frequency is lowered. These relationships can be used to evaluate the strength of a material, since strength is related to radius of gyration and elasticity.

Plots of sonic modulus vs strength for across- and with-grain orientations are exhibited in Figures 15 through 18. The comparisons are for flexural samples whose dimensions were 3 x 1/4 x 1/4 in. Data for billets 7-F-12, 7-F-14, and 14-G-1 are combined and compared to data for billet 14-G-3. The strength and the sonic modulus for the with-grain orientation varied randomly. However, the across-grain orientation exhibited a narrow strength range and a wide sonic-modulus range. This contrast is due to the differences in bonding mechanism between with- and across-grain orientations of graphite. The bonds for the with-grain orientation are extremely strong and intermediate between covalent and metallic bonds. Therefore failure is apt to be random and related to the flaw structure in the material. Since the material is a composite having a fractured phase, scatter of the fracture stress can be expected to be very large. On the other hand, the bonds in the across-grain orientation are fewer[8] and consist of weak Van der Walls forces; in this case, the bond forces govern the flaws in the composite. For this reason the scatter in the fracture stress is much less than that for the with-grain orientation. However, the wide scatter in the sonic-modulus values indicates that while sonic modulus can be used to separate with- and across-grain orientations, it cannot be used to characterize the mechanical strength within a particular grain orientation.

The relationship between sonic modulus and density (Figure 19) could also be used to characterize JTA graphite. This plot also shows wide scatter and little or no correlation between these two properties and confirms the conclusion that sonic modulus can be used only for gross identification, not true characterization, of properties.

A cross check of a JTA specimen was made with Union Carbide to reference our respective equipment. Union Carbide tested a sample, JTA-9-WRB, and obtained a with-grain sonic modulus of 12.89×10^6 psi $\pm$ 0.4%. There is an approximately 6% difference between the two measurements; this difference can be attributed to variations in equipment and technique, not to gross errors in measurement. These data indicate a close correlation between two different pieces of equipment making the same measurement in different laboratories.

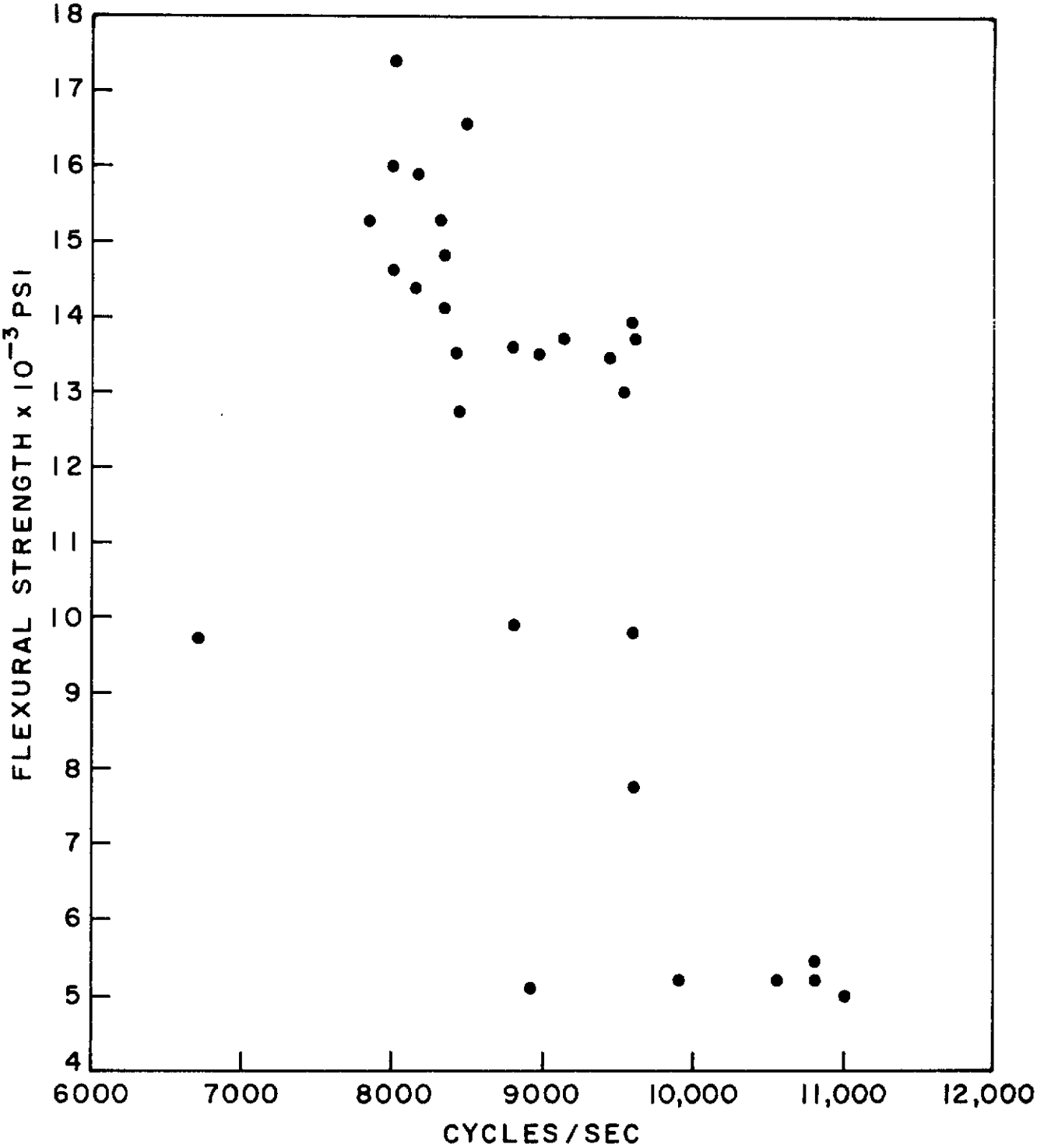

Figure 15. FLEXURAL STRENGTH VS SONIC MODULUS FOR BILLETS 7-F-12, 7-F-14, and 14-G-1 (Across grain)

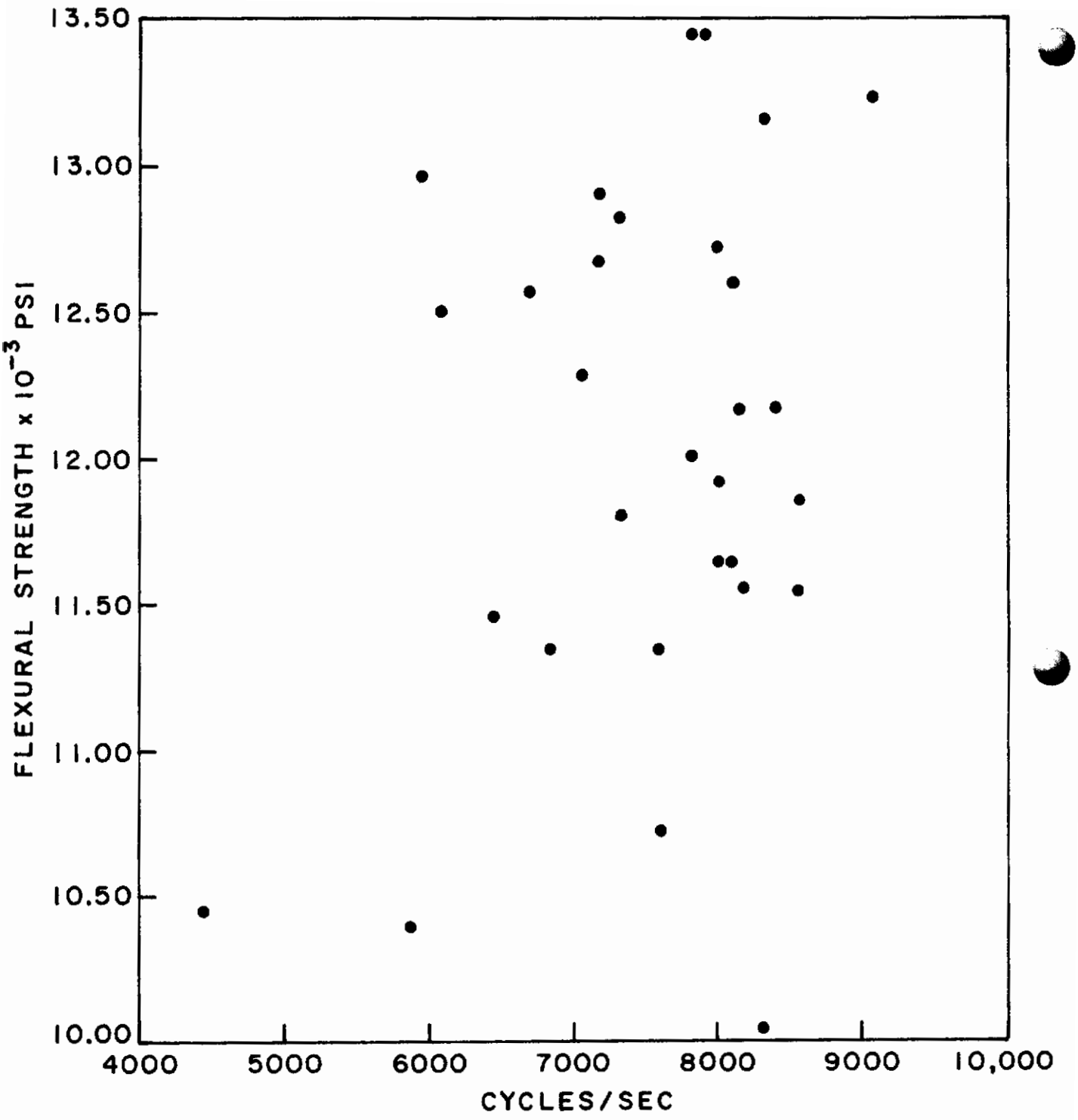

Figure 16. FLEXURAL STRENGTH VS SONIC MODULUS FOR BILLET 14-G-3 (Across grain)

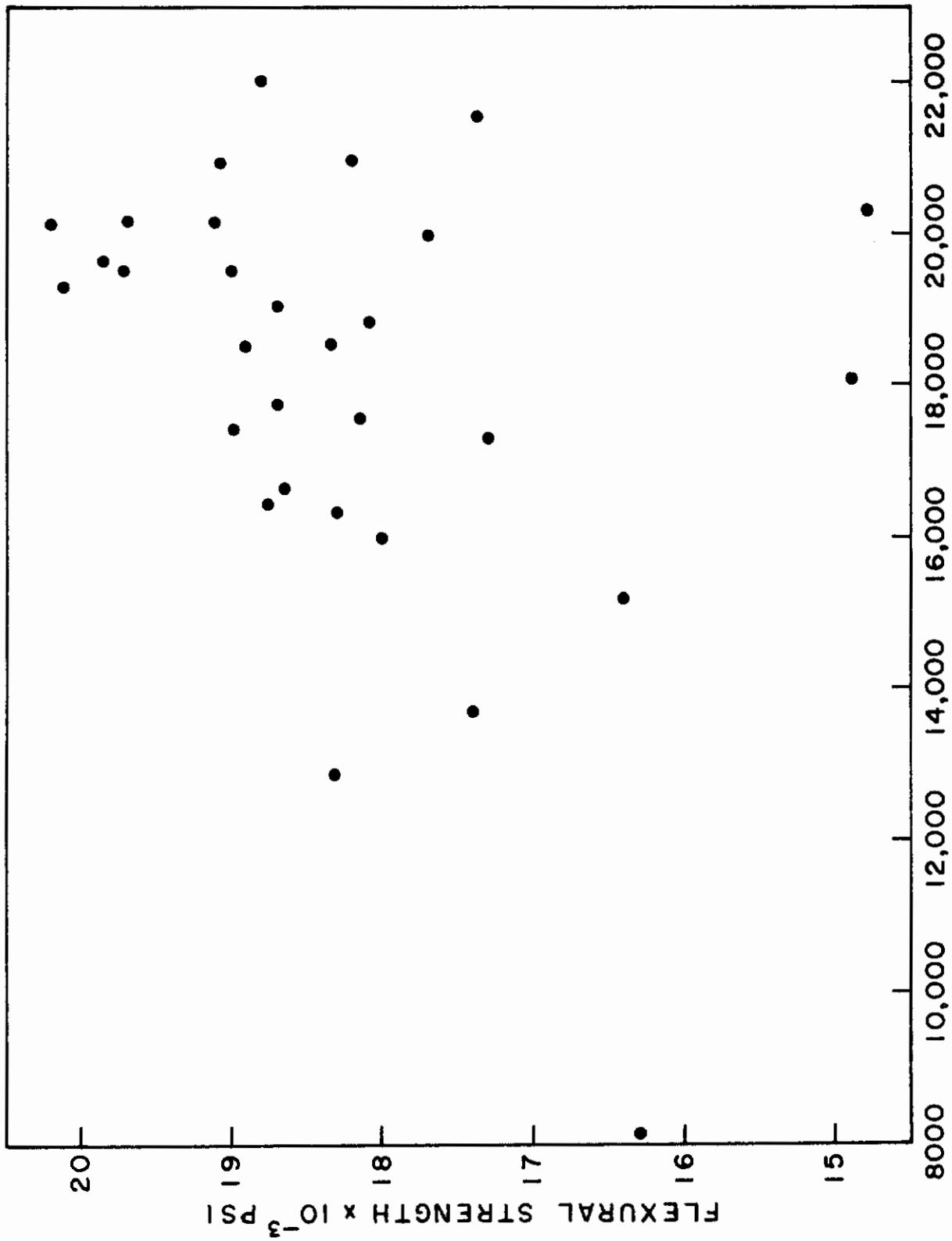

Figure 17. FLEXURAL STRENGTH VS SONIC MODULUS FOR BILLETS 7-F-12, 7-F-14, and 14-G-1 (With grain)

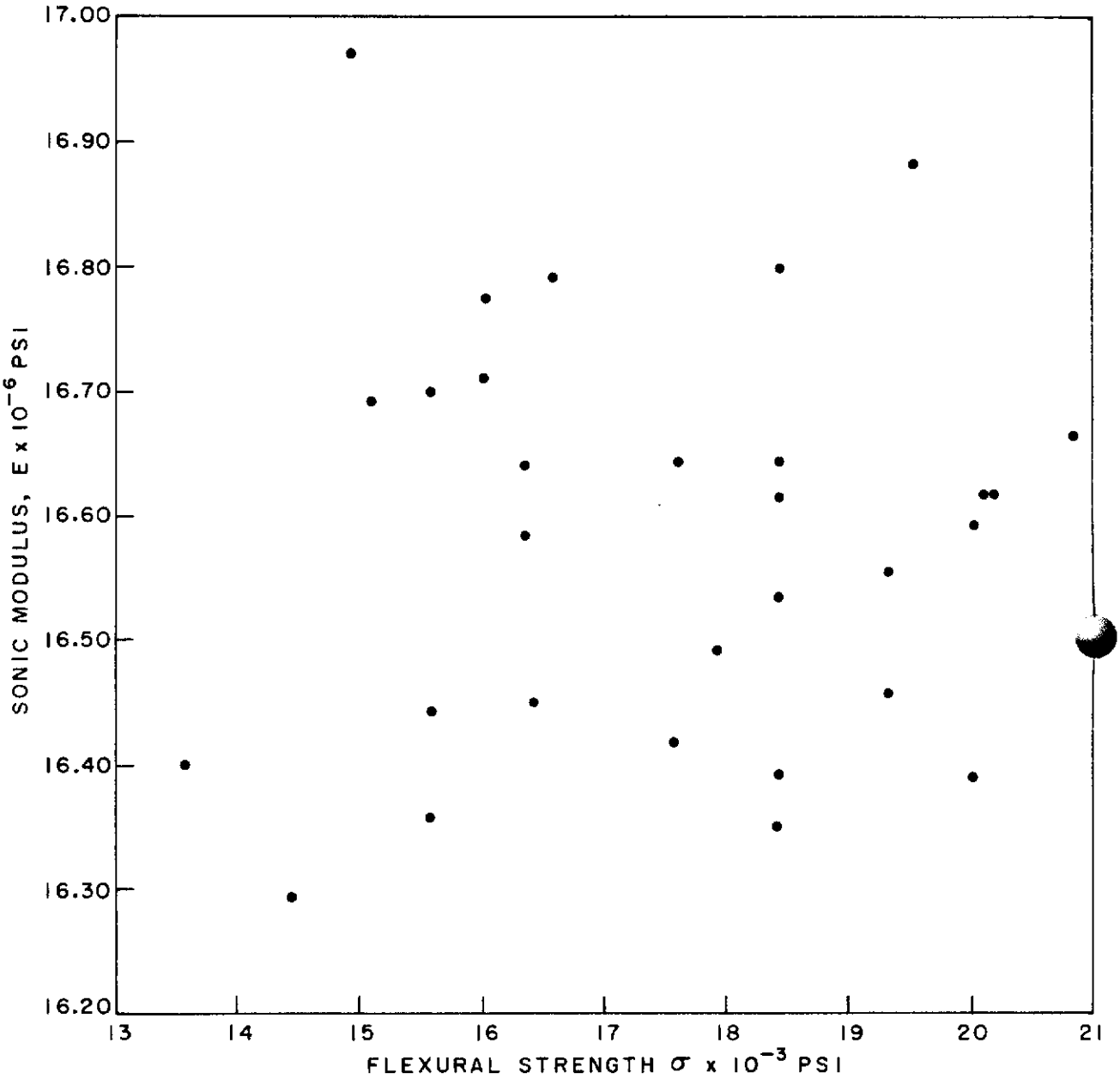

Figure 18. FLEXURAL STRENGTH VS SONIC MODULUS
FOR BILLET 14-G-3 (With grain)

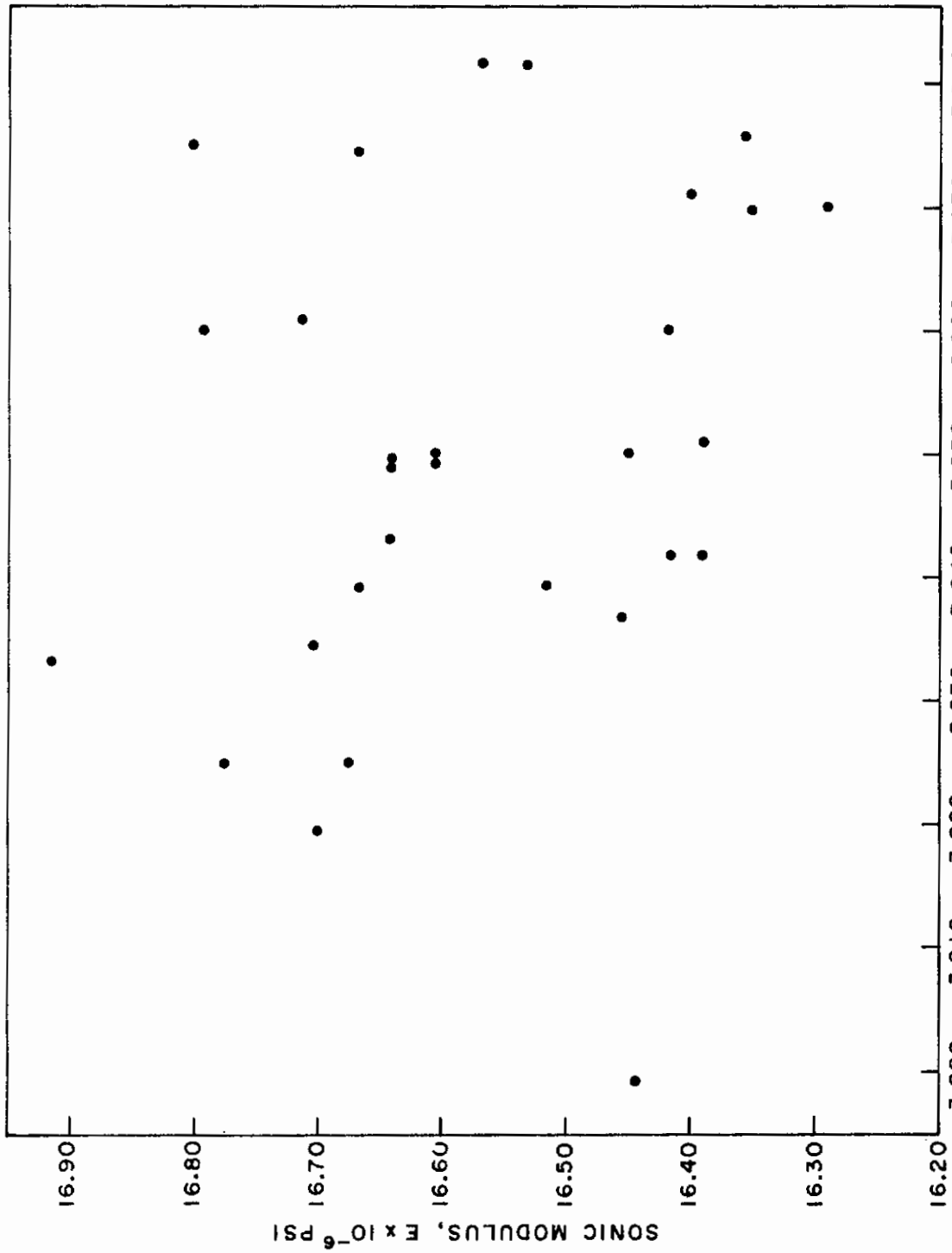

Figure 19. SONIC MODULUS VS DENSITY FOR BILLET 14-G-3 (With grain)

7. PERMEABILITY EXPERIMENTS

Permeability tests were made on specimens 3/4 in. in diameter and 1/2 and 1/4 in. thick. Initial tests were made in a vacuum apparatus. These experiments indicated no gas flow through the system under a 1-atm pressure differential. To obtain greater pressure differentials, a positive-pressure apparatus was assembled; a schematic diagram of this equipment is shown in Figure 20 and a view of the specimen holders and permeability apparatus is shown in Figures 21 and 22. The samples were mounted with epoxy into the holders. A constant pressure of nitrogen was introduced, and the gas passing through the specimen was collected and measured.

With- and across-grain orientations of specimens tested at 150 atm for 1/2 to 1 hr produced no apparent pressure drop. The evidence provided by these experiments indicates that JTA graphite has a closed-pore system that exhibits no measurable permeability.

8. OXIDATION STUDIES

JTA graphite was developed for use at high temperatures under oxidizing conditions. Two methods of observing the effects of oxidation on JTA graphite were studied. The first method consisted of exposing flexural samples to various temperatures and air pressures (Table VI); the effect of oxidation on weight and strength as measured under ambient atmospheric conditions. The second method consisted of measuring strength changes under the exposure conditions; these experiments enabled the translation of mechanical properties in the inert environment into those under oxidizing conditions. The depth or amount of oxidation, the nature of the oxidized material, the rate at which oxidation progressed, and the effect of oxidation on strength were determined. A comparison of strengths obtained by the different test methods is given in Section IV4. The effect of material loss is considered in Section IV3. In this section the effect of oxidation on the character of JTA graphite is discussed.

Under oxidizing conditions a protective coating is formed on the surface of JTA graphite. Figure 23 shows the coating after 1-hr exposures at three temperatures. Figure 24 exhibits how the coating built up with time at a particular temperature. X-ray analysis of the protective coating (Table VII) indicated that it was zirconia. At 2730°F the coating formation was slow. At 3180°F there was a considerable build up of coating and considerable migration of a borosilicate glass to the surface of the specimen, where it formed in globules, as observed in Figure 24. At 3630°F a smooth zirconium oxide coating formed, but there was considerable loss of graphite.

Metallographic examinations of the oxidized surface were made. Figures 25 through 27 exhibit the appearance of the oxidized surface of with-grain orientations at 1832°F, 2732°F and 3182°F.

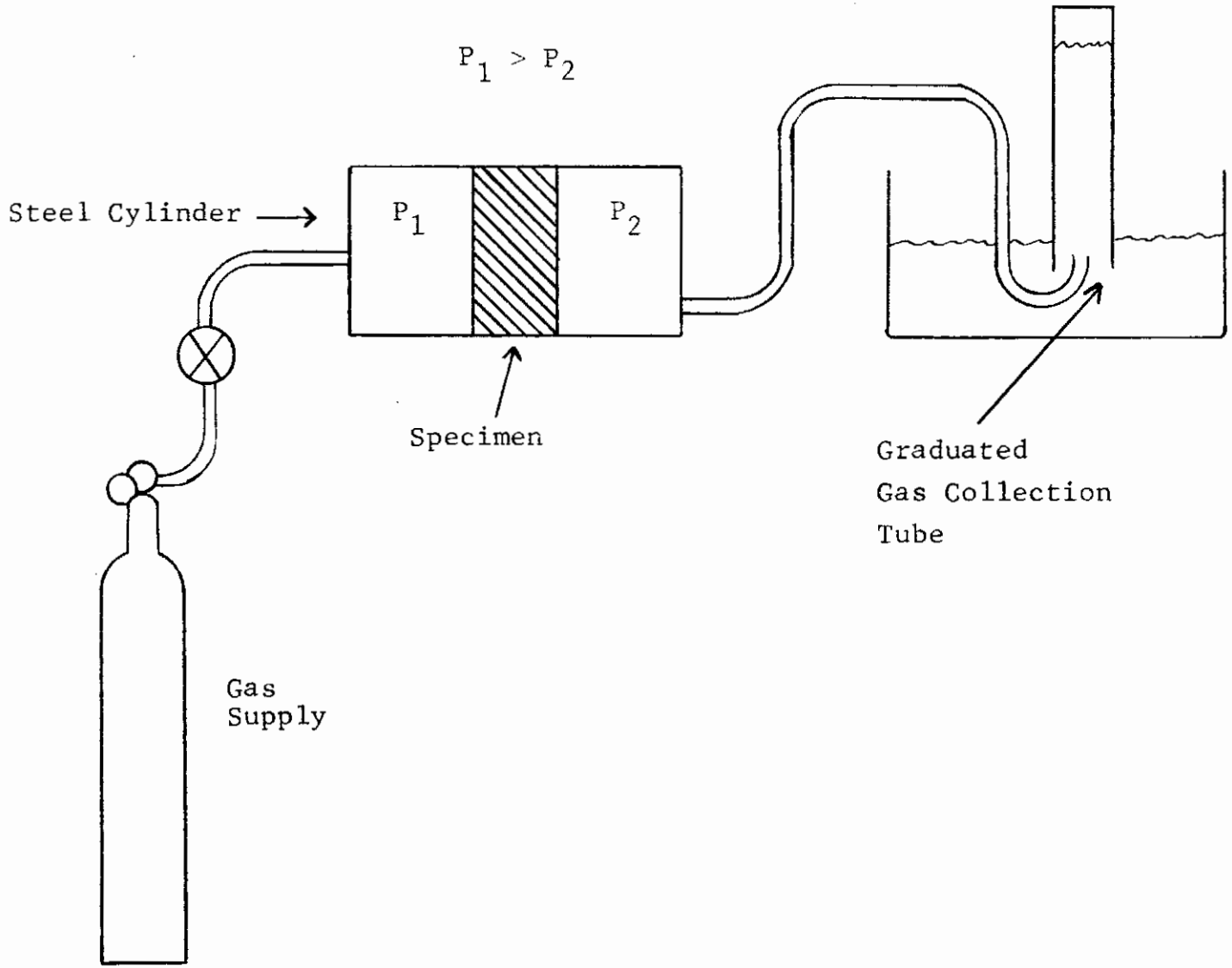

Figure 20. SCHEMATIC DIAGRAM OF PERMEABILITY MEASURING SYSTEM

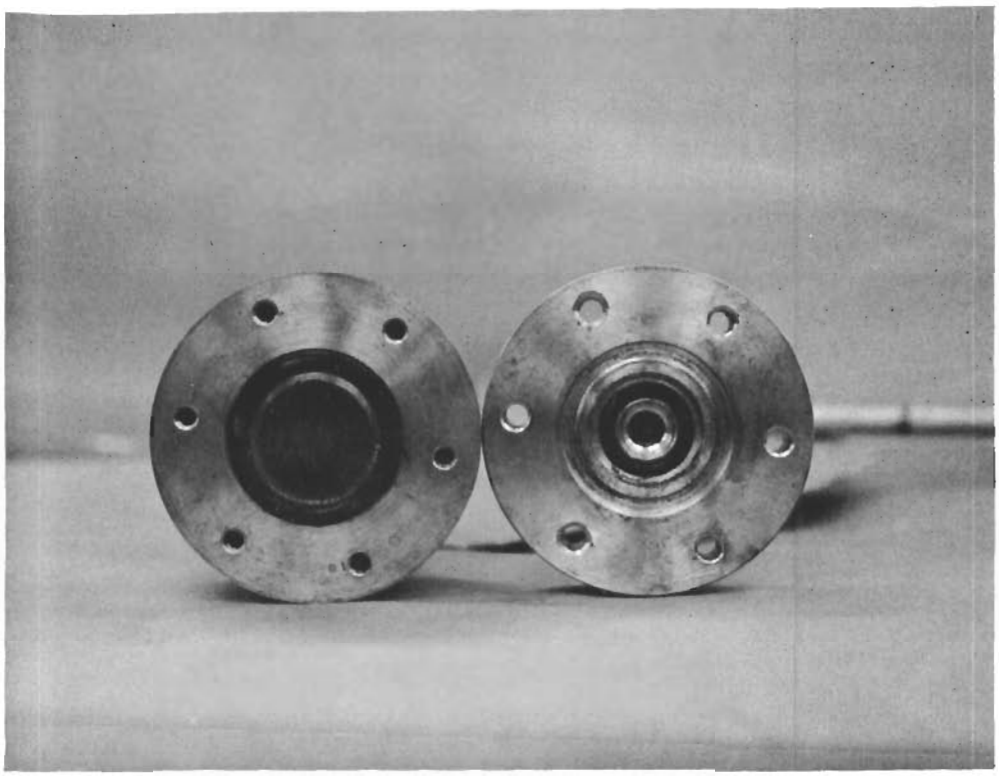

Figure 21. VIEW OF SPECIMEN HOLDER

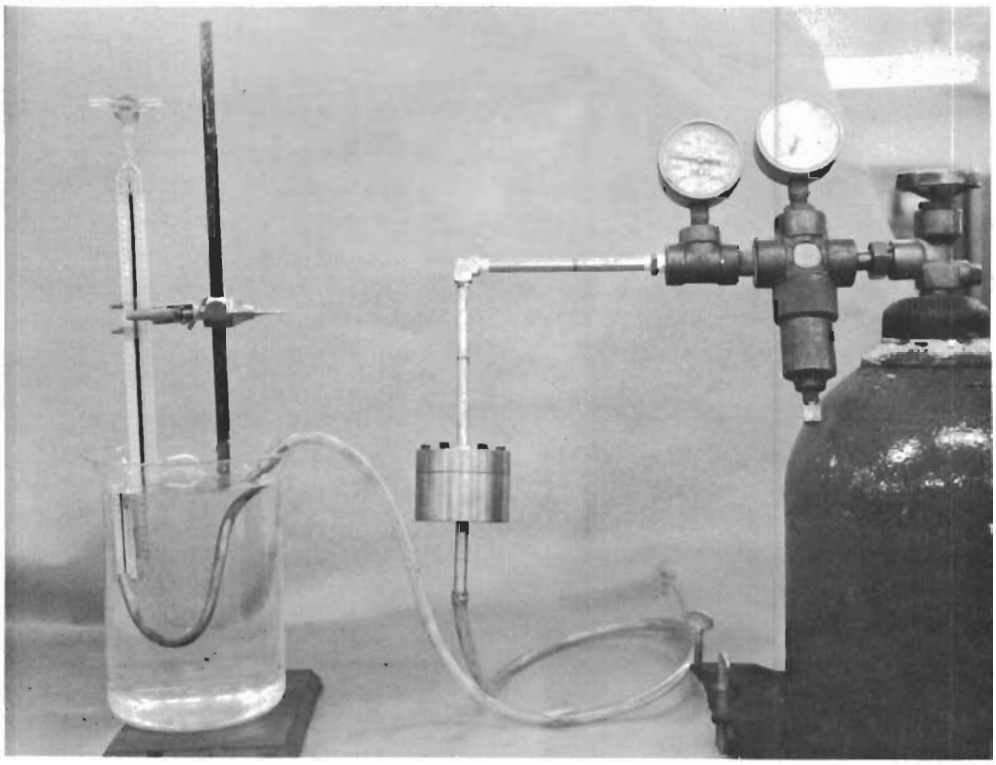

Figure 22. PERMEABILITY APPARATUS: SPECIMEN HOLDER, COMPRESSED AIR, AND GRADUATED GAS-COLLECTION TUBE

Table VI. EXPERIMENTAL CONDITIONS OF OXIDATION TESTS OF JTA GRAPHITE

Property	Crystal orientation	Number of specimens tested Temperature, °F 1832	3182	3632
Tension	With grain	10	10	10
	Across grain	10	10	10
Flexure	With grain	10	10	10
	Across grain	10	10	10
Compression	With grain	10	10	10
	Across grain	10	10	10

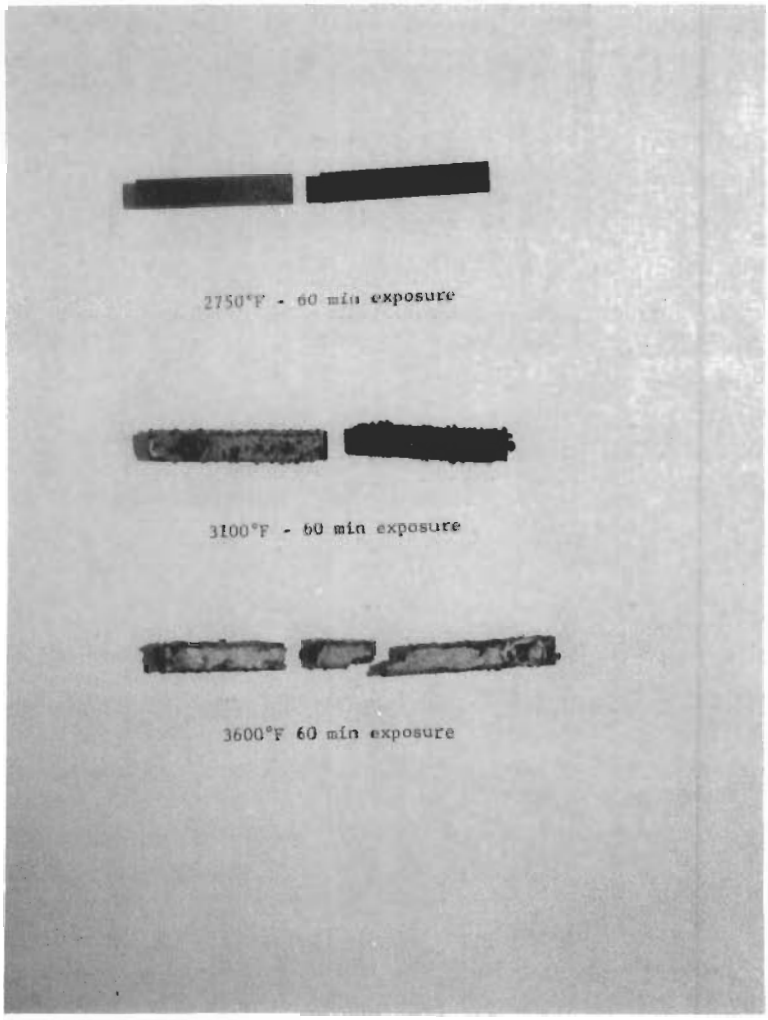

Figure 23. APPEARANCE OF FLEXURAL SPECIMENS AFTER 60-MIN SOAK AND TESTING IN AIR

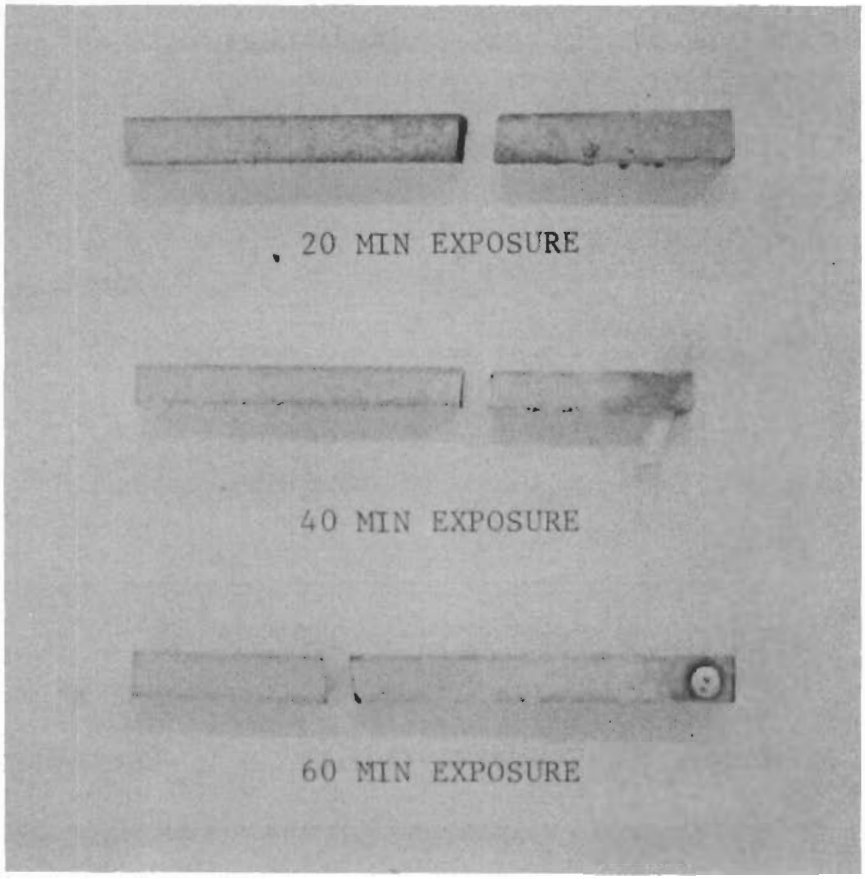

Figure 24. DEVELOPMENT OF OXIDE COATING ON JTA SAMPLES DUE TO EXPOSURE TO AIR AT 3100°F

Table VII. RESULTS OF X-RAY ANALYSIS OF PROTECTIVE JTA COATING FORMED AT 3100°F IN AIR

Exposure time, min	Composition	
	Component	wt. %
20	Graphite	25-35
	Zirconia	65-75
40	Graphite	10-15
	Zirconia	85-90
60	Graphite	0-5
	Zirconia	95-100

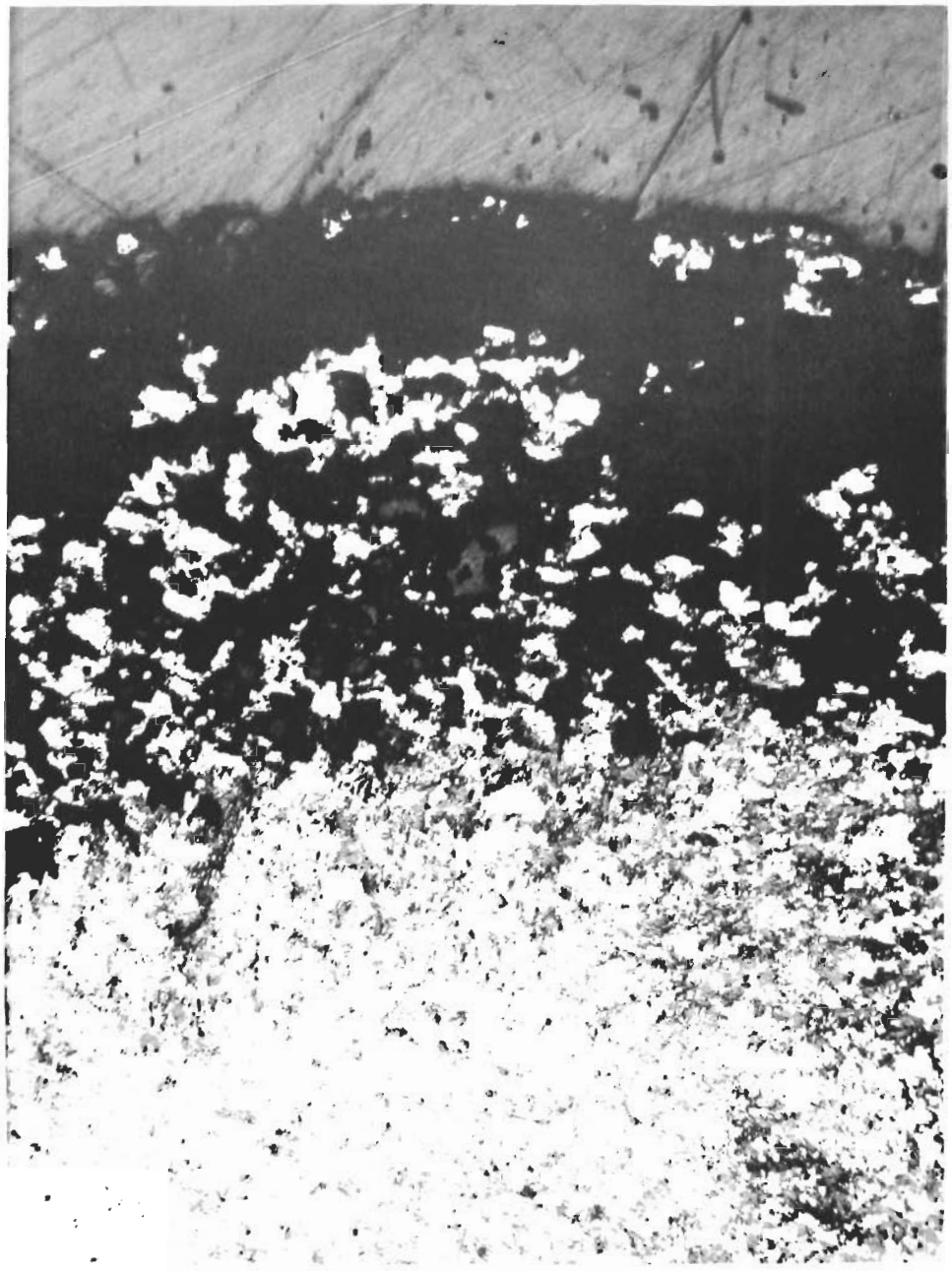

Figure 25. METALLOGRAPH OF EDGE OF JTA
AFTER EXPOSURE TO AIR AT 1832°F FOR 60 MIN

Figure 26. METALLOGRAPH OF EDGE OF JTA AFTER EXPOSURE TO AIR AT 2732°F FOR 60 MIN

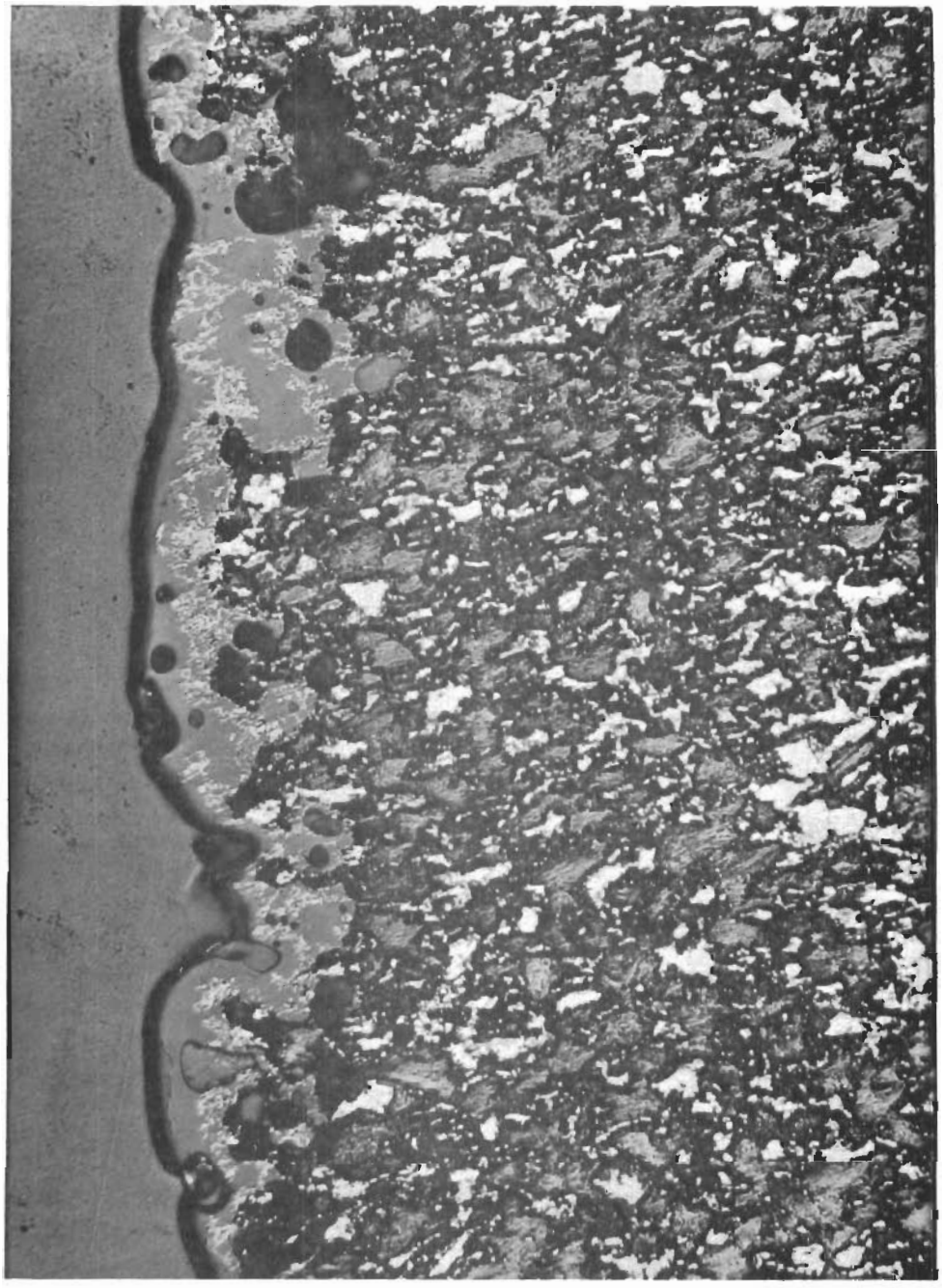

Figure 27. METALLOGRAPH OF EDGE OF JTA AFTER EXPOSURE TO AIR AT 3100°F FOR 20 MIN

At 3632°F the coating and the graphite were too friable for metallography. No real coating was observed until exposure at 3182°F. The build up of this coating can be observed in Figures 27 through 29. Figure 27 exhibits graphite loss with time. It is interesting to note that material loss was higher at 1832°F than at 2732°F and then increased from 2732°F to 3632°F, the end-point temperature for these experiments. Coating formation was observed at 3182°F, but there was greater material loss at this temperature than at 2732°F.

Weight-loss and strength-loss experiments were performed for all the temperatures and atmospheric pressures studied. Weight-loss data are shown in Figures 30 through 34. At ambient air pressure and 1832°F, there was a rapid weight loss during the first 20 min of exposure, a rapid weight gain due to build up of protective coating during the second 20 min, and a slower weight loss due to diffusion and/or spalling of the coating during the third 20 min. At 10^{-1} torr, a similar pattern was observed, except weight loss was about two orders of magnitude slower than that in an ambient air atmosphere. At 10^{-3} and 10^{-5} torr, the pattern was somewhat different. The initial weight loss was comparable to that observed under 10^{-1} torr, but there was no weight gain; the weight loss leveled off after 20 min of exposure. The with-grain orientation appeared to be more sensitive to oxidation than the across-grain orientation at these pressures.

Weight-loss behavior in an air atmosphere was different when the exposure temperature was raised from 1832°F, to 3182°F. There was a slower initial rate of material loss, but no rapid build up of coating. After 1-hr exposure at 3182°F, the rate of weight loss appeared to level off. The material exposed to static air exhibited about twice the weight loss of material exposed to 10^{-1} torr. A comparison of the low-pressure plots indicates that the weight loss at 3182°F was an order of magnitude greater than that at 1832°F. However, the high-temperature curves show a hump between 20 and 60 min. The weight loss at 10^{-1} torr was about twice that at 10^{-3} and 10^{-5} torr. The effect of grain orientation on material exposed to 3182°F was much less than that on material exposed to 1832°F.

At 3632°F the JTA exposed to ambient air conditions lost 40% of its weight. Material exposed to 3632°F and 10^{-1} or 10^{-3} torr exhibited about the same behavior as material exposed to 3182°F and 10^{-1} or 10^{-3} torr. However, material exposed to 3632°F and 10^{-5} torr exhibited the behavior exhibited at 3182°F and ambient air pressure.

Changes in flexural strength of material exposed to the conditions used for the weight-loss experiments are shown in Figures 35 through 37. The important factor indicated by these tests is that the strength loss of JTA exposed to low pressures is minimal as compared with that of JTA exposed to high temperatures and ambient atmospheric conditions.

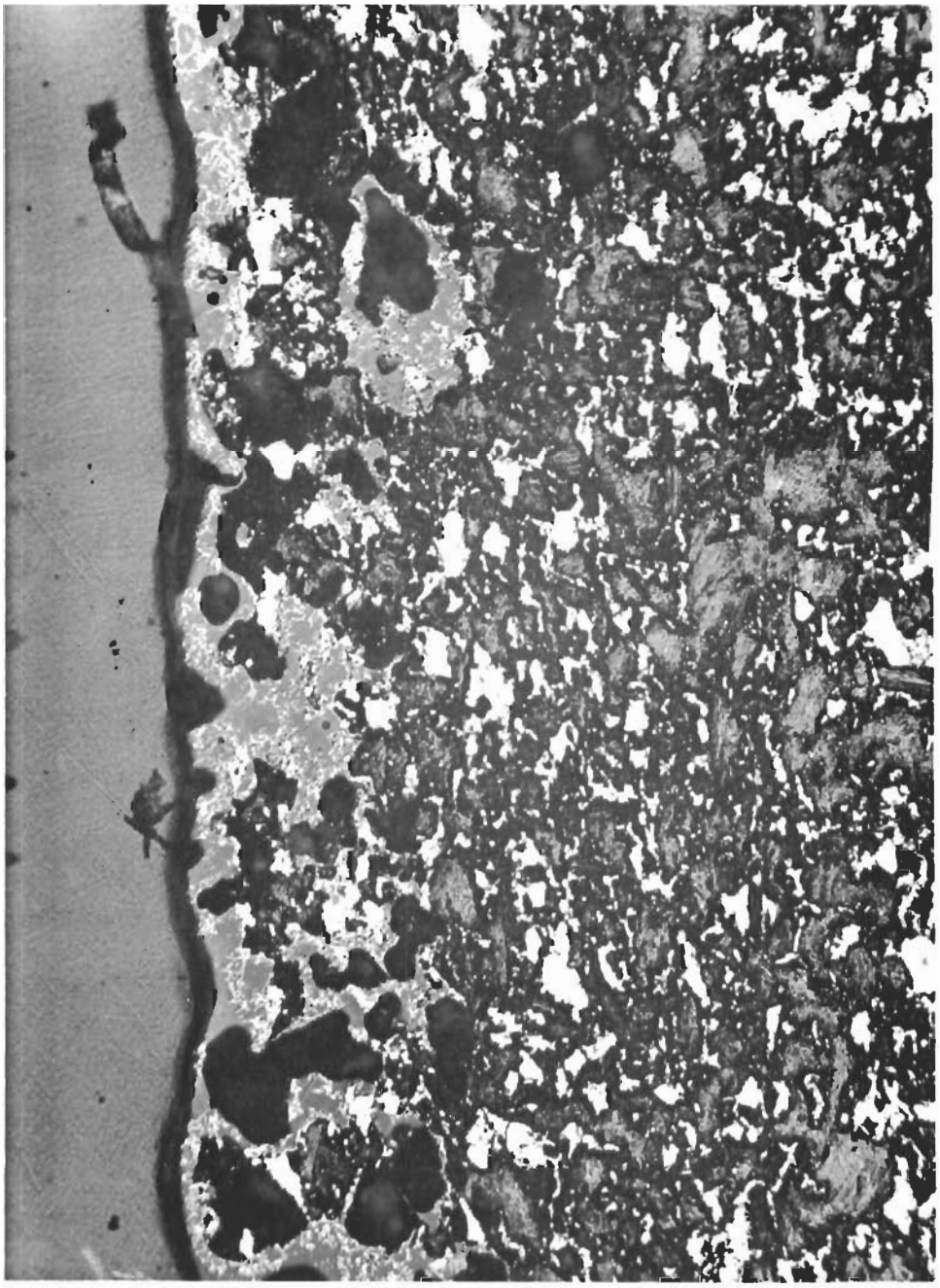

Figure 28. METALLOGRAPH OF EDGE OF JTA
AFTER EXPOSURE TO AIR AT 3100°F FOR 40 MIN

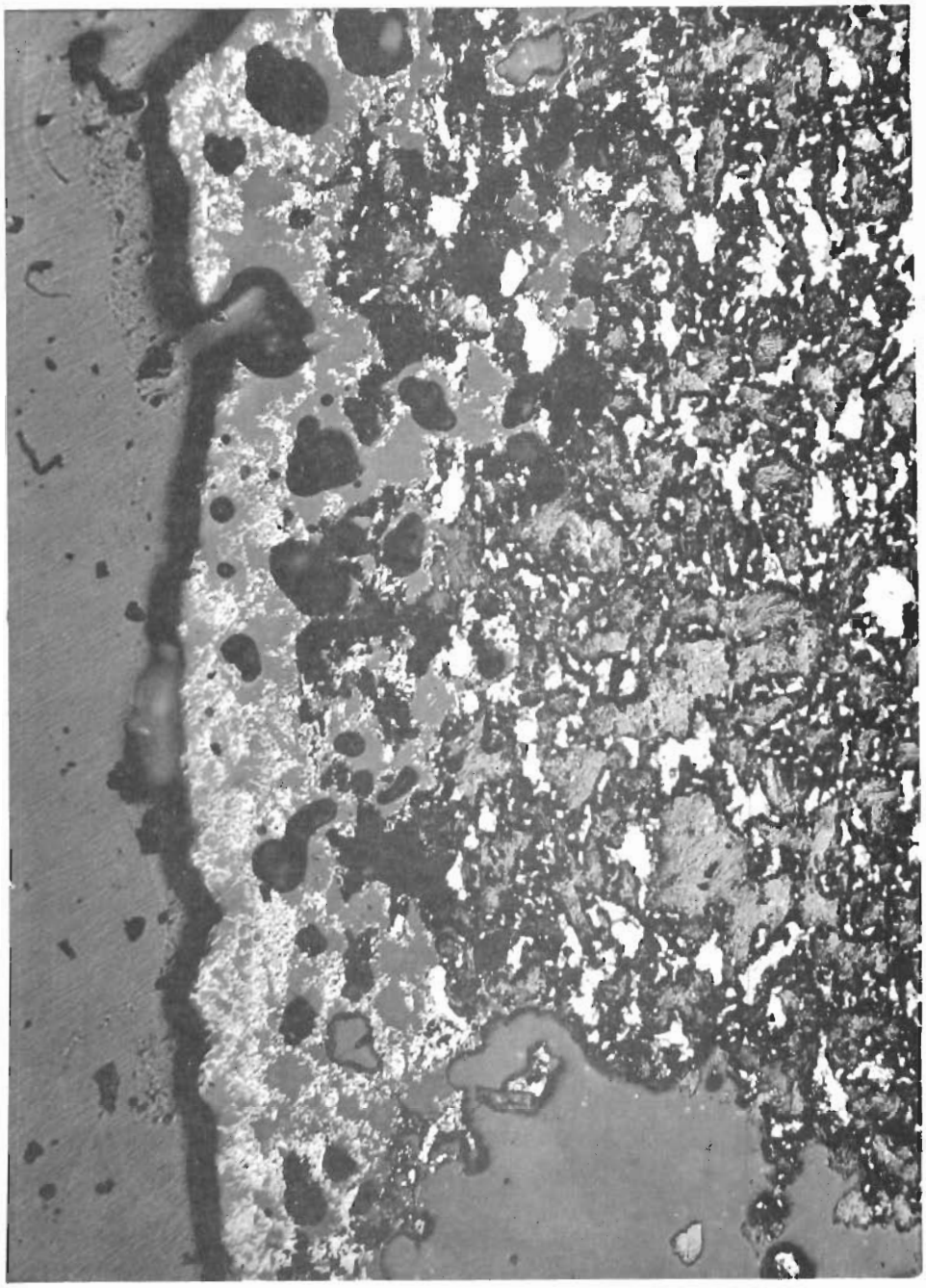

Figure 29. METALLOGRAPH OF EDGE OF JTA AFTER EXPOSURE TO AIR AT 3100°F FOR 60 MIN

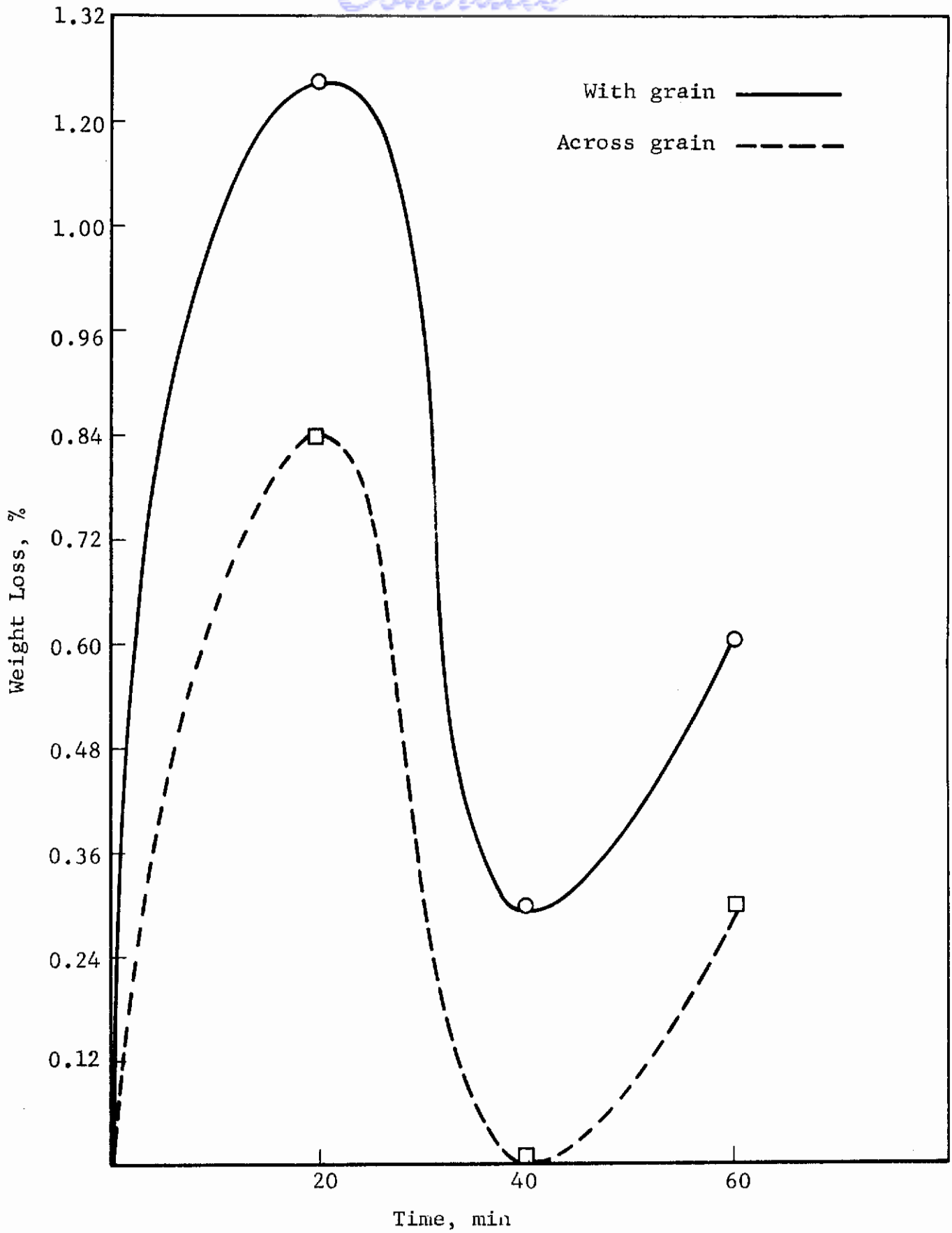

Figure 30. WEIGHT LOSS OF JTA GRAPHITE AT 1800°F IN STATIC AIR

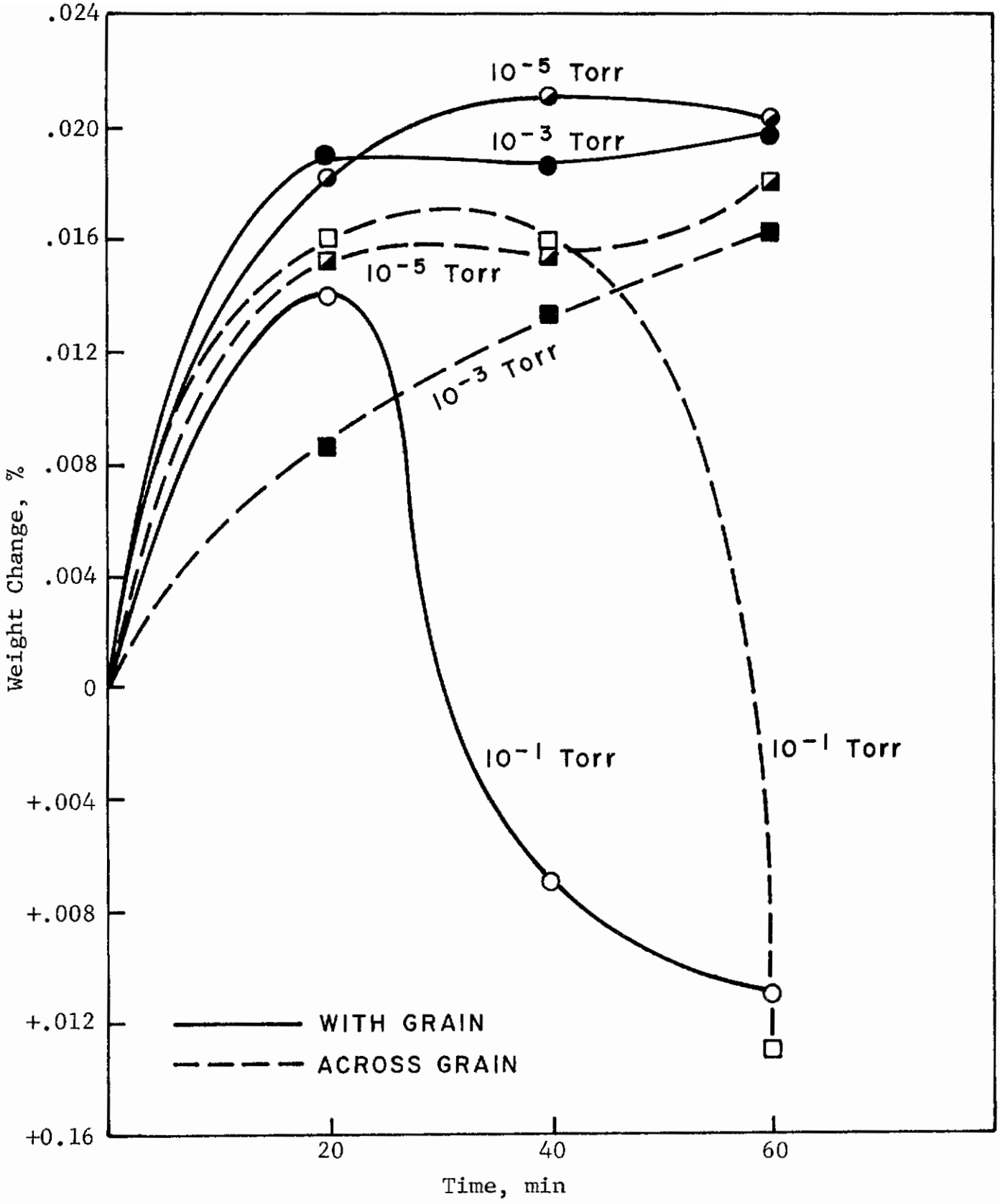

Figure 31. WEIGHT LOSS OF JTA GRAPHITE AT 1800°F, IN AN AIR ATMOSPHERE

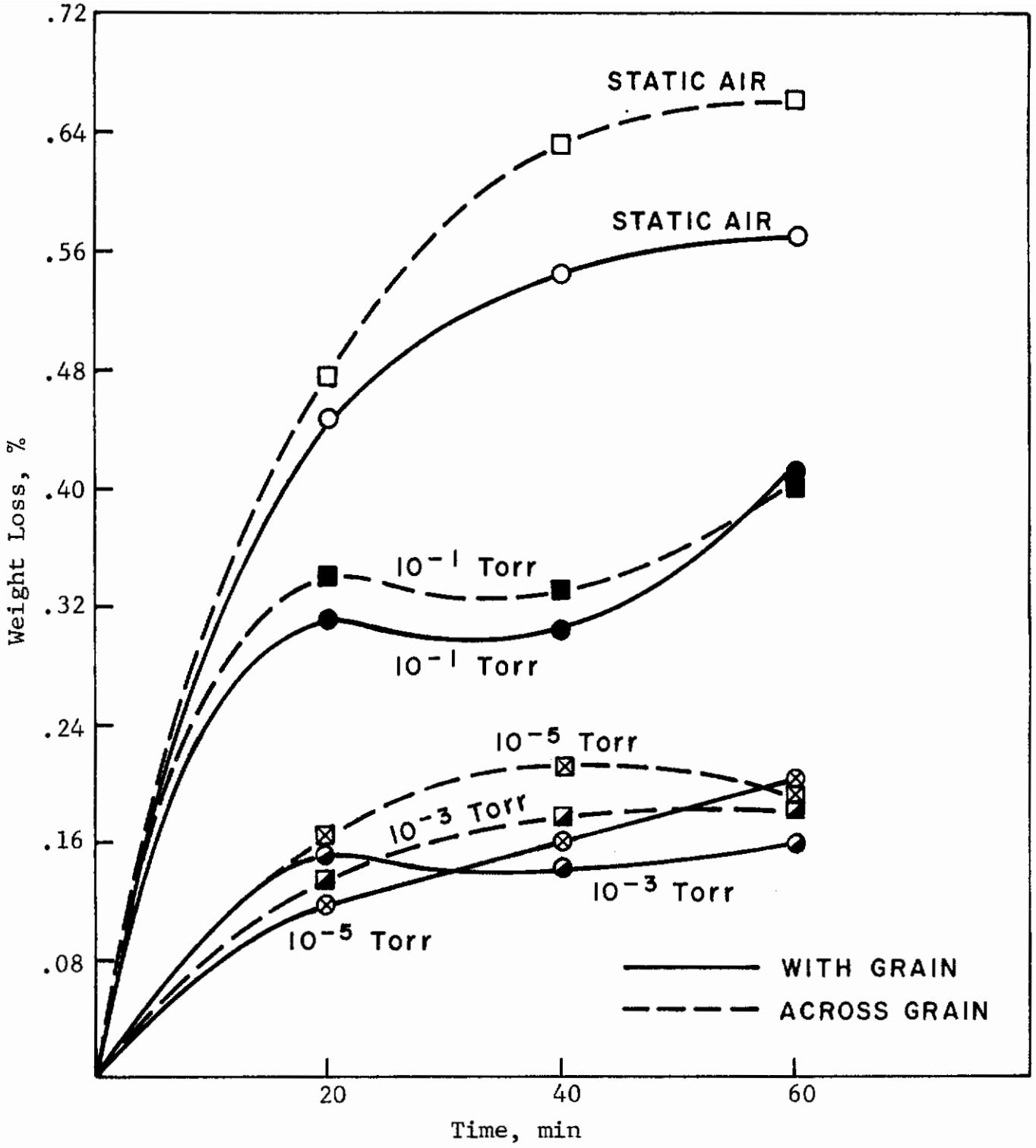

Figure 32. WEIGHT LOSS OF JTA GRAPHITE AT 3100°F, IN AN AIR ATMOSPHERE

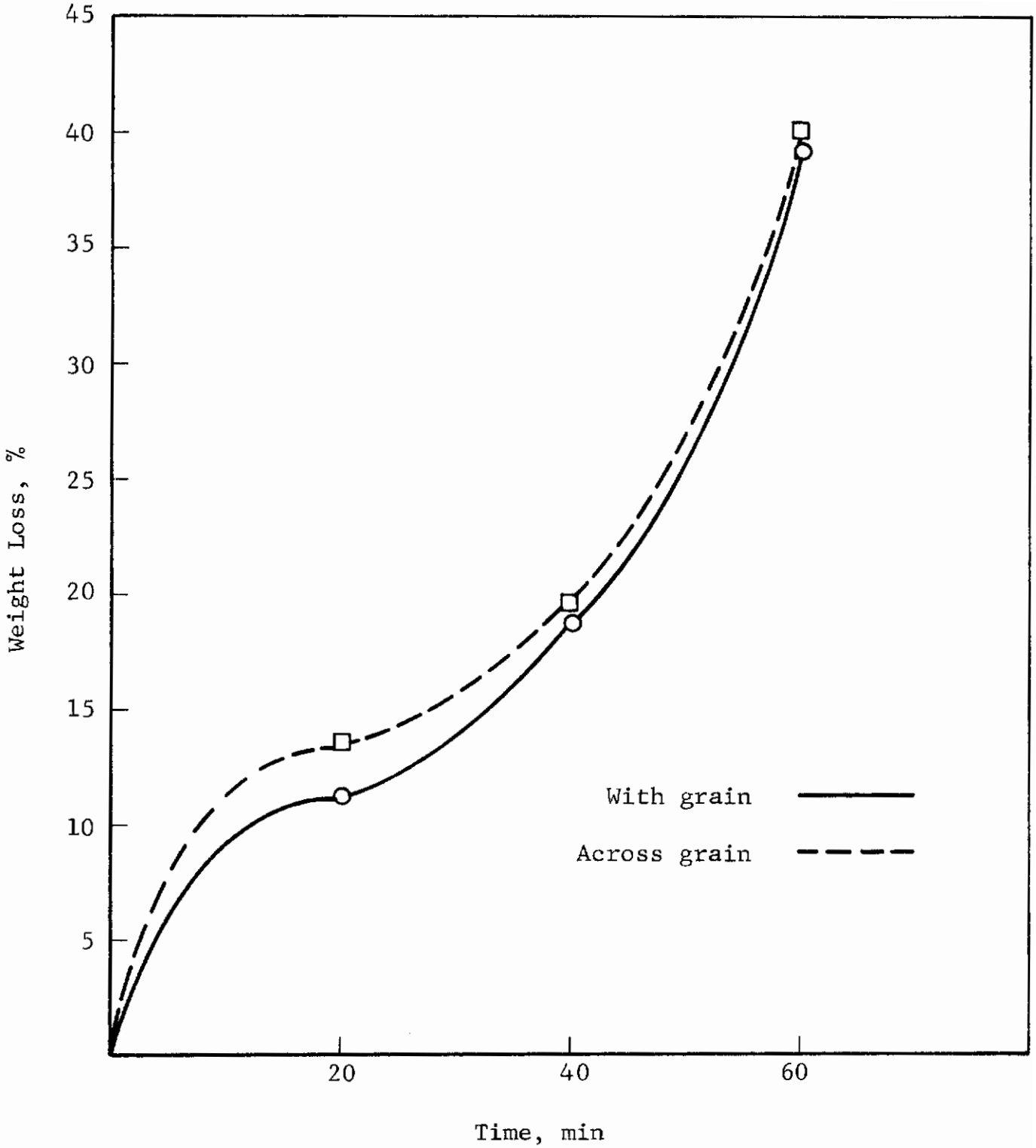

Figure 33. WEIGHT LOSS OF JTA GRAPHITE AT 3600°F IN STATIC AIR

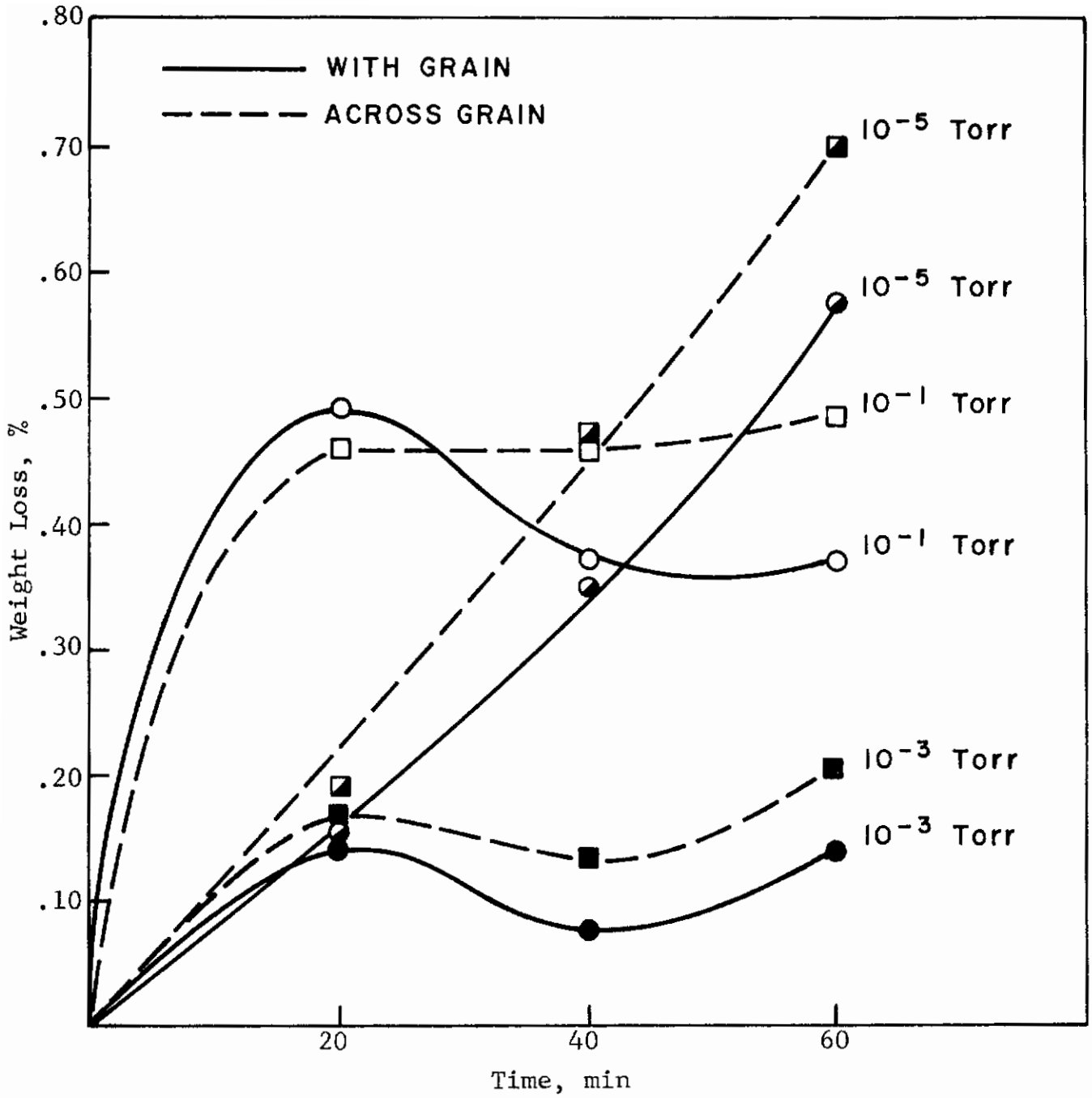

Figure 34. WEIGHT LOSS OF JTA GRAPHITE AT 3600°F, IN AN AIR ATMOSPHERE

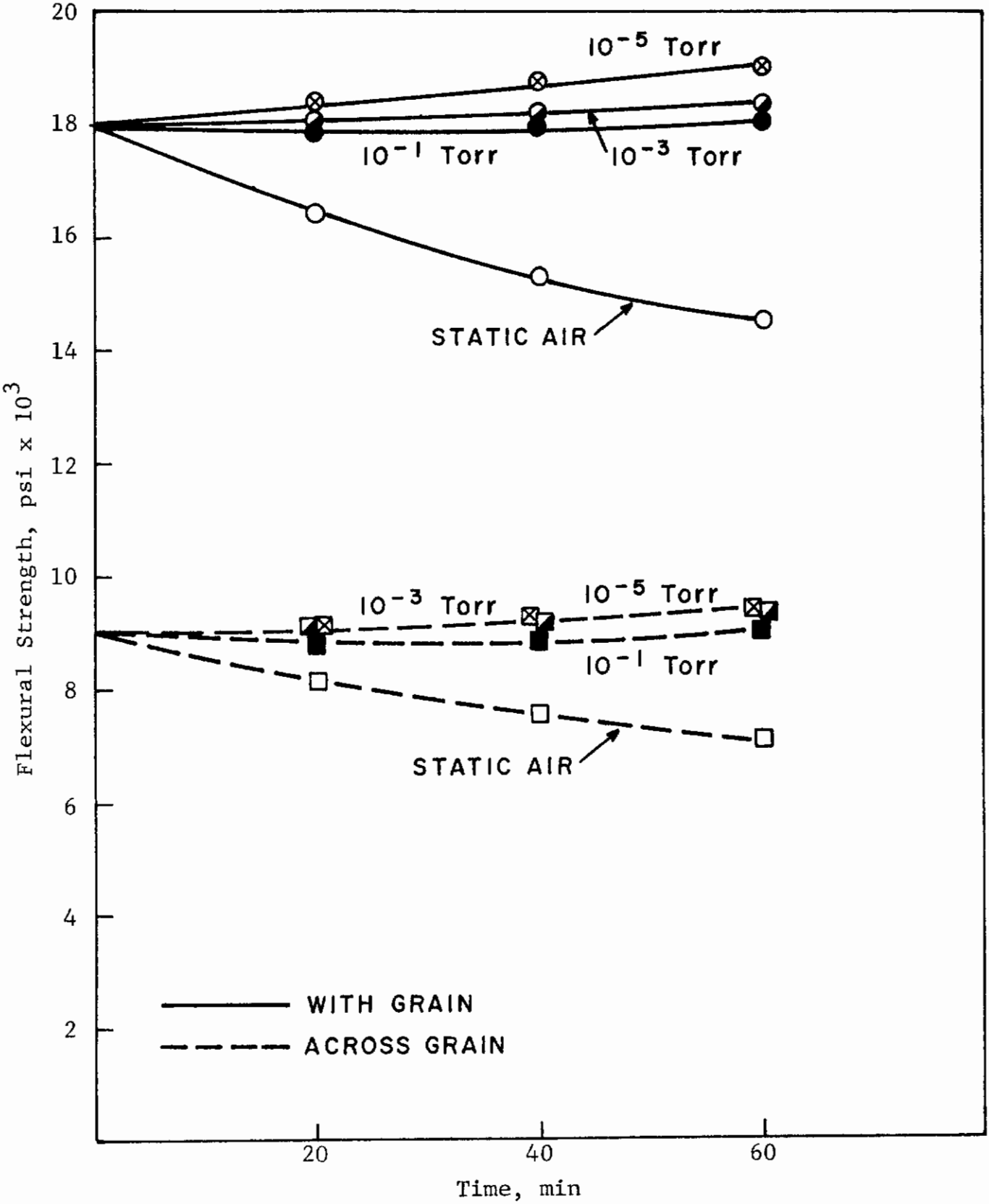

Figure 35. STRENGTH OF JTA GRAPHITE AT 1800°F, IN AN AIR ATMOSPHERE

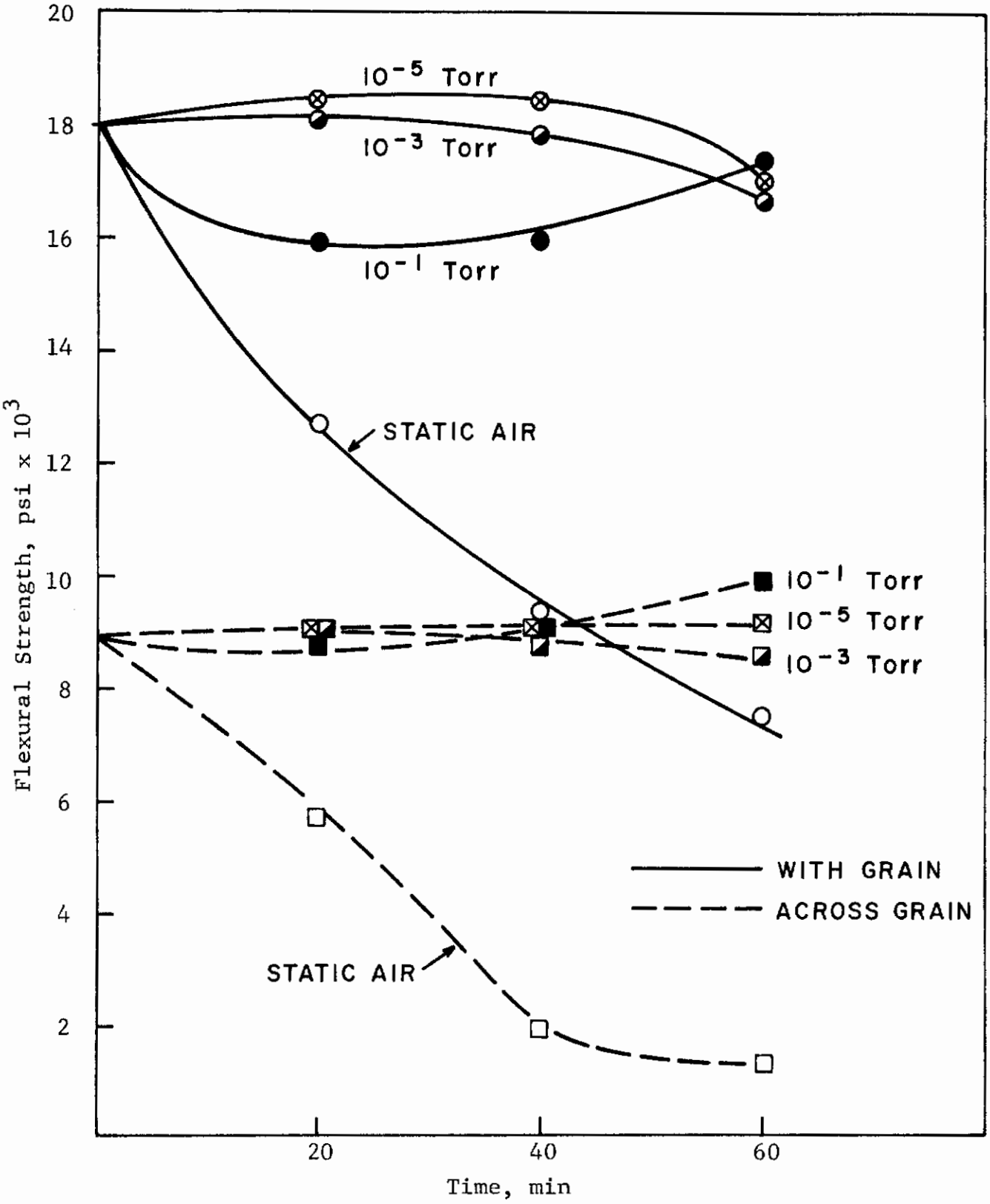

Figure 36. STRENGTH OF JTA GRAPHITE AT 3100°F, IN AN AIR ATMOSPHERE

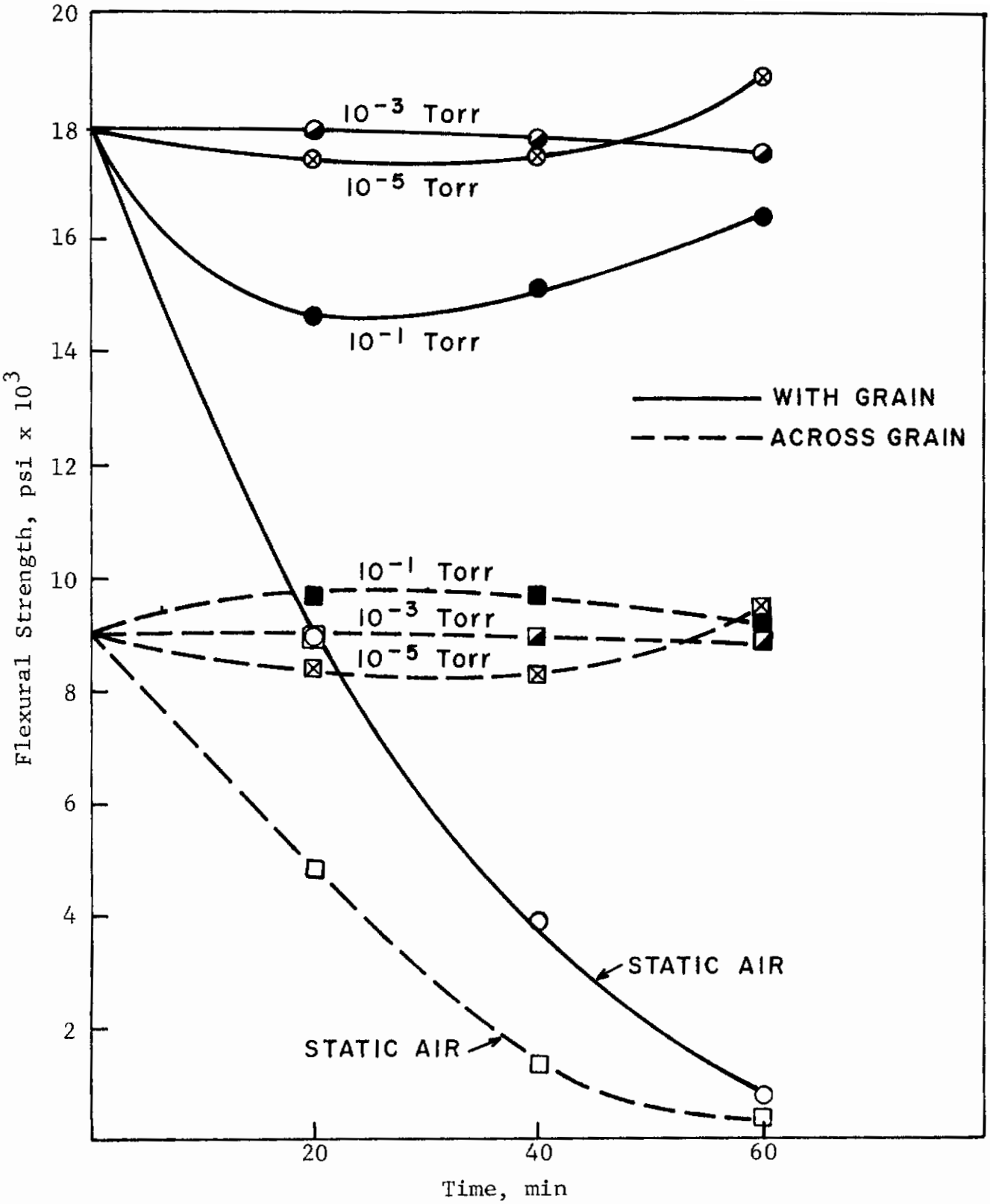

Figure 37. STRENGTH OF JTA GRAPHITE AT 3600°F, IN AN AIR ATMOSPHERE

The data indicate that effective oxidation resistance begins to occur between 1832°F and 2732°F. The coating becomes visible but less effective between 2732°F and 3182°F, and at 3632°F diffusion is so rapid that the coating protection is not effective. At pressures lower than 10^{-1} torr, oxidation protection is effective at all temperatures as high as 3632°F.

While the weight-loss experiments verified the metallographic studies, metallography appears to be the most effective means of studying oxidation resistance of this type of material. The findings show that JTA graphite is sensitive to partial oxygen pressure and temperature. Resistance to oxidation is greatest at 2732°F under ambient conditions and at pressures lower than 10^{-1} torr.

SECTION IV

MECHANICAL PROPERTIES

The use of JTA graphite requires a complete knowledge of its properties and an understanding of its behavior. Therefore mechanical-property data were obtained at ambient temperatures in an ambient environment, at several elevated temperatures in an oxidizing atmosphere at various pressures, and at the same elevated temperatures in an inert-gas atmosphere.

The number of specimens observed was sufficient for obtaining an accurate average strength for the various properties measured. A statistical evaluation was performed to obtain the distribution parameters, which, in turn, can be used in scaling laws(9) and in determining safe working loads. Twenty to fifty tests were made for each grain orientation.

1. SIZE

To establish the minimal specimen dimensions that would not adversely effect the test results, a size-effect study was performed prior to the overall evaluation program. These experiments were performed by using flexural data obtained at room temperature. Table VIII lists the specimen sizes and numbers involved in this study. The effect of friction on the test results was eliminated through the use of rollers. The specimens had a square cross section and were loaded with four-point flexure at the third point. The distance between the supports was maintained at a 10:1 ratio with regard to the depth of the beam. Six of the 1/2-in.-cross-section beams from each of the billets (7-F-12, 7-F-14, and 14-G-1) were instrumented with SR-4 electrical strain gages so that both longitudinal and lateral strains could be measured in the constant-moment gage section under both compressive and tensile loads. For each set evaluated, three beams from each billet were tested in the with-grain orientation and three tested in the across-grain orientation. Young's elastic modulus and Poisson's ratio were calculated from this information.

Tables IX through XI and Figure 38 summarize the results. There was an apparent increase in strength with a decrease in cross section for all specimens except the 1/16- x 1/16- x 10-in. specimens, which exhibited about the same strength or a loss in strength. Since the average graphite grain is about 120 ± 30 μ (0.00485 in.) long and 70 ± 15 μ (0.027 in.) wide, the 1/16- (0.0625-) in.-cross-section grain is approximately 13 times larger than the average grain. These experiments apparently verify the rule-of-thumb relationship that the depth of the beam must be greater than ten times the largest dimension of the average grain in the cross section. Since the grain dimensions are average, the large variability exhibited by the across-grain 1/16-in.-cross-section

Table VIII. JTA GRAPHITE SPECIMENS
USED FOR DETERMINATION OF SIZE EFFECT
BY FLEXURAL TESTING AT ROOM TEMPERATURE

Billet no.	Specimen length, in.	Cross-sectional dimensions, in.	Number of specimens Orientation With grain	Across grain
7-F-12	1	1/16 x 1/16	10	10
	3	1/4 x 1/4	10	10
	6	1/2 x 1/2	10	10
7-F-14	1	1/16 x 1/16	10	10
	3	1/4 x 1/4	10	10
	6	1/2 x 1/2	10	10
14-G-1	1	1/16 x 1/16	10	10
	3	1/4 x 1/4	10	10
	6	1/2 x 1/2	10	10

Table IX. EFFECT OF SIZE ON STRENGTH AND ELASTIC MODULUS OF BILLET 7-F-12

Property	Values for specimens: Cross-sectional dimensions, in. 6 x 1/2 x 1/2 With grain	6 x 1/2 x 1/2 Across grain	3 x 1/4 x 1/4 With grain	3 x 1/4 x 1/4 Across grain	1 x 1/16 x 1/16 With grain	1 x 1/16 x 1/16 Across grain
Avg. flexural strength, psi	14,820	8,640	17,320	9,370	23,220	7,580
Avg. tangent modulus, psi	9.4	4.2	13.0	4.0	7.2	4.6
Avg. sonic modulus, psi	14.6	10.5	17.1	6.8	5.1	5.25
Coef. of error, %						
Flexural strength	22.3	8.1	21.2	11.5	19.0	43.5
Tangent modulus	21.5	8.3	21.3	44.6	29.1	17.7
Sonic modulus	9.5	8.5	2.5	3.9	21.8	15.7

Table X. EFFECT OF SIZE ON STRENGTH AND ELASTIC MODULUS OF BILLET 7-F-14

Property	Values for specimens: Cross-sectional dimensions, in. 6 x 1/2 x 1/2 With grain	6 x 1/2 x 1/2 Across grain	3 x 1/4 x 1/4 With grain	3 x 1/4 x 1/4 Across grain	1 x 1/16 x 1/16 With grain	1 x 1/16 x 1/16 Across grain
Avg. flexural strength, psi	14,972	7,100	18,352	9,306	20,428	8,704
Avg. tangent modulus, psi	8.36	3.26	10.42	4.56	---	---
Avg. sonic modulus, psi	18.00	9.78	19.36	13.57	4.20	3.65
Coef. of error, %						
Flexural strength	9.89	7.91	6.73	3.88	7.49	16.29
Tangent modulus	10.10	10.61	11.13	10.09	---	---
Sonic modulus	5.94	5.62	1.86	3.54	9.29	3.56

Table XI. EFFECT OF SIZE ON STRENGTH AND ELASTIC MODULUS OF BILLET 14-G-1

Property	Values for specimens: Cross-sectional dimensions, in. 6 x 1/2 x 1/2 With grain	6 x 1/2 x 1/2 Across grain	3 x 1/4 x 1/4 With grain	3 x 1/4 x 1/4 Across grain	1 x 1/16 x 1/16 With grain	1 x 1/16 x 1/16 Across grain
Avg. flexural strength, psi	15,818	8,800	17,880	8,160	24,190	9,045
Avg. tangent modulus, psi	9.32	4.13	9.83	4.99	---	---
Avg. sonic modulus, psi	15.30	10.50	18.31	15.47	4.58	3.72
Coef. of error, %						
Flexural strength	15.99	5.32	13.23	2.92	11.58	22.54
Tangent modulus	14.37	8.92	13.22	10.62	---	---
Sonic modulus	9.67	7.00	4.15	3.04	10.26	7.80

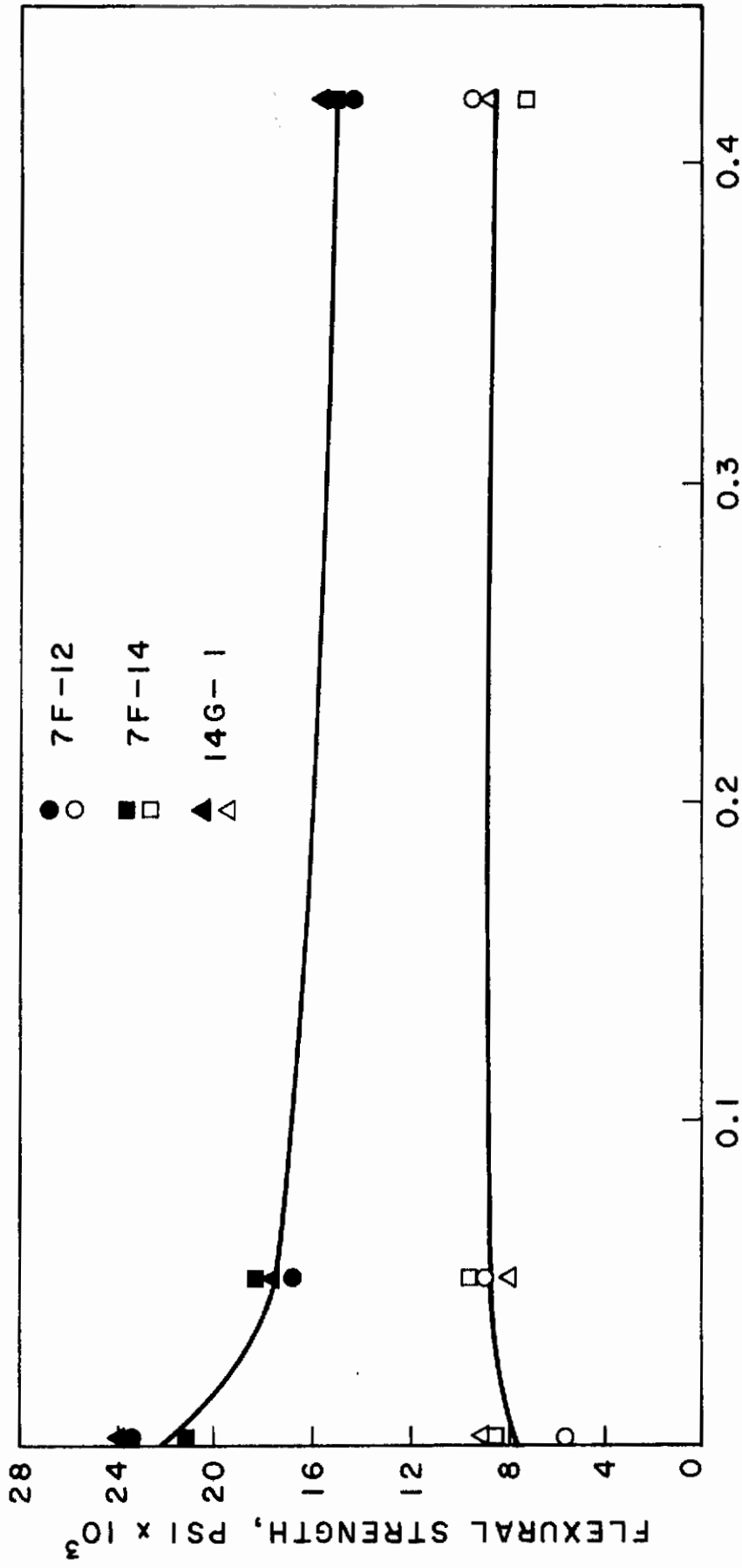

Figure 38. EFFECT OF SPECIMEN SIZE ON FLEXURE STRENGTH

specimens is easily explained. This series of experiments indicated that the smallest sample dimension of JTA graphite that would not adversely effect the results was 1/4 in.

One of the goals of this program was to study the variability of test data within and among the billets. Failure distributions for the 1/4-in.-cross-section flexural-strength data are shown in Figures 39 and 40. An analysis of variance showed that the strength data for the original three billets (7-F-12, 7-F-14 and 14-G-1) could be considered to have come from the same test population at the 95% confidence level. A similar analysis was made between the combined data and data obtained from flexural tests of billet 14-G-3 (Appendix III). Examination of the curves, however, revealed several factors of additional interest.

A rank sum test comparing the four sample populations revealed that while the with-grain orientation data could be considered to have come from the same material population, the across-grain populations were not the same. However, because of the narrow range of failure distribution shown by the across-grain population, it showed average strengths that were very nearly the same. Therefore test data for the three billets were considered as part of the same data population, and the strengths among the four billets were within the statistical variability of those within the billets. Table XII indicates the rationale behind this statement. The statistical error of the combined data was less than the percent error shown by billets 7-F-12 and 14-G-1 for the with-grain data and about the same as that for the across-grain data. The results of this analysis lead to the conclusion that the test specimens from all four billets could be randomly mixed to provide useful engineering data.

A similar study was made for specimens used for tensile testing. Tensile specimens having circular cross sections with diameters of 1/8-, 3/16-, and 1/4-in. were examined. Figure 41 is a plot of these data. The with-grain plot exhibits a certain amount of inconsistency, and the dotted line may be a better average plot of values than the solid curved line because of the small population (10 specimens) used. The conclusion is that a 1/4-in.-diameter cross section provides an accurate representation of the JTA graphite strength in tension as well as in flexure.

In addition to experimental data, strength differences due to volume (size) effects can be analytically investigated. The scaling technique(1) that assumes a single series material as a load-redistribution model (Figure 42) does not depend on a specific type of probability distribution or on the direct determination of any of the descriptive parameters of the distribution. It projects points from a probability curve obtained at one volume simply on the basis of the load-redistribution model. It is generally a conservative technique and gives greater reduction in strength for larger volumes than is usually found in real materials.

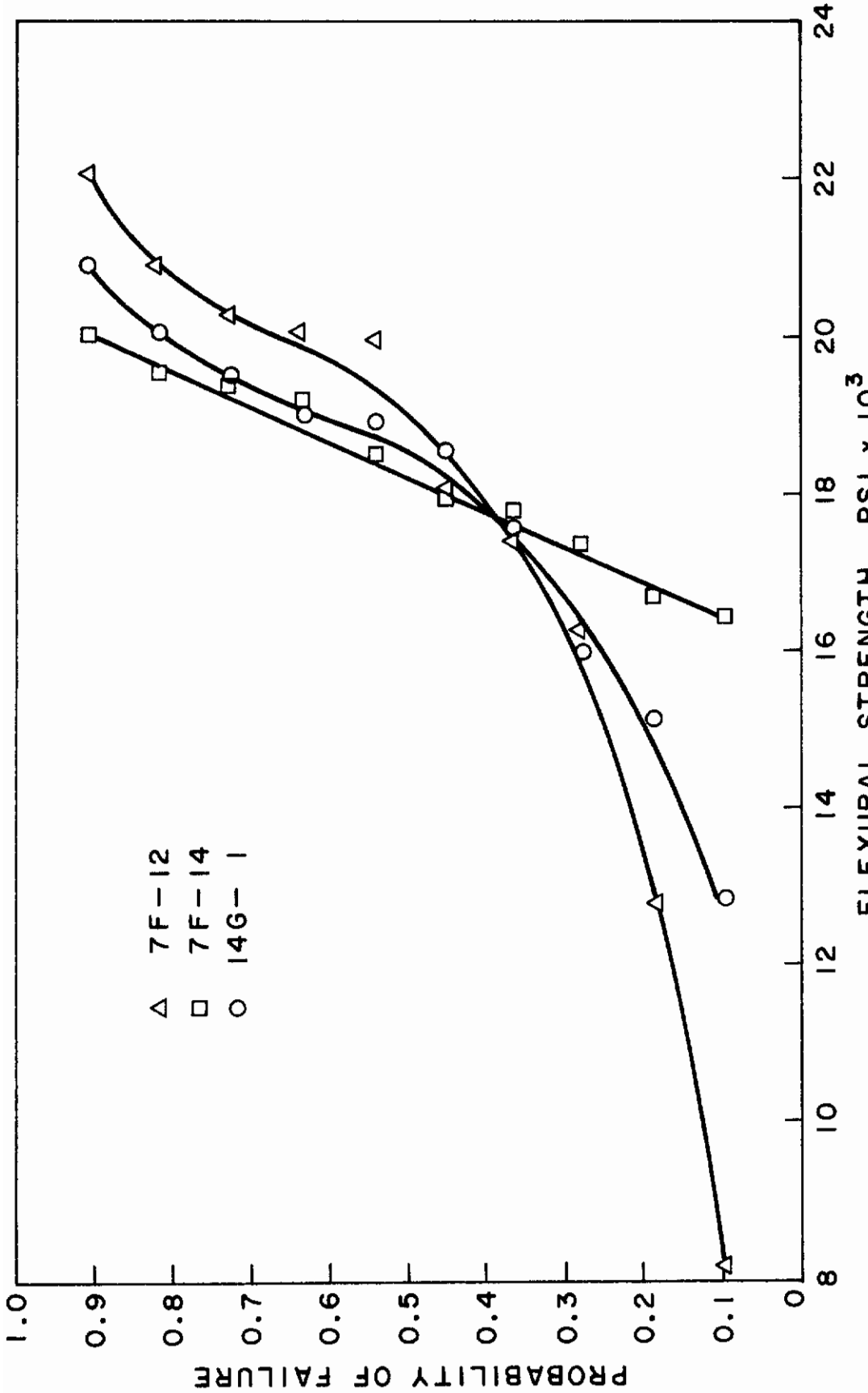

Figure 39. FLEXURAL-STRENGTH DISTRIBUTION OF WITH-GRAIN ORIENTATION

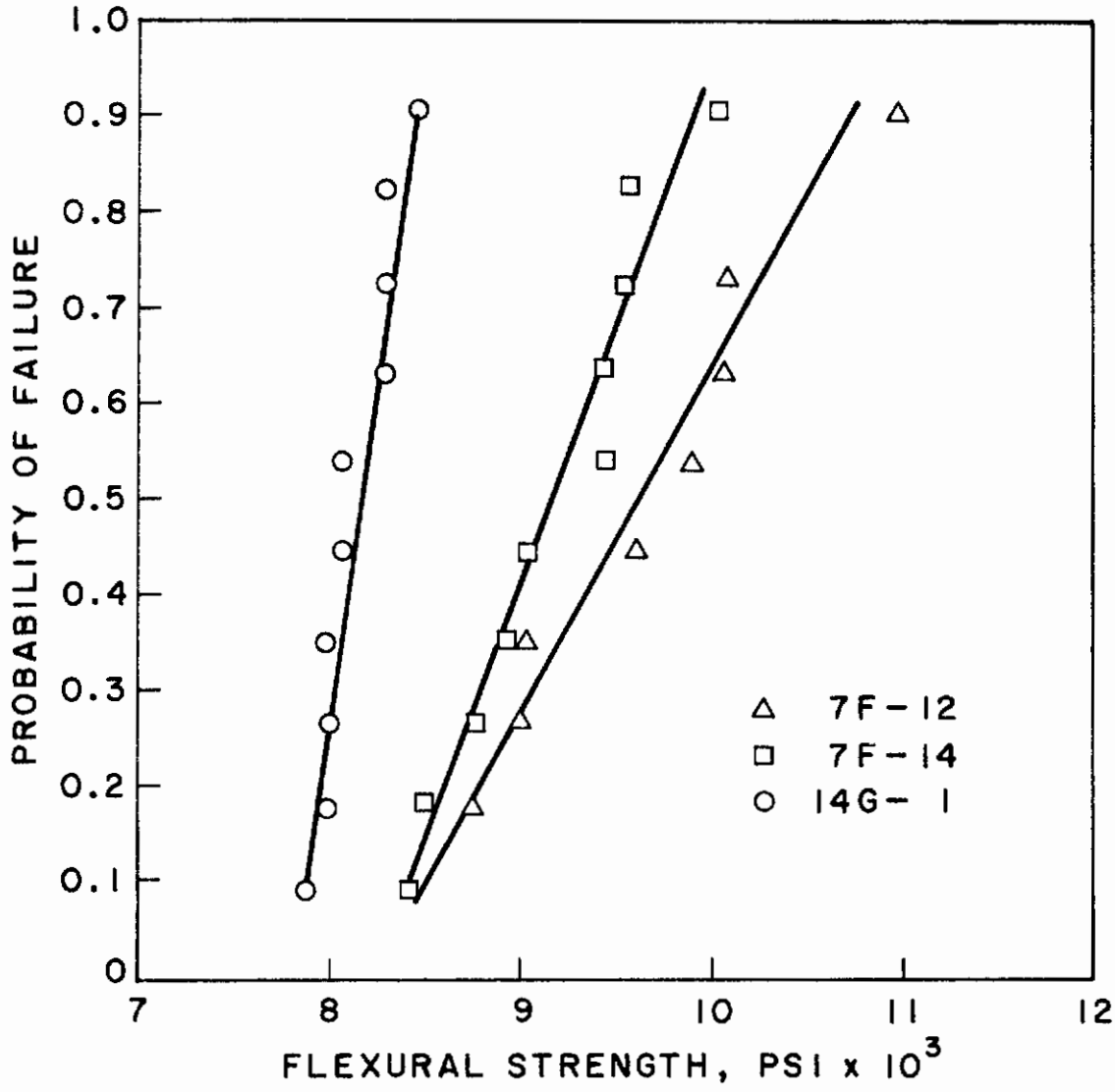

Figure 40. FLEXURAL-STRENGTH DISTRIBUTION OF ACROSS-GRAIN ORIENTATION

Table XII. COMBINED SPECIMEN SIZE-EFFECT DATA FOR BILLETS 7-F-12, 7-F-14, AND 14-G-1

Property	Values for specimens: Cross-sectional dimensions, in. 6 x 1/2 x 1/2 With grain	6 x 1/2 x 1/2 Across grain	3 x 1/4 x 1/4 With grain	3 x 1/4 x 1/4 Across grain	1 x 1/16 x 1/16 With grain	1 x 1/16 x 1/16 Across grain
Avg. flexural strength, psi	15,203	8,180	17,850	8,945	22,613	8,443
Avg. tangent modulus, psi	9.26	3.86	11.08	4.52	---	---
Avg. sonic modulus, psi	15.97	10.26	18.26	11.95	4.63	4.21
Coef. of error, %						
Flexural strength	14.37	11.77	14.87	9.73	15.59	29.18
Tangent modulus	16.63	14.22	21.14	26.06	---	---
Sonic modulus	12.52	7.89	5.46	30.79	17.71	21.31

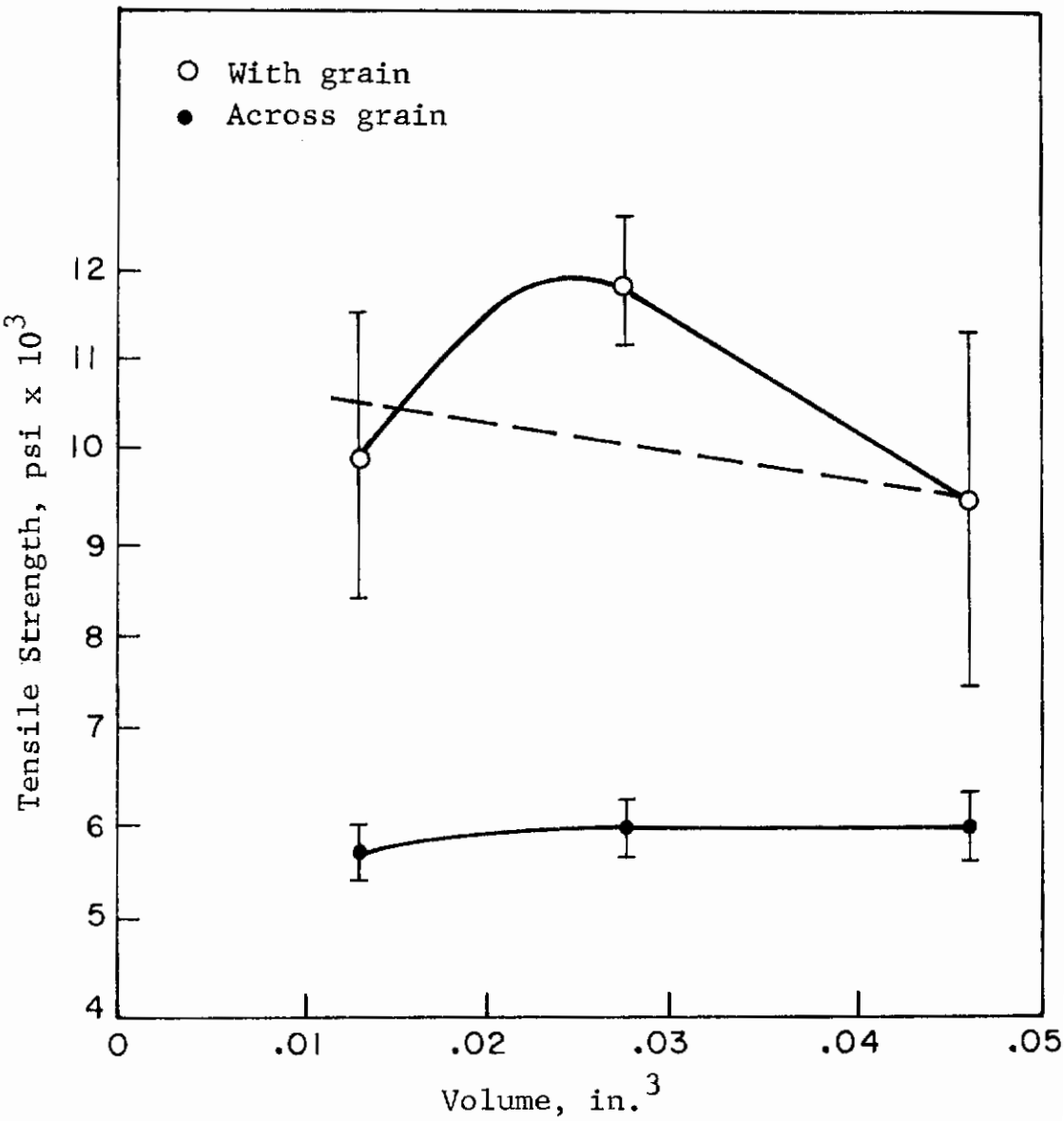

Figure 41. EFFECT OF SIZE ON TENSILE STRENGTH

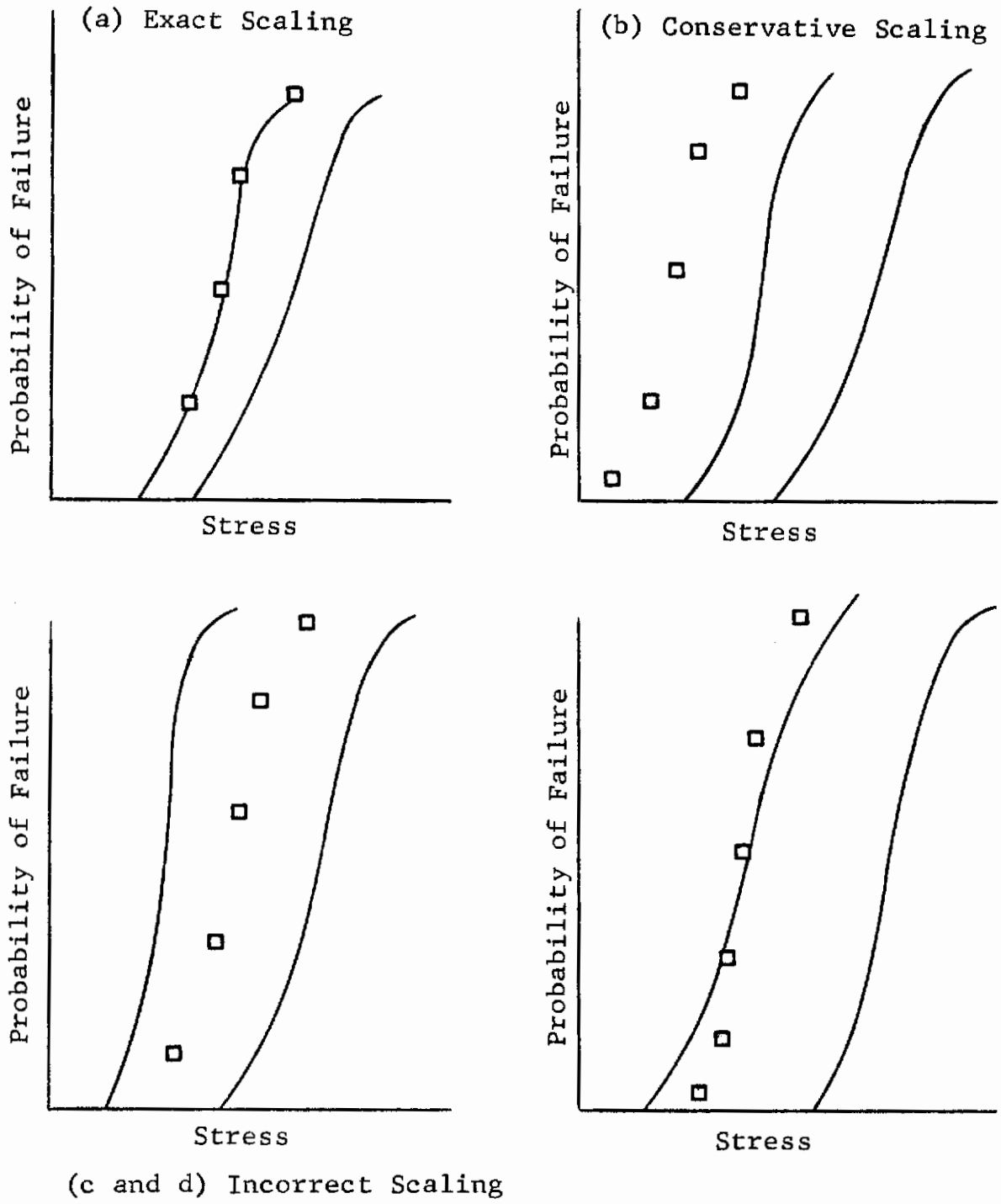

(c and d) Incorrect Scaling

Figure 42. POSSIBLE RESULTS OF MODEL SCALING
[Solid lines represent experimental distribution curves. Squares are points from the curve for a small volume sample (right solid line) scaled to the larger volume (left solid line).]

It should provide accurate predictions for a material that approaches a true series material. The scaling relationship is given by:

$$1 - F_{\sigma_2} = \left(1 - F_{\sigma_1}\right)^{V_2/V_1} \tag{6}$$

where

F_{σ} is the probability of failure at some stress (σ)
V_1 and V_2 are the gage volumes.

A second method of analysis is the Weibull[1] equation:

$$\frac{\sigma_1}{\sigma_2} = \left(\frac{V_2}{V_1}\right)^{1/m} \tag{7}$$

where

m is the flaw density of the material
σ is stress
V is volume.

For this phase of the analysis, m can be calculated by using an approximation theory[1]:

$$m = \frac{1.2}{Z} \tag{8}$$

where Z is the coefficient of variation of the test series.

Figures 43 and 44 exhibit distribution curves for the 1/4- x 1/4- x 3-in. and the 1/2- x 1/2- x 6-in. test specimens and the predicted distribution curve obtained by using the scaling laws. Scaling the with-grain data indicated that techniques will produce conservative values for design use. Scaling the across-grain data, however, revealed a peculiar relationship between the scaled and the actual data. The predicted failure distribution crossed the actual distribution curve at the 25% probability-of-failure level; therefore the scaling law did not predict a conservative failure-distribution curve. This phenomenon may be due to the deterministic behavior of the across-grain material. This behavior is discussed further in Section IV4.

A Weibull analysis predicted that the 1/2- x 1/2- x 6-in. specimens will have an average strength of 12,300 psi for the with-grain orientation. The scaling law predicted 13,800 psi and 15,203 psi was actually measured. The predicted across-grain average strength was 7800 psi, as compared with 7520 psi predicted by the scaling law and 8180 psi actually measured.

For a failure distribution having a large coefficient of error the Weibull analysis is more conservative than the scaling

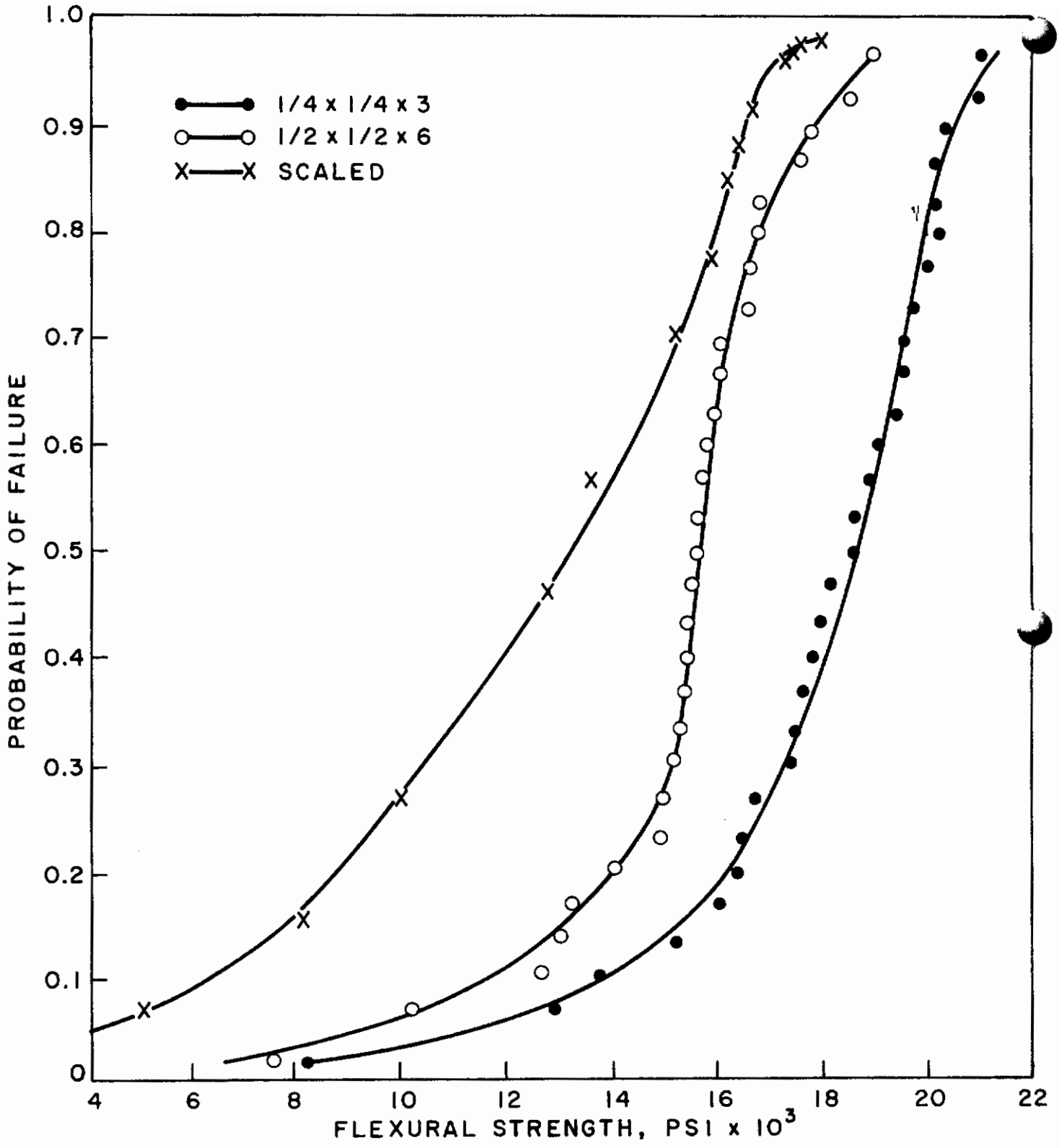

Figure 43. COMBINED FLEXURAL STRENGTH DISTRIBUTION CURVE
(With grain)

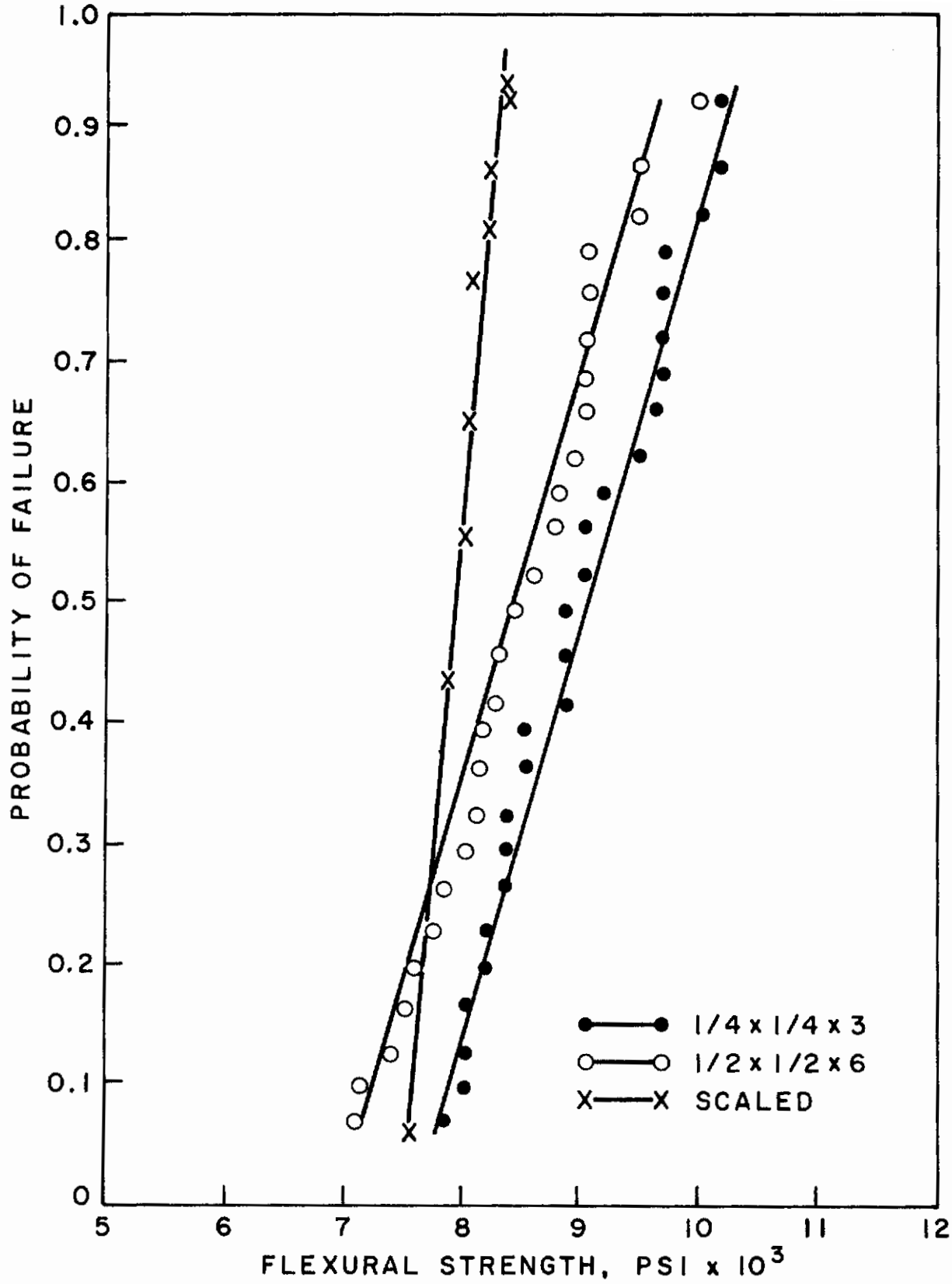

Figure 44. COMBINED FLEXURAL STRENGTH DISTRIBUTION CURVE (Across grain)

law for the with-grain distribution. The reverse situation is true for the across-grain orientation, for which the variability is much less. Therefore the analysis appeared to show that for materials having large variances, a Weibull analysis provides a more conservative scaling method than the probability scaling law. The reverse appears to be true for materials having coefficients of error of less than 10.

2. STRAIN RATE

A series of tensile strain-rate experiments with JTA graphite was performed. The purpose of this investigation was to determine whether this material shows large strength changes with strain changes of several orders of magnitude. The experiments were performed with crosshead rates of 0.02, 0.2, 2.0 and 20.0 in./min. A standard tensile specimen having a 1/4-in.-diameter circular cross section was used for these experiments. The tests were conducted on a 20,000-lb Instron Universal testing machine. Five specimens were tested at each strain rate. The data, shown in Figure 45, indicate that there were no strain-rate effects at room temperature.

No experiments were run at elevated temperatures. However, strain-rate effects can be expected to occur at the temperatures at which JTA graphite shows evidence of creep under load.

3. TENSION

Tensile strength was measured by using a direct uniaxial test[1] under ambient conditions and a uniaxial tensile test at elevated temperatures. Specimens had a 1/4-in.-diameter circular gage section. A collet grip (Figure 46) was used to hold the test specimens. The grip consists of a split ring machined on the inside to fit the transition radius of the test specimen and on the outside to a spherical surface. The split ring is held together by a circular spring. The split ring fits into grip holders whose inside surface is machined to mate with the spherical surface of the split ring. The grip holder fits into the load train of the test machine. Graphite grips were used for all ambient- and inert-atmosphere tests. Water-cooled stainless steel grips were used for the elevated-temperature oxidation tests. Typical fractures are shown in Figure 47.

In the burst test, a ring-shaped specimen (Figure 48) is subjected to hydrostatic pressure acting radially through an inner rubber bulb and causing a tangential tensile stress in the specimen wall. The maximal tensile-stress accuracy on the inside surface ($\sigma_{t_{max}}$) is calculated from:

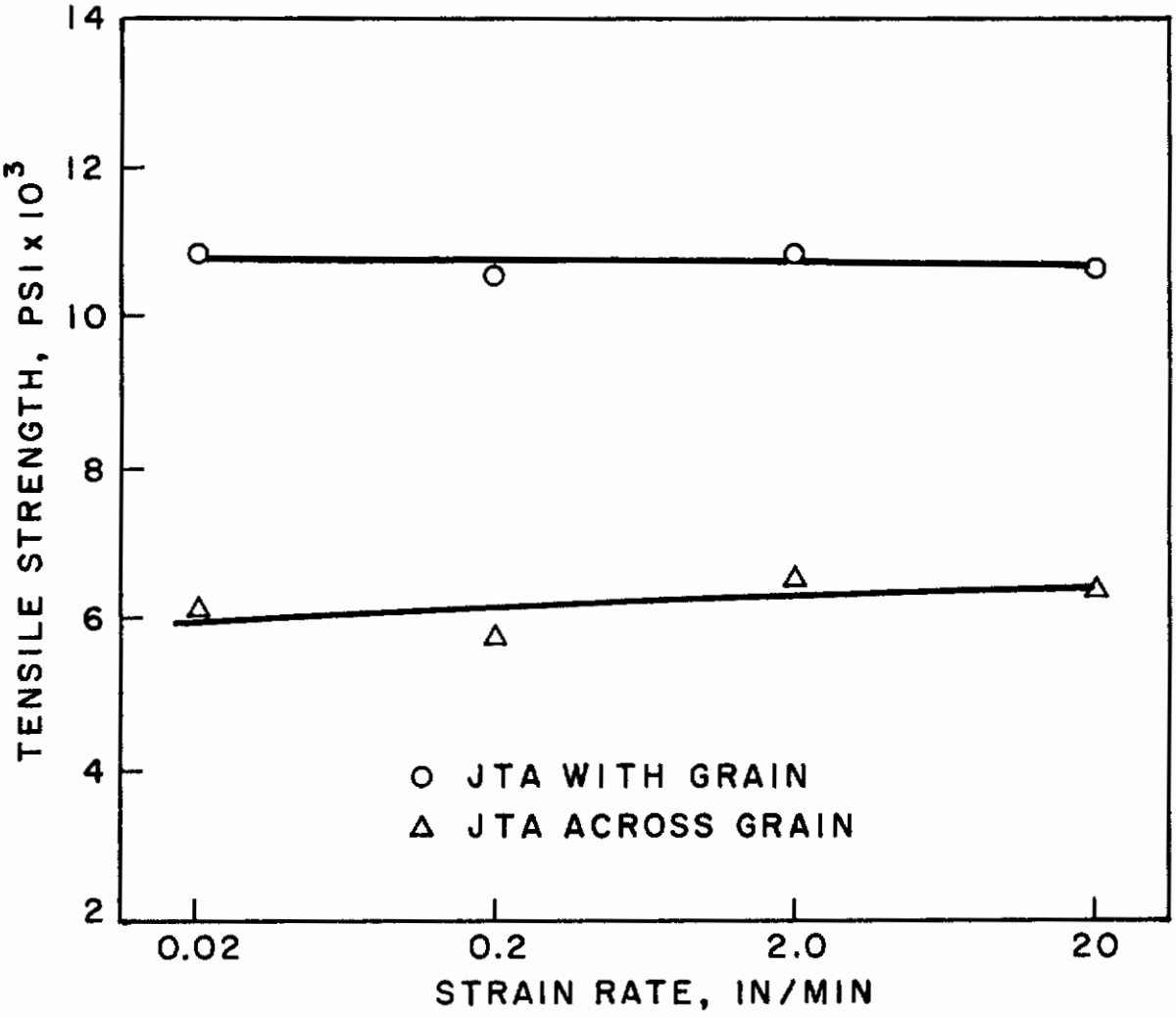

Figure 45. STRAIN RATE EFFECT ON TENSILE STRENGTH OF JTA GRAPHITE

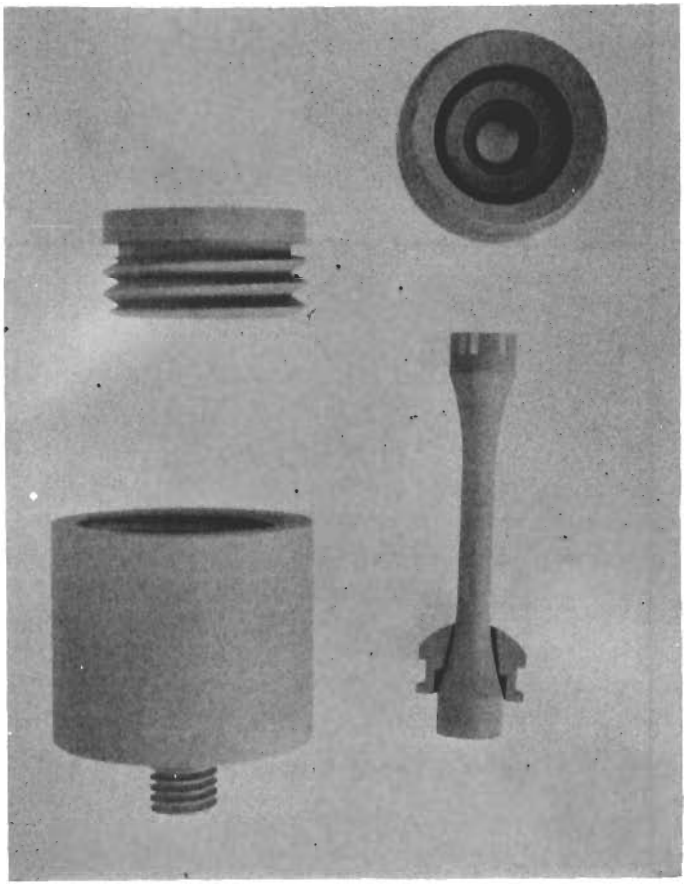

Figure 46. TENSILE GRIPS DEVELOPED AT IITRI AND USED WITH COLLET SAMPLES

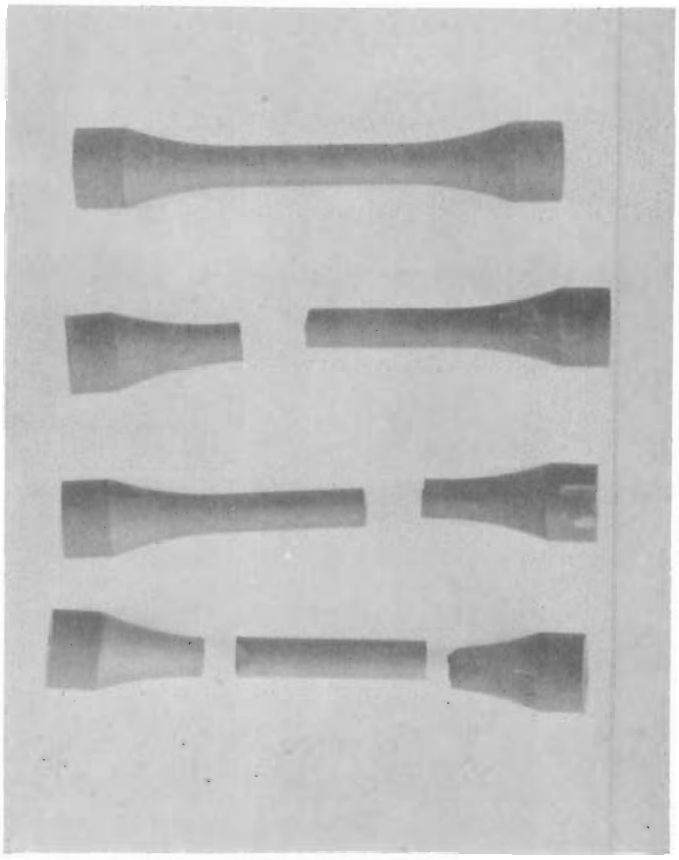

Figure 47. DUMBBELL TENSILE SPECIMEN
WITH AND WITHOUT TYPICAL FRACTURES

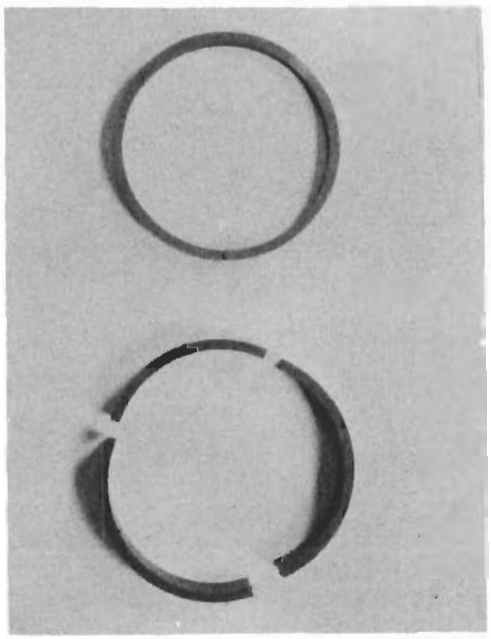

Figure 48. BURST TEST FAILURES
TOP: TEST RUN AT STANFORD RESEARCH INSTITUTE
BOTTOM: TEST RUN AT IITRI

$$\sigma_{t_{max}} = \frac{Pr_1^2}{r_0^2 - r_1^2} \left(1 = \frac{r_0^2}{r_1^2}\right) \quad (9)$$

where

P is the hydrostatic pressure (psi)
r_1 is the inside radius (in.)
r_0 is the outside radius (in.).

The test apparatus is shown in Figure 49.

The test procedure consists of seating the rubber bulb and placing the test specimen in a position concentric with the rubber bulb. Spacer blocks, 1 to 2 mils higher than the test specimen holder, are placed around it, and the upper plate of the specimen holder is lowered into place. The entire assembly is clamped together so that the hydrostatic pressure does not alter the spacing of the specimen-holder plates. The hydrostatic pressure as a function of time is recorded on a strip chart. During testing the holder must be free of compressive constraint and the distance between the holder plates must remain constant.

a. Ambient-Environment Tests

The results obtained from the ambient-environment tests are listed in Table XIII. The strength data obtained by the two test procedures exhibited close agreement. The effect of a small population size can be noted by observing the differences between the estimated m values. The large populations showed relatively close correlation between estimated and graphically determined m factors; while the small populations exhibited a difference in variability, which made a true comparison difficult. The distribution curves and the Weibull plots are shown in Figures 50 through 55. The variability of the test data appeared to be within the limits observed for other graphitic materials in tension[10,11]. The room-temperature tensile data appeared to be consistent enough to use the appropriate scaling laws by allowing for statistical safety factors. Therefore if three standard deviations are assumed to produce a reasonable safety factor and the conservative scaling laws are applied, a reasonable design allowable for JTA graphite for a specific design problem is produced.

b. High-Temperature Inert-Atmosphere Tests

Studies were conducted to determine whether samples tested in vacuum produce results different from those tested in an argon atmosphere. Test data showed no observable differences in strength. High-temperature tensile tests were made in vacuum by using a Brew furnace having a mechanical extensometer attachment (Figure 56). Strain elongation is transferred to a differential transformer

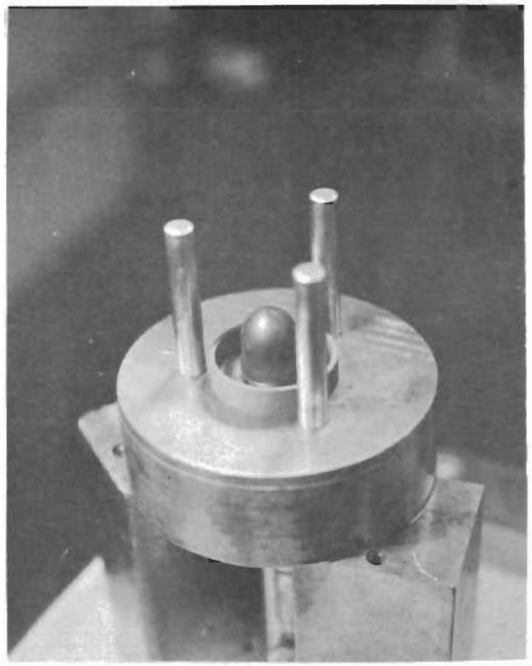

a) Detail of Burst Test Fixture

b) Apparatus in Tinius-Olsen Machine

Figure 49. INTERNAL PRESSURE BURST TEST

Table XIII. RESULTS OF TENSILE TESTS UNDER AMBIENT CONDITIONS

Orientation	Type of test	Number of tests	Avg. stress, $(\bar{\sigma})$, psi	Coef. of variation (ν), %	Flaw density (m), g/cc	
					Est.	Calc.
With grain	Uniaxial	30	12,140	9.398	12.75	11.0
	Burst	9	12,620	3.734	32	
Across grain	Uniaxial	30	6,300	6.708	17.90	15.0
	Burst	13	6,270	8.044	14	

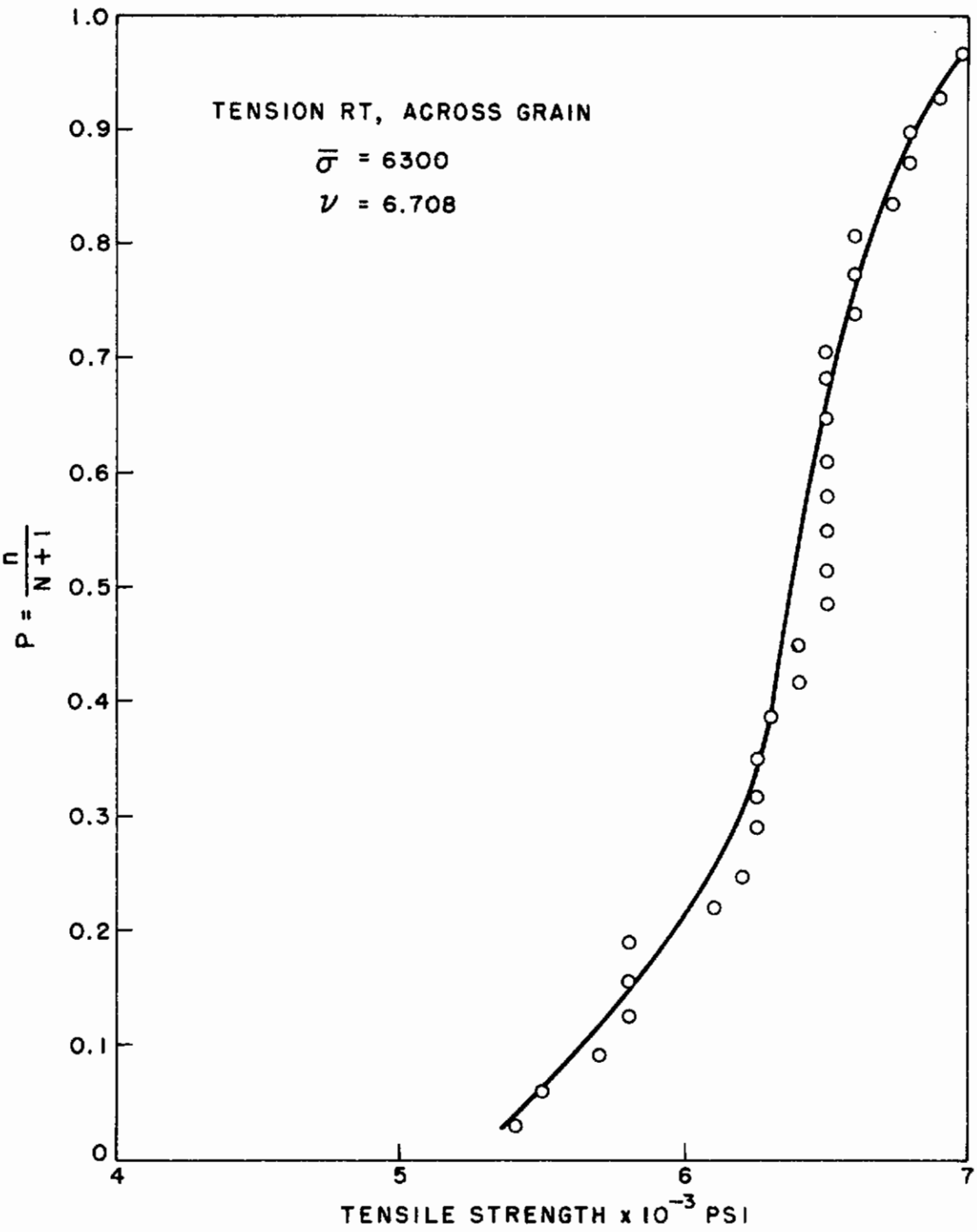

Figure 50. DISTRIBUTION CURVE FOR ROOM TEMPERATURE ACROSS GRAIN TENSION TESTS

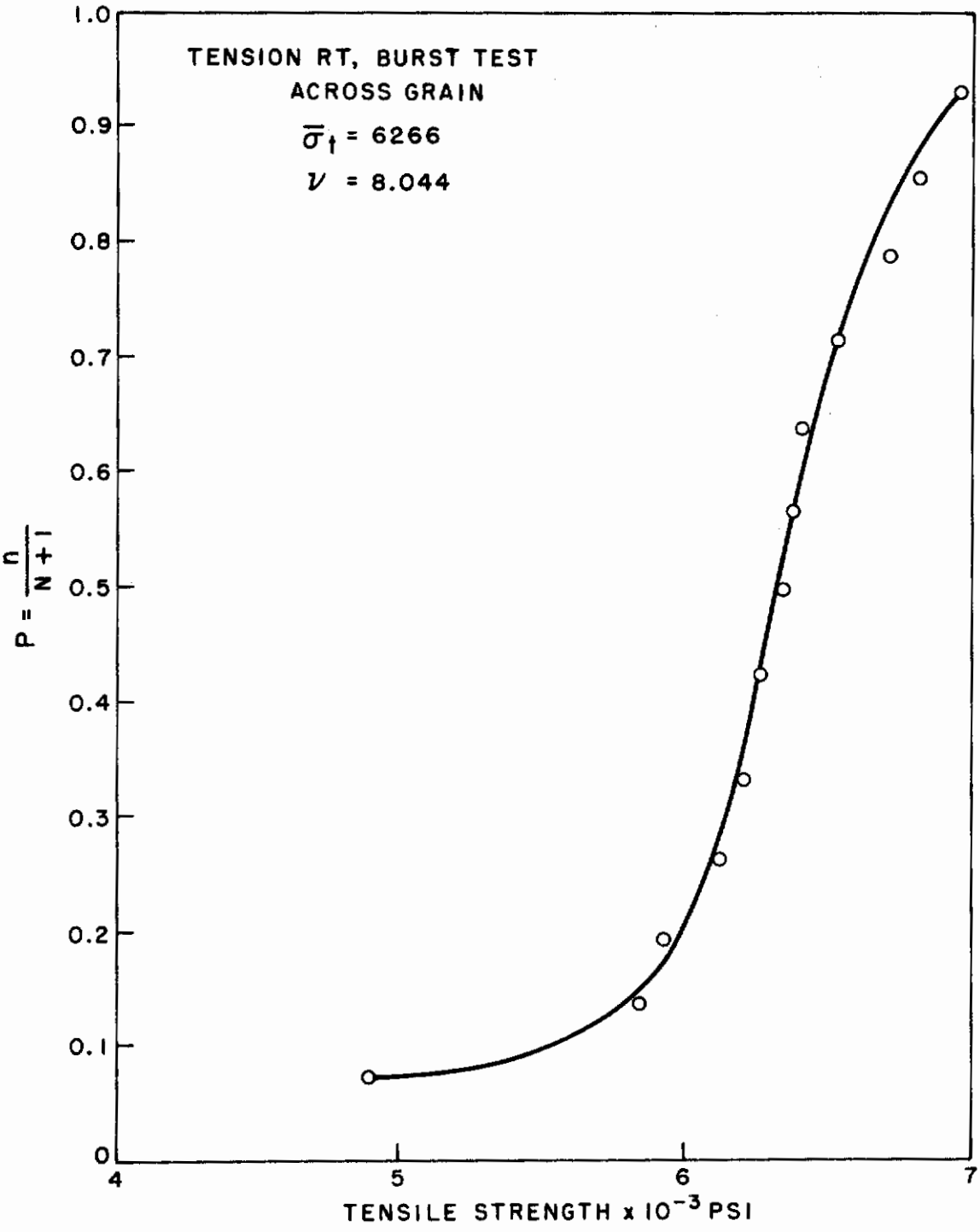

Figure 51. DISTRIBUTION CURVE FOR ROOM TEMPERATURE ACROSS GRAIN BURST TENSION TESTS

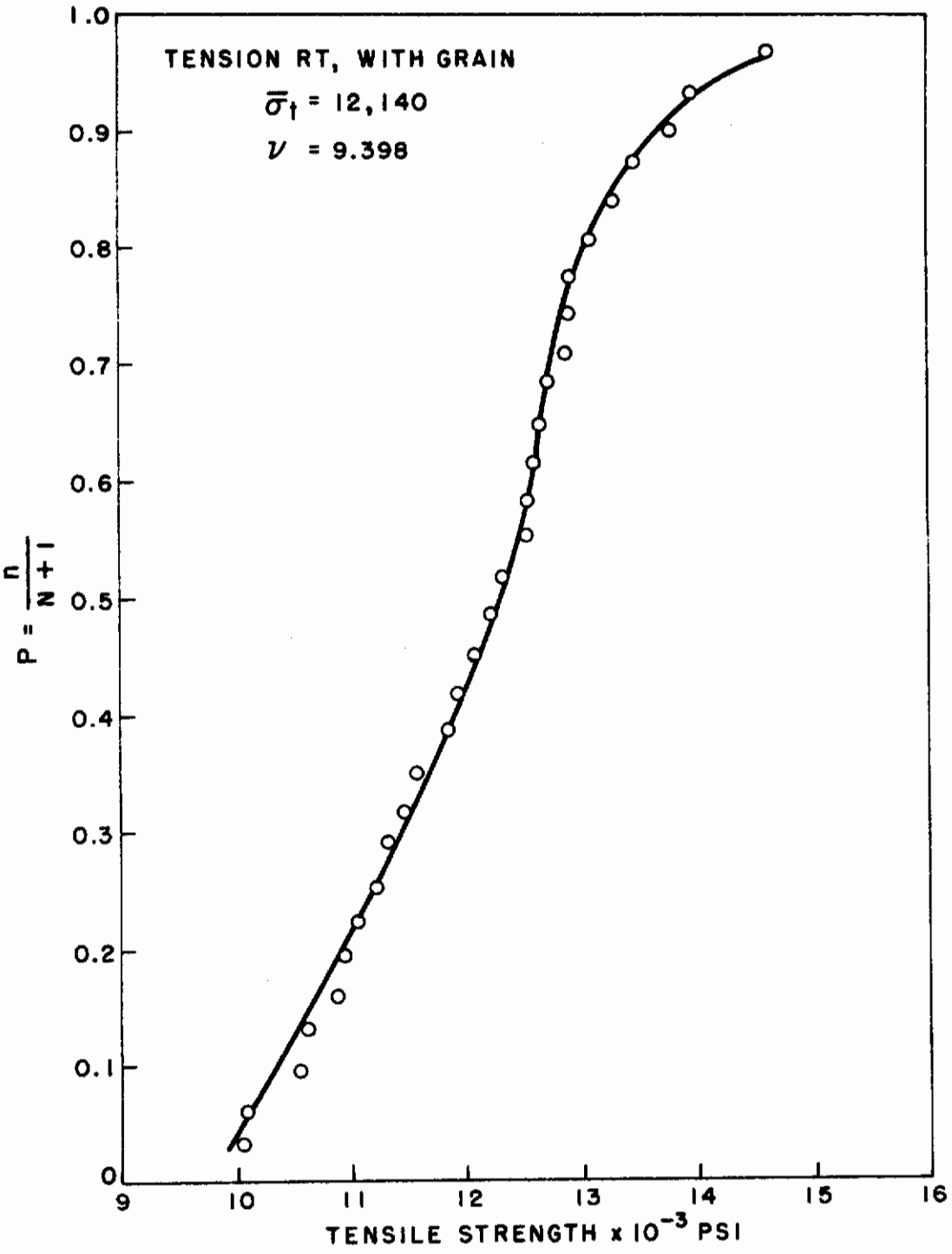

Figure 52. DISTRIBUTION CURVE FOR ROOM TEMPERATURE WITH GRAIN TENSION TESTS

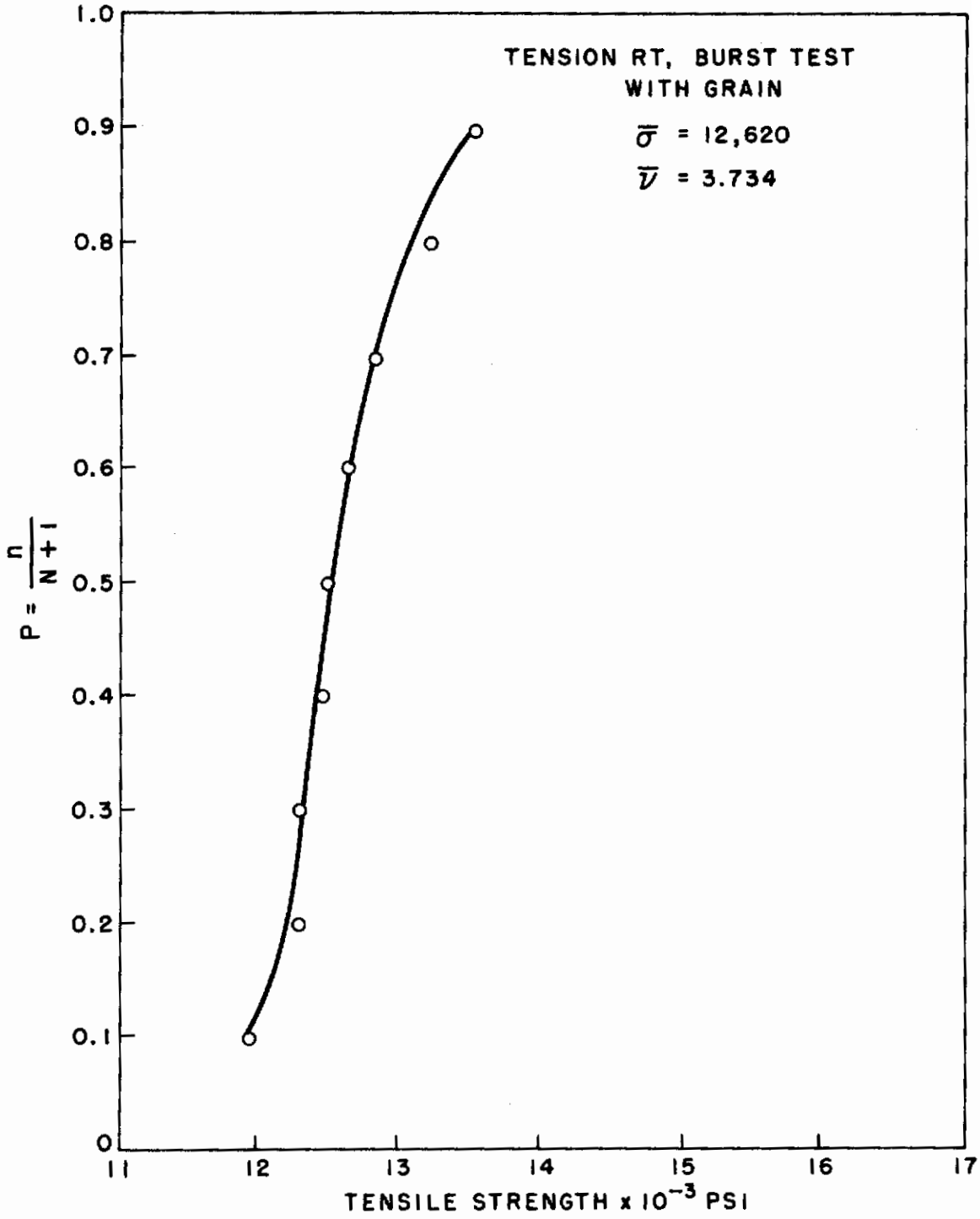

Figure 53. DISTRIBUTION CURVE FOR ROOM TEMPERATURE WITH GRAIN BURST TENSION TESTS

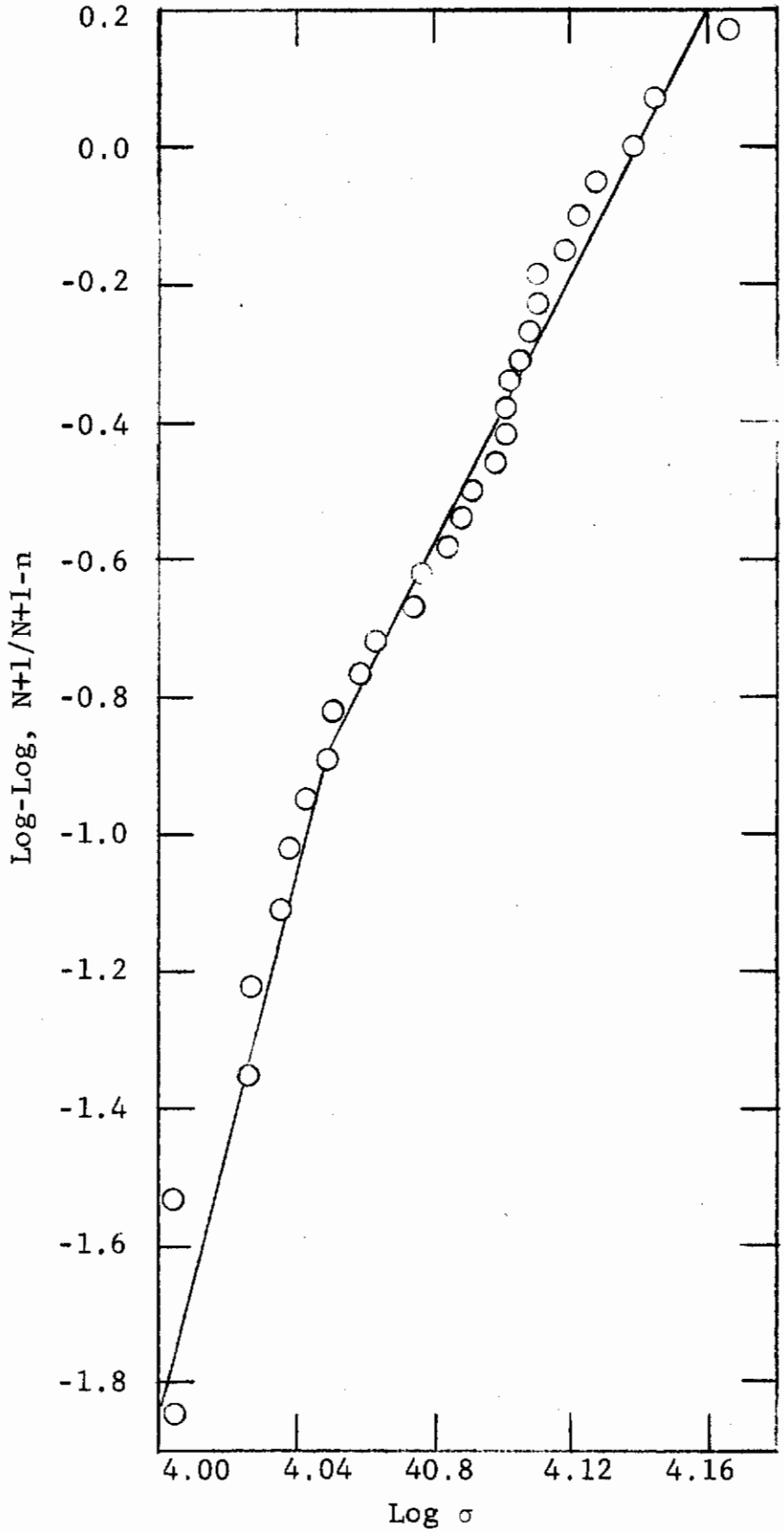

Figure 54. WEIBULL PLOT FOR JTA TESTED IN TENSION (With grain, 77°F, air)

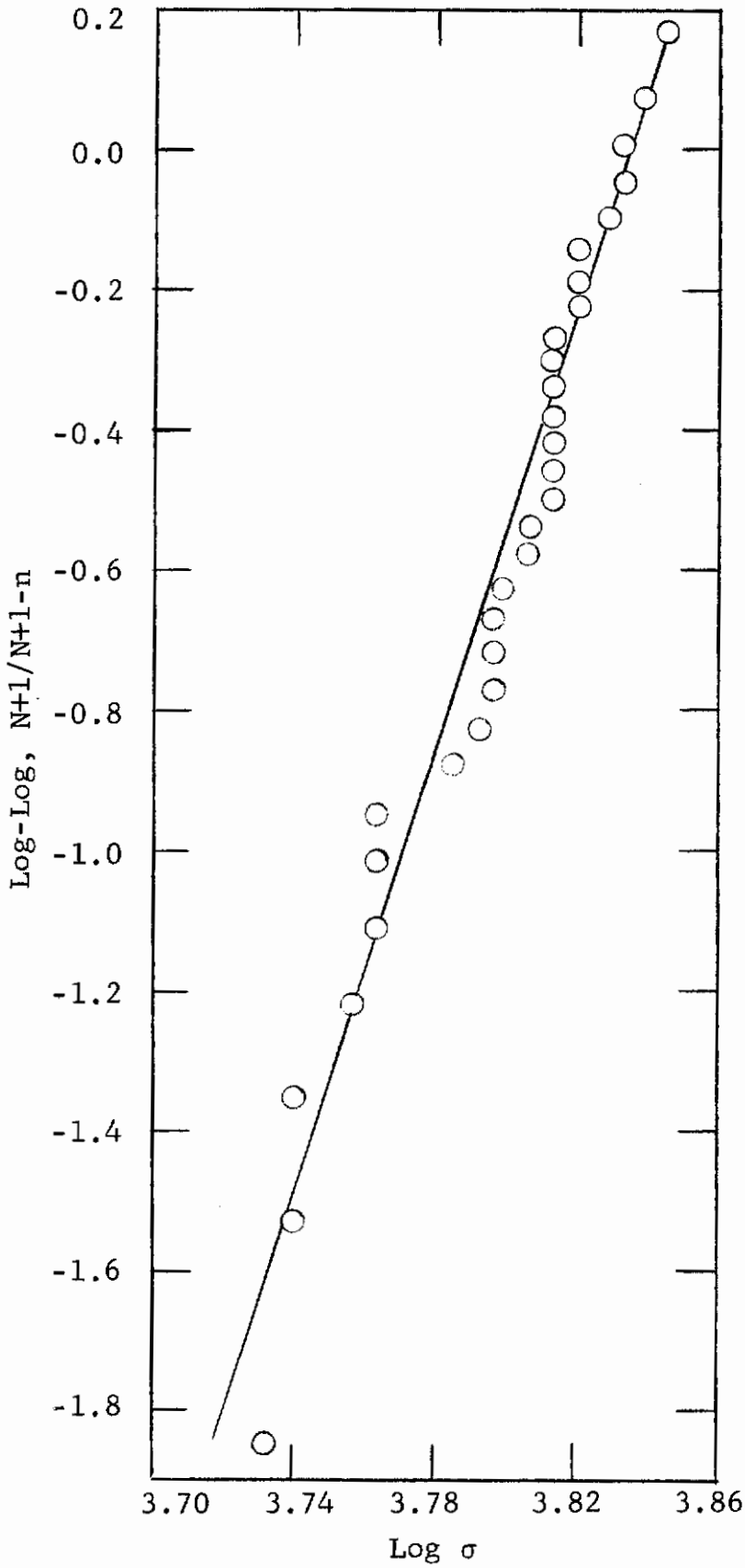

Figure 55. WEIBULL PLOT FOR JTA TESTED IN TENSION (Across grain, 77°F, air)

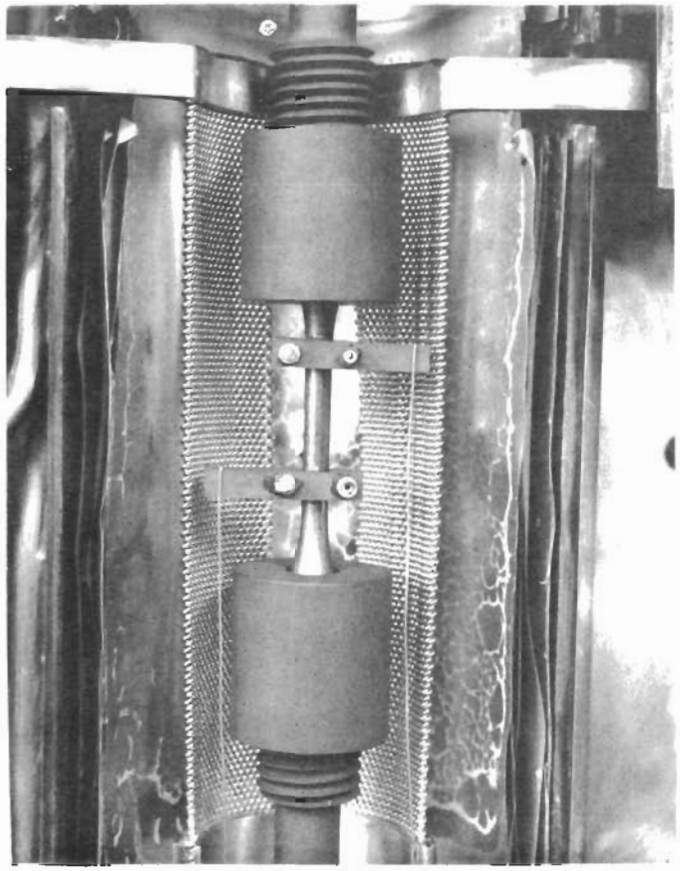

a) Extensometer Setup for Tension

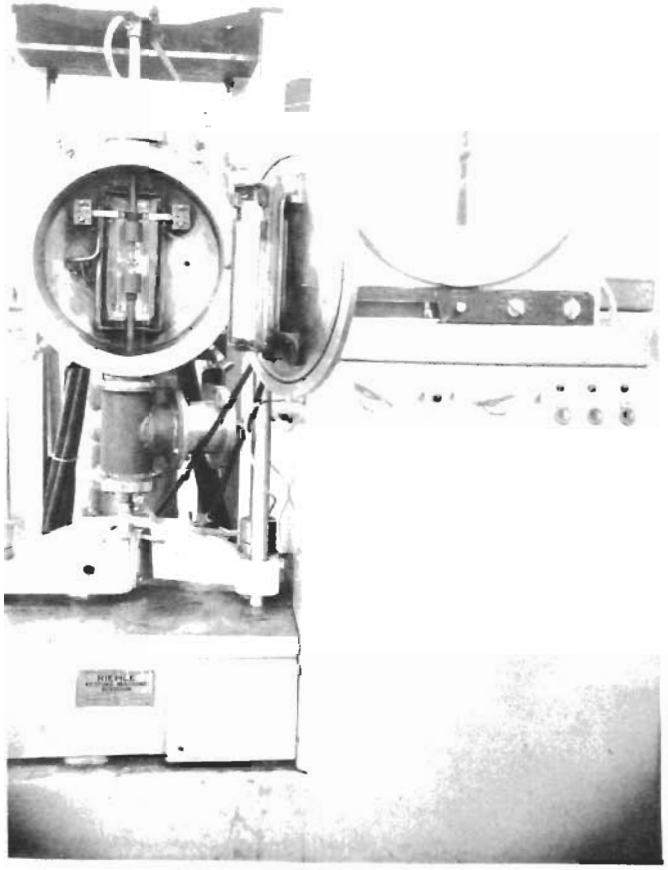

b) Extensometer in Relation to Brew Furnace

Figure 56 HIGH-TEMPERATURE EXTENSOMETER

by attaching high-temperature extension arms to the gage length of the sample. Stress-strain data at as much as 60% of the average failure load were taken because release of elastic energy at failure fractures the extension arm rods and may damage the heating elements. The test was stopped, the load removed from the sample, the temperature returned to ambient, the extension arm rod removed and the test rerun to failure.

Average tensile-strength data through 3580°F are shown in Table XIV, and normalized stress-strain curves are shown in Figures 57 through 60. The stress-strain behavior appeared to be linear to 1830°F and became increasingly nonlinear above 2750°F.

The variability of the high-temperature data was within the range exhibited by the ambient test data. Examination of the distribution curves (Figures 61 through 68) indicates that the with-grain data produced a linear, or deterministic, relationship as compared to the more typical nonlinear S-shaped distribution shown by the across-grain data. These results are the opposite of the observed relationships indicated by the flexural test data taken during the size-effect experiments.

c. High-Temperature Air-Atmosphere Tests

Special test procedures were developed for making high temperature tensile tests in an air atmosphere. The test sample was held in water-cooled grips. Induction heating was used to heat the samples to and hold them at the desired temperature for the required exposure period. The induction coils were fabricated so that the load train was accessible for applying the load (Figure 69). Direct temperature readings for the samples were made by using an optical pyrometer. After the specimens were exposed to the high-temperature atmosphere, stress-strain in tension was recorded by using a mechanical gage consisting of two low-voltage differential transformers to make strain measurements.

Table XV lists the tensile strengths in an air atmosphere. Strength loss occurred during a 60-min exposure in air at increasing temperatures until at 3580°F the JTA sample fell apart when handled. Reducing the exposure time to 20-min at 3580°F produced oxidation damage about the same as that resulting from a 60-min exposure at 3180°F. Although perhaps coincidental, the strength variability of the test samples exposed to air at 3580°F for 20-min was also the same as that of samples exposed to air at 3180°F for 60-min. The variabilities of the other samples exposed to air at elevated temperatures were much greater.

A correlation of material loss (Figures 70 and 71) with strengths based on nominal cross-sectional dimensions revealed that interior material not affected by oxidation retained its original strength. The material-loss curves can be used to estimate strength loss up to the limitations of the experiments attempted during this program. Figure 70 indicates that the rate of oxidation was nonlinear. However, to estimate strength loss the assumption

Table XIV. RESULTS OF TENSILE TESTS IN INERT ATMOSPHERE

Temp., °F	Orientation	Atmosphere	Number of tests	$\bar{\sigma}$, psi	ν, %	Avg. Young's modulus ($\bar{E}$), psi
Room	With grain	Air	30	12,140	9.398	10.65
	Across grain	Air	30	6,300	6.708	3.74
1832	With grain	Vacuum	10	9,940	4.128	9.52
	Across grain	Vacuum	10	5,460	8.142	3.74
2732	With grain	Vacuum	10	9,050	4.185	7.46
	Across grain	Vacuum	10	4,980	7.675	3.61
3182	With grain	Vacuum	10	9,260	4.167	4.41
	Across grain	Vacuum	10	4,165	5.906	2.74
3632	With grain	Vacuum	10	6,950	15.751	3.54
	Across grain	Vacuum	10	4,545	6.251	2.08
3992	With grain					
	Across grain					

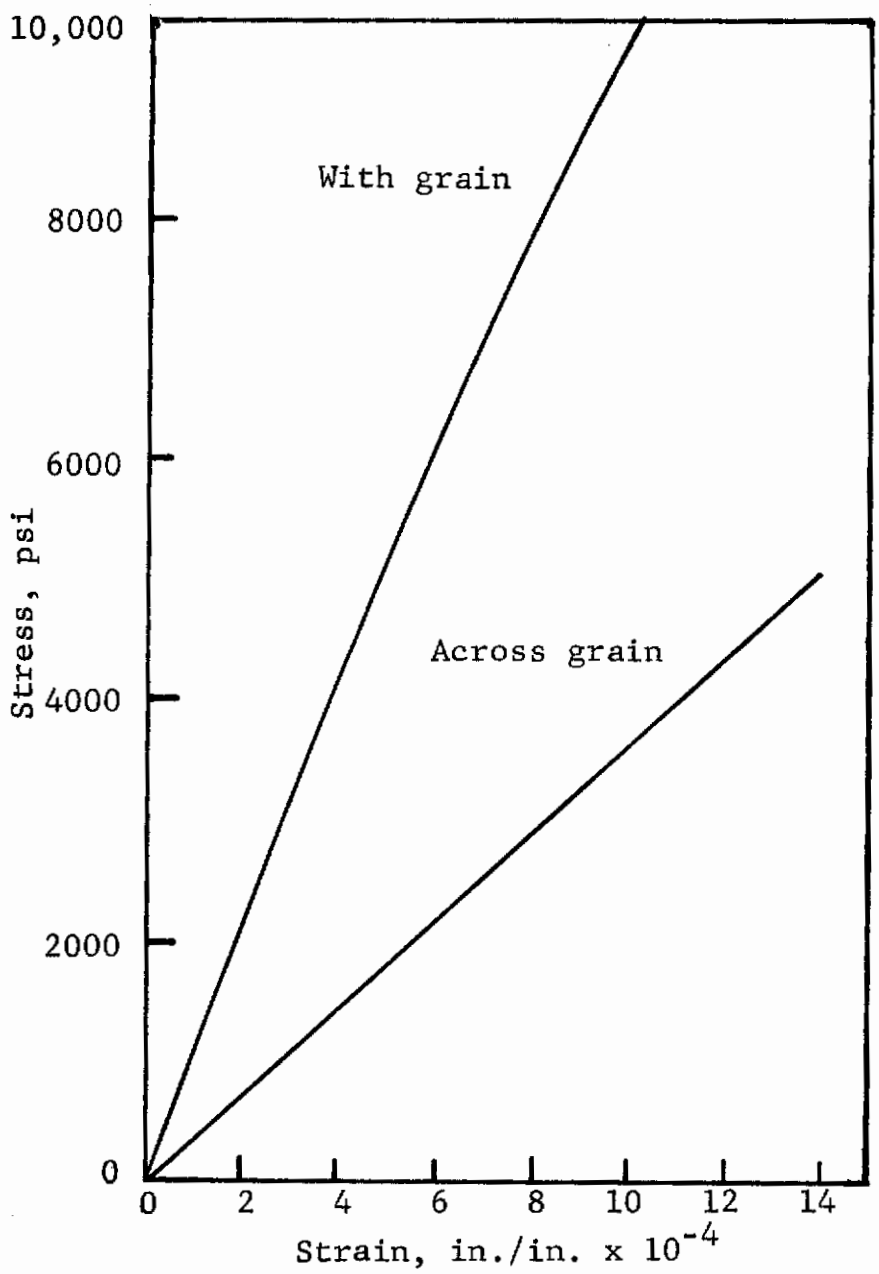

Figure 57. TYPICAL STRESS-STRAIN CURVE OF JTA IN TENSION AT 1830°F

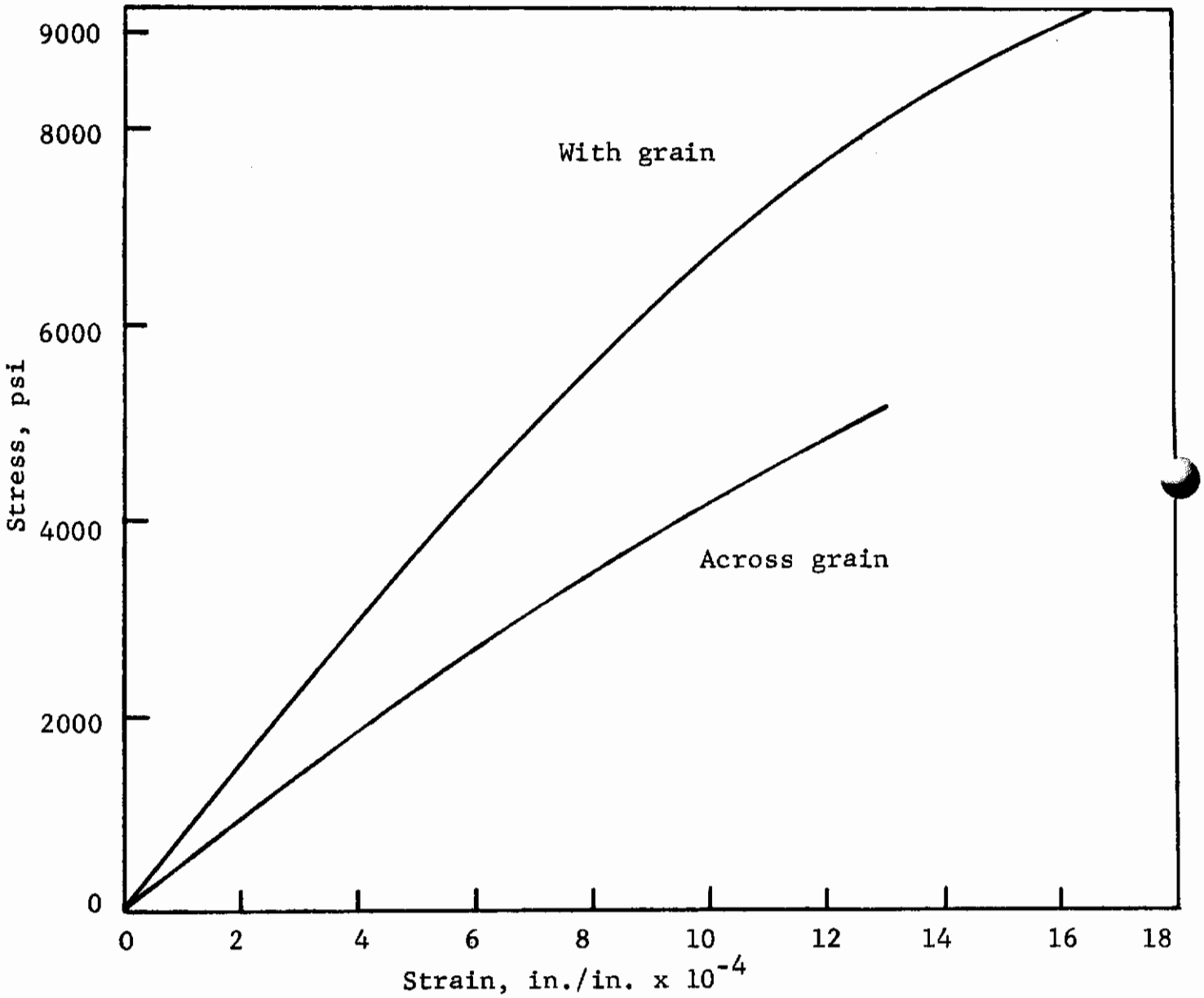

Figure 58. TYPICAL STRESS-STRAIN CURVE OF JTA IN TENSION AT 2750°F

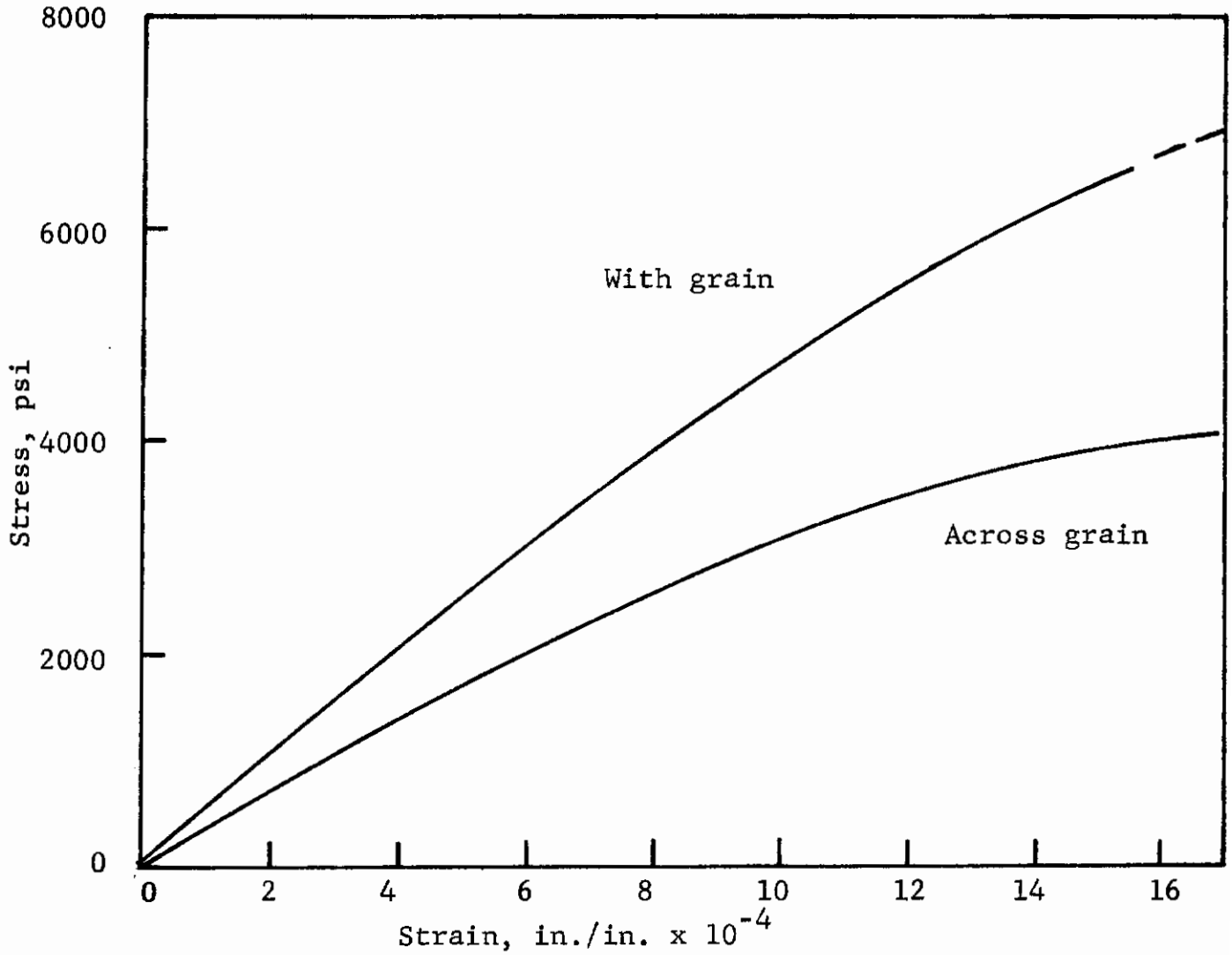

Figure 59. TYPICAL STRESS-STRAIN CURVE OF JTA IN TENSION AT 3100°F

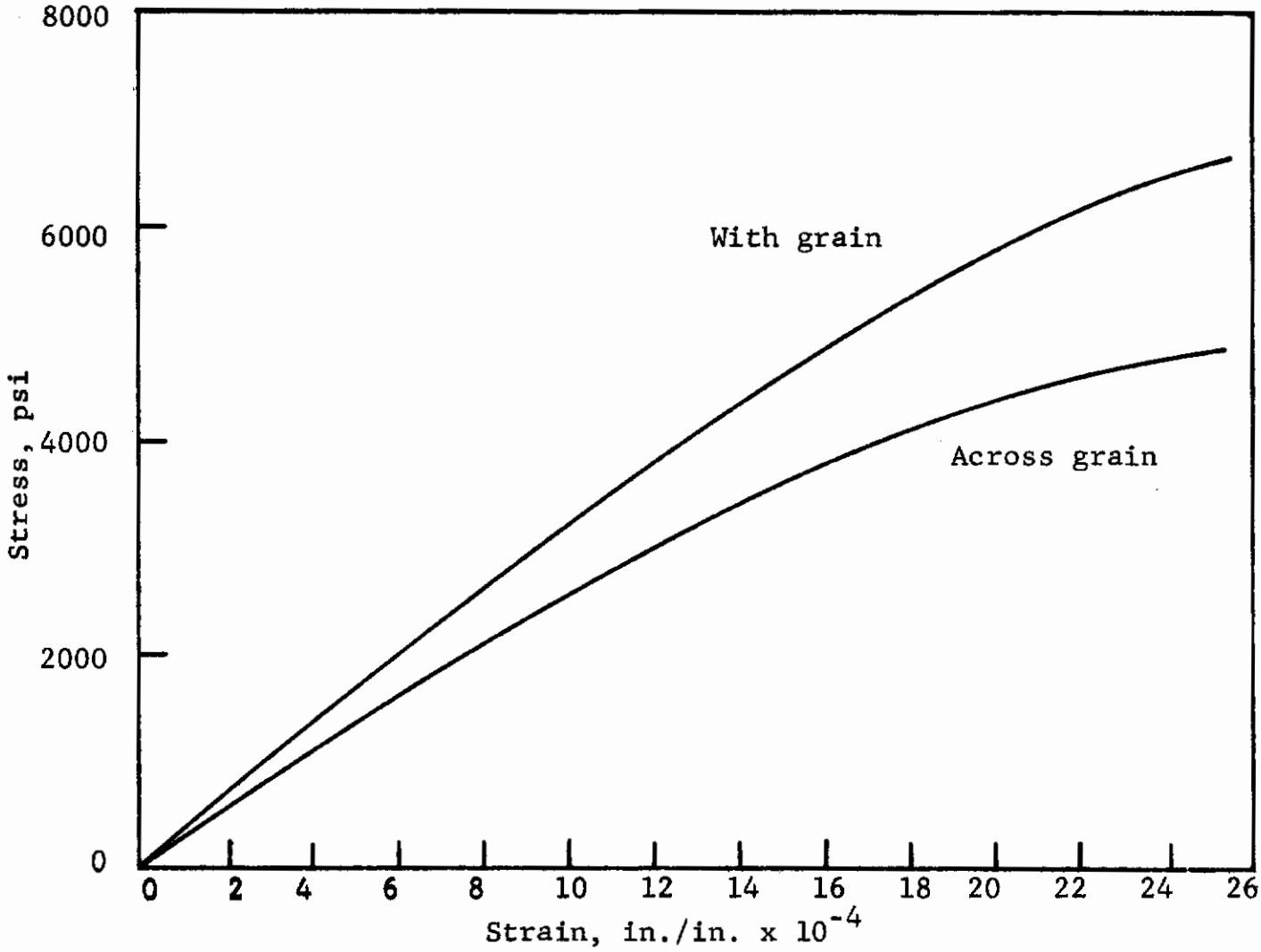

Figure 60. TYPICAL STRESS-STRAIN CURVE OF JTA IN TENSION AT 3600°F

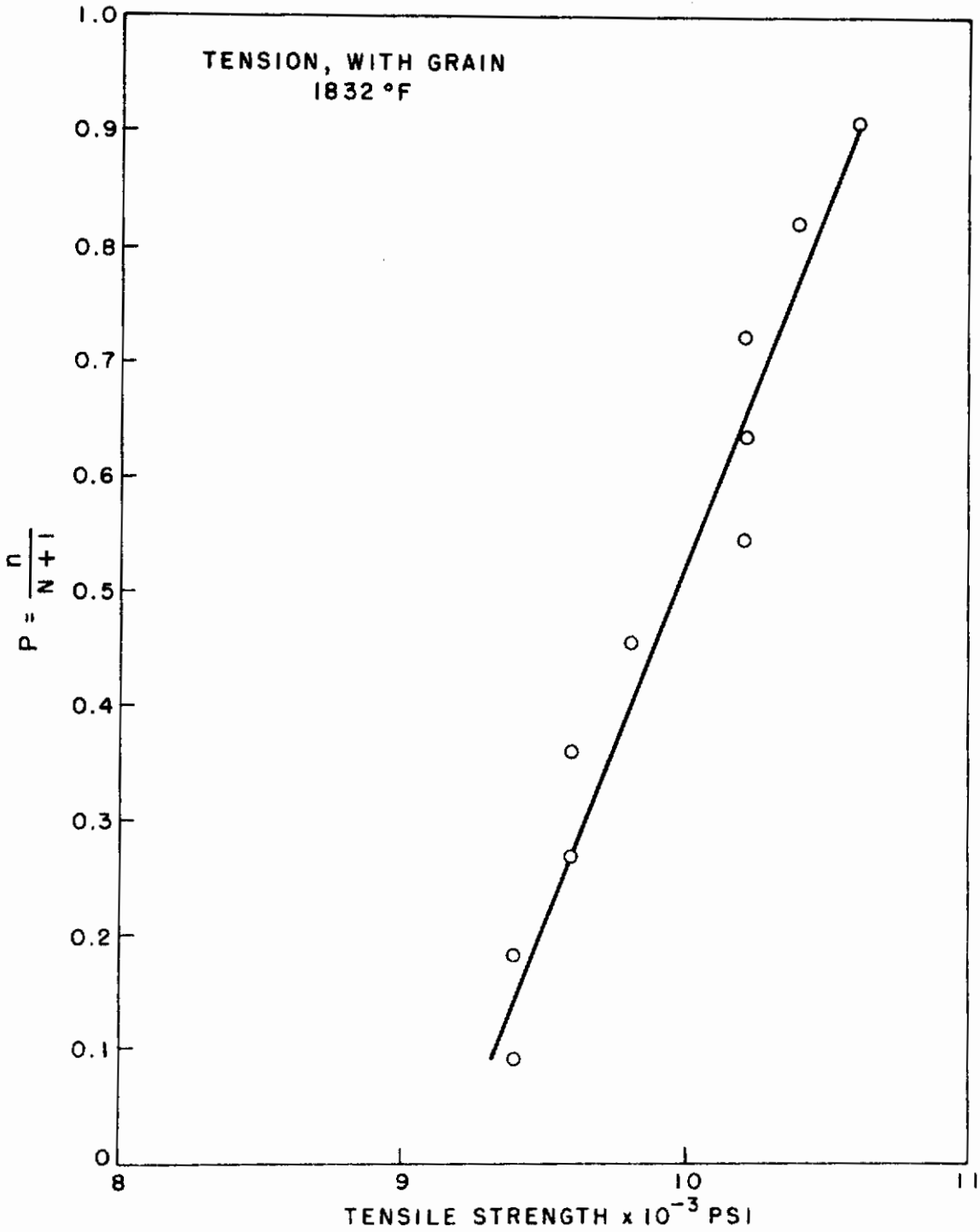

Figure 61. DISTRIBUTION CURVE IN WITH GRAIN TENSION AT 1832°F

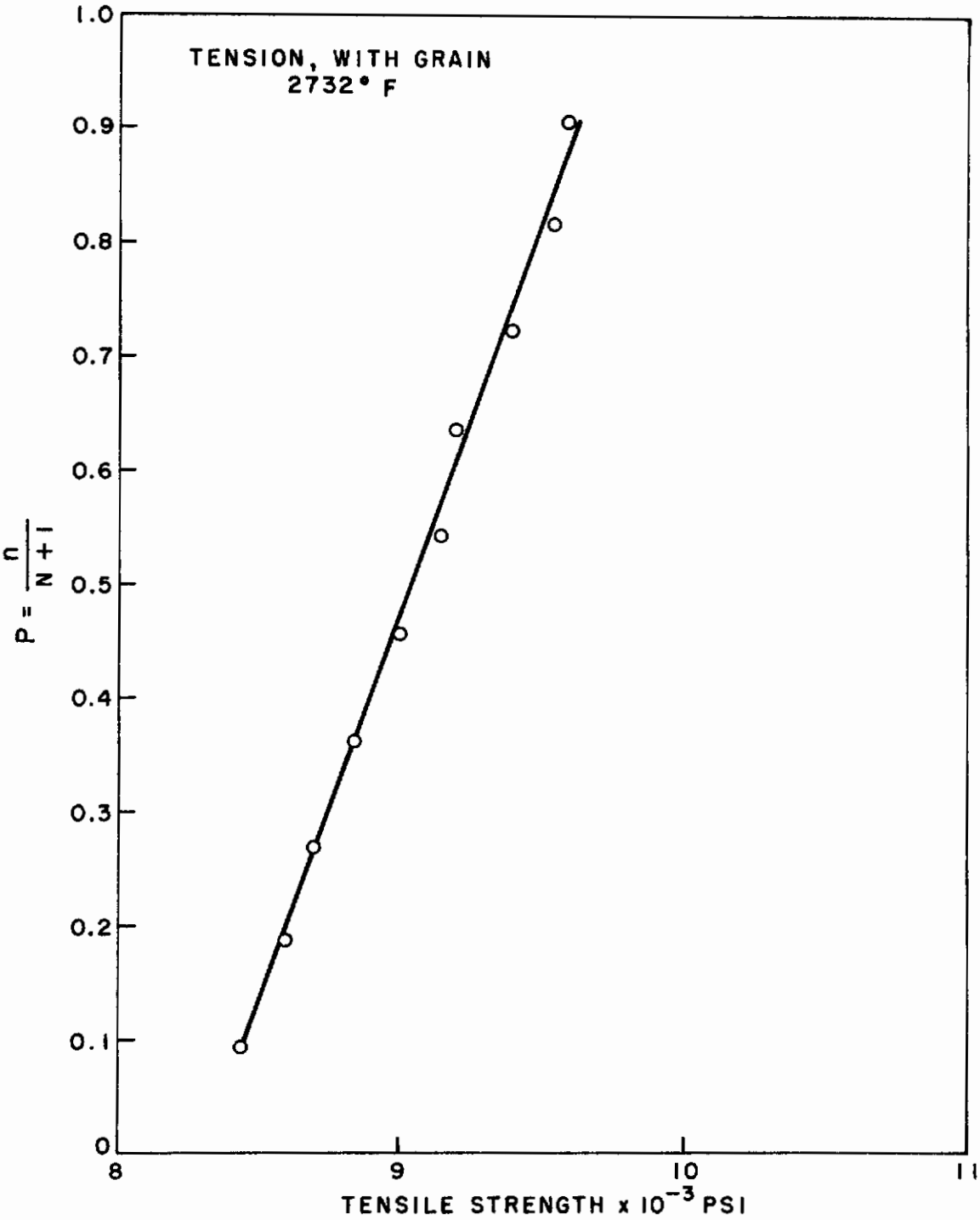

Figure 62. DISTRIBUTION CURVE IN WITH GRAIN TENSION AT 2732°F

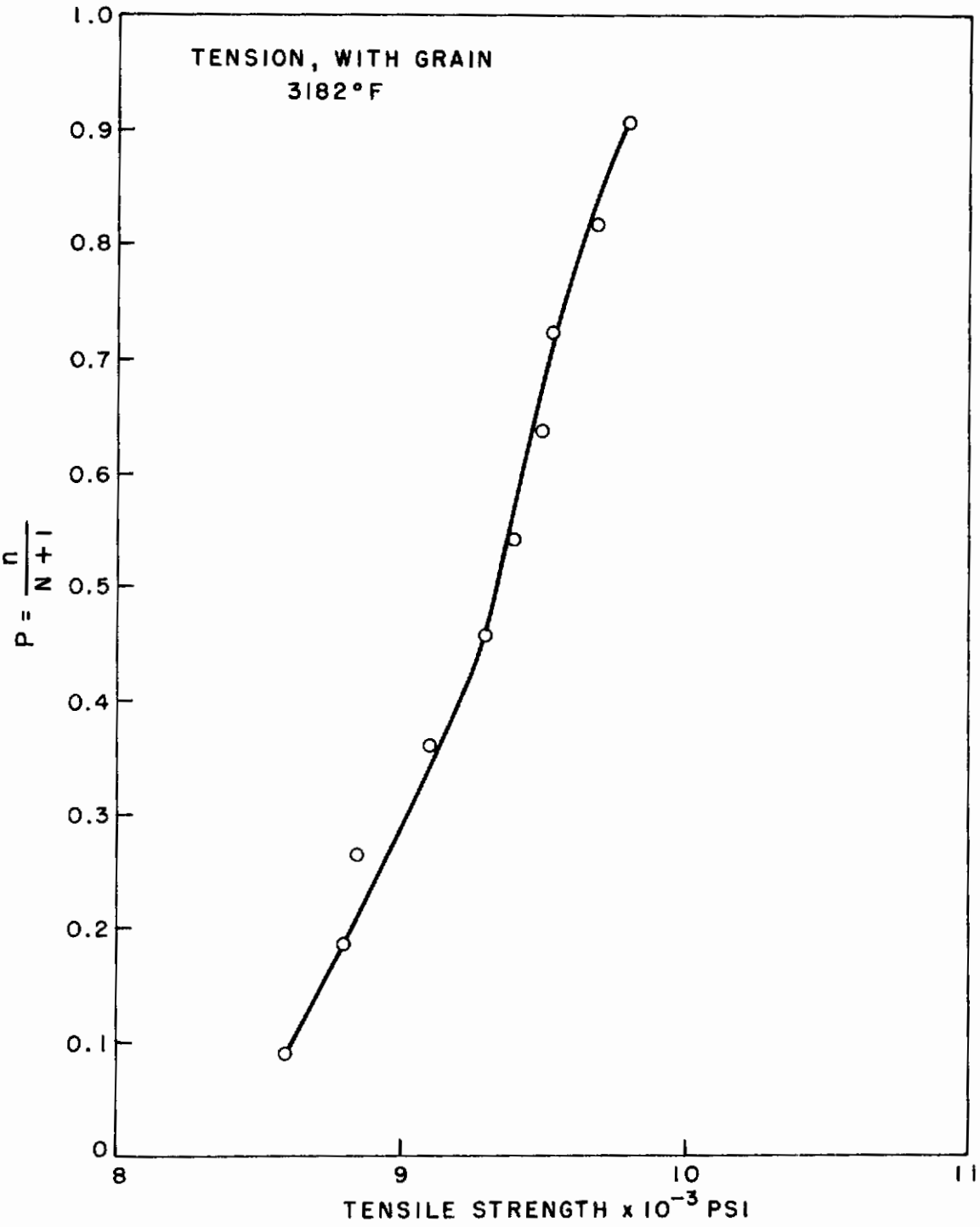

Figure 63. DISTRIBUTION CURVE IN WITH GRAIN TENSION AT 3182°F

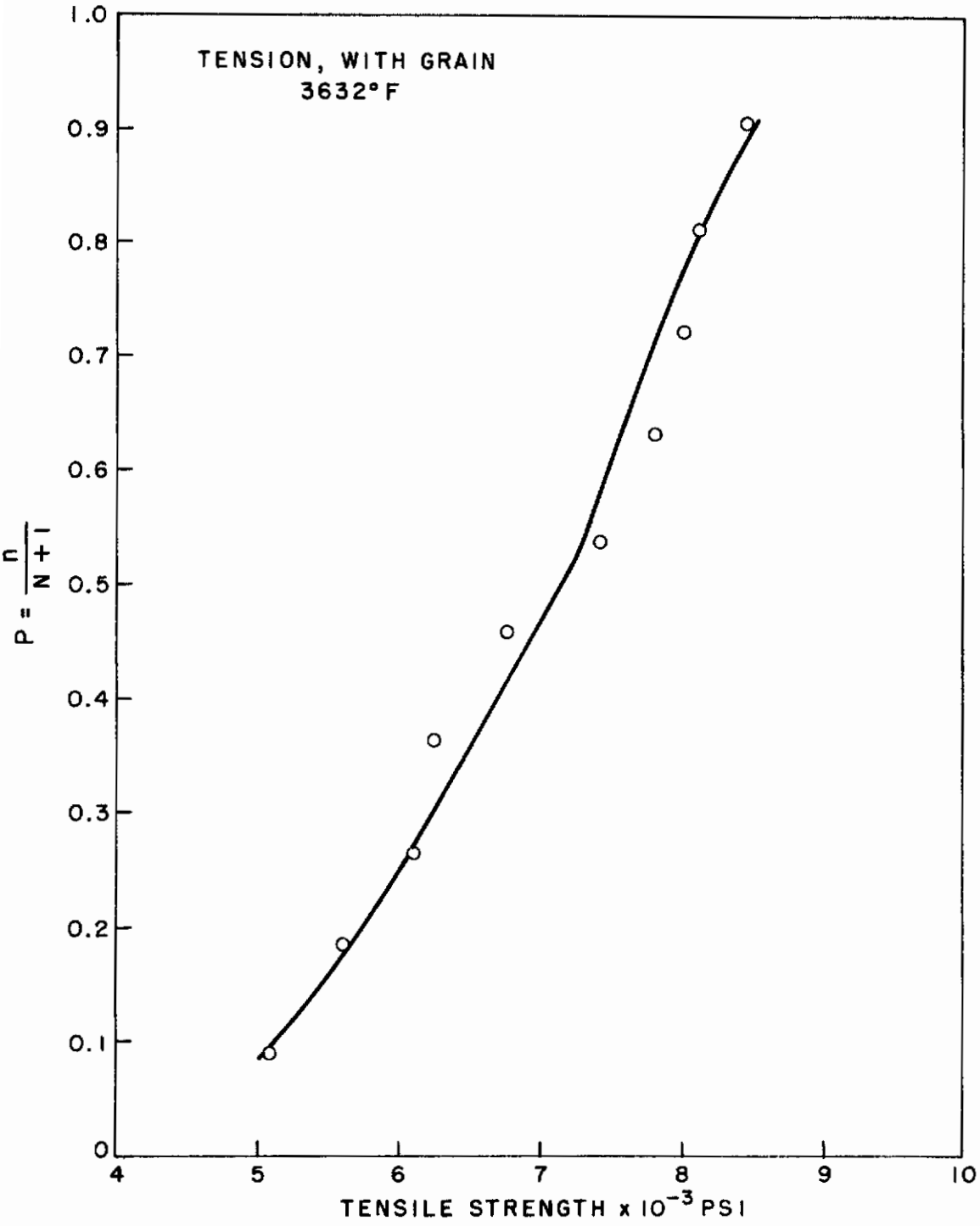

Figure 64. DISTRIBUTION CURVE IN WITH GRAIN TENSION AT 3632°F

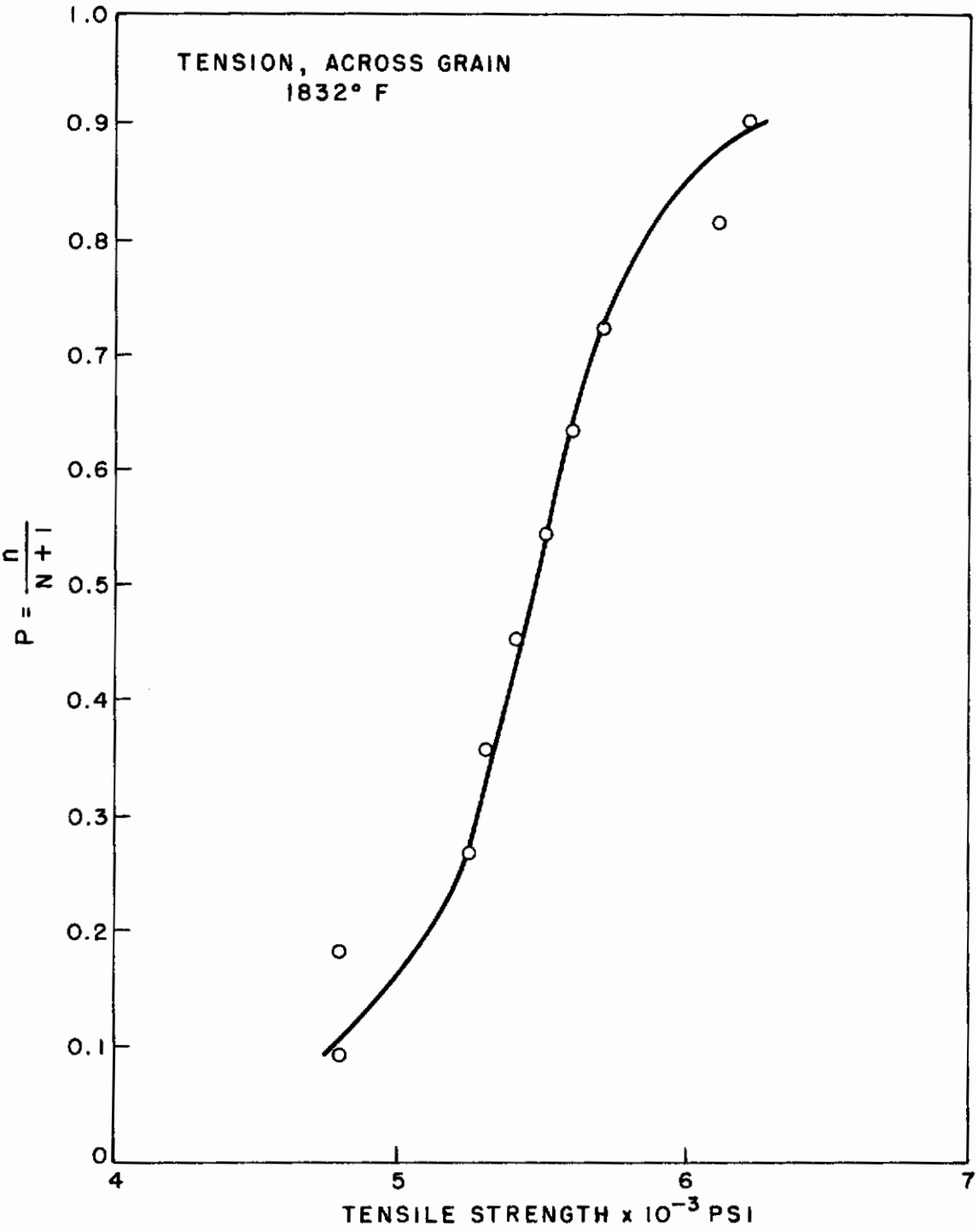

Figure 65. DISTRIBUTION CURVE IN ACROSS GRAIN TENSION AT 1832°F

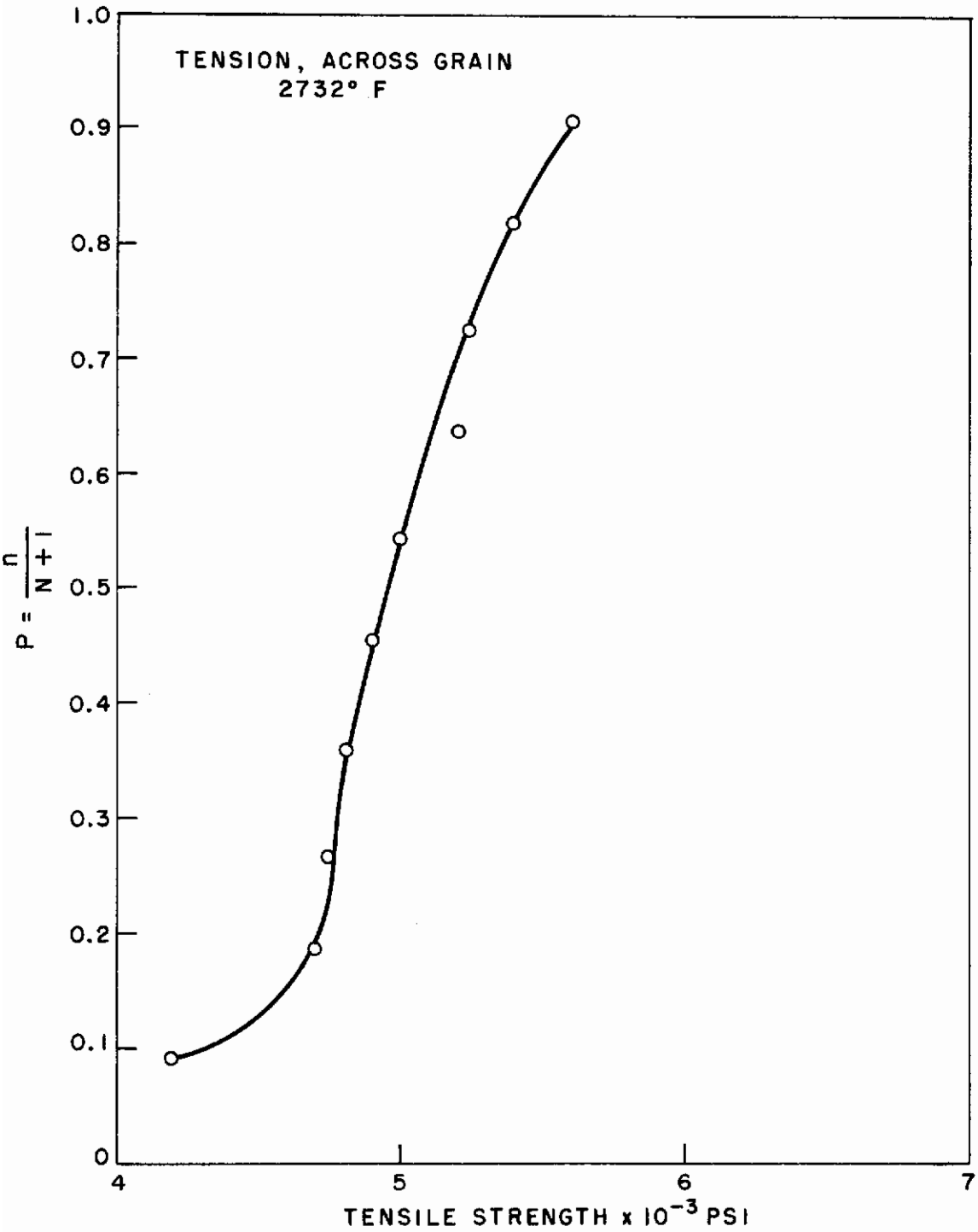

Figure 66. DISTRIBUTION CURVE IN ACROSS GRAIN TENSION AT 2732°F

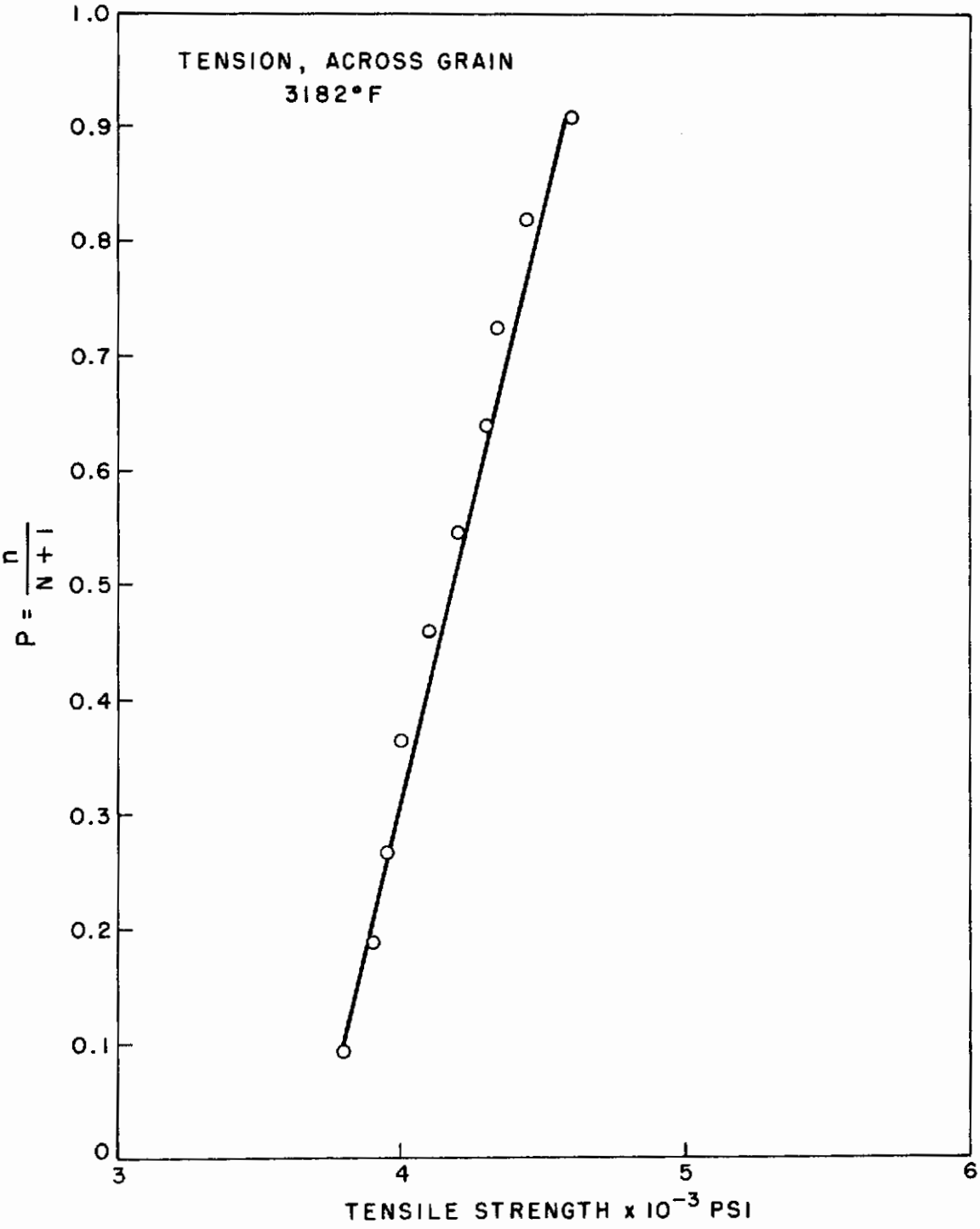

Figure 67. DISTRIBUTION CURVE IN ACROSS GRAIN TENSION AT 3182°F

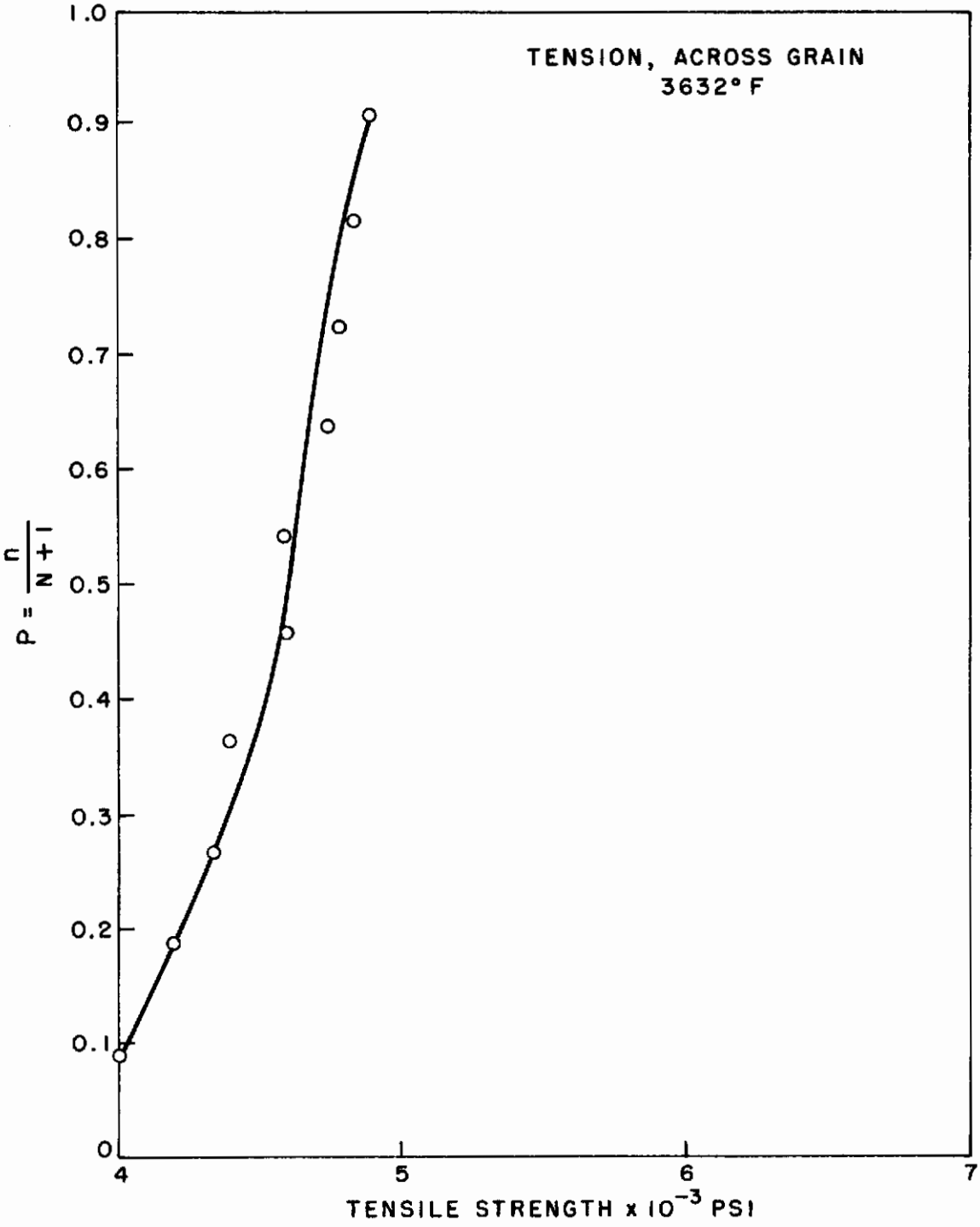

Figure 68. DISTRIBUTION CURVE IN ACROSS GRAIN TENSION AT 3632°F

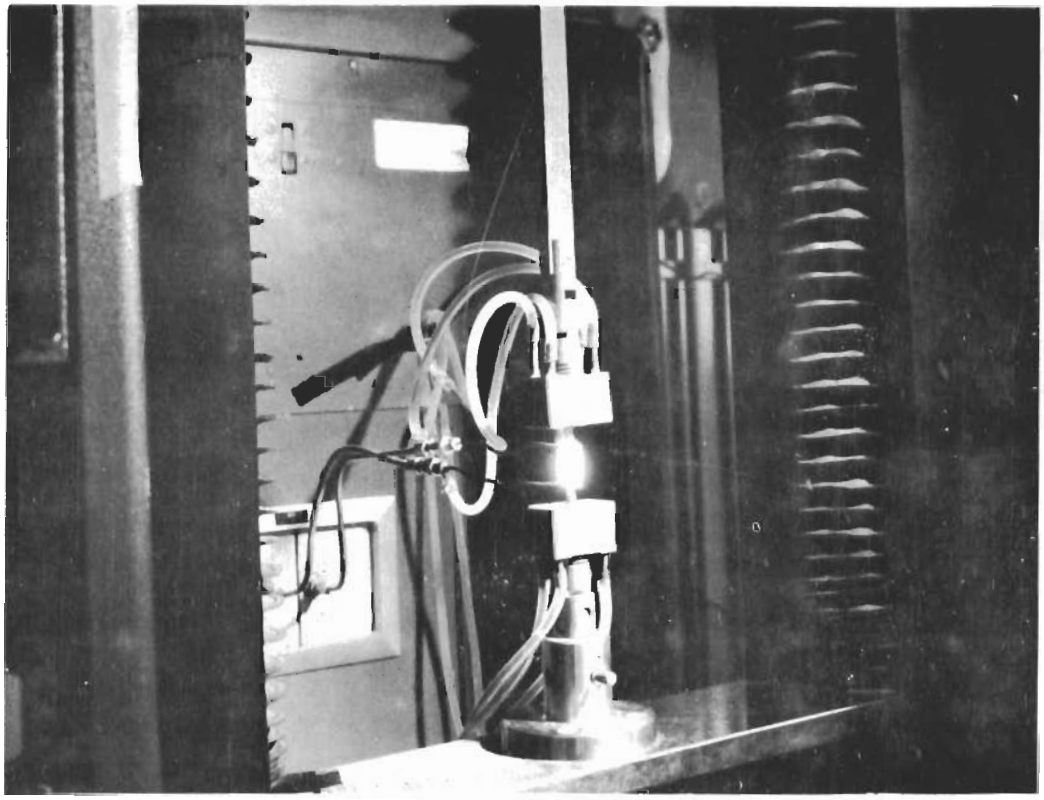

Figure 69. TENSION TEST FIXTURE FOR AIR TESTING OF JTA GRAPHITE SHOWING INDUCTION COILS HEATING SAMPLE DURING SOAK PERIOD

Table XV. RESULTS OF TENSILE TESTS IN AIR ATMOSPHERE

Temp., °F	Orientation	Number of tests	Exposure time, min	$\bar{\sigma}$, psi	ν, %	$\bar{E}$, psi x 10^6
Room	With grain	30		12,140	9.398	
	Across grain	30		6,300	6.708	
1832	With grain	5	60	4,120	28.446	
	Across grain	5	60	1,400	29.965	
2732	With grain	3	60	5,630	---	
	Across grain	5	60	2,220	46.148	
3092	With grain	5	60	2,700		0.91
	Across grain	5	60	1,610		0.43
3182	With grain	5	60	2,700	6.625	
	Across grain	5	60	1,610	4.120	
3596	With grain	3	20	2,630		0.47
	Across grain	3	20	1,500		0.25
	With grain	3	40	266		---
	Across grain	3	40	250		---
	With grain	3	60	0		---
	Across grain	3	60	0		---
3632	With grain	3	20	2,630	4.736	
	Across grain	3	20	1,500	6.774	
	With grain	3	40	266	17.677	
	Across grain	3	40	250	16.329	
	With grain	3	60	0	---	
	Across grain	3	60	0	---	

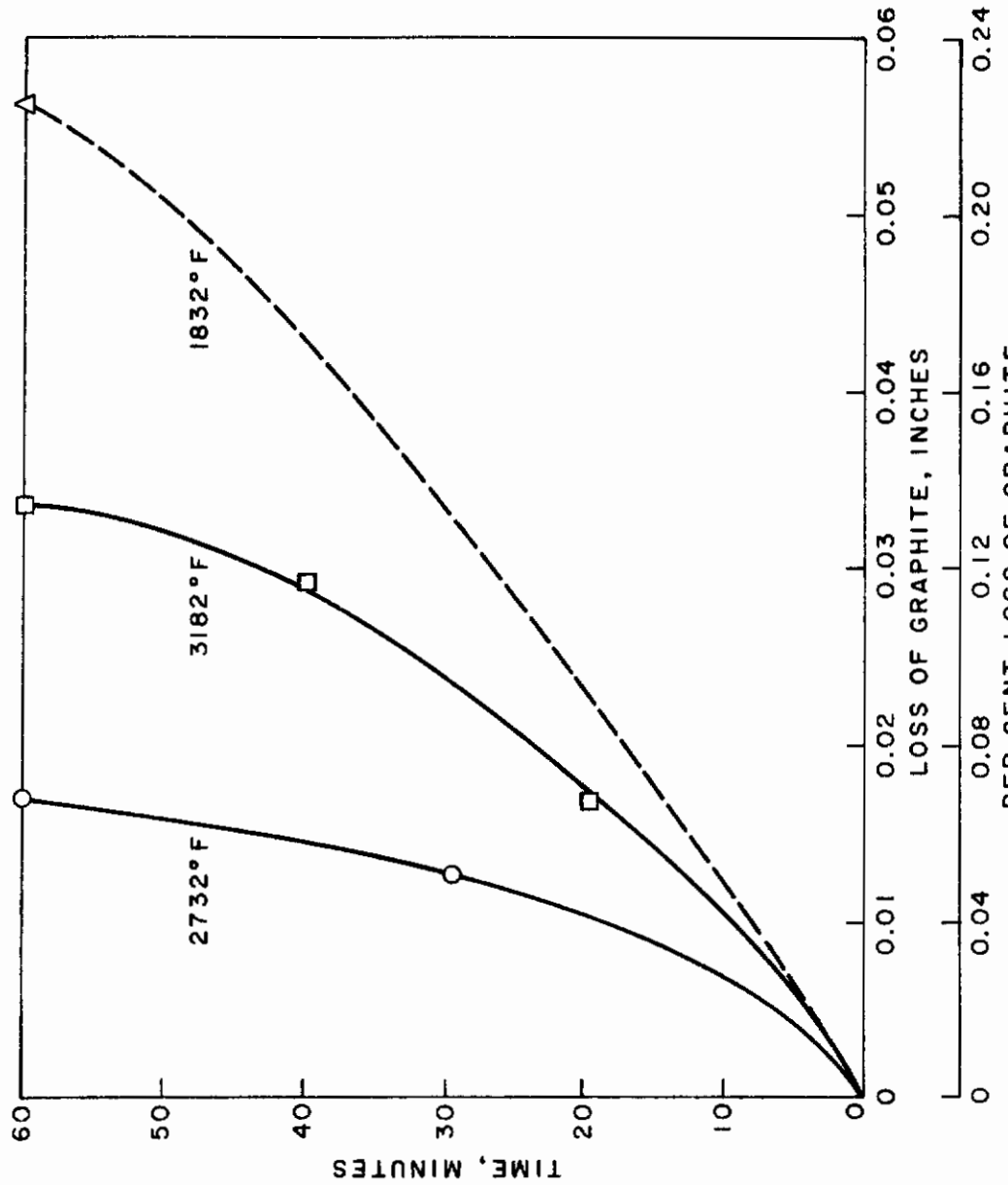

Figure 70. % LOSS OF JTA GRAPHITE IN RELATION TO TEMPERATURE AND TIME

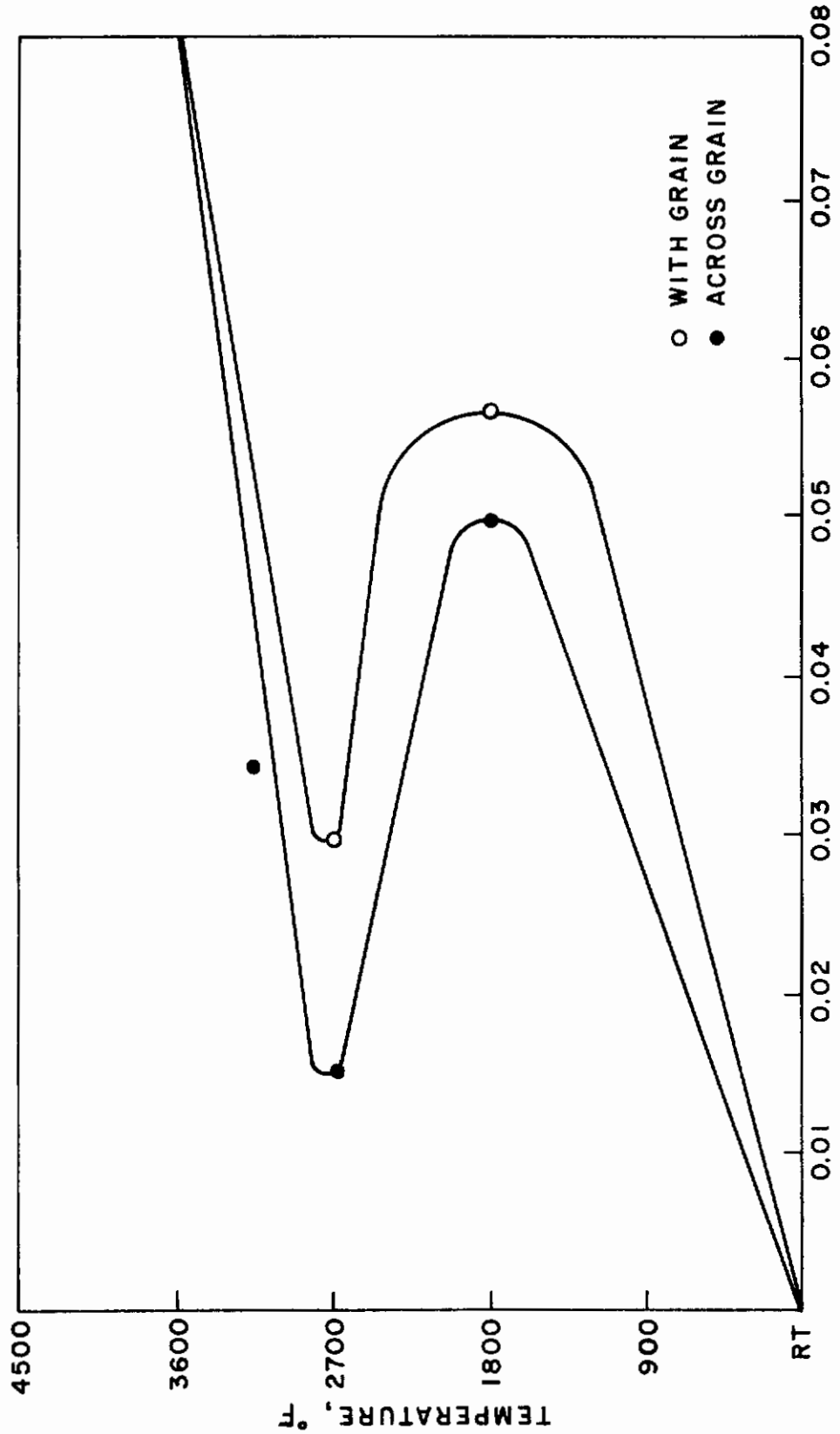

Figure 71. MATERIAL LOSS OF JTA GRAPHITE IN RELATION TO TEMPERATURE

that a linear rate of oxidation that produces a conservative residual strength in the material occurs and helps to compensate for the variability of the results. Therefore the rate of material loss under static oxidation conditions is approximately 3/64 in./hr for the across-grain orientation and 1/16 in./hr for the with-grain orientation at 1830°F in air, 1/64 in./hr for the across-grain orientation and 1/32 in./hr for the with-grain orientation at 2730°F in air, and 3/32 in./hr loss for both orientations at 3580°F in air.

A summation of the 1-hr-exposure tensile data taken in inert and oxidation environments is shown in Figure 72. The general shapes of the curves are about the same. The oxidized material had about half the strength of material tested in an inert environment.

4. FLEXURE

The test method used to obtain flexural strength of JTA graphite is described in Section IV1. Elevated-temperature tests were performed in a similar manner, except the test fixtures were made from Poco graphite instead of metal.

Tests were run in a graphite resistance-heated tube furnace. Stress-strain was determined from load-deflection curves obtained from optical readings of sample deflection of specific load points.

For testing in air, a water-cooled metal jig was used. Induction heating similar to that described for tensile testing was used for making high-temperature air tests in flexure (Figure 73). Temperature readings were taken directly by using an optical pyrometer. Elastic moduli were obtained at various temperatures from load-deflection relationships obtained from a mechanical strain gage activated by a remote deflection plunger.

a. High-Temperature Inert-Atmosphere Tests

The flexural data were more extensive than data obtained by other test methods because of the greater ease in making this test with brittle materials. Table XVI lists the average strengths obtained from this series of experiments. The strength of the with-grain orientation of JTA graphite remained level or possibly increased somewhat up to 3180°F; it was 17,800 psi at room temperature and 20,660 psi at 3180°F; then the strength decreased rapidly. The across-grain strength evidenced the same type of behavior.

The variability within the group was reasonable and, as expected, increased with increasing temperature. Elastic-modulus values behaved in a manner similar to that of the strength values. Figure 74 compares the present data with test results taken from a previous program.(12) While the data comparison is not exact, it is as good as that observed for most ceramic or graphites when

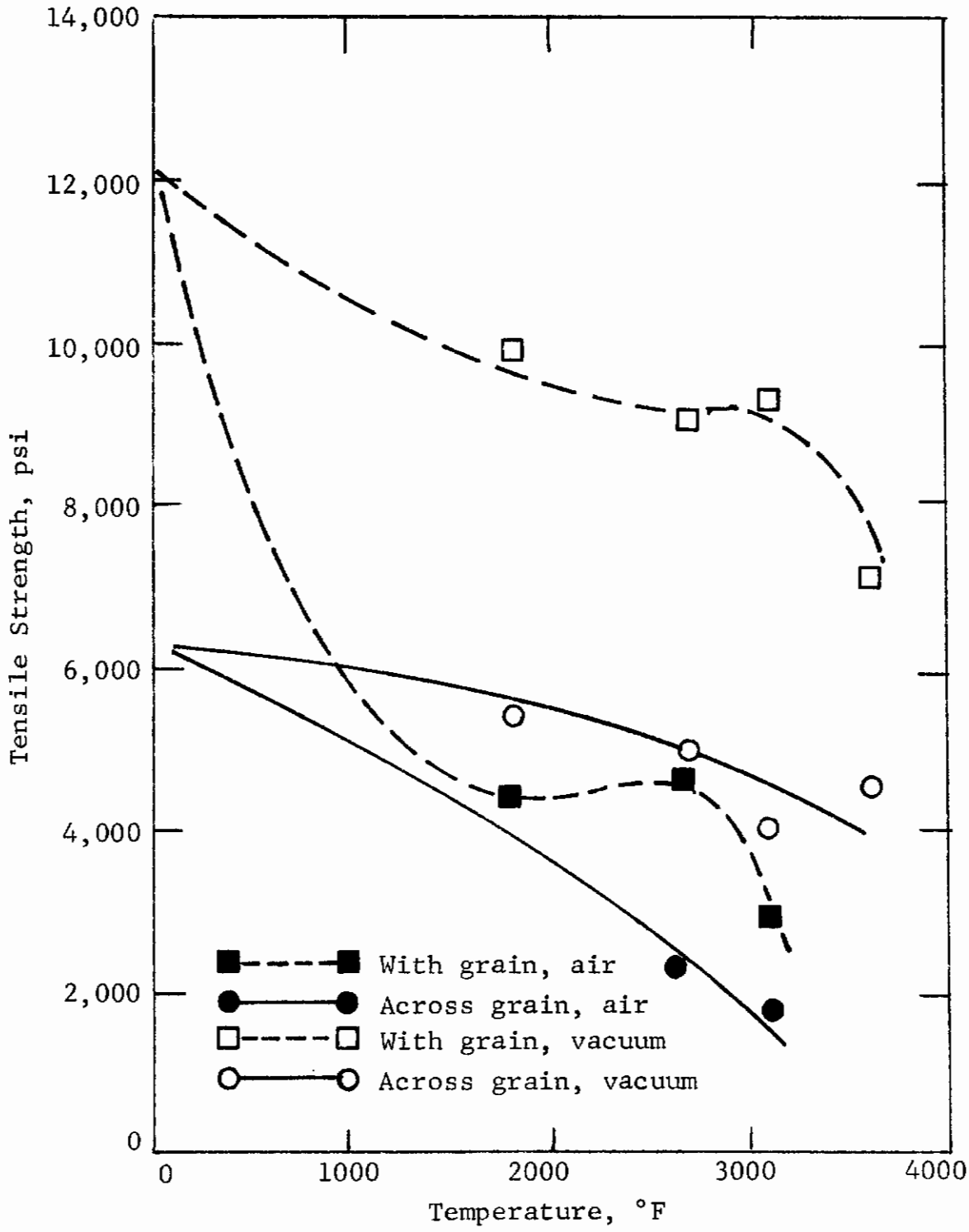

Figure 72. EFFECT OF TEMPERATURE ON TENSILE STRENGTH OF JTA IN INERT AND AIR ATMOSPHERES

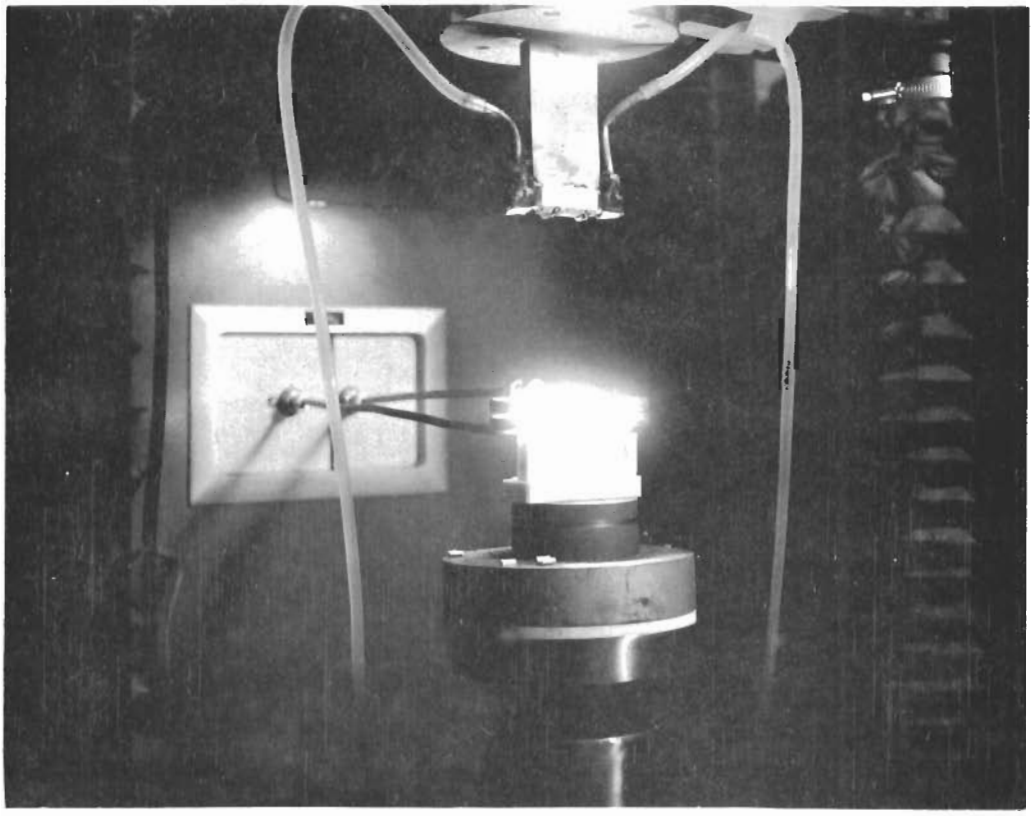

Figure 73. FLEXURAL TEST FIXTURE FOR AIR TESTING JTA GRAPHITE, SHOWING INDUCTION COILS HEATING SAMPLE DURING SOAK PERIOD

Table XVI. RESULTS OF FLEXURAL TESTS IN VARIOUS ATMOSPHERES

Temp., °F	Orientation	Number of tests	Atmosphere	$\bar{\sigma}$, psi	ν, %	$\bar{E}$, psi x 10^6
Room	With grain	30		17,800	14.8	11.80
			Air	17,520		10.69
	Across grain	30		8,945	9.7	4.52
			Air	7,510		4.32
1796	With grain	30	Argon	18,450		6.88
	Across grain	30	Argon	8,150		3.28
1832	With grain	30		18,450	8.4	6.88
	Across grain	30		8,140	21.9	3.24
2732	With grain	30		19,200	9.0	7.20
	Across grain	30		9,315	10.9	2.62
2750	With grain	30	Argon	18,875		7.21
	Across grain	30	Argon	9,500		2.62
3182	With grain	30		20,660	8.3	7.57
	Across grain	30		9,120	15.4	2.72
3200	With grain	30	Argon	20,660		7.57
	Across grain	30	Argon	8,822		2.72
3596	With grain	30	Argon	14,670		4.54
	Across grain	30	Argon	6,836		2.51
3632	With grain	30		14,670	11.59	4.53
	Across grain	30		6,836	13.17	2.51
3992	With grain	30		7,367	15.41	2.75
			Argon	7,366		2.75
	Across grain	30		4,950	18.53	1.57
			Argon	4.950		1.57

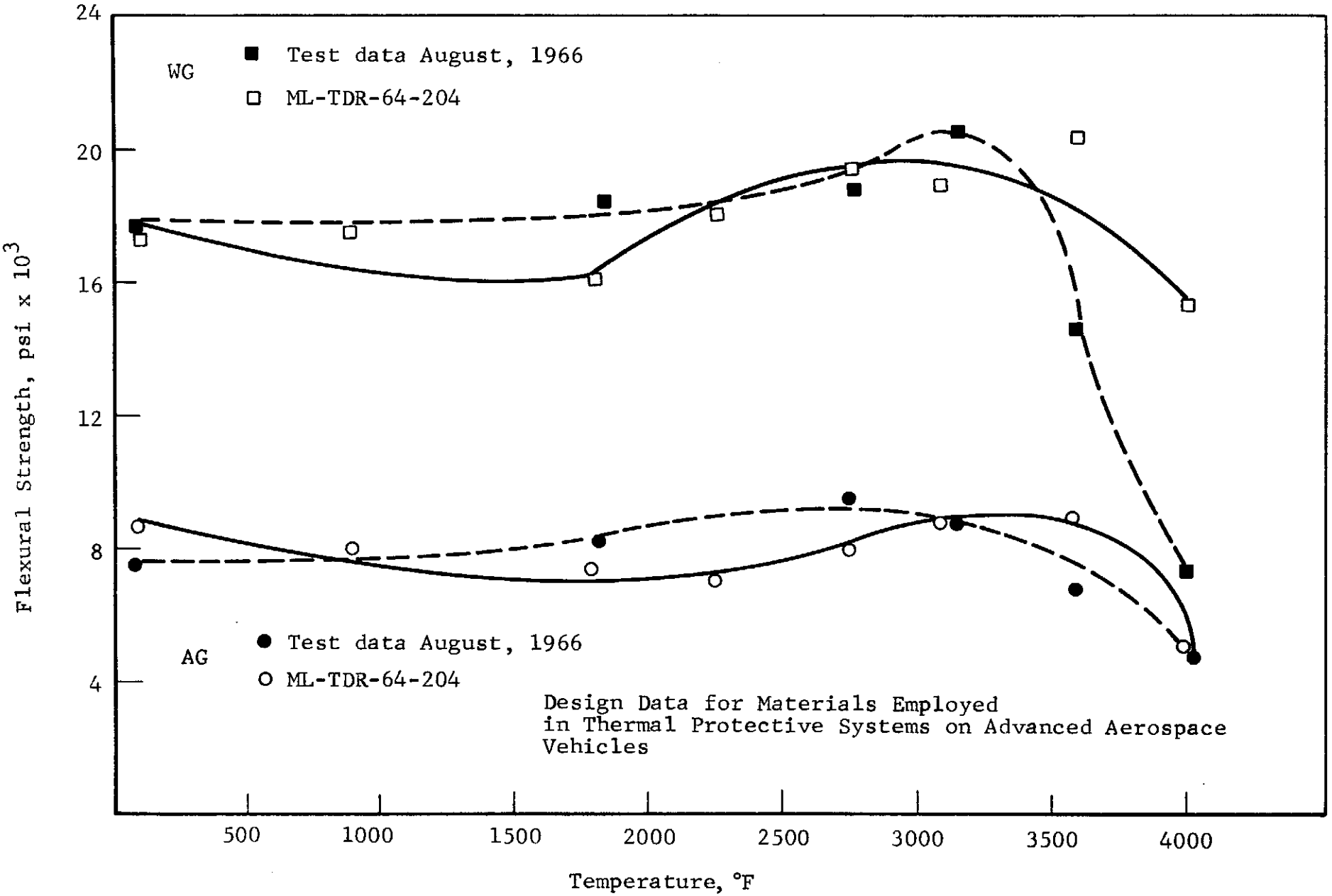

Figure 74. FLEXURAL STRENGTH OF JTA GRAPHITE

different batches are compared. If a material variability of 10% is taken as normal (test evidence indicates that this figure is reasonable), the overlap in individual test results makes the data from these two different testing programs appear to come from the same test population. For design purposes, the designer can use the scaling laws or must take observed variability into account when determining safe design load factors. Stress-deflection curves in flexure are shown in Figures 75 through 80.

Distribution curves for strengths obtained at different temperatures are exhibited in Figures 81 through 90. These distribution plots show a general tendency for the with-grain data to show an S-curve configuration, while the across-grain plots show a tendency to be a straight line with a small tail attached at the lower strengths. It is interesting to note that the tension data, for test populations of 30 samples, indicate S curves for both grain orientations. The indication is that the mode of failure between tension and flexure is sufficiently different to produce different types of distribution curves when across-grain data are compared. However, the anisotropy of with- and across-grain strength is approximately 2 to 1 for both tension and flexure.

Table XVII provides a comparison of Weibull's material constant (m) obtained from graphic plots and the estimation method using the coefficient of variability. When the data indicate that $\sigma_u = 0$, i.e., when the plot is a straight line, the agreement between m values obtained from data plots and the estimation formula was good. The data thus show that m is related to the variability of JTA. The with-grain variability is about half the across-grain variability at temperatures as high as 3180°F. While the m factors for JTA graphite tested in flexure appear to be constant for temperatures as high as 3180°F, a comparison of similar calculations for tensile data reveals an apparent agreement for the with-grain orientation, but not for across-grain orientation. This phenomenon makes it difficult to relate the Weibull parameters to a meaningful design concept. Also, there is enough variation between m factors developed on the present program and those developed by Bell Aerosystems(5) on a companion program to cast doubt on the significance of attempting to relate design concepts to Weibull constants. At this time materials are not consistent enough, our test procedures' reliability not established well enough, and our understanding of brittle failure not good enough to determine true material constants and to understand their significance.

b. Air-Atmosphere Tests

Flexural experiments in oxidizing environments were carried out by using two different test conditions.

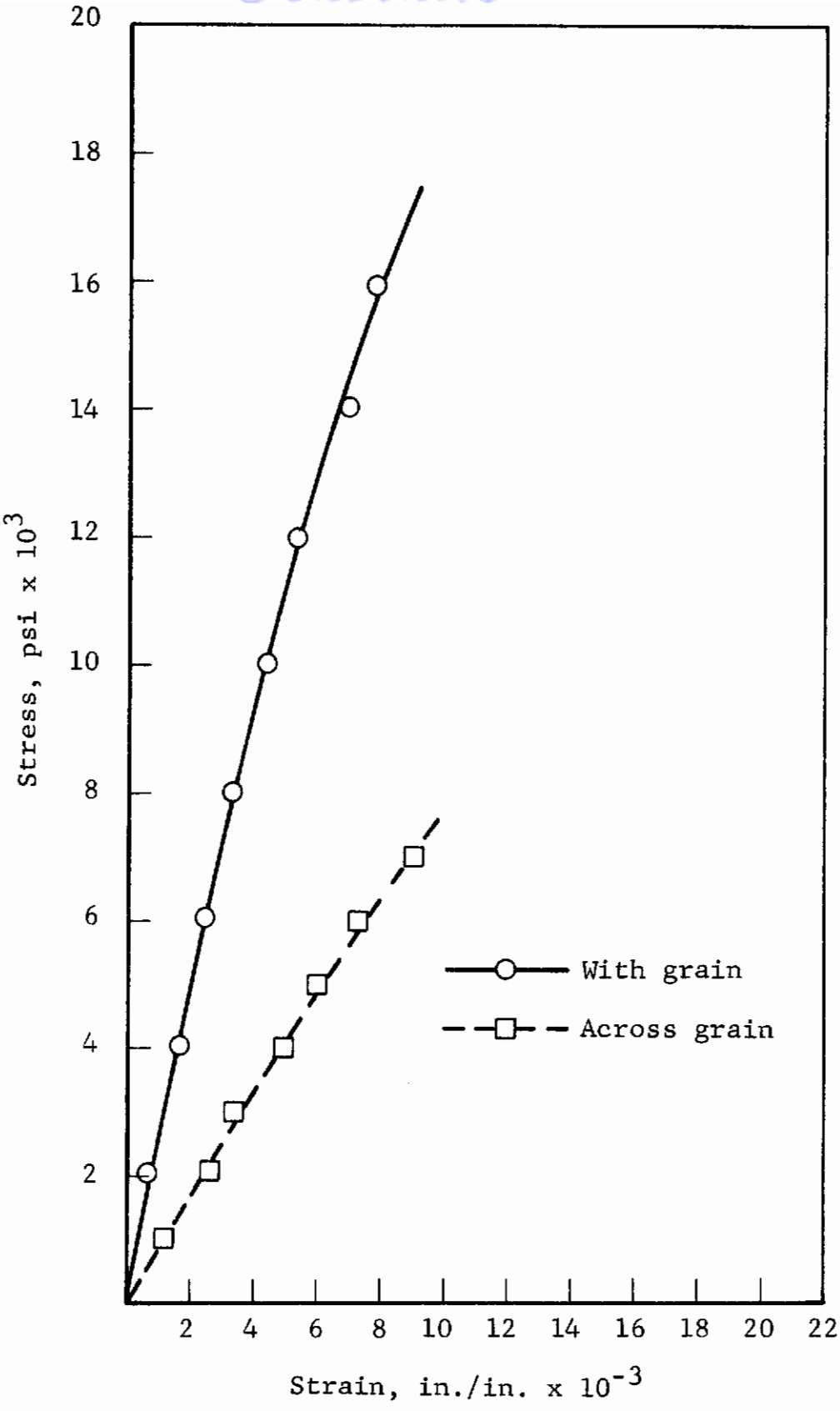

Figure 75. ROOM-TEMPERATURE FLEXURAL STRESS VS DEFLECTION OF JTA GRAPHITE

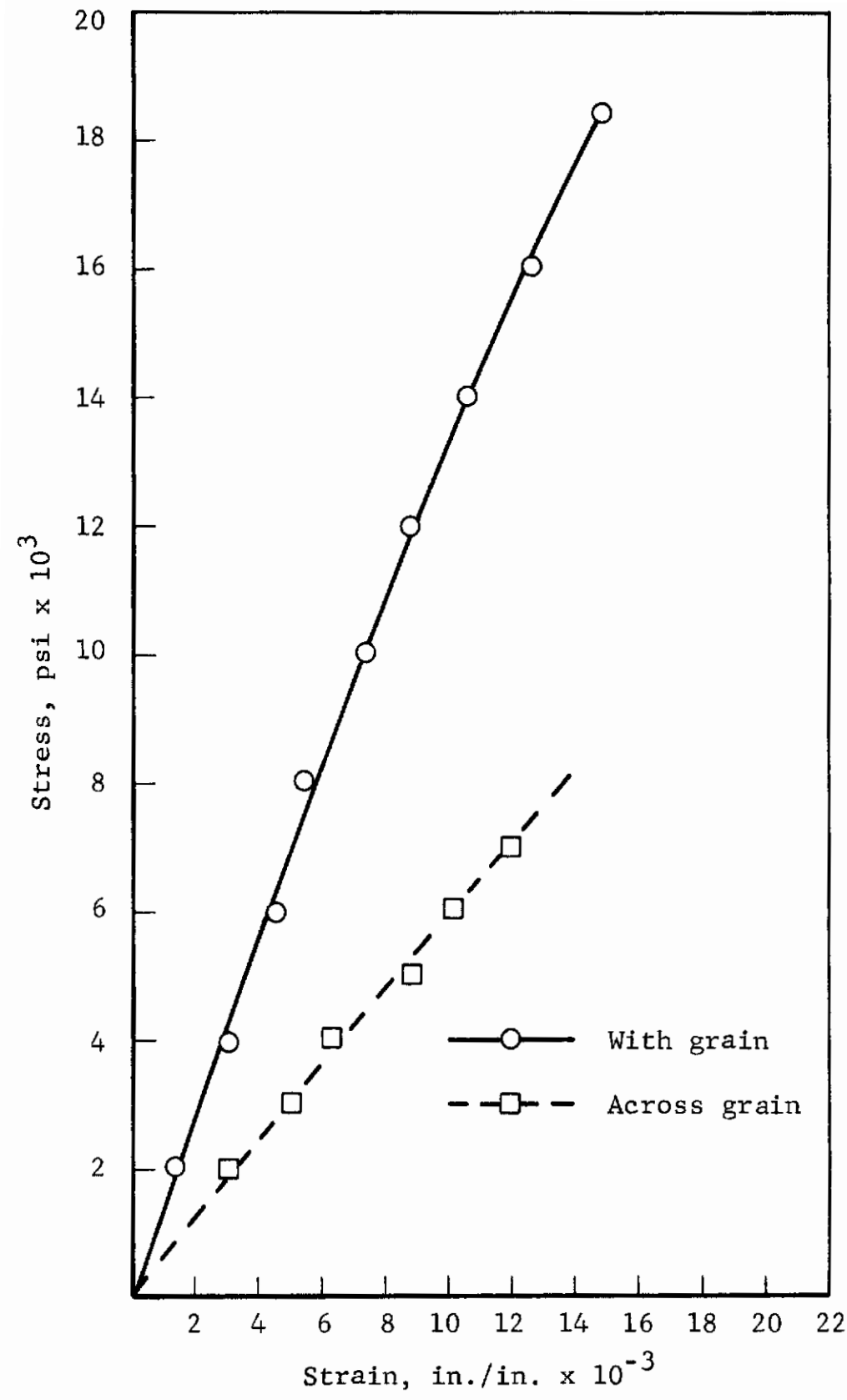

Figure 76. FLEXURAL STRESS VS DEFLECTION CURVE OF JTA GRAPHITE AT 1800°F

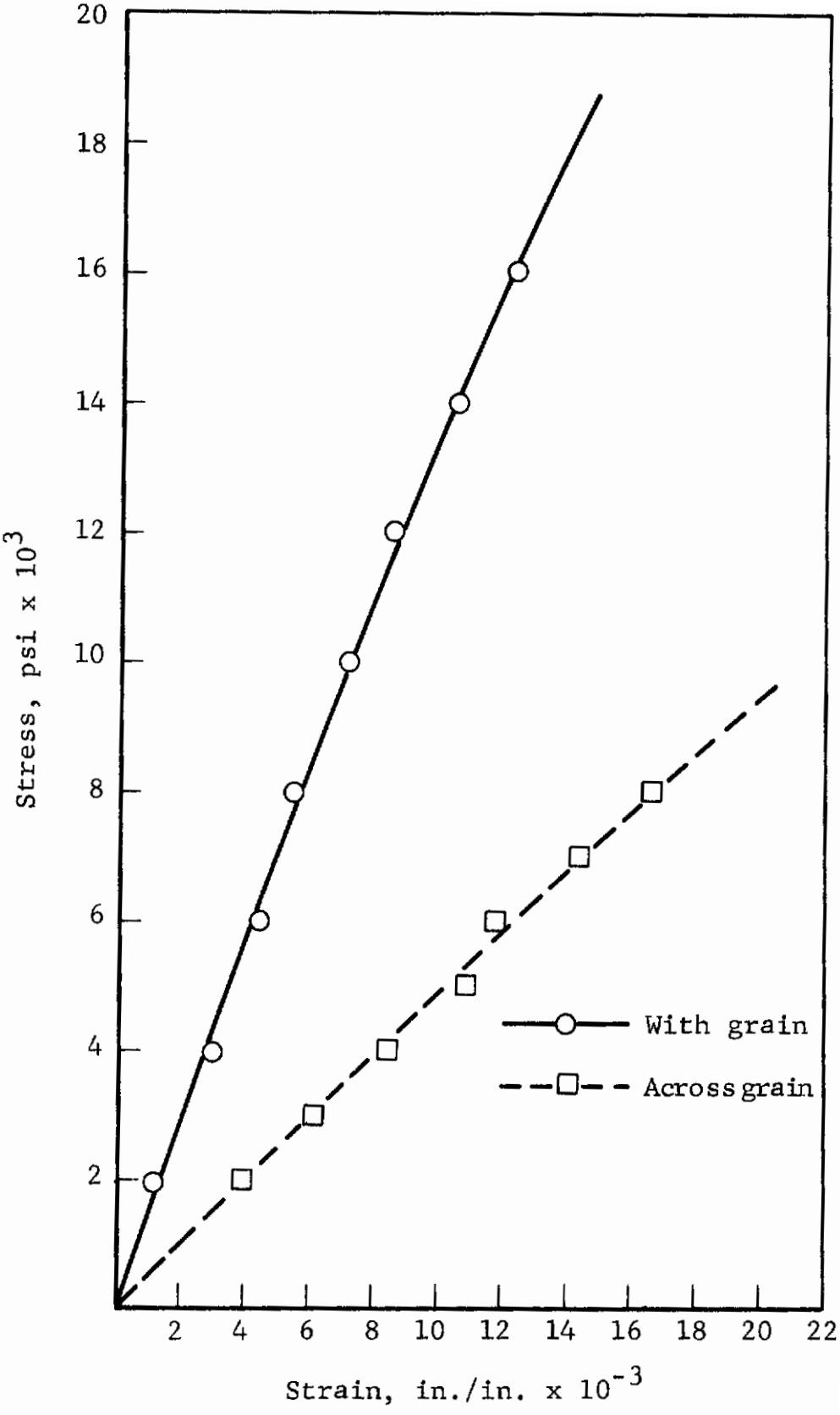

Figure 77. FLEXURAL STRESS VS DEFLECTION CURVE OF JTA GRAPHITE AT 2750°F

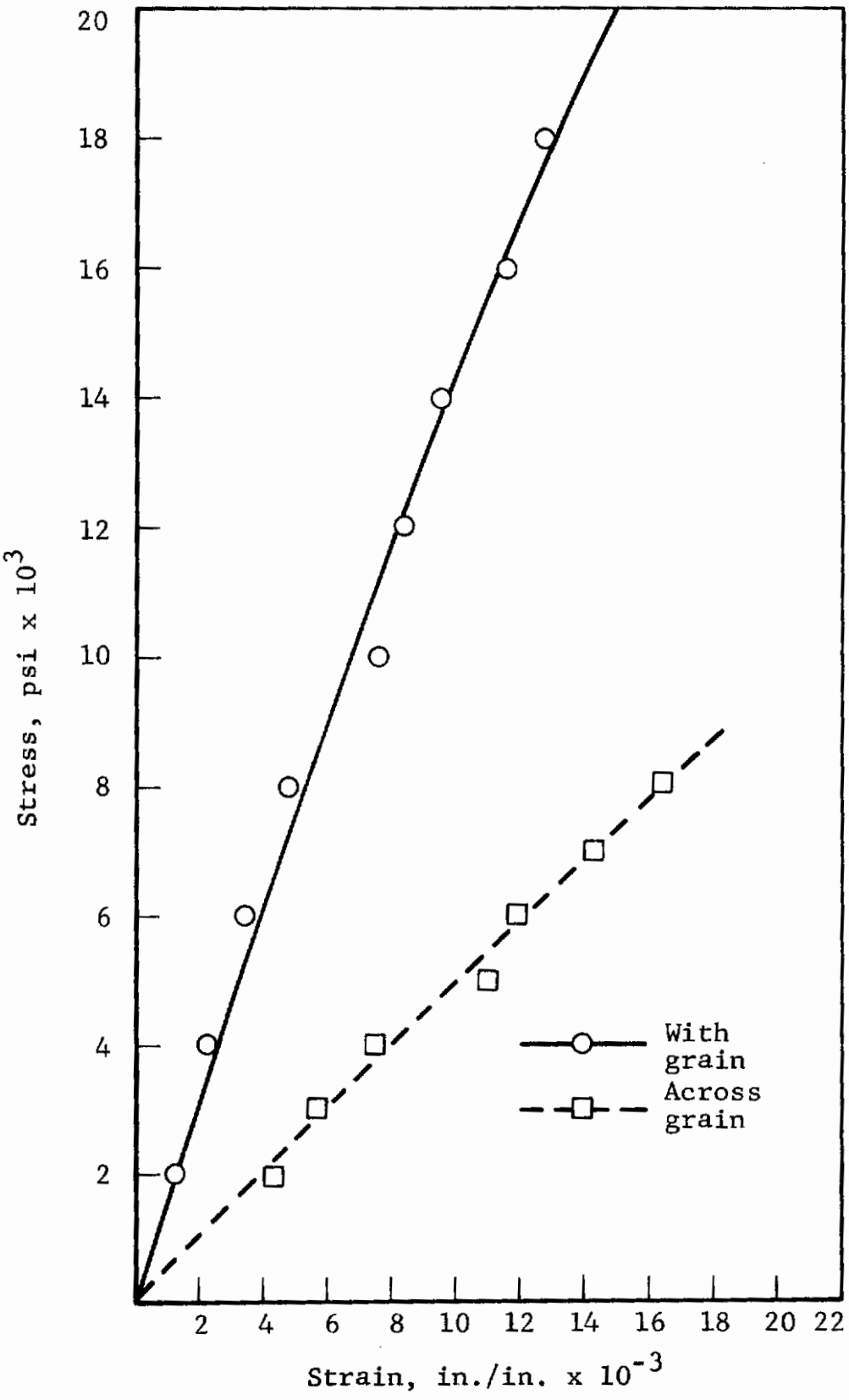

Figure 78. FLEXURAL STRESS VS DEFLECTION CURVE OF JTA GRAPHITE AT 3200°F

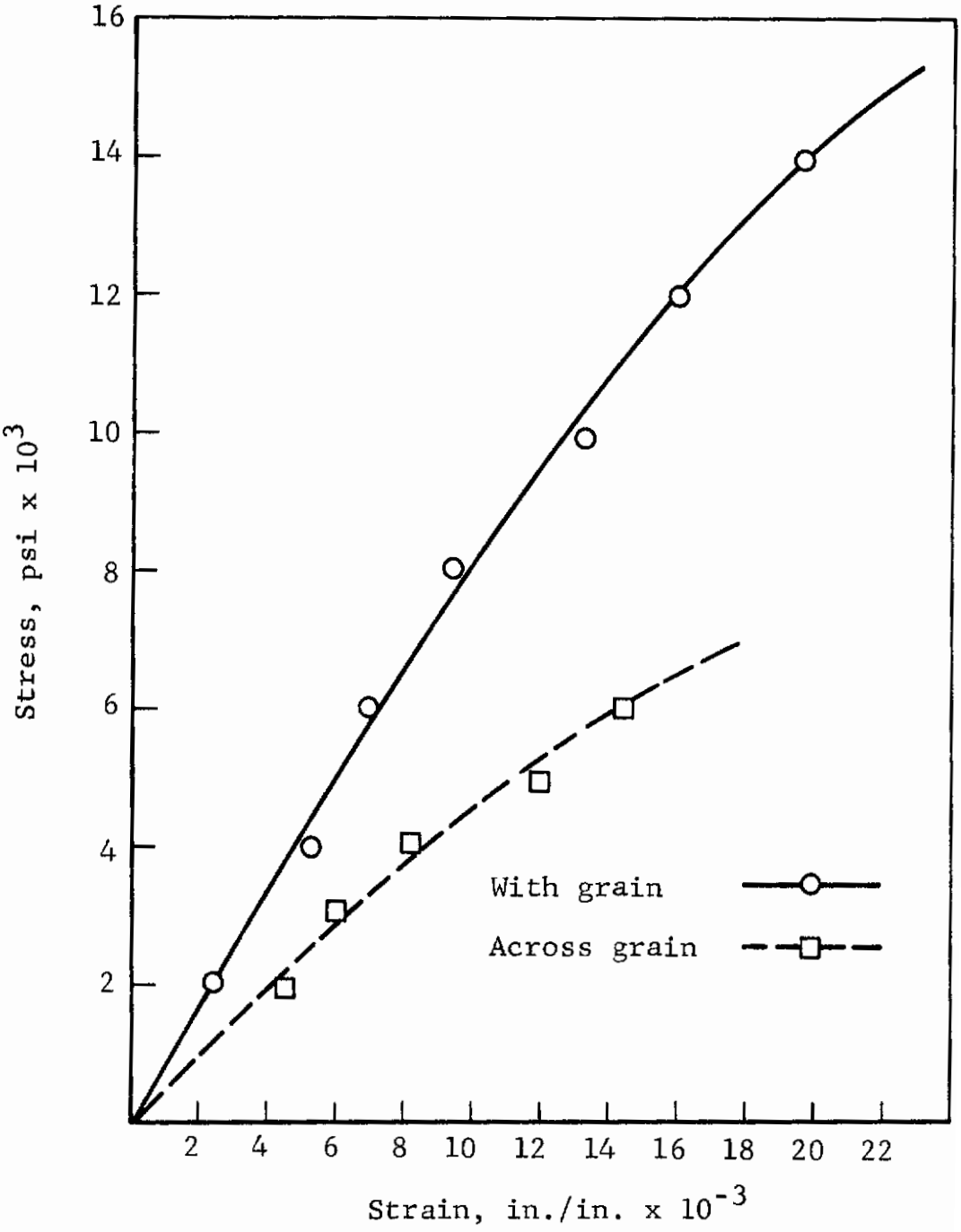

Figure 79. FLEXURAL STRESS VS DEFLECTION CURVE OF JTA GRAPHITE AT 3600°F

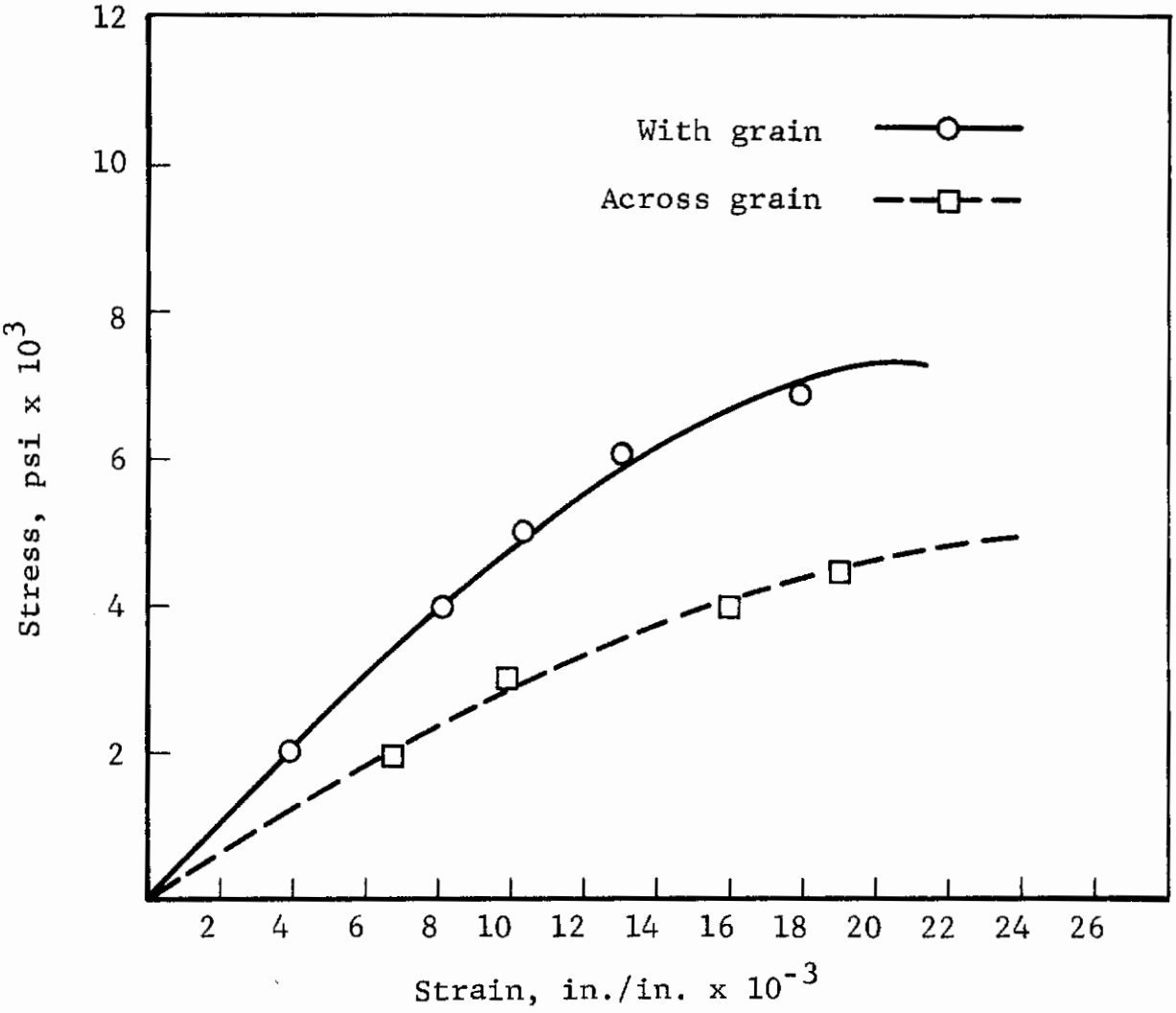

Figure 80. FLEXURAL STRESS VS DEFLECTION CURVE OF JTA GRAPHITE AT 4000°F

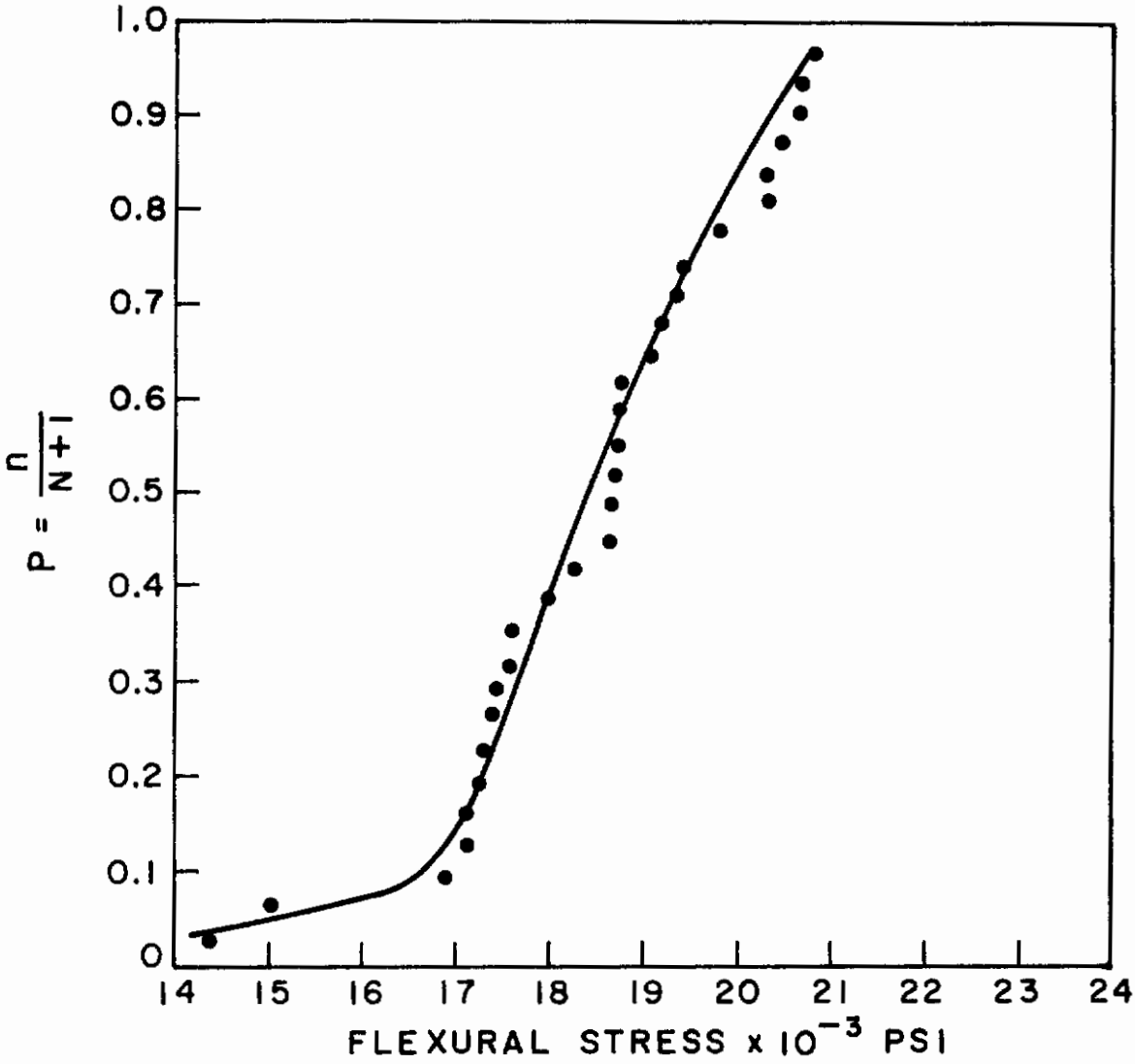

Figure 81. DISTRIBUTION CURVE FOR WITH GRAIN FLEXURAL STRENGTH IN AN INERT ATMOSPHERE AT 1832°F

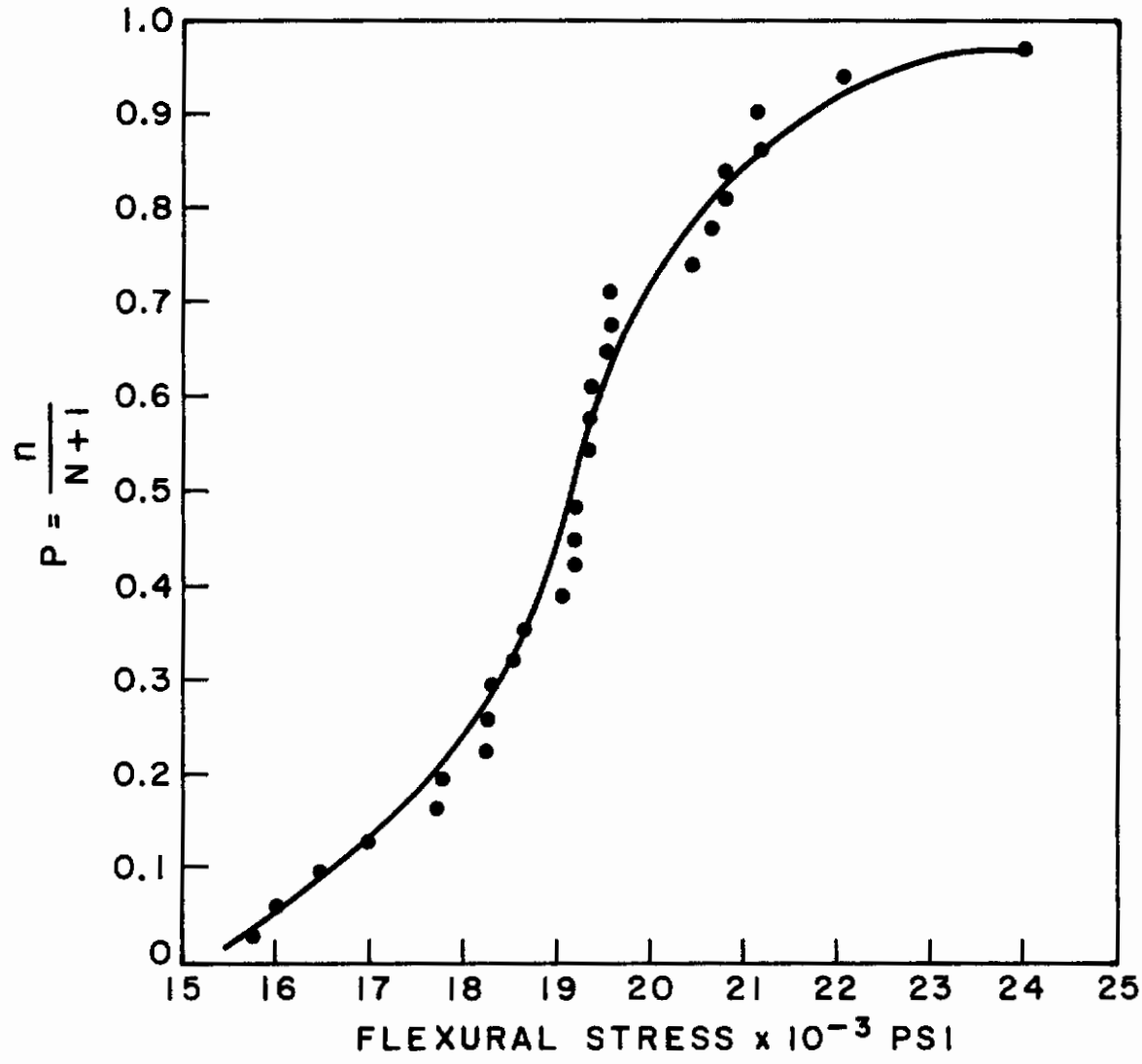

Figure 82. DISTRIBUTION CURVE FOR WITH GRAIN FLEXURAL STRENGTH IN AN INERT ATMOSPHERE AT 2732°F

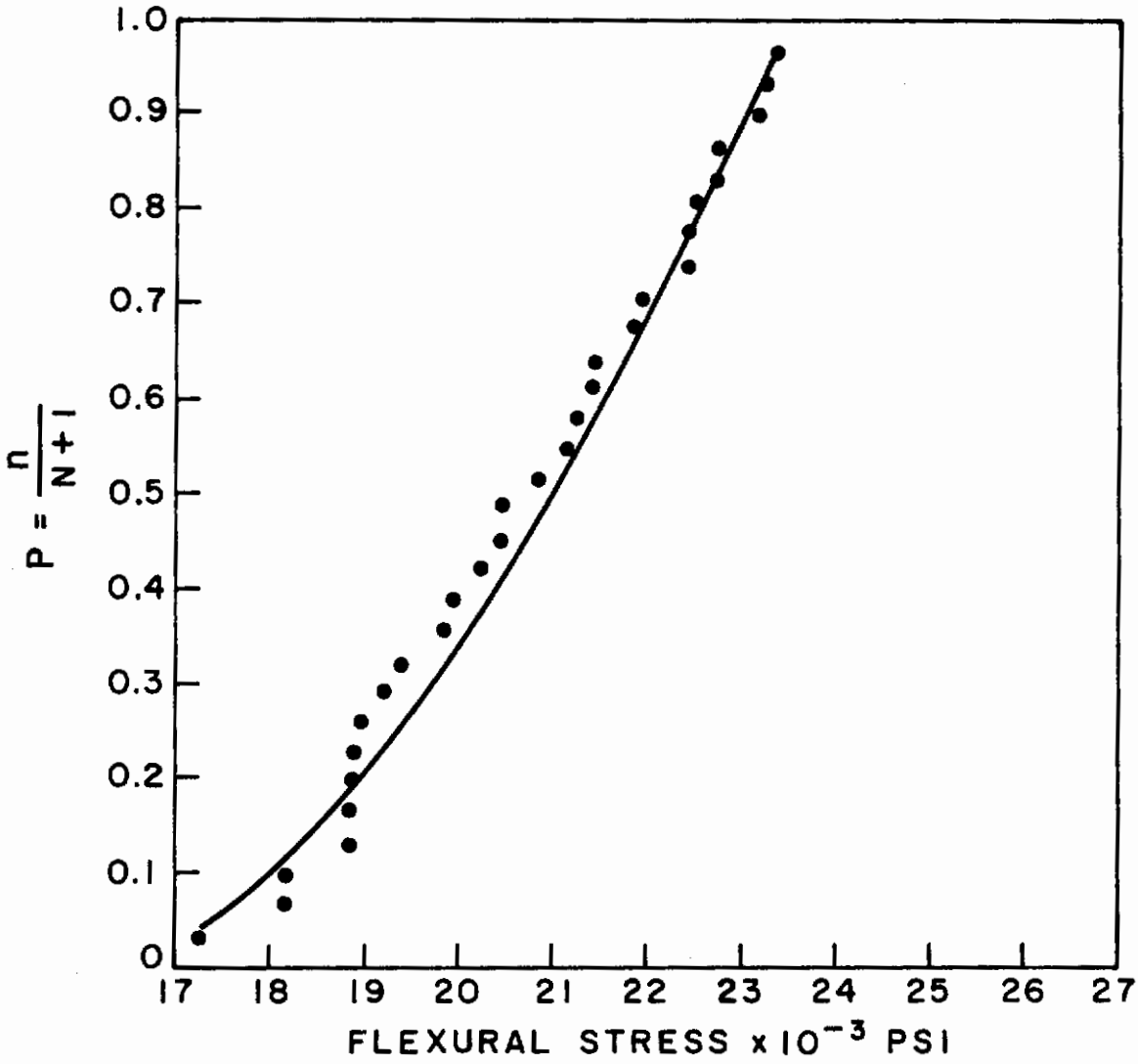

Figure 83. DISTRIBUTION CURVE FOR WITH GRAIN FLEXURAL STRENGTH IN AN INERT ATMOSPHERE AT 3182°F

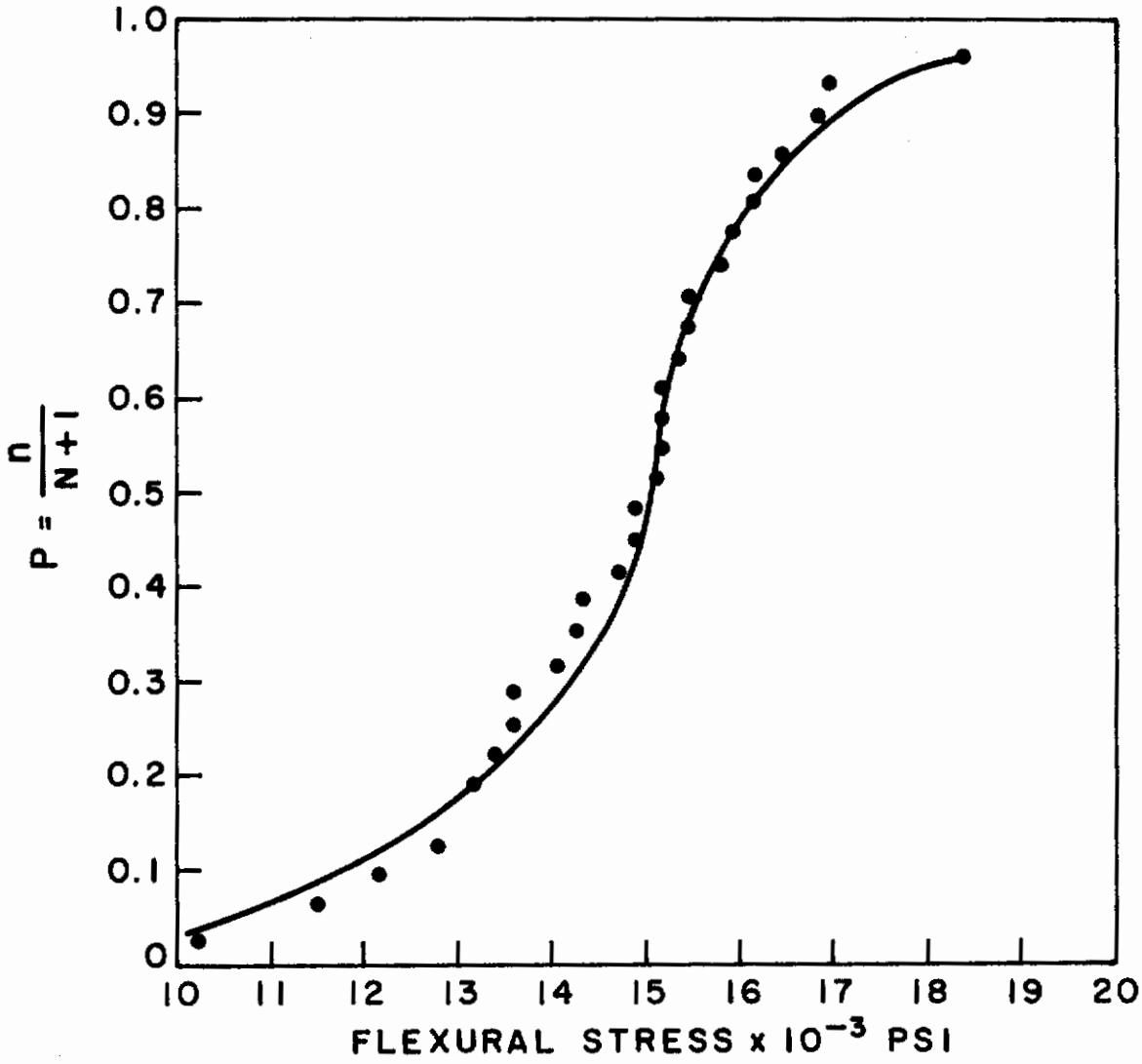

Figure 84. DISTRIBUTION CURVE FOR WITH GRAIN FLEXURAL STRENGTH IN AN INERT ATMOSHPERE AT 3632°F

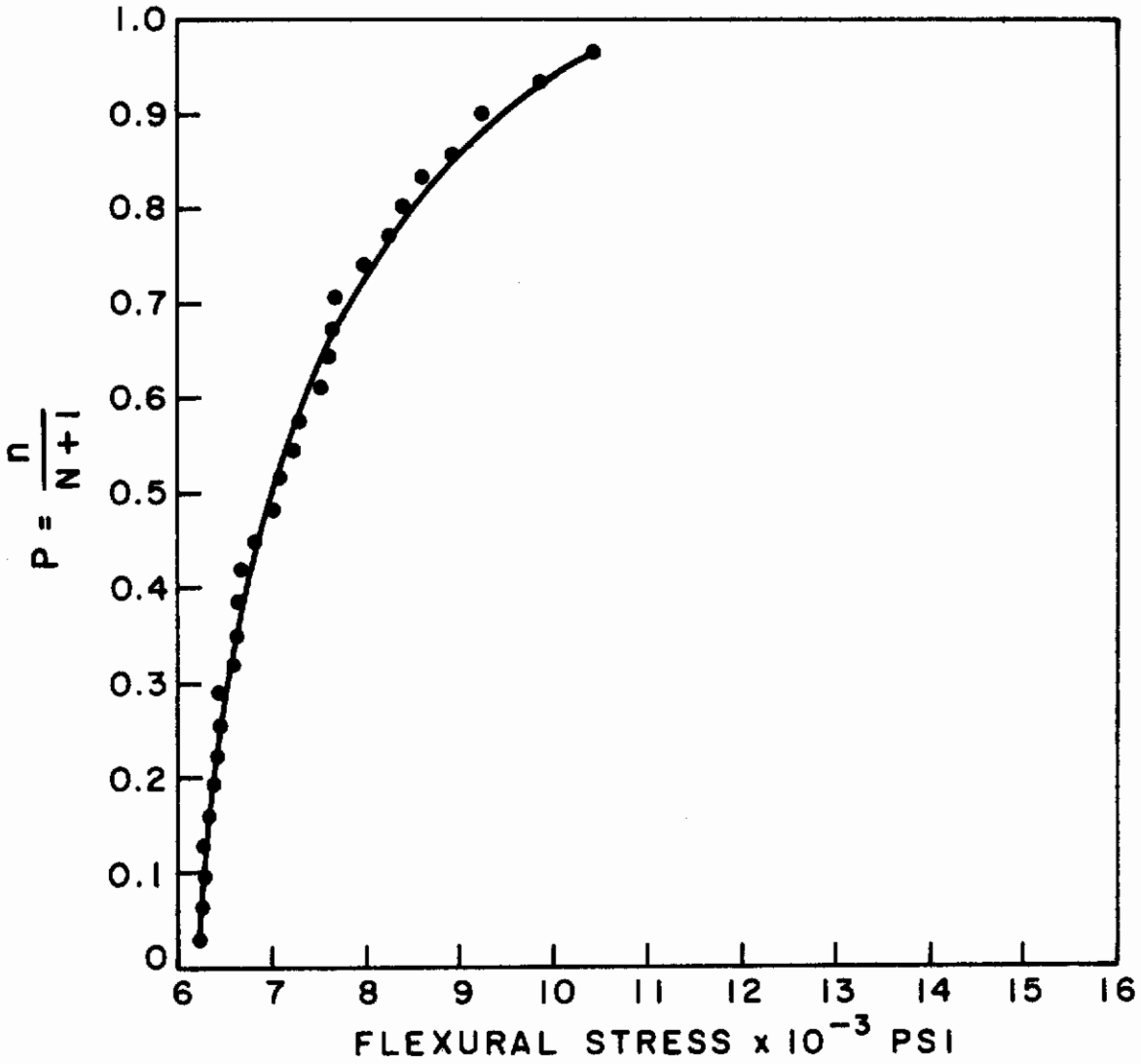

Figure 85. DISTRIBUTION CURVE FOR WITH GRAIN FLEXURAL STRENGTH IN AN INERT ATMOSPHERE AT 3992°F

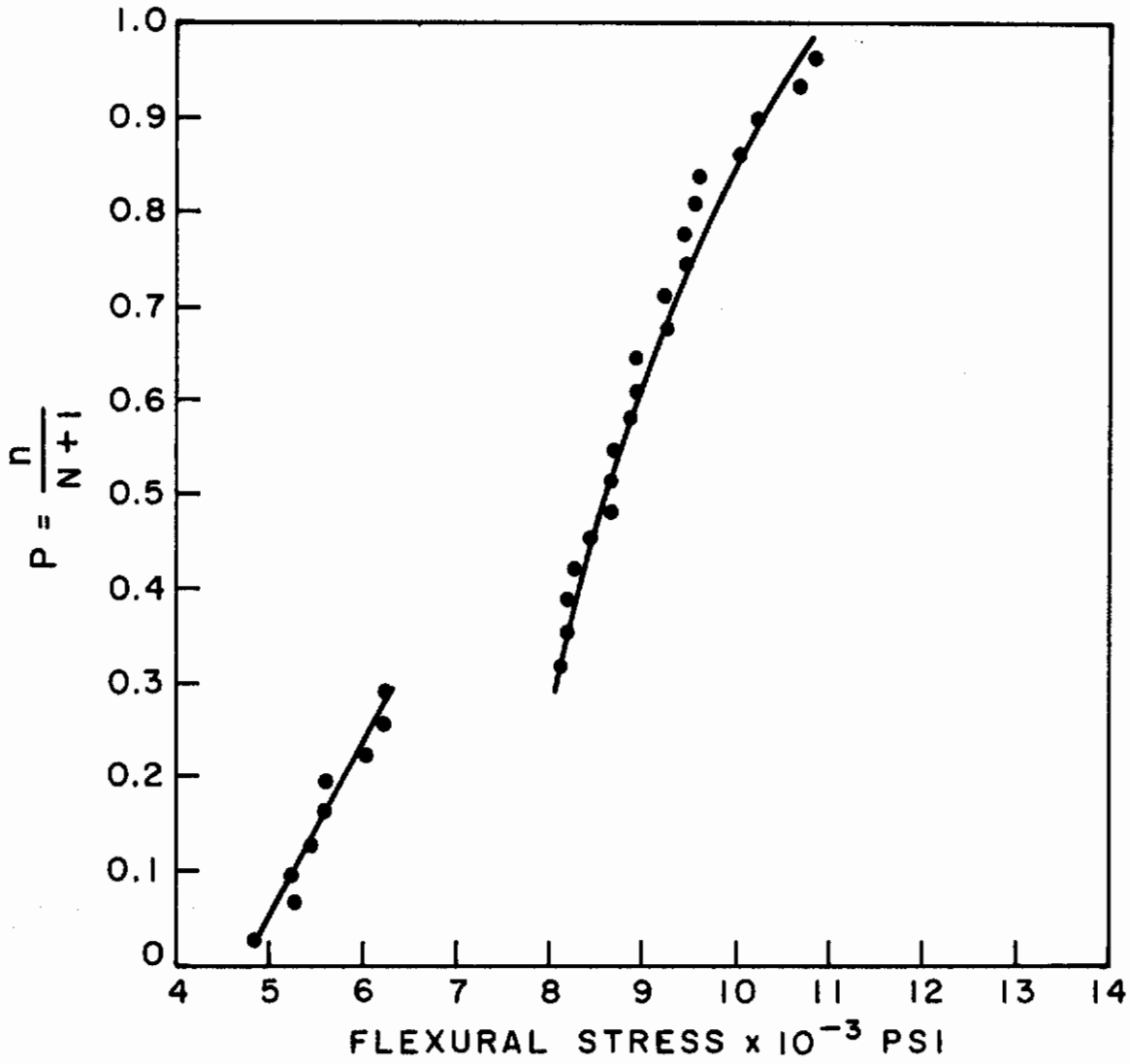

Figure 86. DISTRIBUTION CURVE FOR ACROSS GRAIN FLEXURAL STRENGTH IN AN INERT ATMOSPHERE AT 1832°F

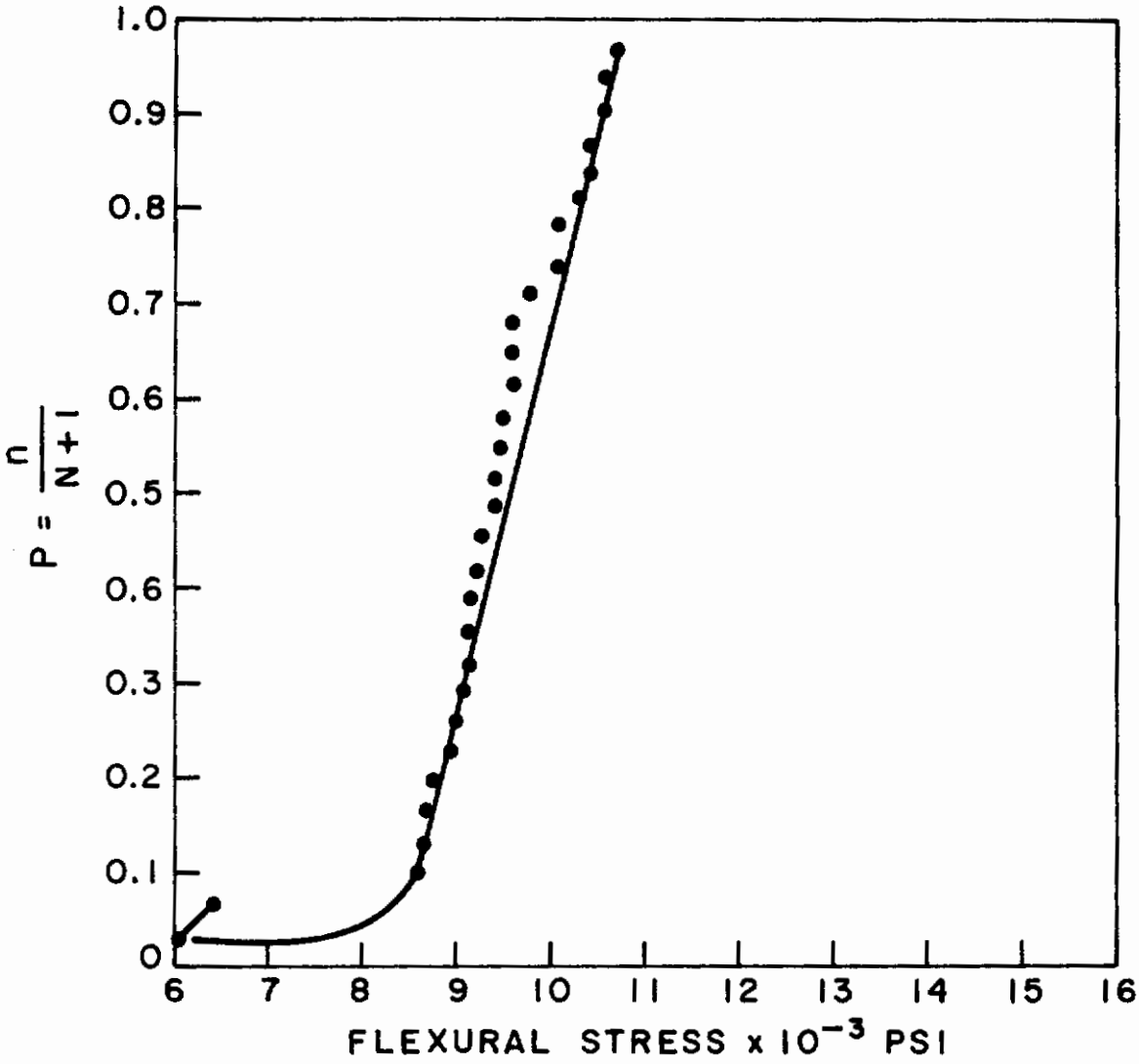

Figure 87. DISTRIBUTION CURVE FOR ACROSS GRAIN FLEXURAL STRENGTH IN AN INERT ATMOSPHERE AT 2732°F

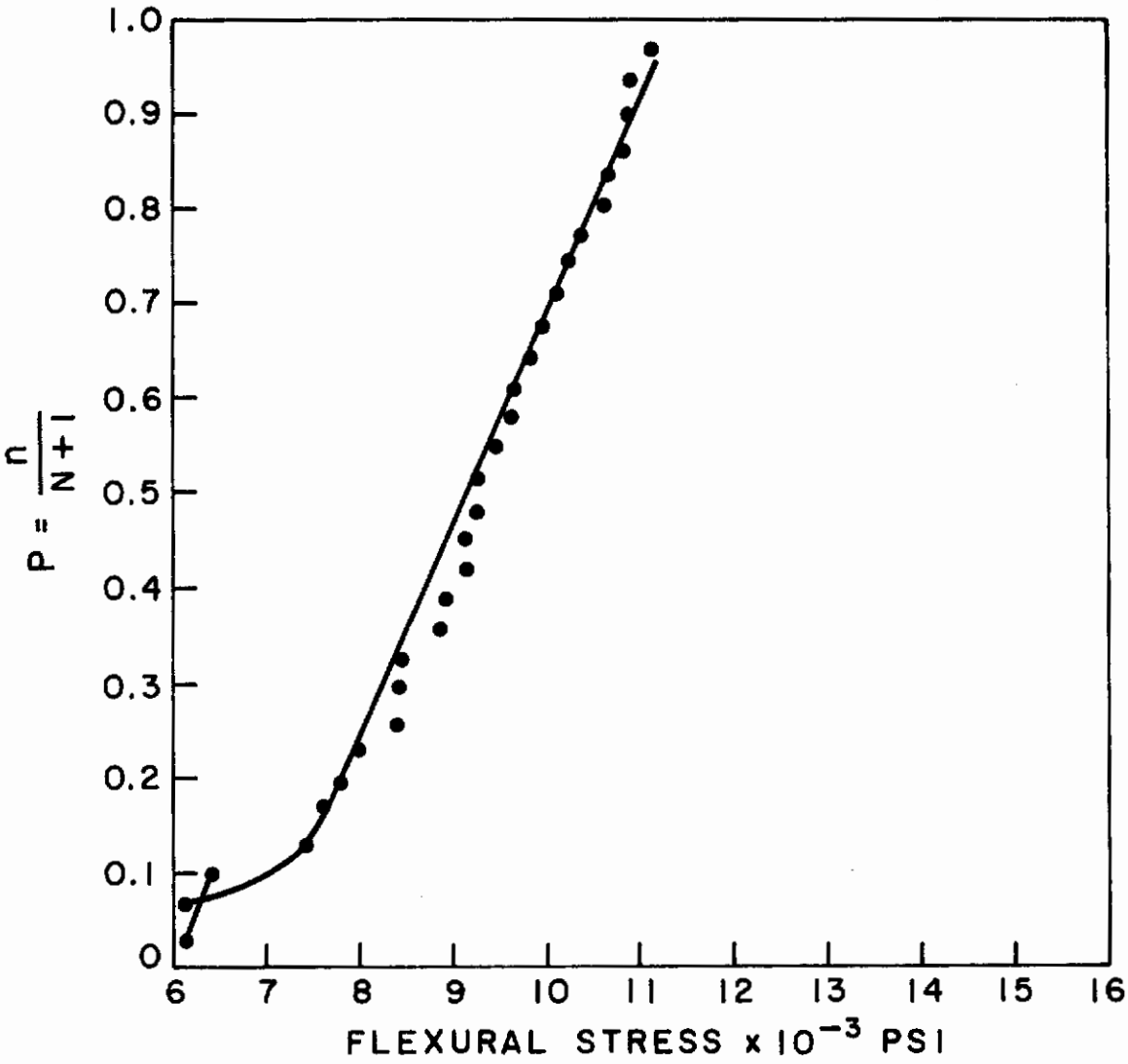

Figure 88. DISTRIBUTION CURVE FOR ACROSS GRAIN FLEXURAL STRENGTH IN AN INERT ATMOSPHERE AT 3182°F

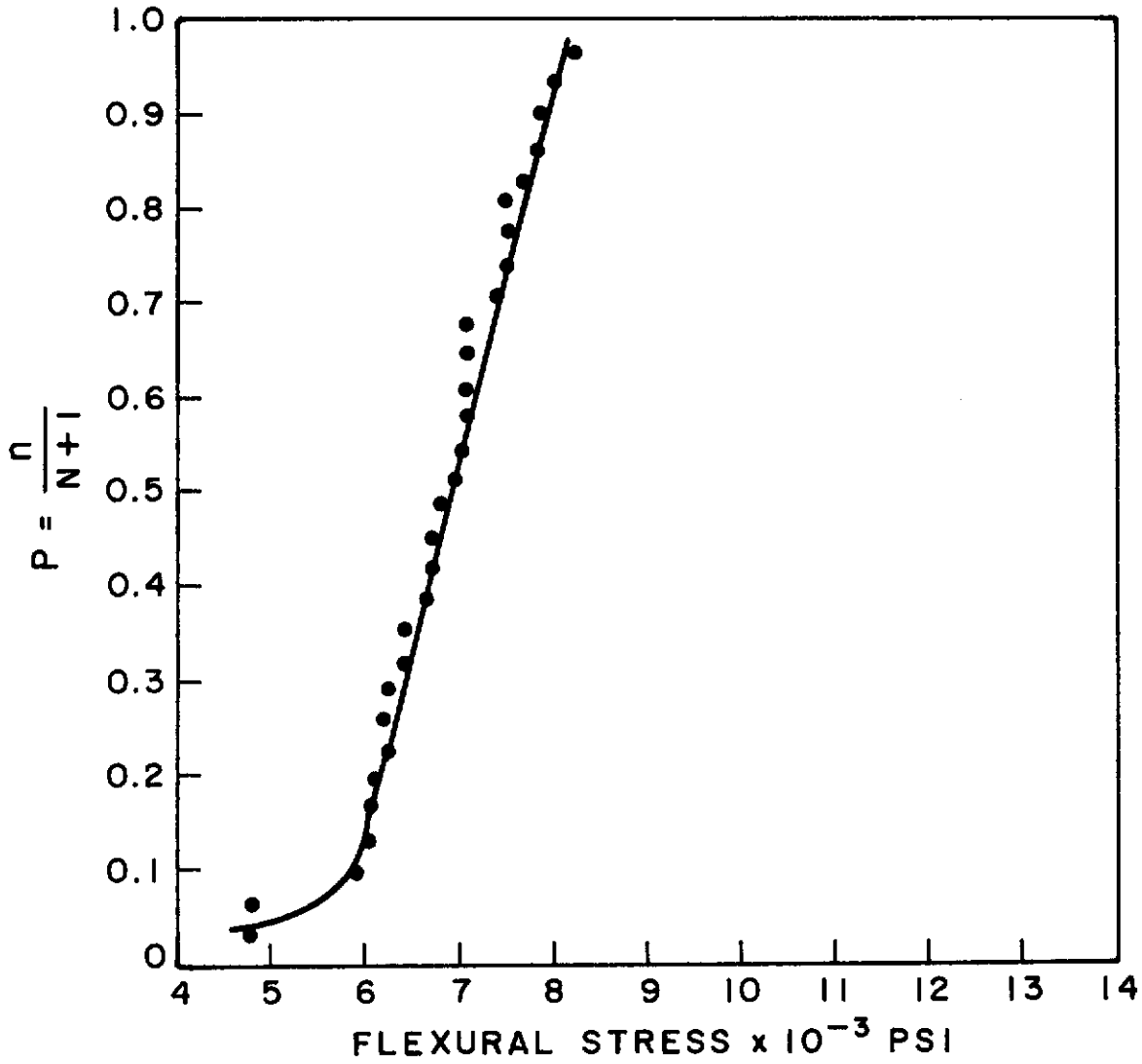

Figure 89. DISTRIBUTION CURVE FOR ACROSS GRAIN FLEXURAL STRENGTH IN AN INERT ATMOSPHERE AT 3632°F

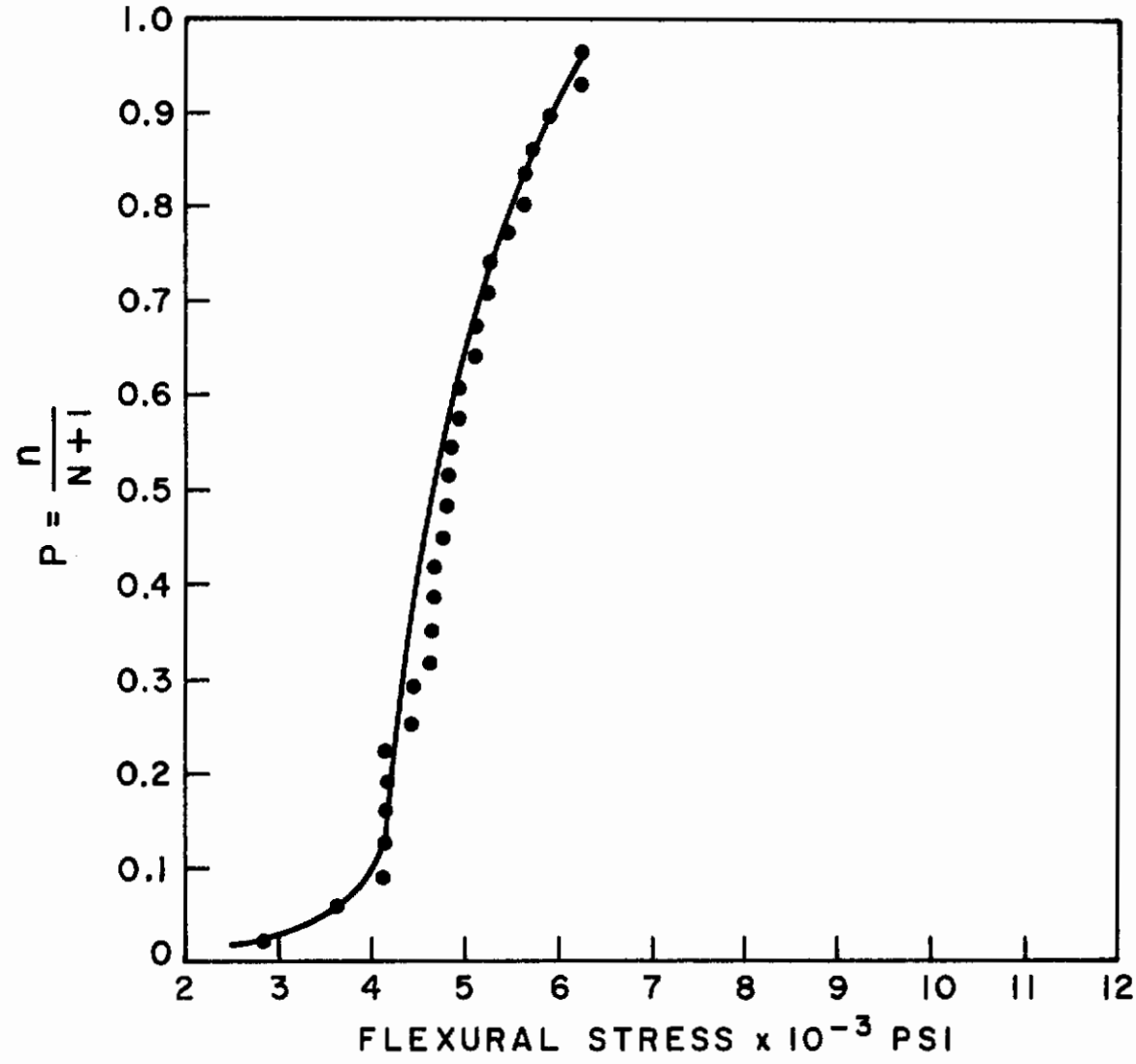

Figure 90. DISTRIBUTION CURVE FOR ACROSS GRAIN FLEXURAL STRENGTH IN AN INERT ATMOSPHERE AT 3992°F

Table XVII. FLEXURAL DATA FOR JTA GRAPHITE

Temp., °F	Orientation	Number of tests	Atmosphere	m_1	m_2	ν, %	m_{calc} ($m = 1.2\nu$)
Room	With grain		Air				
	Across grain		Air				
1832	With grain	30	Argon	14.7	8.00	8.40	14.300
	Across grain	30	Argon	7.5	8.33	21.85	5.504
2732	With grain	30	Argon	12.5		9.33	12.903
	Across grain	30	Argon	22.5	8.33	16.24	7.389
3182	With grain	30	Argon	32.5	10.00	8.27	14.510
	Across grain	30	Argon	7.00	10.00	15.76	7.595
3632	With grain	30	Argon	9.85		11.58	10.360
	Across grain	30	Argon	9.25		13.40	8.955
3992	With grain	30	Argon	3.33	28.33		
	Across grain	30	Argon	6.875		18.58	6.451
	With grain		Argon	4.00	37.50	16.08	7.460
	Across grain		Argon	1.17			

For one set of test conditions, test samples were exposed to the temperatures, air pressures, and exposure times shown in Table VI. After exposure, the test samples were tested under ambient conditions. The effect of exposure environment is shown in Figures 35 through 37. JTA graphite exhibited no loss in strength at temperatures as high as 3632°F and air pressures of 10^{-6} torr. However, under atmospheric air pressures, it began to show strength loss at 1830°F after 20 min and an approximately 20% strength loss after 1 hr. At 3180°F the strength loss was greater than 60% after 1 hr, and at 3632°F there was almost complete strength loss after 1 hr. It must be remembered that 1/4-in.^{2}-cross-section specimens were exposed. It is suggested that the reader refer back to Section IV3c to understand the true meaning of these tests.

The second test environment consisted of high temperatures and ambient conditions. The flexural data from inert- and the two types of air-environment conditions are summarized in Figures 91 and 92. Specimens exposed to an air environment and tested under ambient conditions exhibited an increasingly rapid strength loss with temperature. However, the data obtained from tests made at high temperatures under ambient atmospheric conditions exhibited the same type of behavior as samples tested at high temperatures under inert environmental conditions. The strengths were about one third lower than those obtained for JTA tested in an inert atmosphere.

These experiments showed quite graphically that to estimate true behavior of a material in a specific environment, the environment must be simulated when testing is performed.

5. COMPRESSION

Compressive strength of JTA graphite was obtained for cylindrical specimens 1/4 in. in diameter x 3/4 in. long. Tests were performed under ambient conditions in a 20,000-lb Instron universal testing machine. The specimens were axially loaded, and a 1-in. spherical loading head was used to help align the axis of force with the axis of the specimens. Elastic moduli were obtained by using SR-4 electrical strain gages at the sides of the specimens.

The high-temperature tests were performed in a Brew testing furnace, and stress-strain curves were obtained by using a Baldwin high-temperature mechanical extensometer. High-temperature oxidation tests were made in a manner similar to that of the tensile and flexural tests. Figure 93 shows the setup for these tests. Deflectometer readings were made by using a double LVDT extensometer.

a. Ambient-Environment Tests

Distribution curves for tests conducted at room temperature are shown in Figures 94 and 95. The average strength of the with-grain orientation was 33,000 psi, with a coefficient of

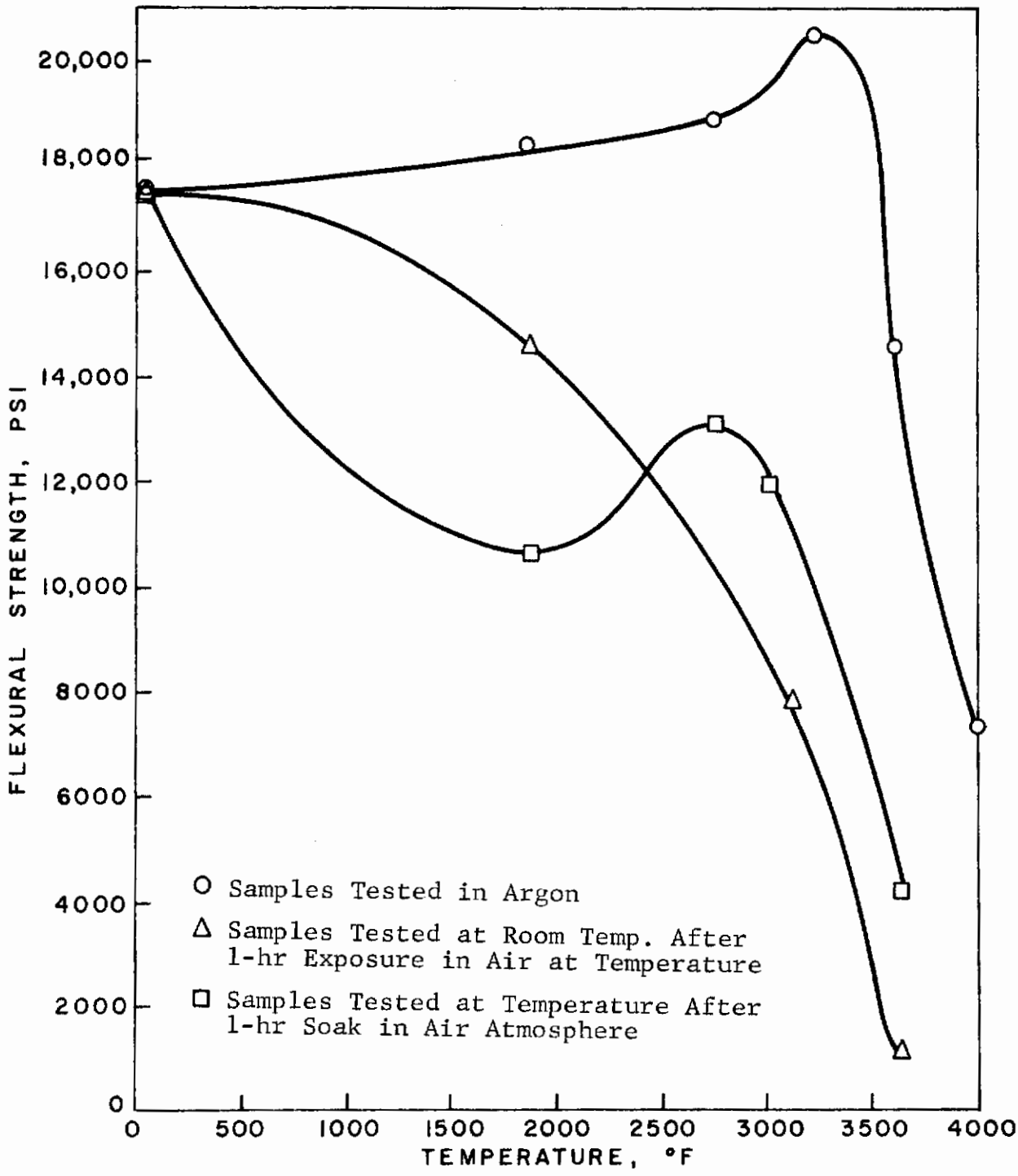

Figure 91. EFFECT OF ATMOSPHERE ON FLEXURAL STRENGTH WITH GRAIN ORIENTATION OF JTA

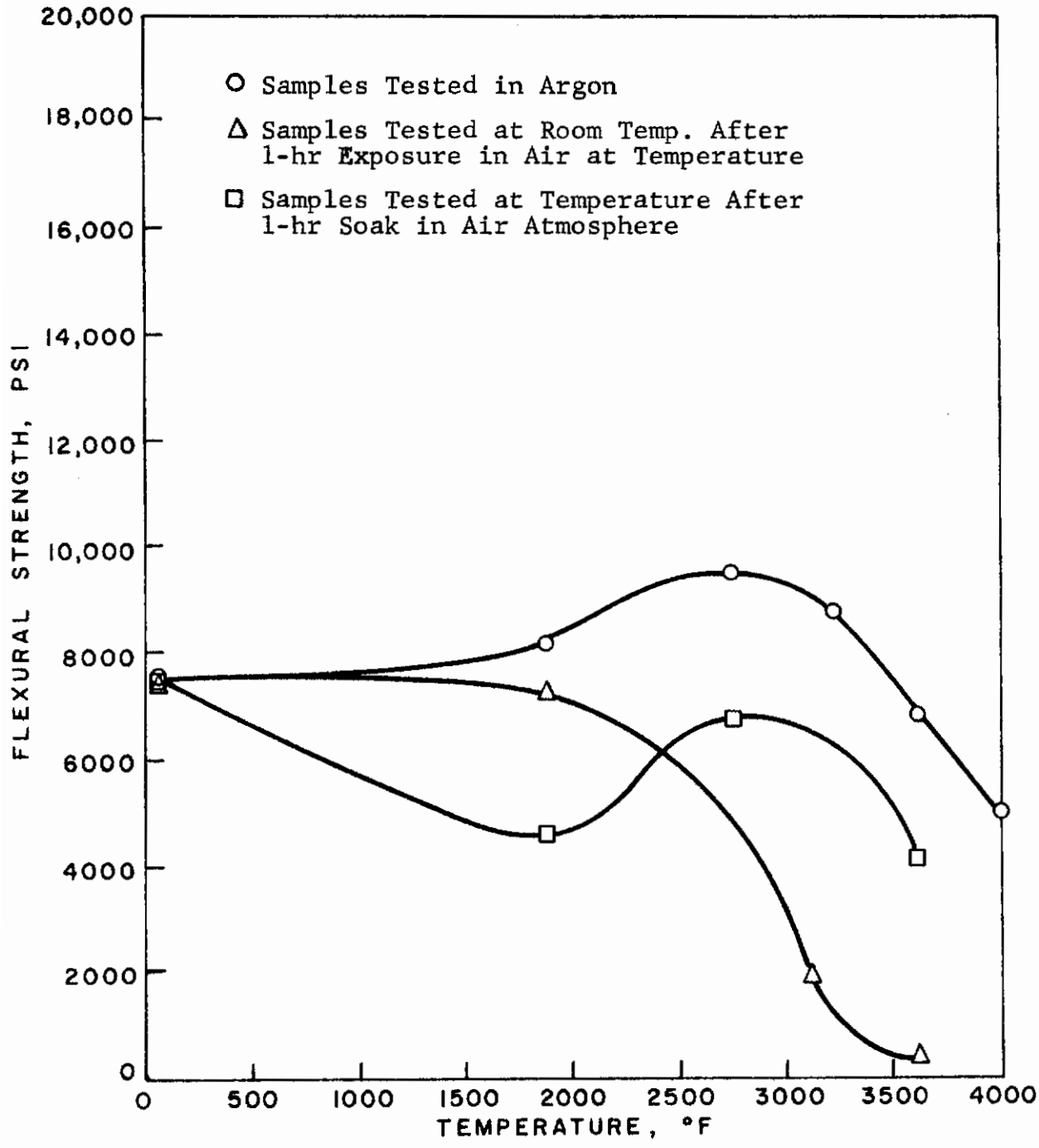

Figure 92. EFFECT OF ATMOSPHERE ON FLEXURAL STRENGTH OF ACROSS GRAIN ORIENTATION OF JTA

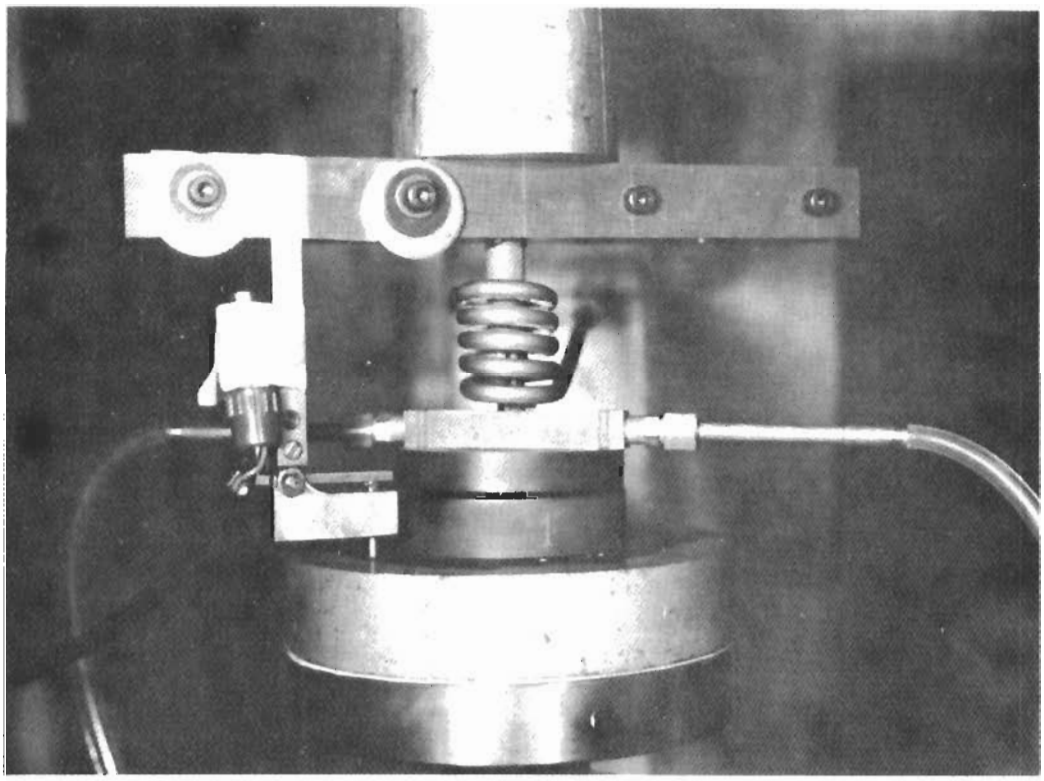

Figure 93. COMPRESSION DEFLECTOMETER
FOR HIGH-TEMPERATURE TESTS

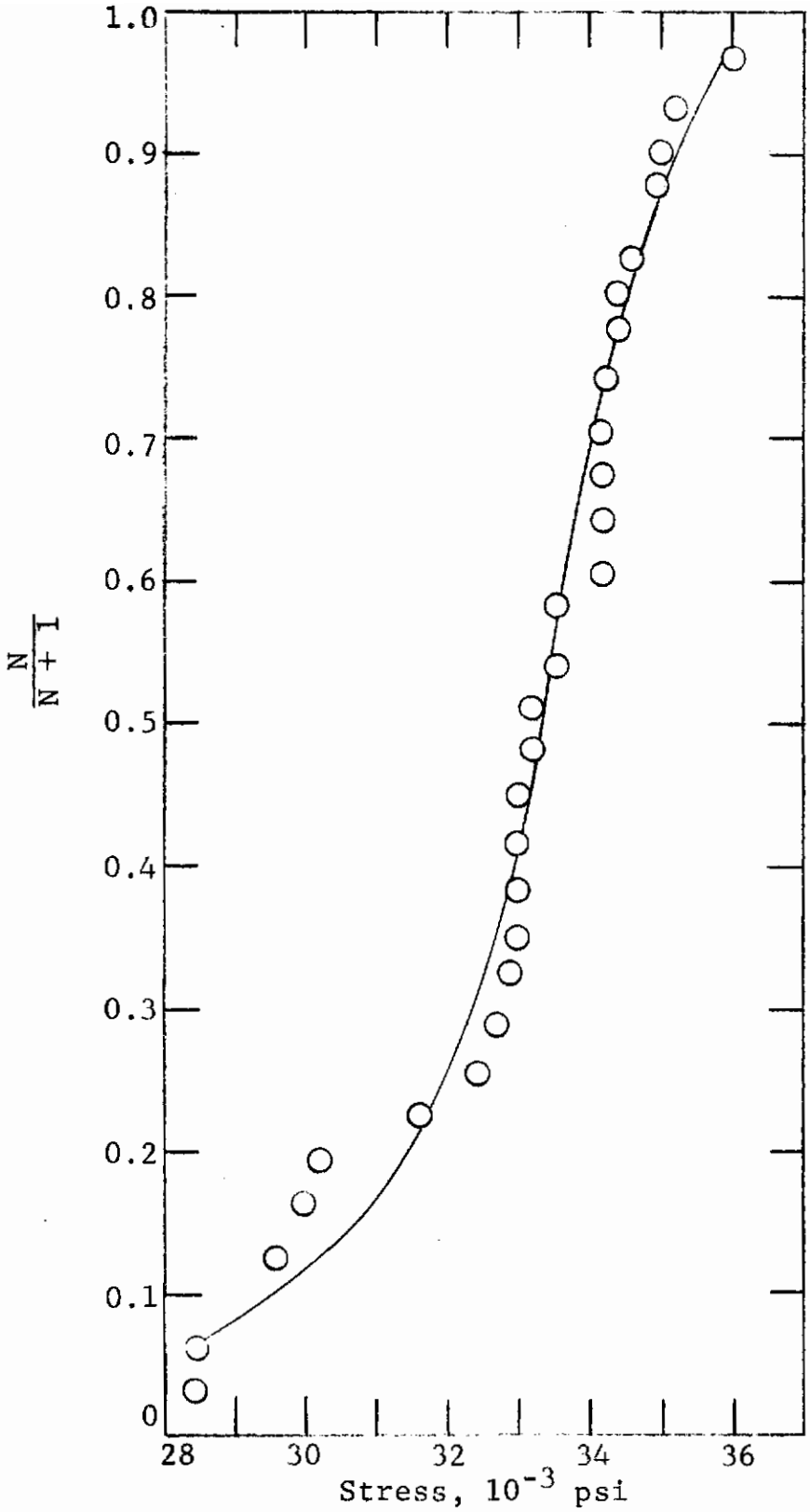

Figure 94. DISTRIBUTION CURVE FOR JTA TESTED IN COMPRESSION (W/G, 77°F, in air)

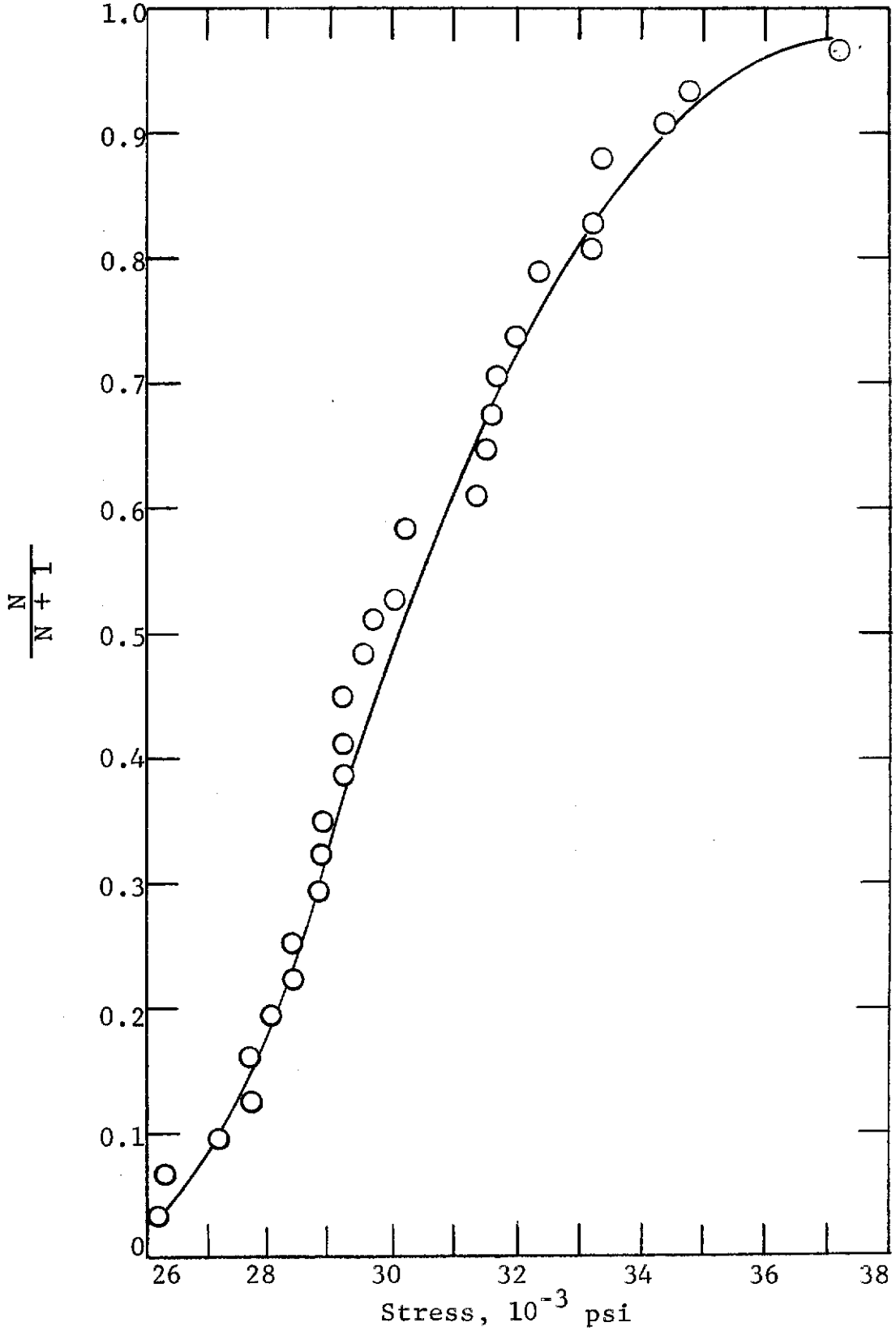

Figure 95. DISTRIBUTION CURVE FOR JTA TESTED IN COMPRESSION (A/G, 77°F, in air)

variation of 5.00%; the average strength of the across-grain orientation was 30,325 psi, with a coefficient of variation of 9.46%. It is interesting to note that the strength distributions were similar to those for flexure -- S shaped for the with-grain orientation and almost straight for the across-grain orientation. However, this observed phenomenon does not hold for the high-temperature strength-distribution plots, as discussed in Section IV5b.

b. High-Temperature Inert-Atmosphere Tests

Data obtained from these experiments are listed in Table XVIII, and distribution curves are shown in Figures 96 through 101. It is interesting to note that the with- and the across-grain flexural-strength-distribution curves are similar to those observed for tensile data in that there is no real difference in the plots. At this time no reason can be given for the different behavior. However, the different behavior exhibited by the material tested uniaxially and in flexure is interesting.

A Weibull analysis of the data (Figures 102 through 109) indicate that when $\sigma_u = 0$, m is approximately 12. However, there are indications that other factors, which may be due to material variability or test procedures, influence the shape of the curves. No clear evidence is available for the observed variations of the Weibull plots or changes in the m values. These results indicate that the conservative design approach discussed in Section IV1 is the only rational method for obtaining design criteria for JTA graphite at this time.

c. High-Temperature Ambient-Atmosphere Tests

The results of these experiments are listed in Table XIX. A comparison of the ambient-temperature and high-temperature inert-atmosphere tests with the high-temperature ambient-atmosphere tests is shown in Figures 110 and 111. The curves show similar behavior for both with- and across-grain orientations. The strengths are about the same, with a secondary strength peak at 3200°F. The strength falls off rapidly beyond this peak. High-temperature strength tests in an ambient atmosphere showed a strength drop of approximately one third that obtained in an inert atmosphere.

6. TORSION

Attempts were made to obtain shear strength through the use of a torsion test. A spherical rig was set up to make these experiments. Since JTA is a brittle material, care had to be observed to make sure the sample was aligned in the axis of the torsion rig. Figure 112 shows a typical fracture for JTA in the across-grain and the with-grain orientations. As expected, the appearance of the fracture surface indicated that failure was due

Table XVIII. RESULTS OF COMPRESSION OXIDATION TESTS

Temp., °F	Orientation	Number of tests	$\bar{\sigma}$, psi	ν, %	E, psi
1832	With grain	12	16,000	2.85	6.46
	Across grain	12	15,200	5.15	2.83
2732	With grain	12	16,800	3.58	6.61
	Across grain	12	16,100	4.10	3.03
3182	With grain	6	21,830	3.82	
	Across grain	6	22,890	8.08	
3632	With grain	6	5,496	59.23	
	Across grain	6	83,700	61.25	

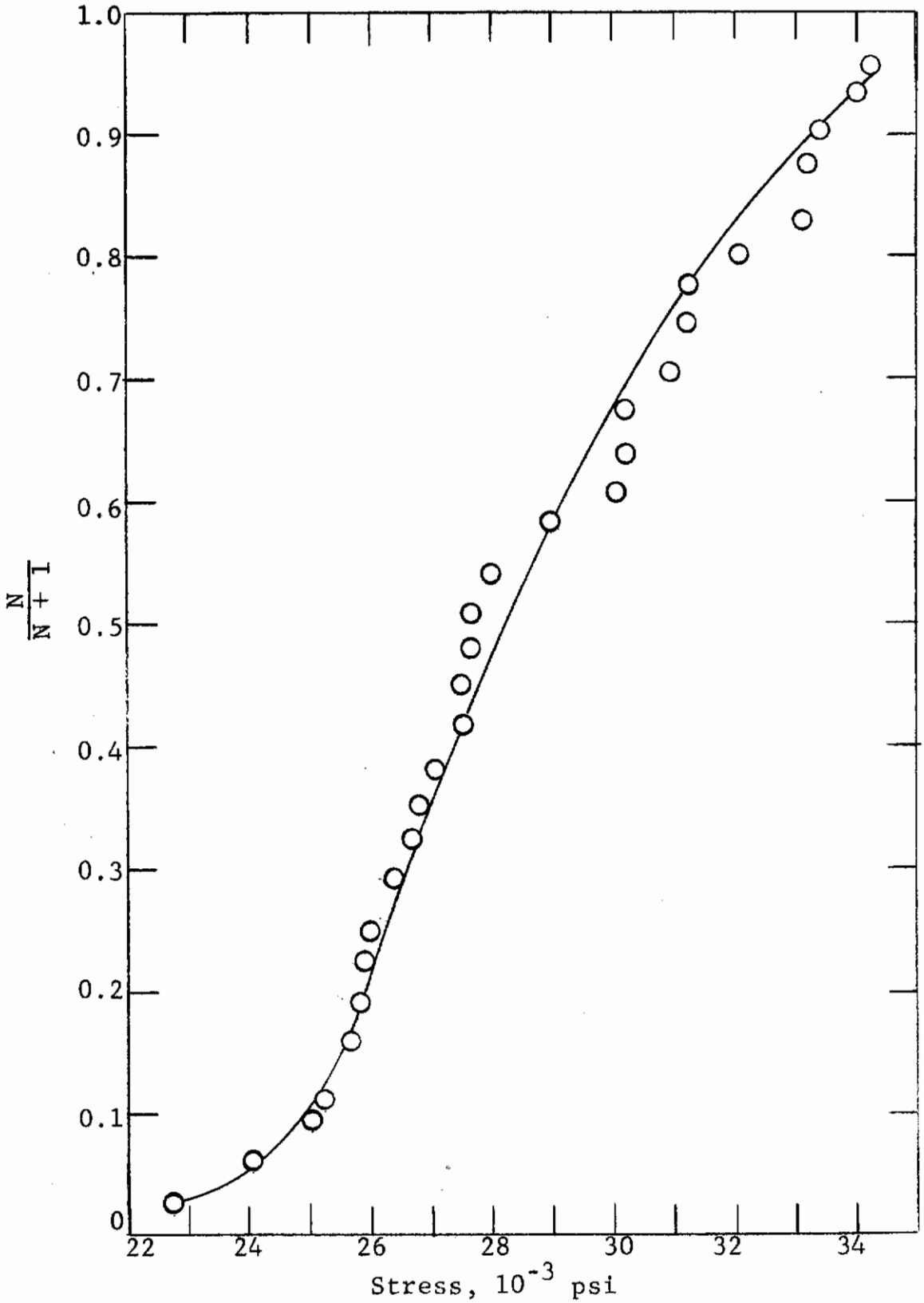

Figure 96. DISTRIBUTION CURVE FOR JTA TESTED IN COMPRESSION (W/G, 1832°F, in vacuum)

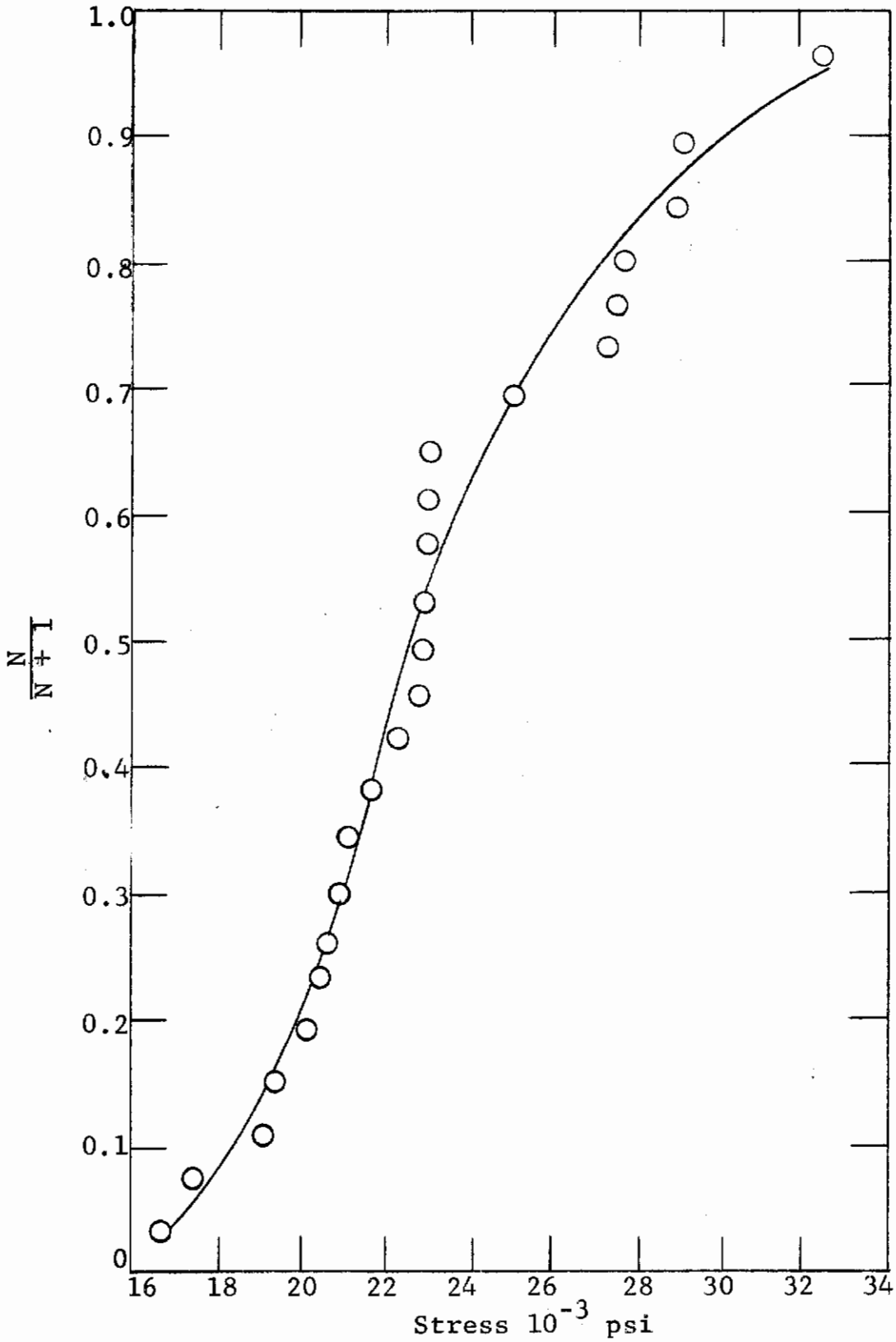

Figure 97. DISTRIBUTION CURVE FOR JTA TESTED IN COMPRESSION (W/C, 2732°F, in vacumm)

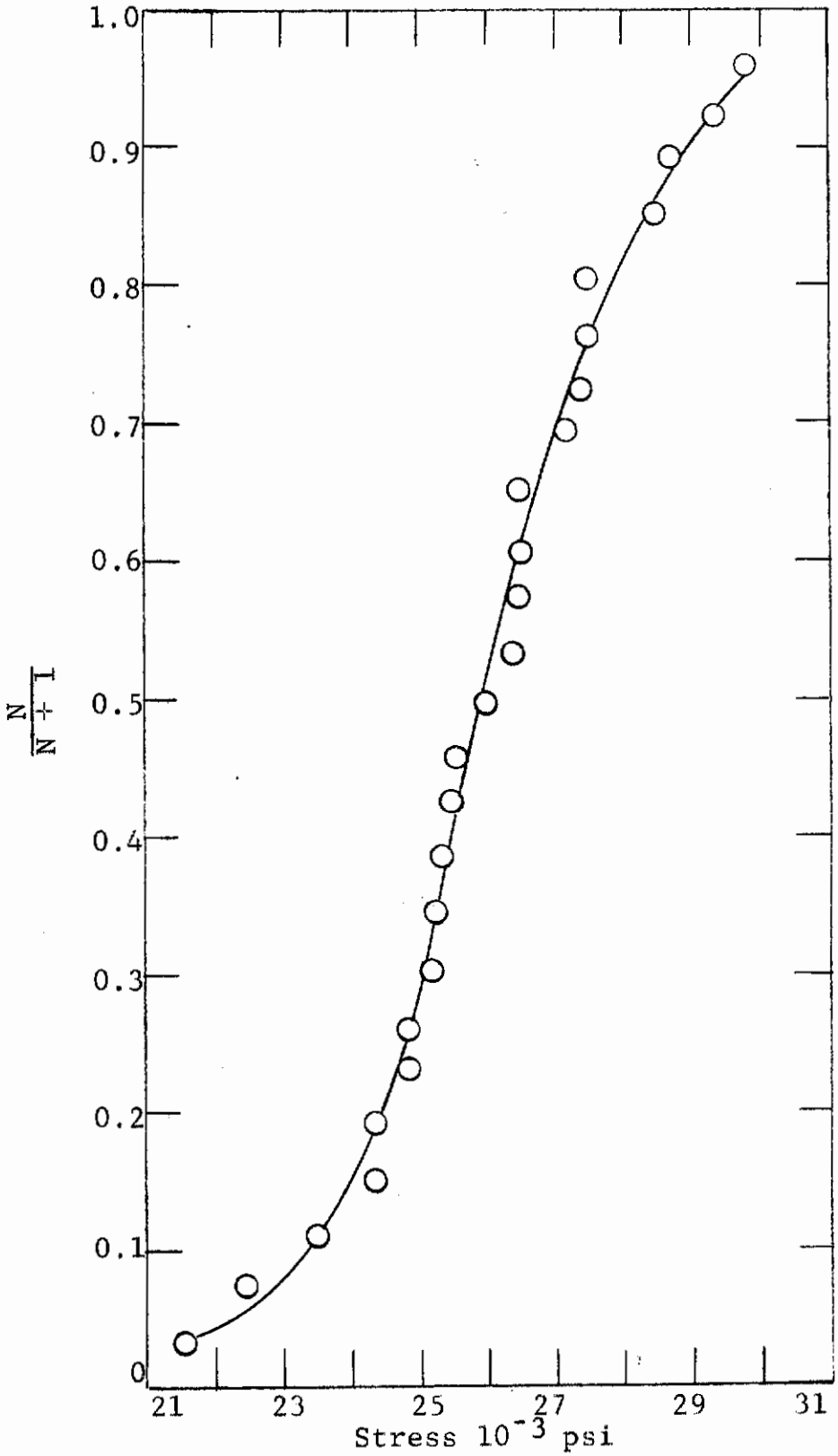

Figure 98. DISTRIBUTION CURVE FOR JTA TESTED IN COMPRESSION (W/C, 3182°F, in vacuum)

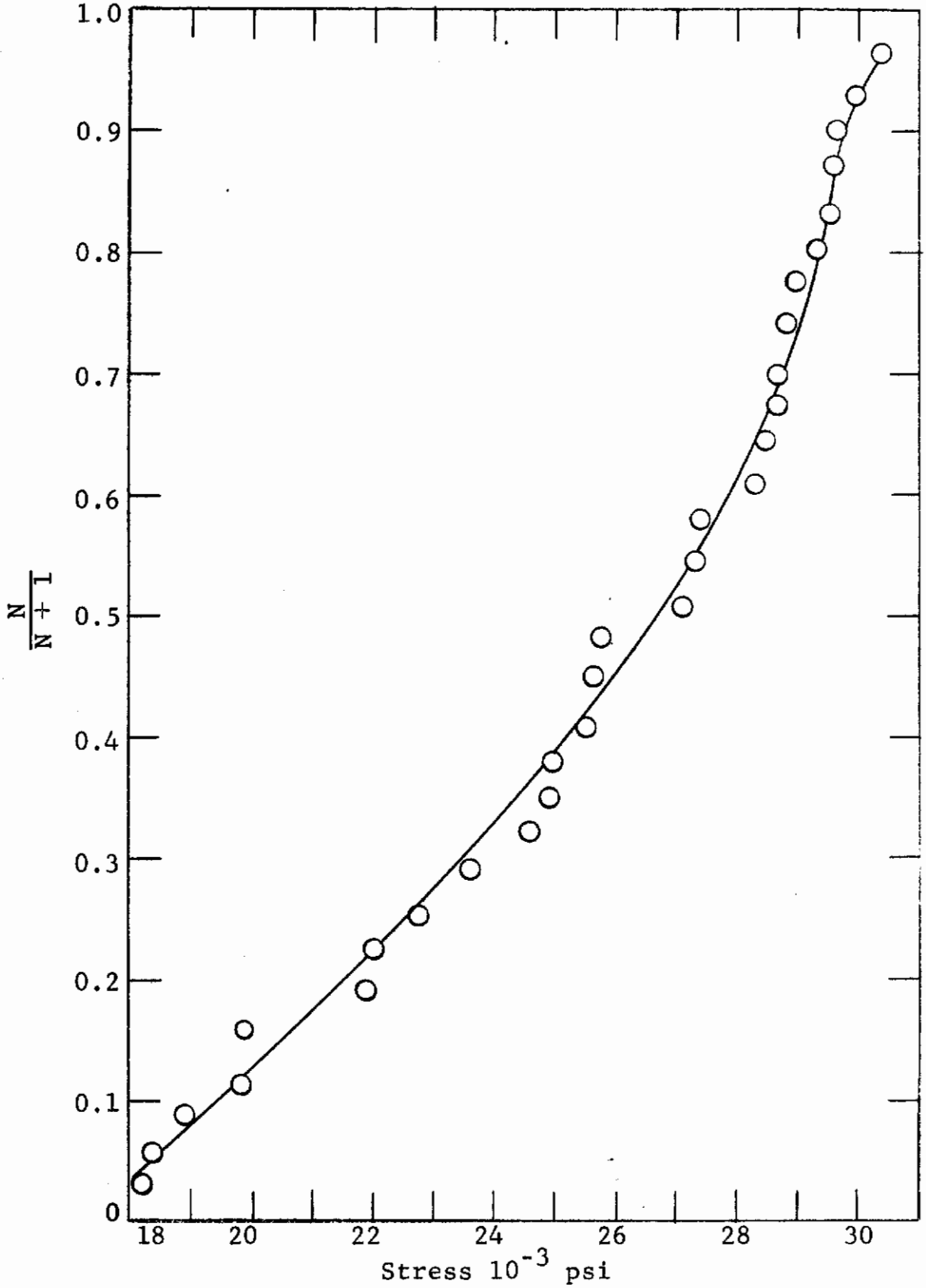

Figure 99. DISTRIBUTION CURVE FOR JTA TESTED IN COMPRESSION (A/G, 1832°F, in vacuum)

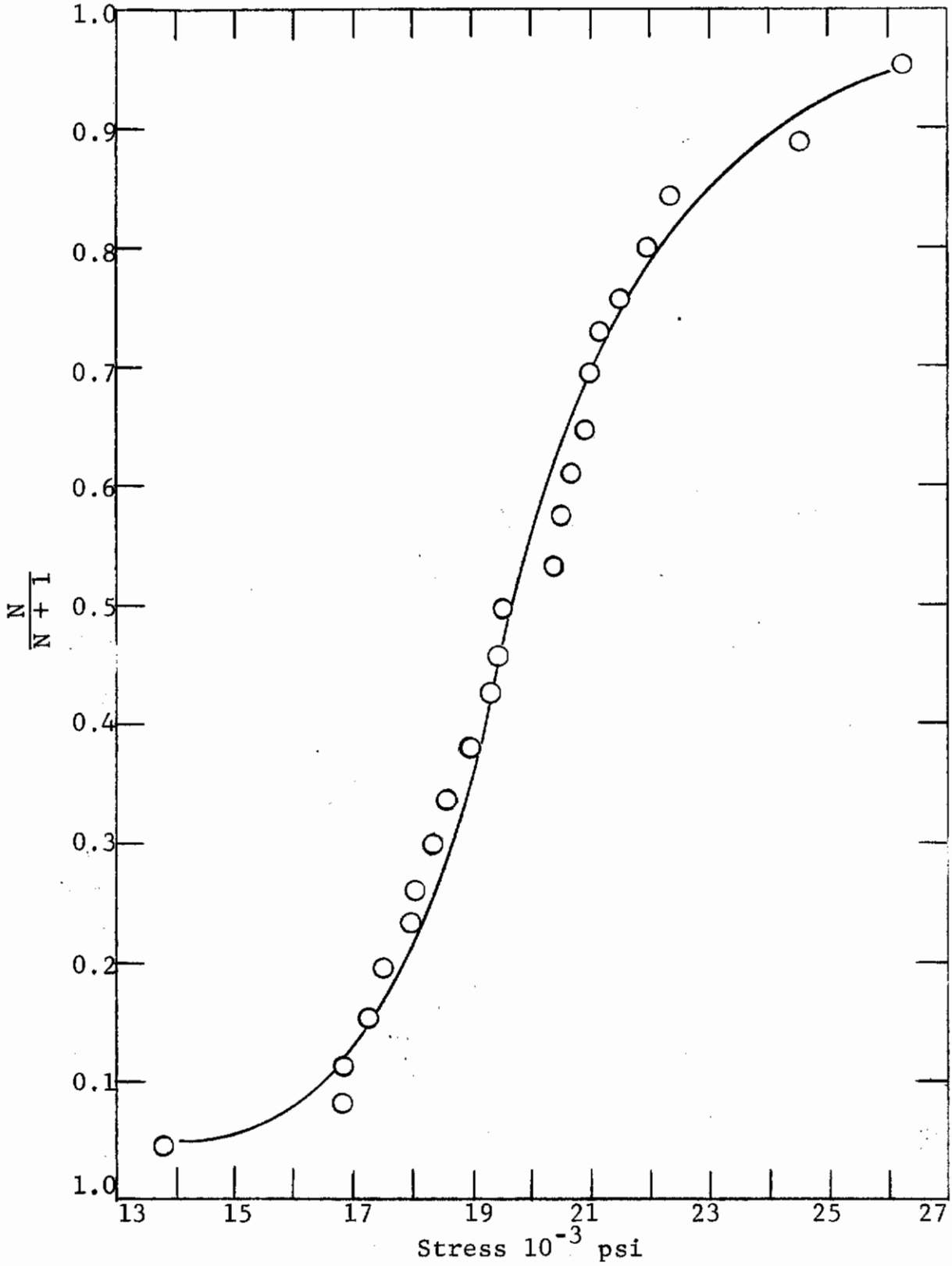

Figure 100. DISTRIBUTION CURVE FOR JTA TESTED IN COMPRESSION (A/G, 2732°F, in vacuum)

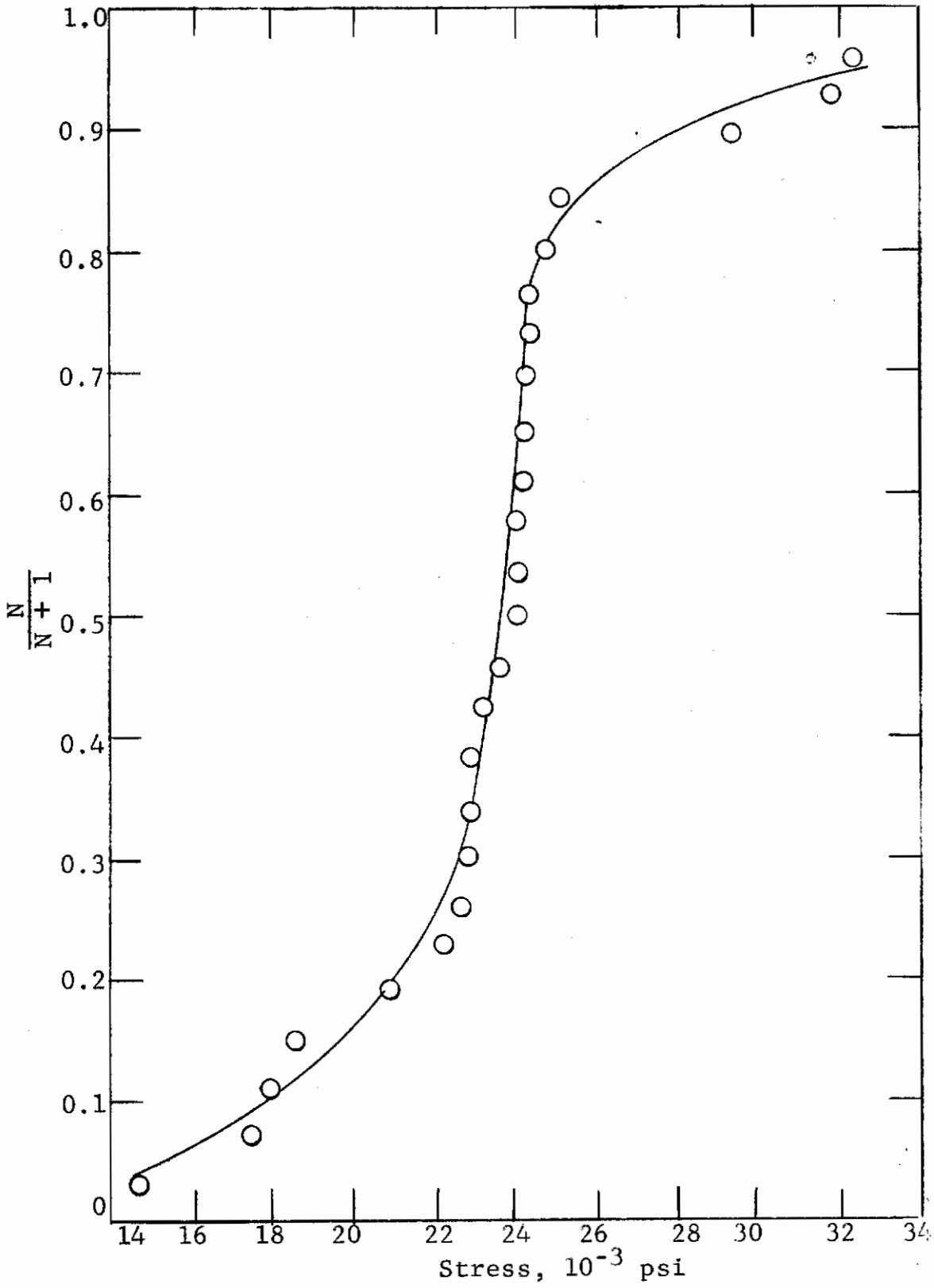

Figure 101. DISTRIBUTION CURVE FOR JTA TESTED IN COMPRESSION (A/G, 3182°F, in vacuum)

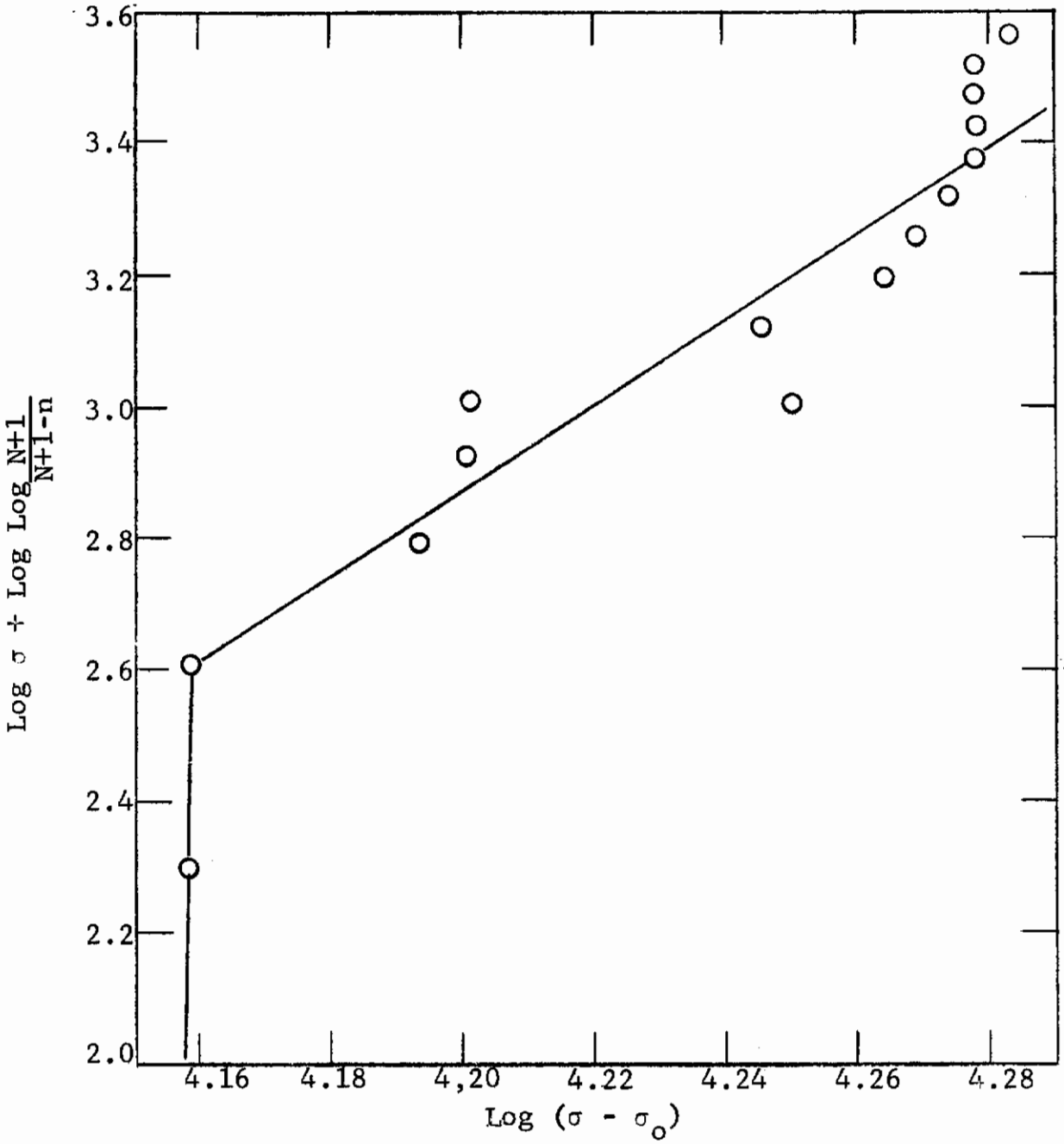

Figure 102. WEIBULL PLOT FOR JTA TESTED IN COMPRESSION (W/G, 77°F, in air)

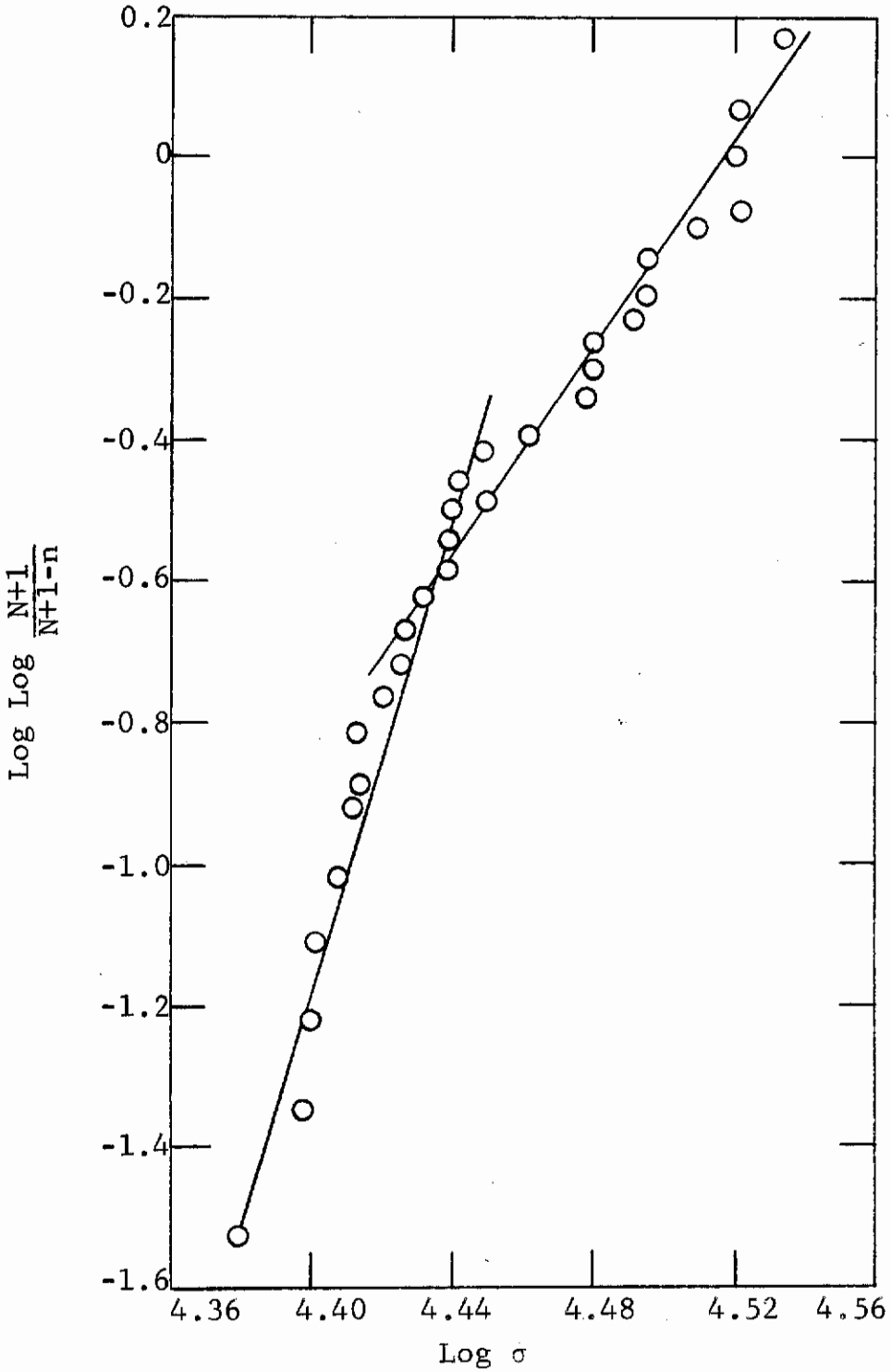

Figure 103. WEIBULL PLOT FOR JTA TESTED IN COMPRESSION (W/G, 1832°F, in vacuum)

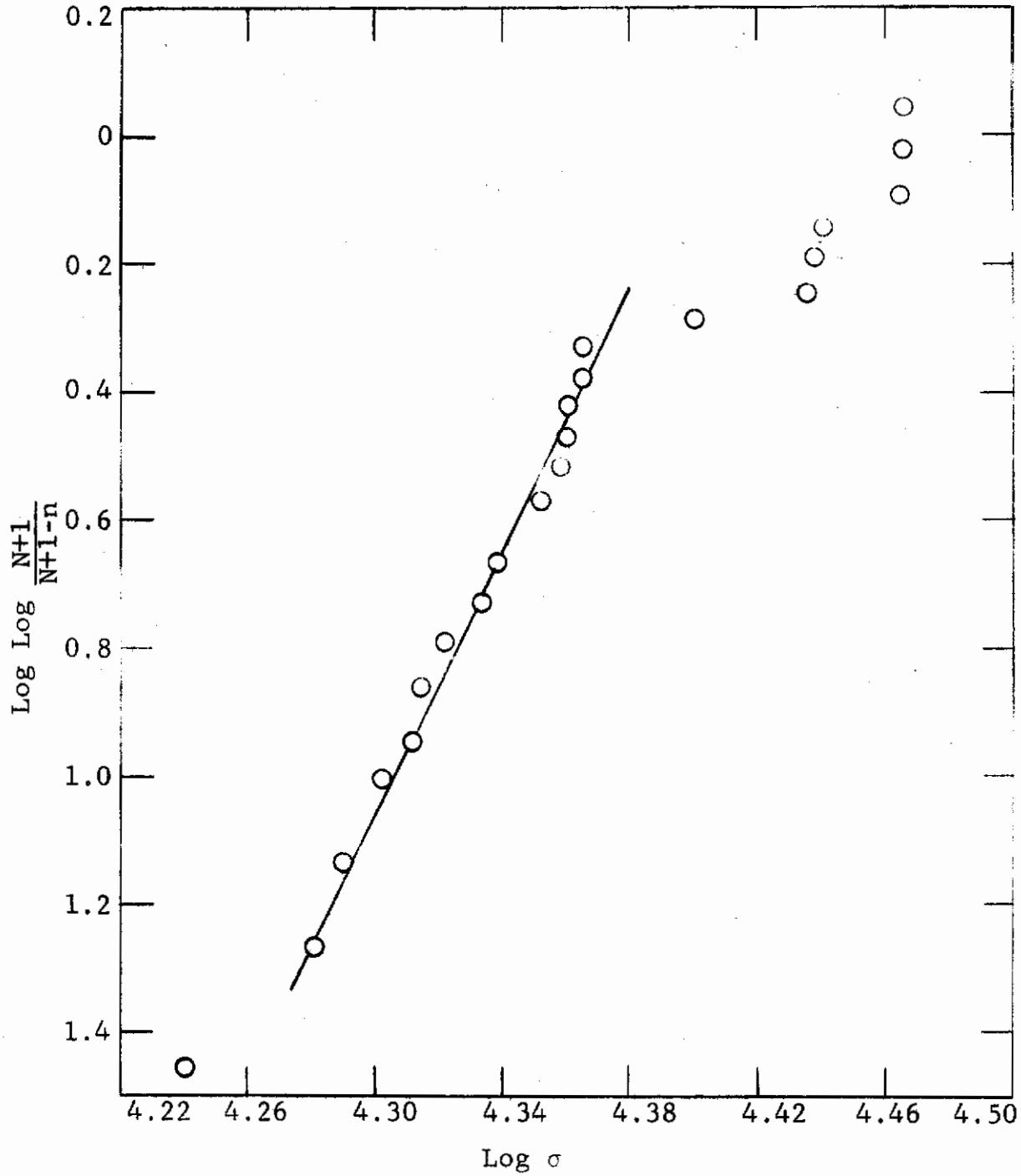

Figure 104. WEIBULL PLOT FOR JTA TESTED IN COMPRESSION (W/G, 2732°F, in vacuum)

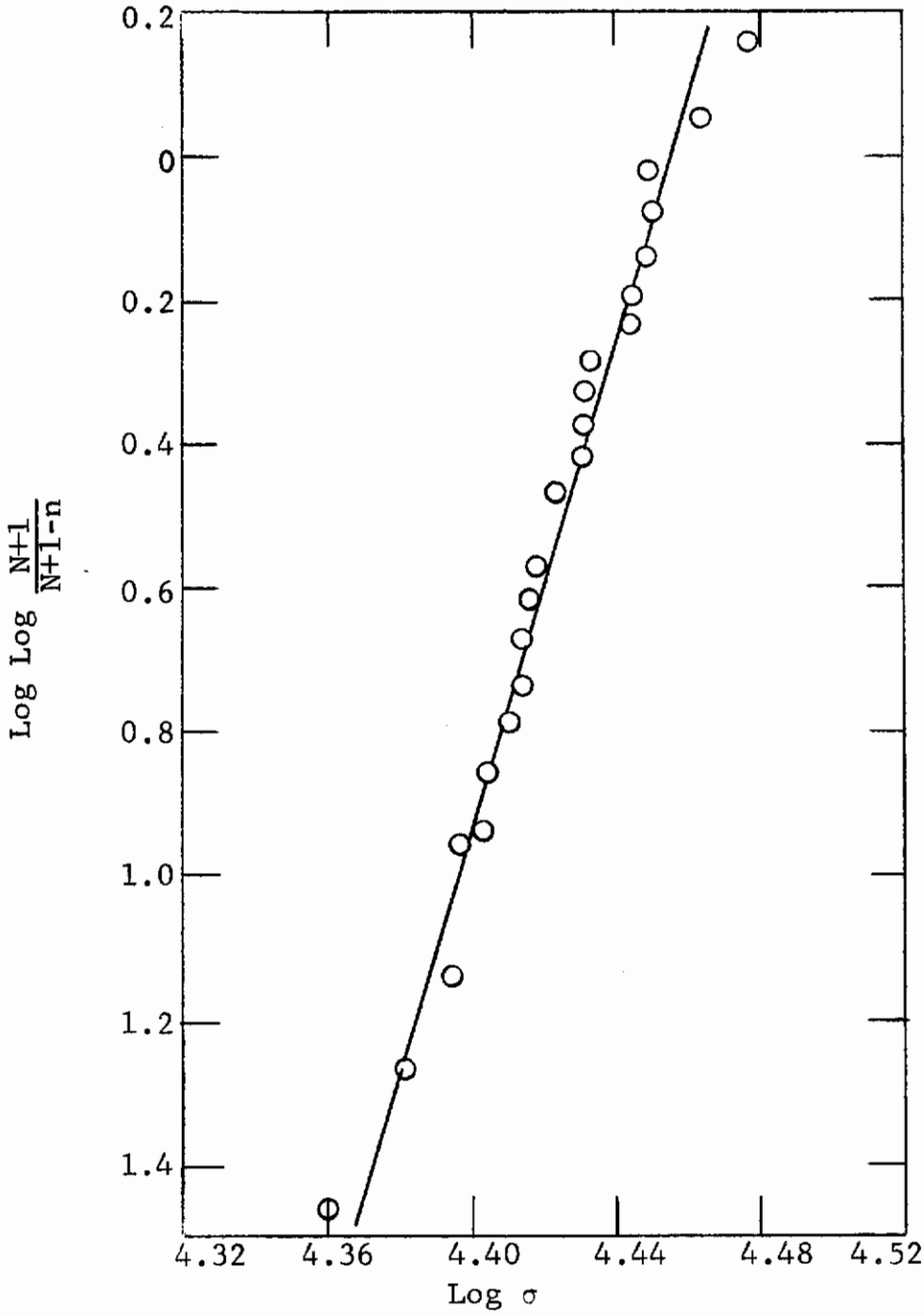

Figure 105. WEIBULL PLOT FOR JTA TESTED IN COMPRESSION (W/G, 3182°F, in vacuum)

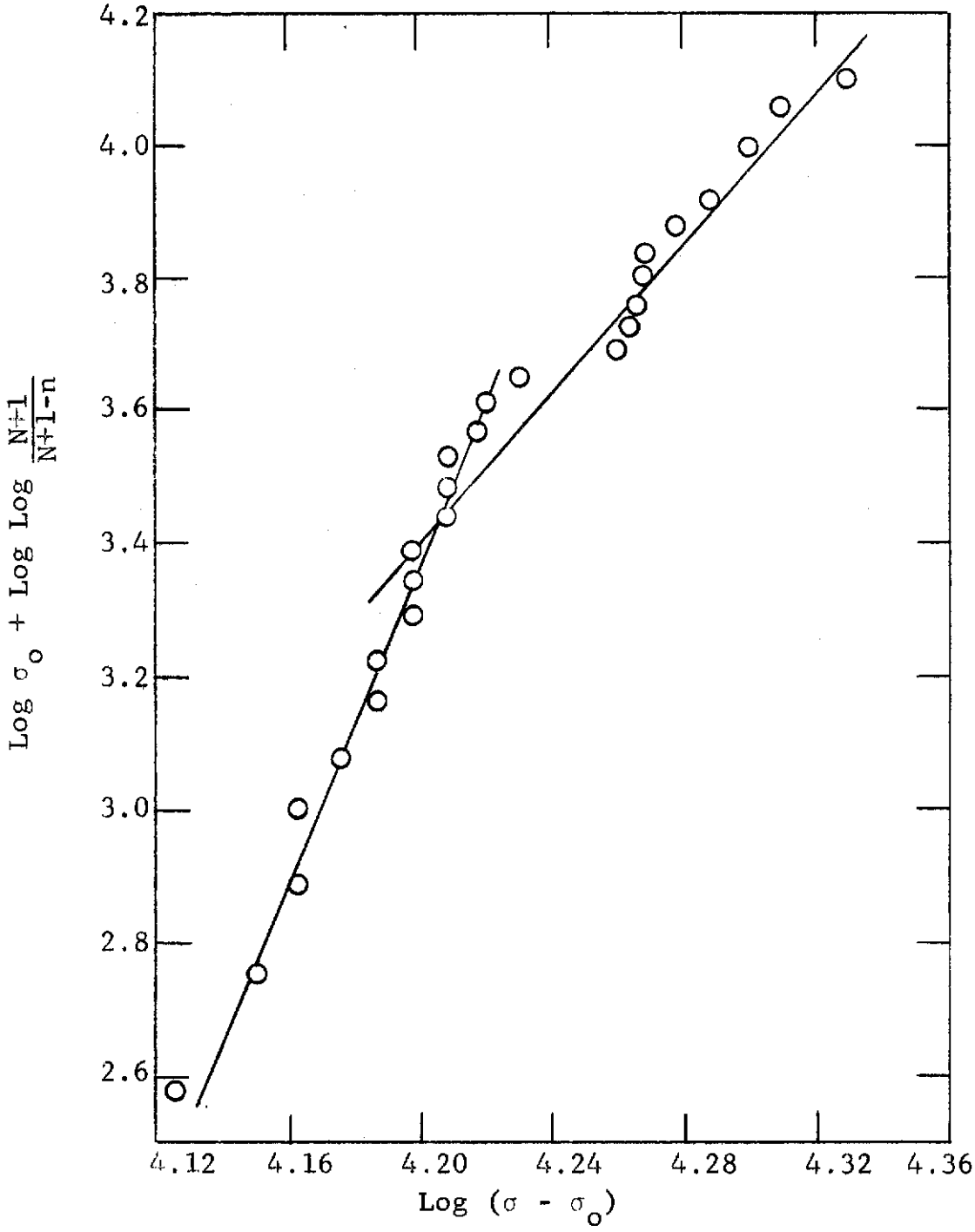

Figure 106. WEIBULL PLOT FOR JTA TESTED IN COMPRESSION (A/G, 77°F, in air)

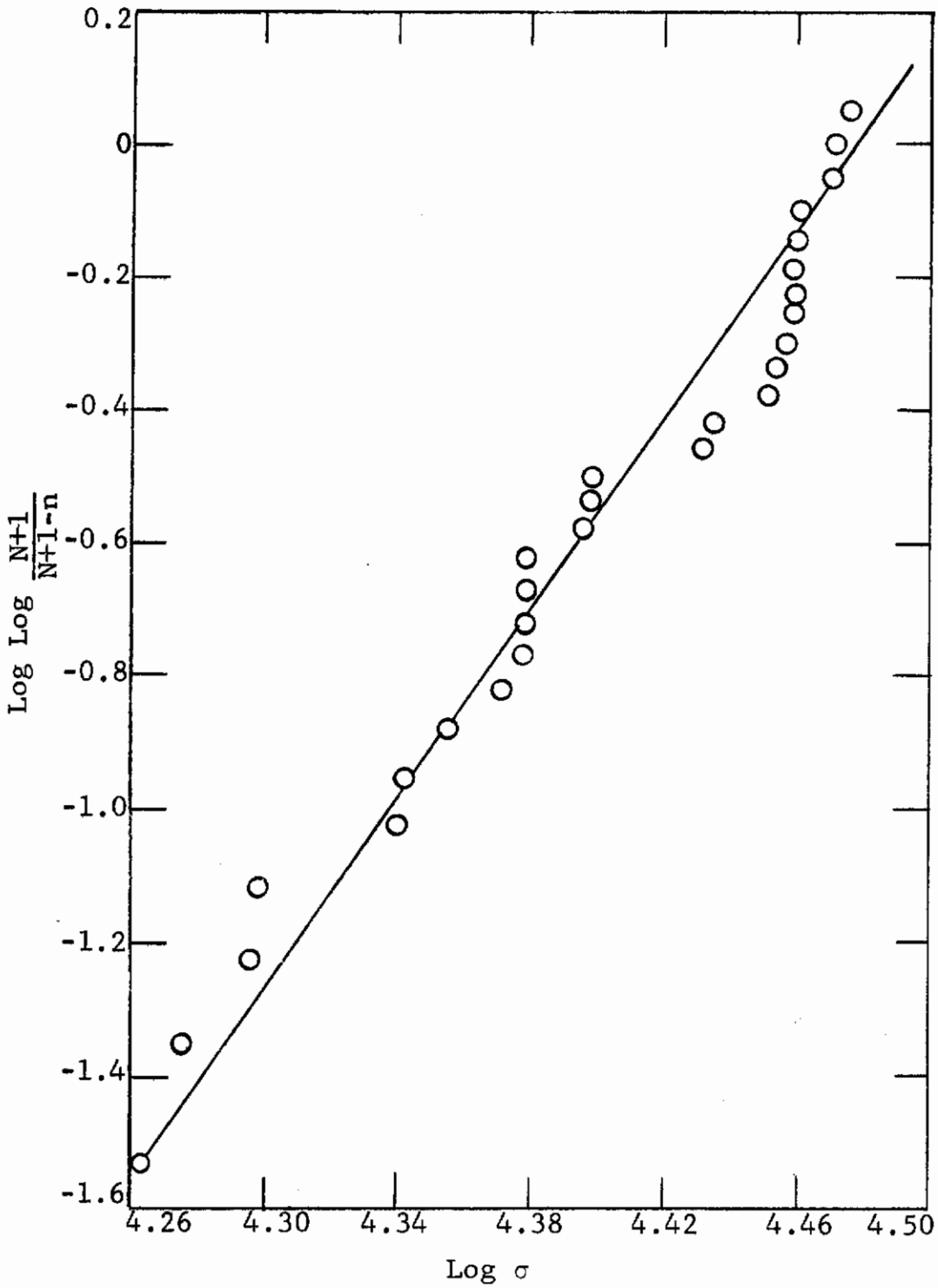

Figure 107. WEIBULL PLOT FOR JTA TESTED IN COMPRESSION (A/G, 1832°F, in vacuum)

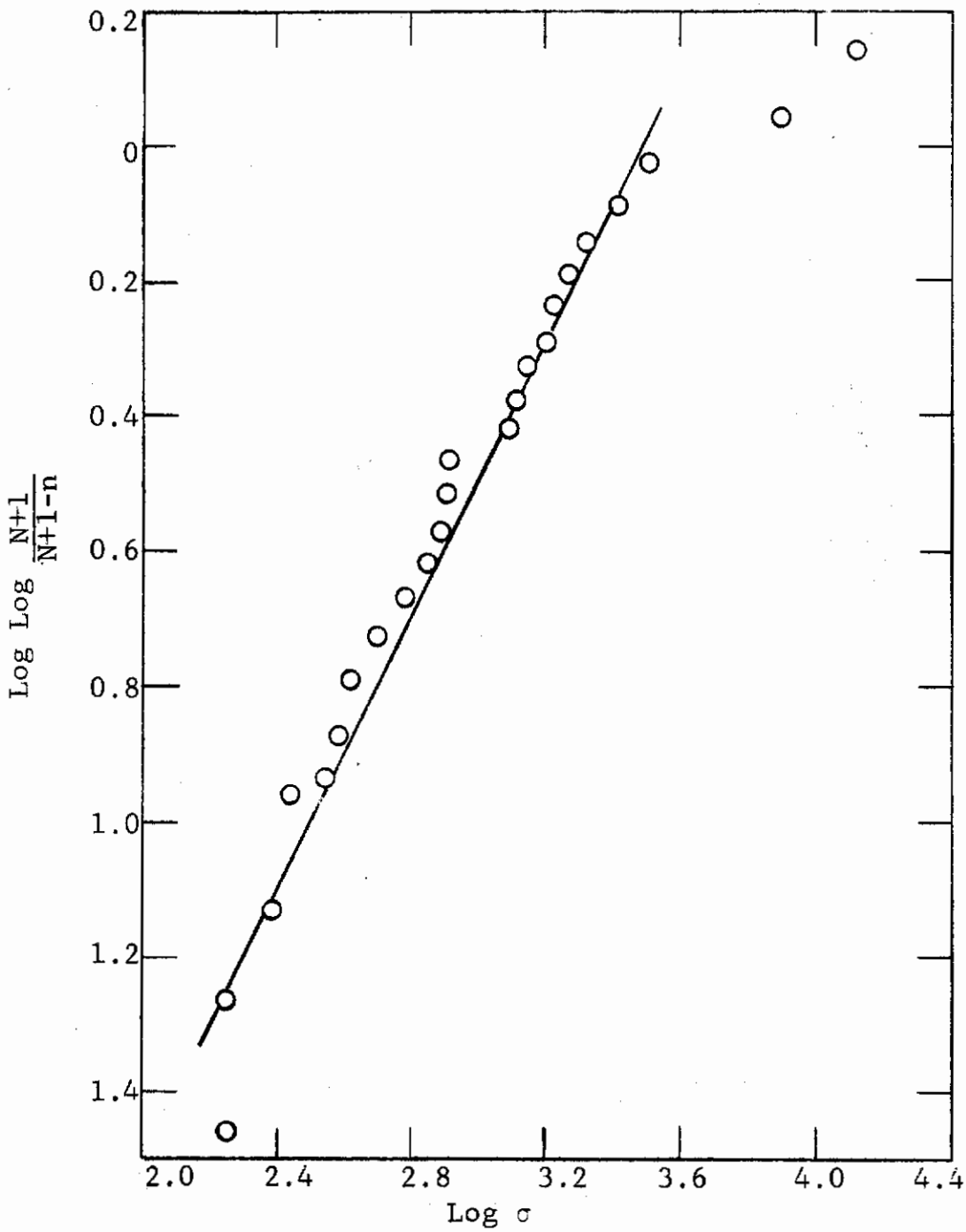

Figure 108. WEIBULL PLOT FOR JTA TESTED IN COMPRESSION (A/G, 2732°F, in vacuum)

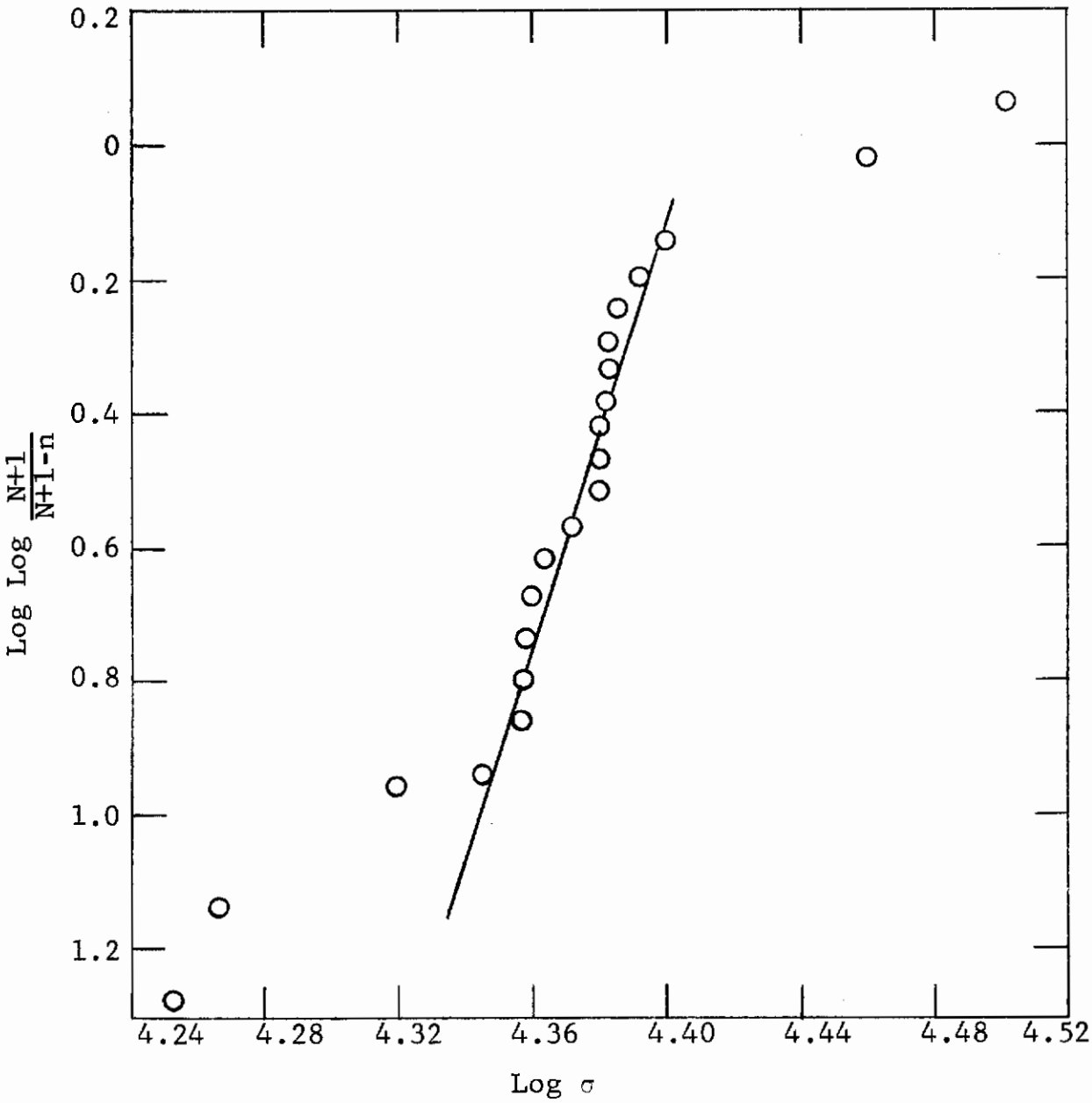

Figure 109. WEIBULL PLOT FOR JTA TESTED IN COMPRESSION (A/G, 3182°F, in vacuum)

Table XIX. COMPRESSION OF JTA GRAPHITE IN AN INERT ENVIRONMENT

Temp., °F	Orientation	Number of tests	$\bar{\sigma}$, psi	ν, %	E, psi
Room	With grain	30	33,070	5.86	3.67
	Across grain	30	30,330	8.61	2.31
1832	With grain	30	28,320	10.67	8.75
	Across grain	30	25,600	14.70	3.08
2732	With grain	25	23,128	16.45	9.14
	Across grain	25	19,720	12.757	3.24
3182	With grain	25	25,930	7.09	3.33
	Across grain	25	23,440	16.46	1.94
3632	With grain	3	15,350	---	--
	Across grain	3	18,120	---	--

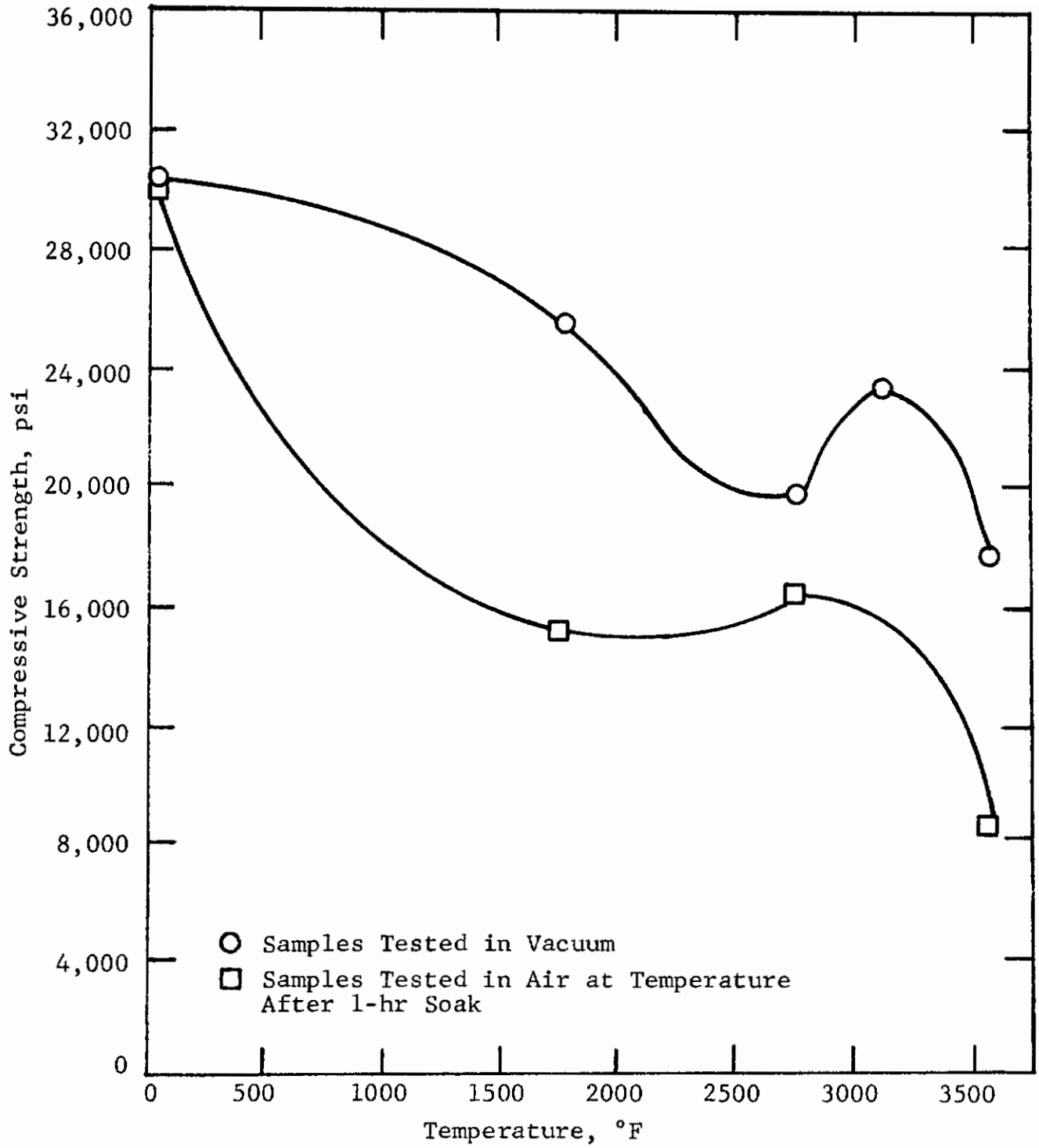

Figure 110. EFFECT OF ATMOSPHERE ON HIGH-TEMPERATURE COMPRESSIVE STRENGTH OF ACROSS GRAIN ORIENTATION OF JTA

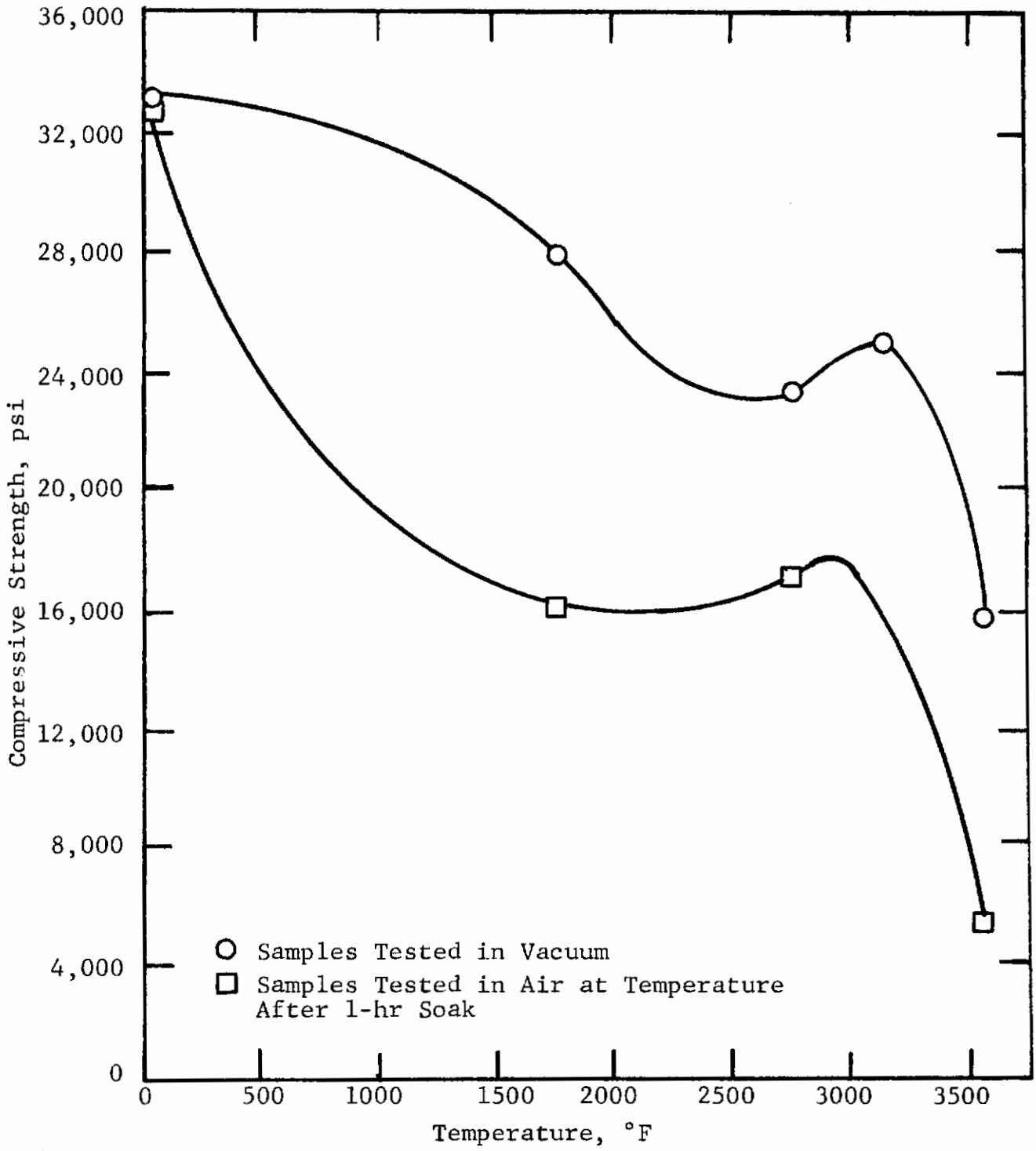

Figure 111. EFFECT OF ATMOSPHERE ON HIGH-TEMPERATURE COMPRESSIVE STRENGTH OF WITH GRAIN ORIENTATION OF JTA

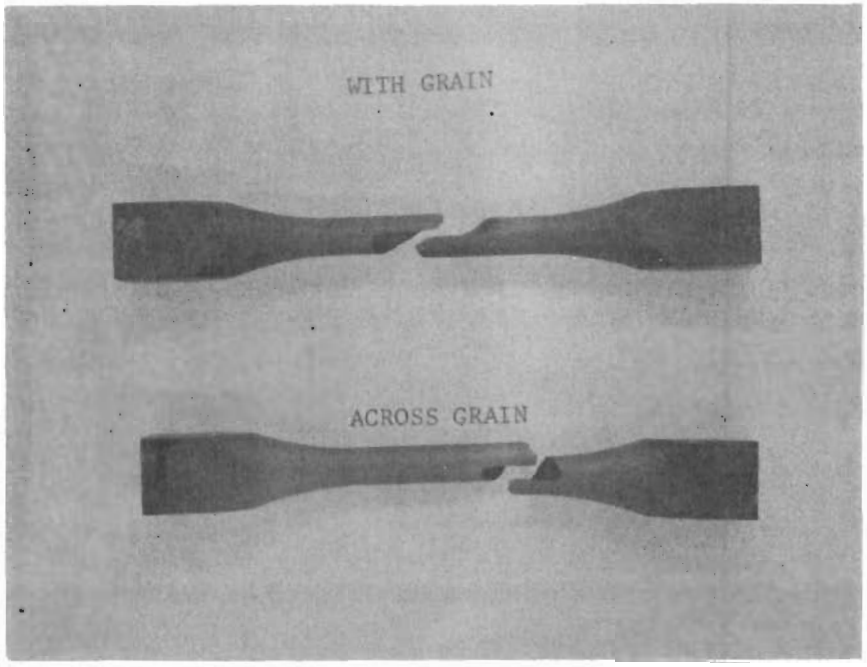

Figure 112. TYPICAL FAILURE OF JTA TORSION SAMPLES

to tensile stresses developed during torsion loading. A distinct difference in fracture between the two orientations can be seen. The calculated shear strength of the with-grain samples was 9,100 psi, and the shear modulus was 2.21×10^6 psi. The calculated shear strength of the across-grain specimens was 9,970 psi, and the shear modulus was 2.00×10^6 psi. Both strength values are approximately equal to the average tensile strength of the with- and across-grain orientations.

Since JTA graphite is anisotropic with respect to grain orientation and since the torsion test loaded the material in tension and compression at a 45° angle to a normal orientation plane, there should be an averaging effect with respect to the anisotropic properties. As anticipated, the averaging effect of the torsion test did not reveal anisotropic characteristics of JTA graphite with respect to strength measurements. However, anisotropy was revealed by the fracture-surface appearance. The length of the spiral fracture surface was different for each orientation. The with-grain ears were longer than the across-grain ears.

Poisson's ratio was calculated by using the relationship:

$$\mu = 1 - \frac{E}{2G} \qquad (10)$$

where

μ is Poisson's ratio
E is Young's elastic modulus
G is the shear modulus.

The values obtained were 1.45 for the with-grain orientation and -0.065 for the across-grain orientation. The with-grain orientation value is theoretically impossible, and the across-grain value is in error as compared to values obtained by using strain gages (Section IV7). The reason for the erroneous data is attributed to the fact that anisotropy of JTA cannot be separated in a torsion test to determine the true shear modulus for either grain orientation.

7. ELASTICITY

Elasticity is the property of a body that permits it to undergo strain from external forces and return to its original shape upon removal of the forces. Hooke's law relates the stress and the strain of materials that behave elastically in that it states that a body acted upon by external forces deforms in proportion to the stress developed ($E = \sigma/e$). The proportionality constant is the modulus of elasticity, the slope of the stress-strain curve over the linear range.

If the stress-strain behavior of a material does not follow Hooke's law (i.e., is nonlinear), the elastic properties are not constant, but vary with stress, although the material can still be elastic. For this case, the average elastic modulus is the best value for design use. This value is obtained from the secant modulus E_{sec}, which represents the average slope of the stress-strain curve or the slope of the secant:

$$E_{sec} = \frac{\sigma_A}{\epsilon_A} \tag{11}$$

The value obtained for the secant modulus obviously depends on the location of point A, which is usually specified in the terms of the stress at A (σ_A). If the modulus associated at a point on the stress-strain curve is wanted, the instantaneous elastic modulus can be found from the slope of the tangent to the curve at that point. This slope is called the tangent modulus (E_t):

$$E_t = \frac{d\sigma_A}{d\epsilon_A} \tag{12}$$

As for the secant modulus, the stress at point A must be specified.

The classic manner of determining Young's modulus (E) and Poisson's ratio (μ) is to subject bars to tension or compression and to measure loads and displacements. This method has the advantage of allowing the determination of the stress-strain relationship beyond the linear elastic range. In spite of its simple appearance, it requires very precise techniques of measuring load and displacement. Loading a bar axially is very difficult. Also, the displacements are measured over a relatively small base length, a procedure that requires gages having high sensitivity and precision.

If the analysis is restricted to elastic behavior, other more convenient specimen shapes, such as a rectangular beam subjected to pure bending, can be used to determine the elastic properties. If both E and μ are to be obtained from one specimen, sensitivity of measurement is again a problem. However, if only E is required, the beam deflections are more easily measured than axial strains. Difficulties are penetration and friction of the supports.

All these measurement difficulties become magnified when high temperature is an environmental condition of the test. However, in the case of certain brittle specimens, indirect methods of obtaining physical properties can be used to determine the elastic constants.

Many specimens for which the state of stress is known at one point can be used to determine the modulus of elasticity and Poisson's ratio. The generalized Hooke's law, solved for E and μ, has the following forms:

$$E = \frac{\sigma_x^2 - \sigma_y^2}{E_x \sigma_y \epsilon \sigma_y \sigma_z} \tag{13}$$

$$\mu = \frac{E_x \sigma_y \epsilon \sigma_y \sigma_x}{E_x \tau_x - \sigma_y \sigma_y} \tag{14}$$

If the strains are determined experimentally for a given load, the stresses are usually determined analytically from the loads, and E and μ can be computed.

If the stresses at every point along some convenient line on a model are known, determining the change in length of a whole line for a given load is sometimes more practical. Since the stresses along the line are known as a function of the load and since the relationship between stresses and strains is also known, the strains along the line are known. The summation of these strains is the displacement. Therefore, a relationship between load and dislpacement is established:

$$E = f(p, \zeta, u) \tag{15}$$

where

p is the load
ζ is the displacement.

If two lines are chosen, two equations, which can be solved for E and u, are obtained. This method uses specimens having a simple geometry, e.g., disks and rings (Figure 113); it has been analyzed by Durelli.(13) The equations for determining the elastic properties of brittle materials by using this method are:

$$\zeta_v = \frac{PR^2}{AE_c}\left\{\frac{\pi}{4} - \frac{2}{\pi}\left(1 - \frac{eL}{RL}\right) + \left[\frac{2E}{R}\ \frac{2}{\pi}\left(1 - \frac{e}{R} - \frac{\pi}{8}\right)\right] + \frac{\pi\ a\ Ee}{4GR}\right\} \tag{16}$$

$$\zeta_h = \frac{PR^L}{AEe}\left[\frac{1}{2} - \frac{2}{\pi} + \frac{e}{R}\left(\frac{4}{\pi} - \frac{1}{2}\right) - \frac{2e^2}{\pi R^2} - \frac{Ee}{2GR}\right] \tag{17}$$

$$u = \frac{Et\zeta_{ho}}{P} - 0.2732 \tag{18}$$

where

ζ_v is the change in length of the vertical diameter
ζ_h is the change in length of the horizontal diameter
P is the load
R is the mean radius of the ring

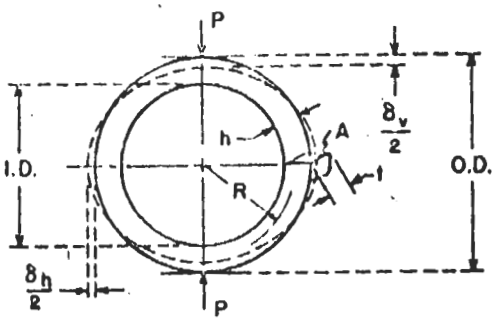

$$\delta_v = \frac{PR^2}{AE_\theta}\left\{\frac{\pi}{4} - \frac{2}{\pi}\left(1-\frac{\theta^2}{R^2}\right) + \frac{2\theta}{R}\left[\frac{2}{\pi}\left(1-\frac{\theta}{R}\right) - \frac{\pi}{8}\right] + \frac{\alpha\pi}{4}\frac{E_\theta}{GR}\right\}$$

$$\delta_h = \frac{PR^2}{AE_\theta}\left[\frac{1}{2} - \frac{2}{\pi} + \frac{\theta}{R}\left(\frac{4}{\pi} - \frac{1}{2}\right) - \frac{2}{\pi}\frac{\theta^2}{R^2} - \frac{\alpha}{2}\frac{E_\theta}{2GR}\right]$$

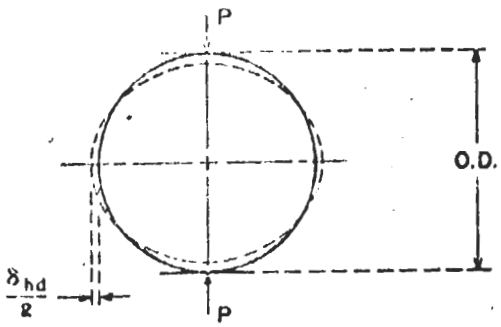

$$\delta_{hd} = \frac{P}{Et}\left[0.2732 + \mu\right]$$

Figure 113. HORIZONTAL AND VERTICAL DEFLECTIONS IN RING AND DISK

A is the cross-sectional area of the ring
E is Young's modulus
e is the distance of the neutral axis from the centroid
a is the numerical factor depending on the shape of the cross section (for rectangular section, a = 1.2)
g is the modulus of elasticity in shear
t is the thickness of the specimen.

The figure suggests computing E from the ring and μ from the disk. However, equations 16, 17, and 18 form two equations having two unknowns that can be solved for E and μ by using either the disk or the ring.

In addition to this simplified technique for determining the elastic properties, the effects of microstructure and temperature must be observed. The material is assumed to be elastic and to obey Hooke's law up to the fracture stress. This technique of obtaining the elastic constant is also applicable to materials that have a nonlinear stress-strain relationship as long as the material behaves in an elastic manner. At temperatures at which creep becomes a factor, the elastic properties no longer have any meaning.

For this work 2-in.-diameter x 1/2-in.-thick disks and 2-in.-OD x 1-in.-ID x 1/2-in.-thick rings were used. The filar microtelescope was used to measure the ring and disk deformations required to obtain elastic modulus and Poisson's ratio for the material studied. The other constants were calculated from these two values.

All methods described were used to obtain the elastic modulus of JTA. However, in this section only the tests performed on beams by using SR-4 electrical strain gages and the ring and disk technique are analyzed. These results are compared to data obtained in the direct measurements.

Young's elastic modulus in bending was obtained from the 1- x 1- x 6-in. size-effect specimens. SR-4 electrical resistance gages were fastened to five specimens from each billet to determine Poisson's ratio. Two gages were applied to each of the four longitudinal faces; one measured the longitudinal strain, and one measured the cross strain. The elastic modulus and Poisson's ratio were thus measured for the two orientations. Table XX presents the results of these experiments. It is obvious from the data that two Poisson's ratios, which depend on the microstructure, have to be considered -- one for the "A" direction and one for the "C" direction. The first represents the broad face of the graphite crystallize, and the second represents the edge of the crystallite. The with-grain orientation exhibits a Poisson's ratio for both axes, depending on how the sample is oriented for measurement.

Table XX. ROOM-TEMPERATURE ELASTIC PROPERTIES OF JTA GRAPHITE

Orientation	Billet no.	Modulus in flexure, 10^6 psi		Poisson's ratio in flexure	
		Tension	Compression	Tension	Compression
With grain	7-F-12	5.535	6.268	0.233[a] 0.082[b]	0.309[a] 0.125[b]
	7-F-14	8.100	9.125	0.252 0.079	0.321 0.135
Across grain	7-F-12	3.139	3.493	0.119	0.145
	7-F-14	3.140	4.074	0.093	0.151
	14-G-1	4.397	4.279	0.110	0.116

[a]Poisson's ratio determined in A direction.

[b]Poisson's ratio determined in C direction.

In addition, as expected, the elastic properties in compression are higher than in tension. Therefore, to obtain a true flexural strength, the data must be corrected for the true position of the neutral axis of the bars.

Young's elastic moduli for tension and compression correlated with similar data obtained from direct tensile and compressive measurements. The direct compressive data were somewhat more variable than the tensile data, a result probably due more to measurement error than material differences.

Attempts to use the ring and disk method of determining Poisson's ratio were not successful. Table XXI lists data obtained from experiments in which this technique was used. While the Young's elastic modulus readings were not too different from those obtained from electrical strain gages and extensometer readings, the data did not show any variability. Therefore the method is not sensitive to differences in the material. Poisson's ratio calculations were in no way similar to those obtained by using strain gages. In view of the type of material used, the data obtained from strain gages appears to be reasonable. The theoretical limits of Poisson's ratio can be obtained from the relationships between the elastic moduli:

$$G = \frac{E}{2(1 + \mu)} \tag{19}$$

$$E_v = \frac{E}{3(1 - 2\mu)} = \frac{2}{3}G\,\frac{(1 + \mu)}{(1 - 2\mu)} \tag{20}$$

In Equation 19, as the value of μ approaches -1, the value of the shear modulus (G) approaches infinity and becomes negative as μ passes -1. Hence, -1 is the minimum value of Poisson's ratio. In a similar manner, in Equation 20, when $\mu = 1/2$, the bulk modulus (E_v) becomes infinity, and when $\mu > 1/2$, the bulk modulus is negative. Hence 1/2 is the maximum value of Poisson's ratio. The data obtained from this work indicated values of from 0.4 for with-grain orientations to approximately 1.0 for across-grain orientations. The indirect technique does not appear to be useful for measurements of Poisson's ratio of anisotropic materials.

8. CREEP RESISTANCE

Creep refers to the continuous deformation of a material as a function of time. Basically, creep behavior of a material should be analyzed in terms of true stress and true deformation; however, for many practical applications in which deformations exceeding 1% or so are not tolerated and when design is based on a low limiting creep deformation, use can be made of the conventional condition of constant load rather than a constant stress on a part. However, this compromise is made in the interest of practicality, and figures calculated are indications or trends, not exact representation of the behavior of the material.

Table XXI. POISSON'S RATIOS OBTAINED BY RING-AND-DISC METHOD

Specimen no.	Load, lb	Gage reading, in. Left Initial	Left Final	Right	δ x 10-4, in.	t, in.	E, 10^6 psi	Etδ/P	μ
27[a]	300	0.0477	0.0491	0.000	1.4	0.127	6.39	0.3787	0.1055
21[a]	300	0.0622	0.6350	0.003	4.3	0.125		1.1449	0.8717
18[a]	300	0.1780	0.1800	0.001	3.0	0.126		0.8051	0.5319
2[a]	300	0.1075	0.1100	0.001	3.5	0.126		0.9393	0.6661
17[a]	300	0.0910	0.0930	0.001	3.0	0.126		0.8051	0.5319
5[a]	300	0.1038	0.1050	0.001	2.2	0.125		0.5858	0.3126
15[a]	300	0.0030	0.0057	0.002	4.7	0.125		1.2513	0.9781
13[a]	300	0.0215	0.0240	0.002	4.5	0.127		1.2173	0.9441
25[a]	300	0.1785	0.1811	0.001	3.6	0.127		0.9738	0.7006
24[a]	300	0.0732	0.0754	0.002	4.2	0.125		1.1183	0.8451
								Average =	0.6487
24[b]	300	0.1010	0.1030	0.001	3.0	0.125	10.72	1.3399	1.0667
23[b]	300	0.1035	0.1058	0.000	2.3	0.126		1.0272	0.7540
22[b]	300	0.0785	0.0795	0.0013	2.3	0.125		1.0354	0.7622
21[b]	300	0.0800	0.0820	0.0015	3.5	0.124		1.5632	1.2900
20[b]	300	0.0345	0.0362	0.0026	4.3	0.125		1.9051	1.6319
19[b]	300	0.1120	0.1140	0.0012	3.2	0.125		1.4292	1.1560
17[b]	300	0.0725	0.0745	0.0006	2.6	0.124		1.1612	0.8880
16[b]	300	0.0410	0.0430	0.001	3.0	0.1275		1.3291	1.0559
15[b]	300	0.1955	0.1975	0.0005	2.5	0.125		1.1154	0.8422
14[b]	300	0.0645	0.0665	0.0005	2.5	0.125		1.1154	0.8422
13[b]	300	0.0828	0.0852	0.001	3.4	0.124		1.5063	1.2331
								Average =	0.9890

[a] Specimen cut from plane parallel to pressing direction.
[b] Specimen cut from plane perpendicular to pressing direction.

A typical plot of creep data is shown in Figure 114. When a specimen is stressed, it first behaves elastically, a reaction that provides an initial deformation before creep actually begins. The first stage of creep is usually characterized by a decreasing creep rate, the second stage by a steady-state rate, and the third by an increasing rate. The portion of the creep curve most commonly used in design work is the steady-state, or second, stage, although the initial deformation is of great importance when dealing with short-life items like reentry structures. The steady-state stage of creep is usually linear on log coordinates defining a creep rate or deformation per unit time.

Consideration was given to a mathematical theory of creep that provides a description of the creep behavior of a material on the basis of test data. The basis of this theory is the relationship:

$$C = B\sigma^{n} \tag{21}$$

where

C is creep rate in tension
σ is the applied tensile stress
n is the slope of creep data on log-log coordinates
B is the stress intercept of a log creep rate equal to 1.0.

This creep law can be applied to problems in bending, the deviation of which is given by Faupel[14]:

$$\delta_{max} = \frac{tP^{n}}{\Phi}\left(\frac{L^{n+2}}{n+2}\right) \tag{22}$$

$$\Phi = \frac{1}{B}\left(\frac{h}{2}\right)^{2n+1}\left(\frac{bn}{2n+1}\right)^{n} \tag{23}$$

where

t is the time under load
P is a concentrated load
L is the span
δ_{max} is the maximum creep deflection
h is the depth of the beam
b is the width of the beam.

Short-term creep data are shown in Figures 115 through 120 for both with- and across-grain data. Longer-term plates are shown in Figures 121 through 123. In all cases, only primary and secondary creep data were obtained. Longer-term tests could not be obtained because of failure in the furnace heating elements, which moved across after 24 hr of continuous use at the temperature of interest. Also, creep at these temperatures was rapid enough so that relatively low stresses were used in order to obtain measurable curves over any length of time. Reproducibility

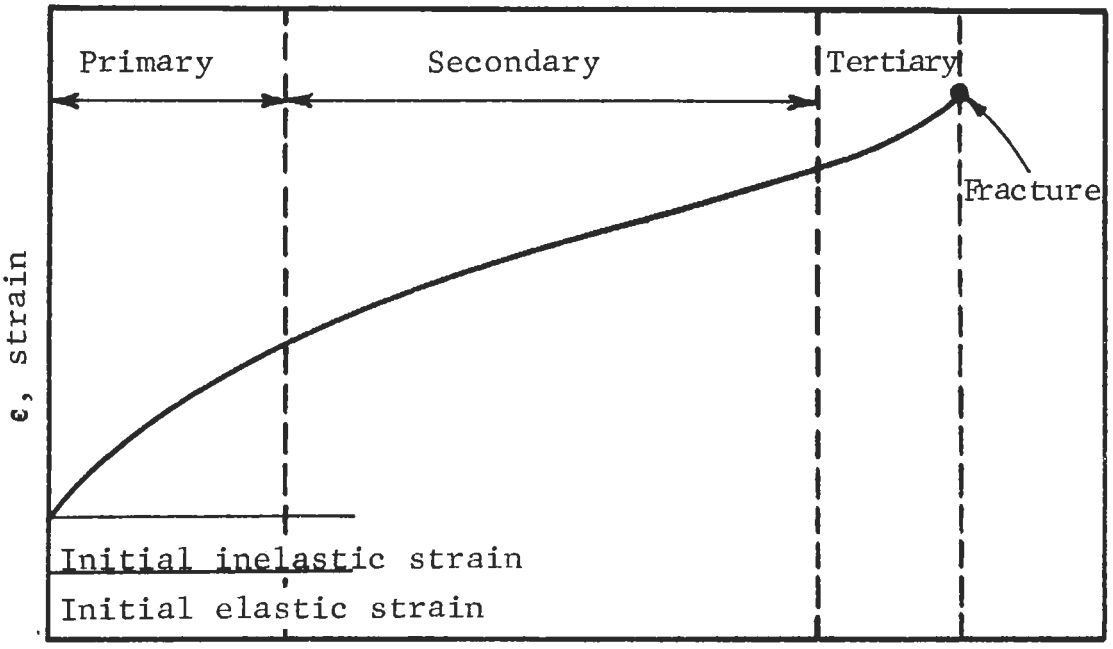

Figure 114. TYPICAL CREEP CURVE

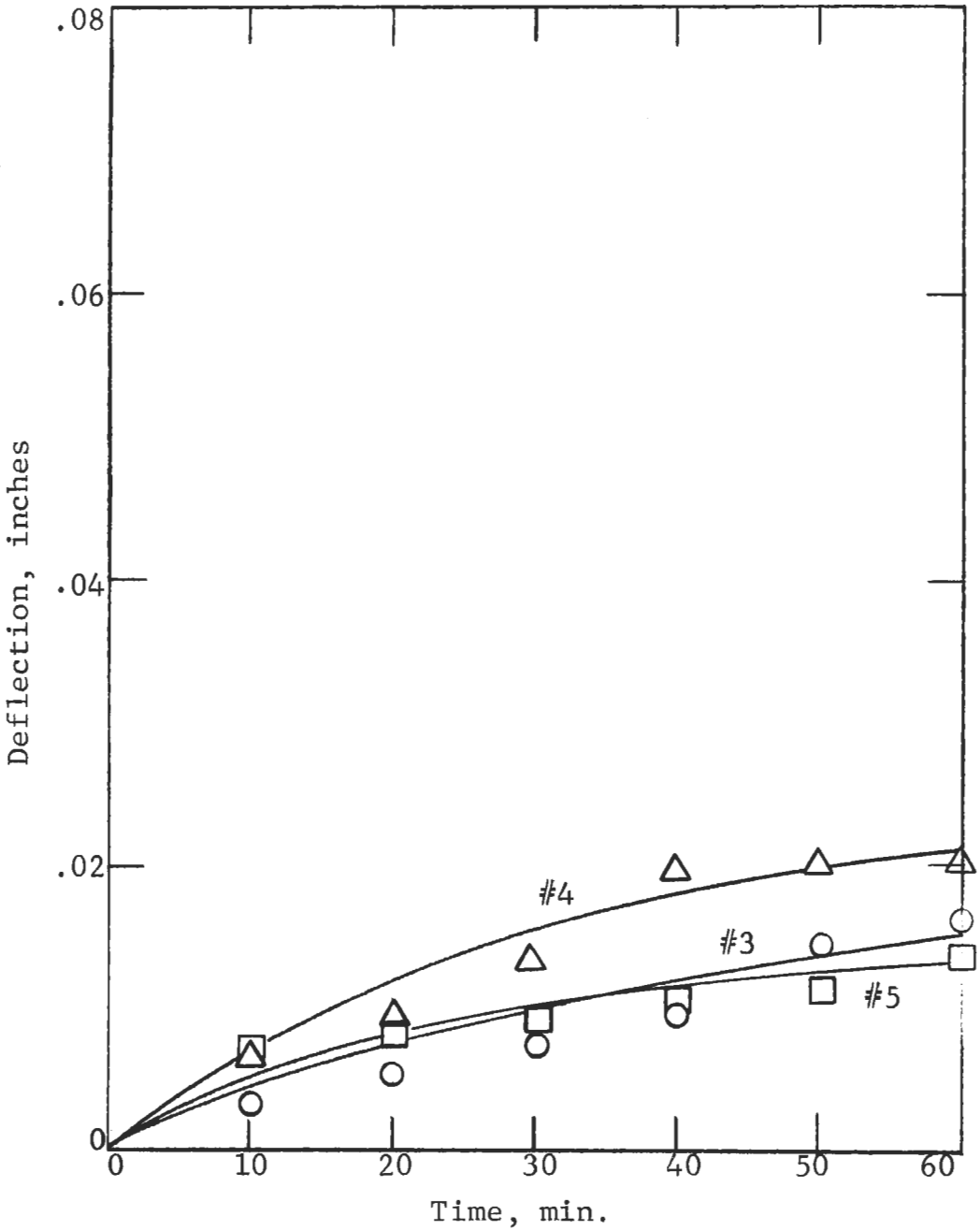

Figure 115. SHORT TERM FLEXURAL CREEP FOR JTA (3182°F, 668 psi, W/G)

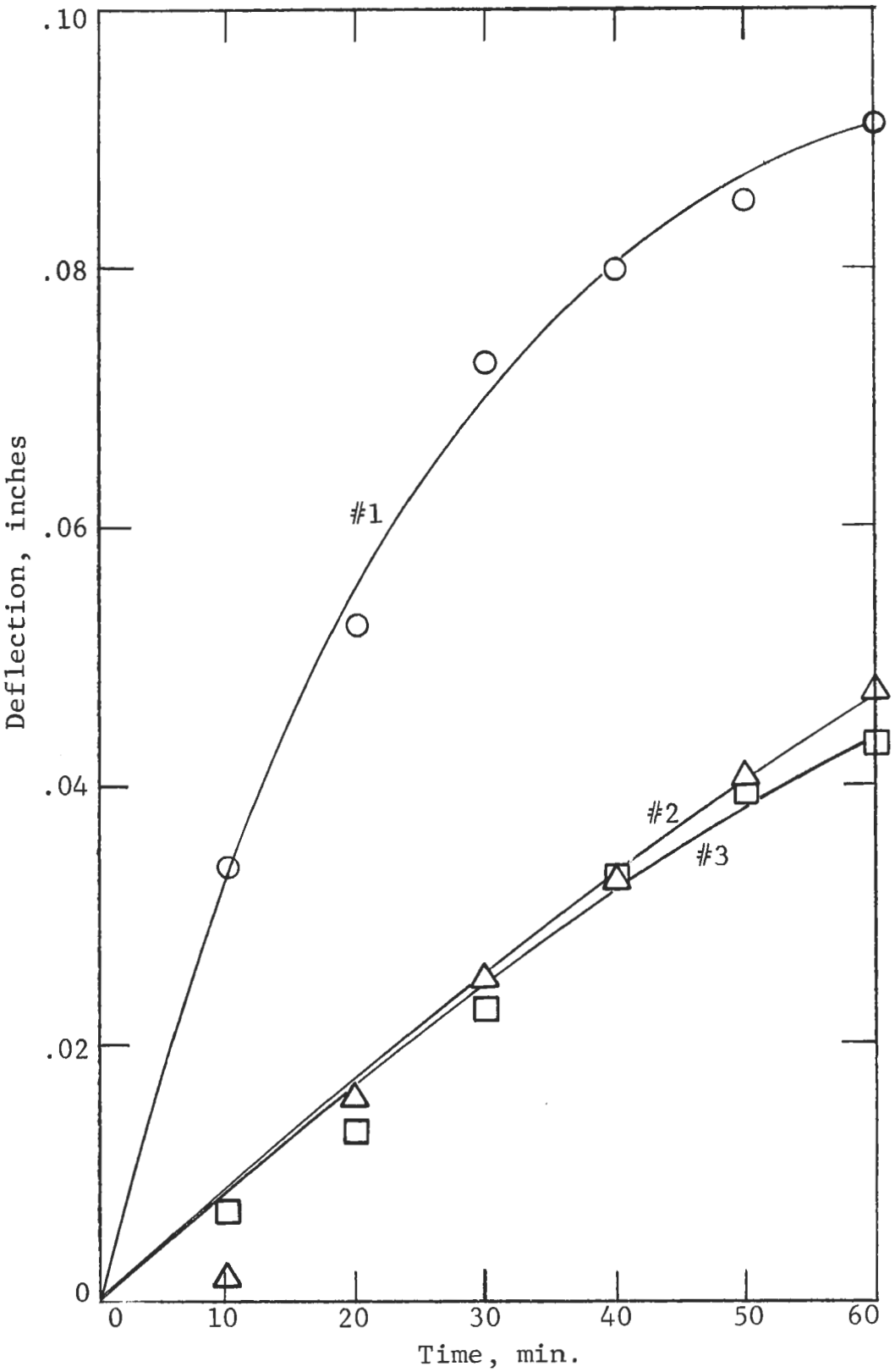

Figure 116. SHORT TERM FLEXURAL CREEP FOR JTA (3632°F, 668 psi, W/G)

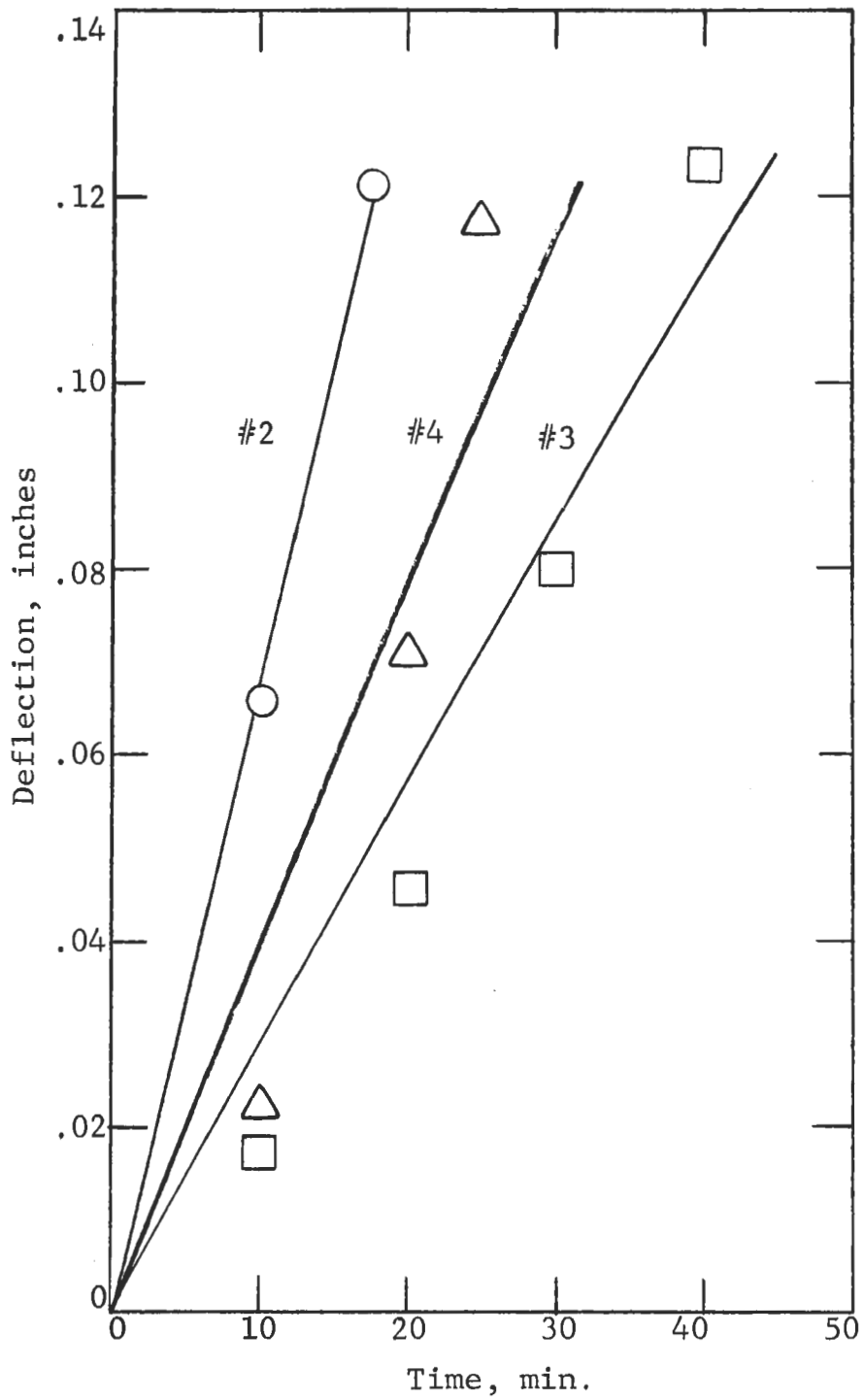

Figure 117. SHORT TERM FLEXURAL CREEP FOR JTA (3992°F, 668 psi, W/C)

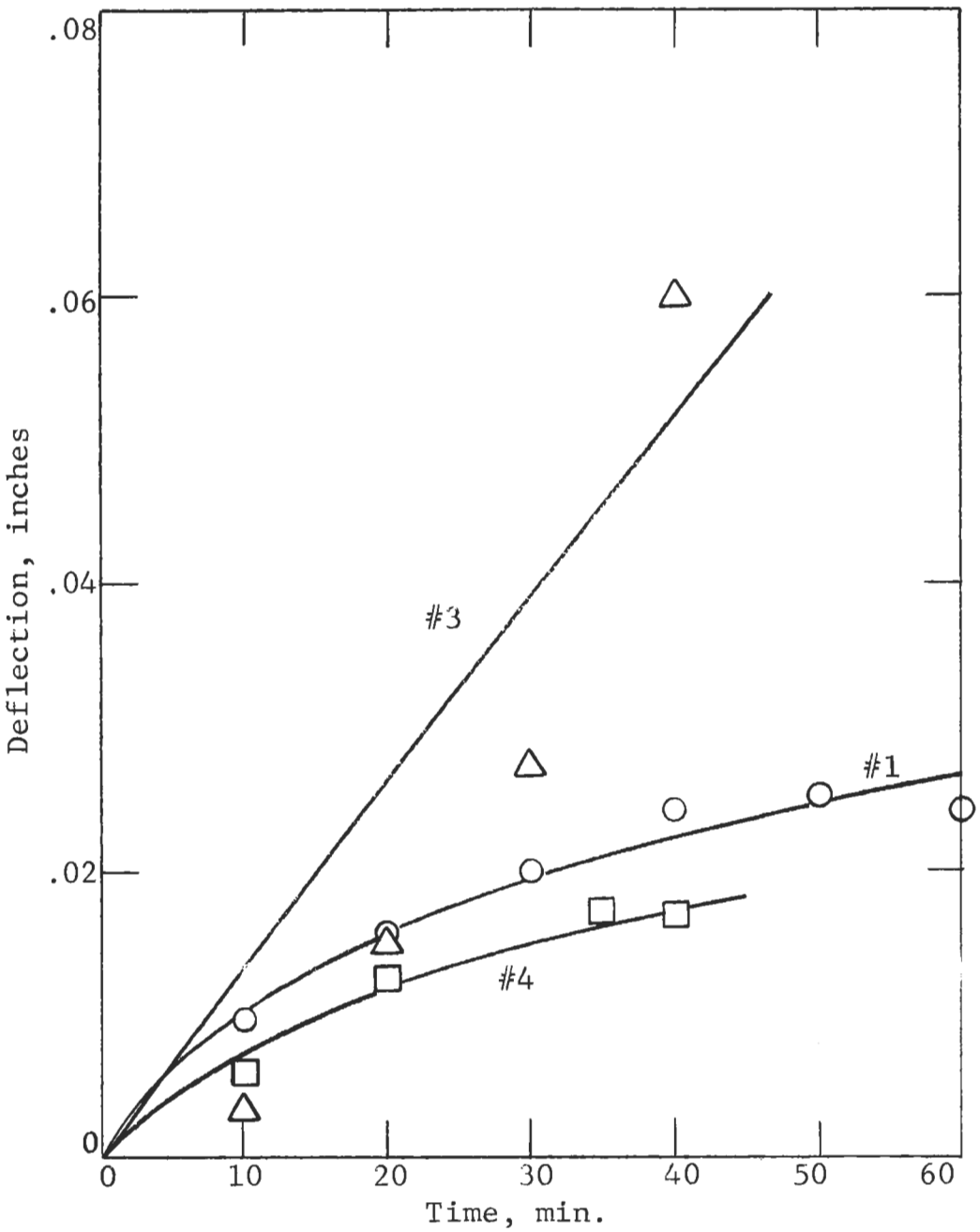

Figure 118. SHORT TERM FLEXURAL CREEP FOR JTA (3182°F, 668 psi, A/G)

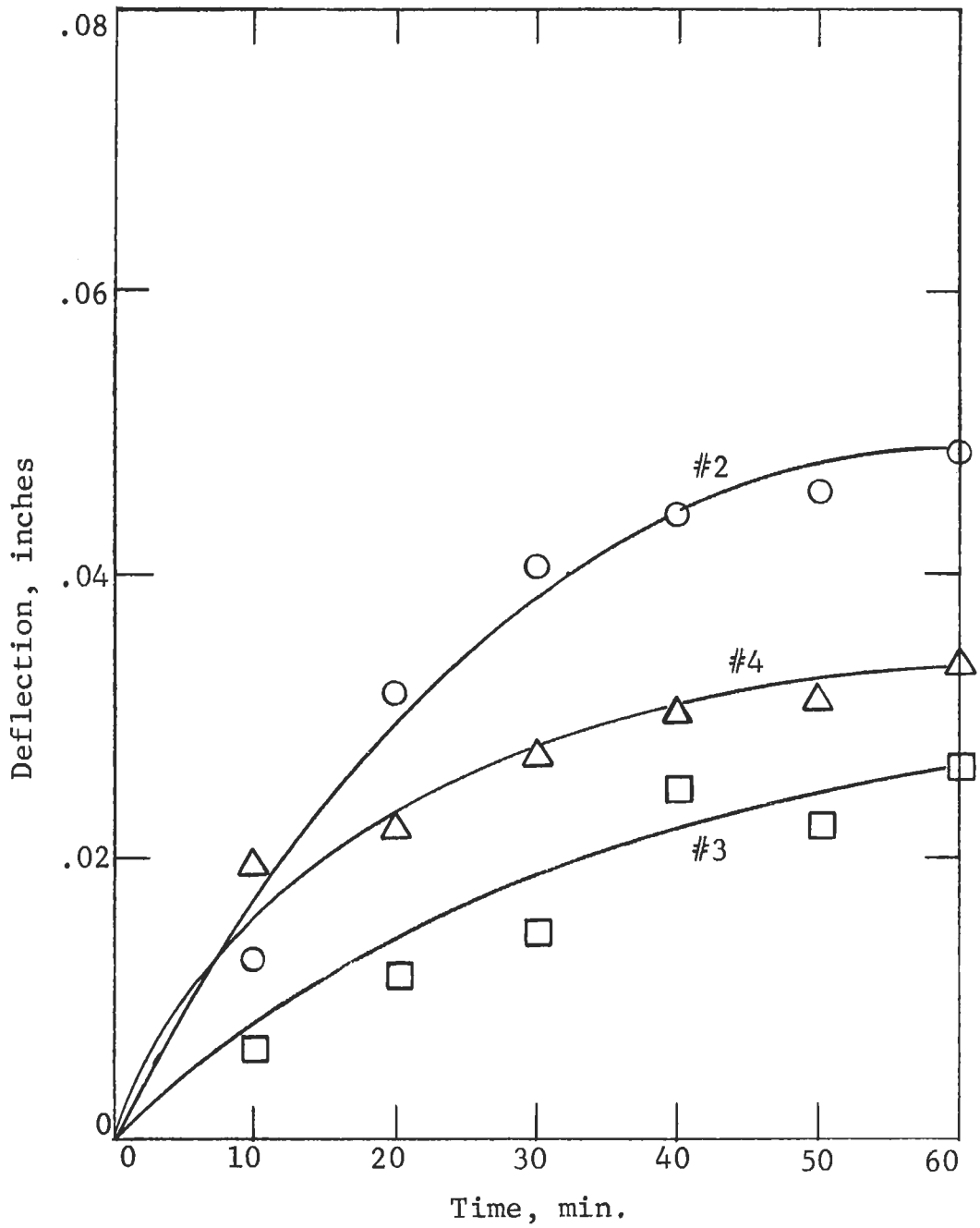

Figure 119. SHORT TERM FLEXURAL CREEP FOR JTA (3632°F, 334 psi, A/G)

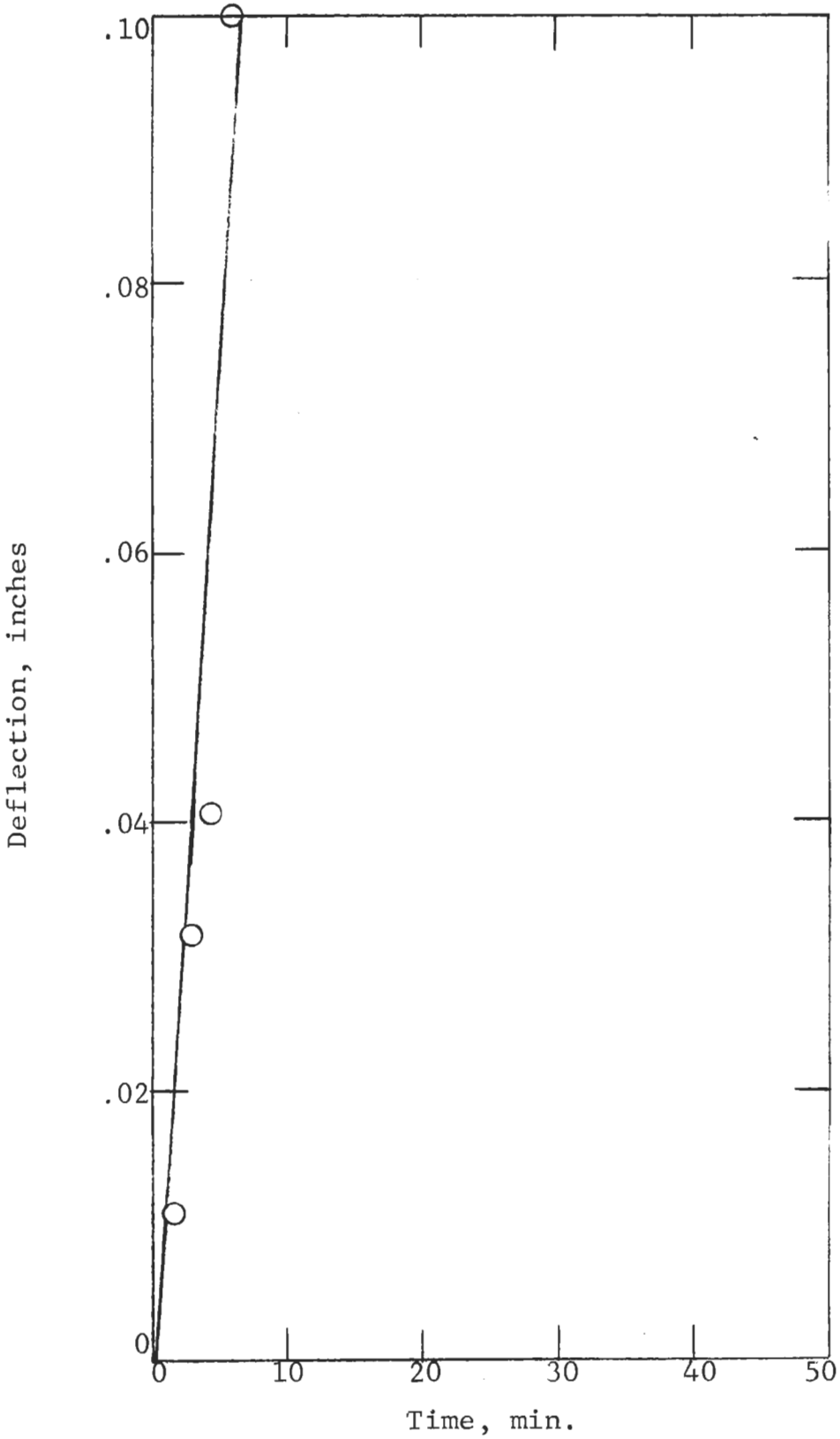

Figure 120. SHORT TERM FLEXURAL CREEP FOR JTA (3992°F, 334 psi, A/G)

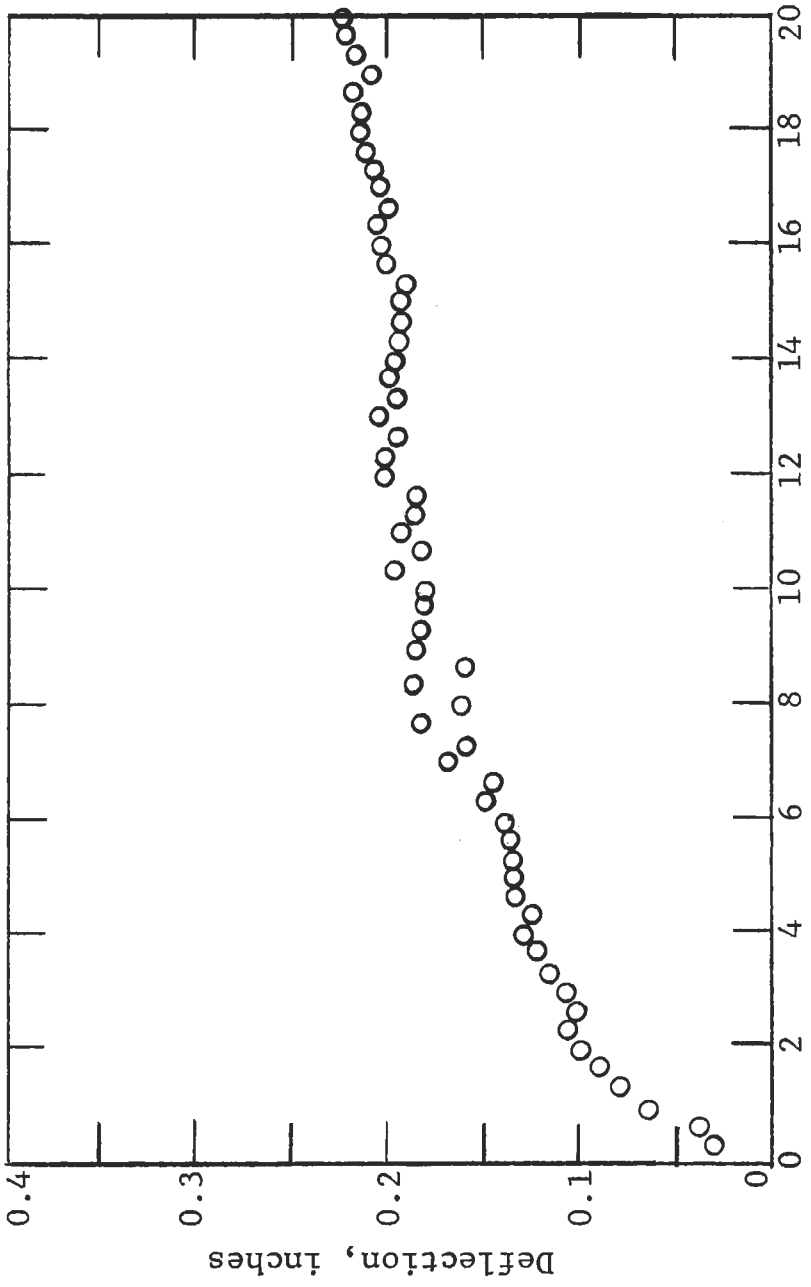

Figure 121. LONG TERM FLEXURAL CREEP FOR JTA (3182°F, 297 psi, W/G)

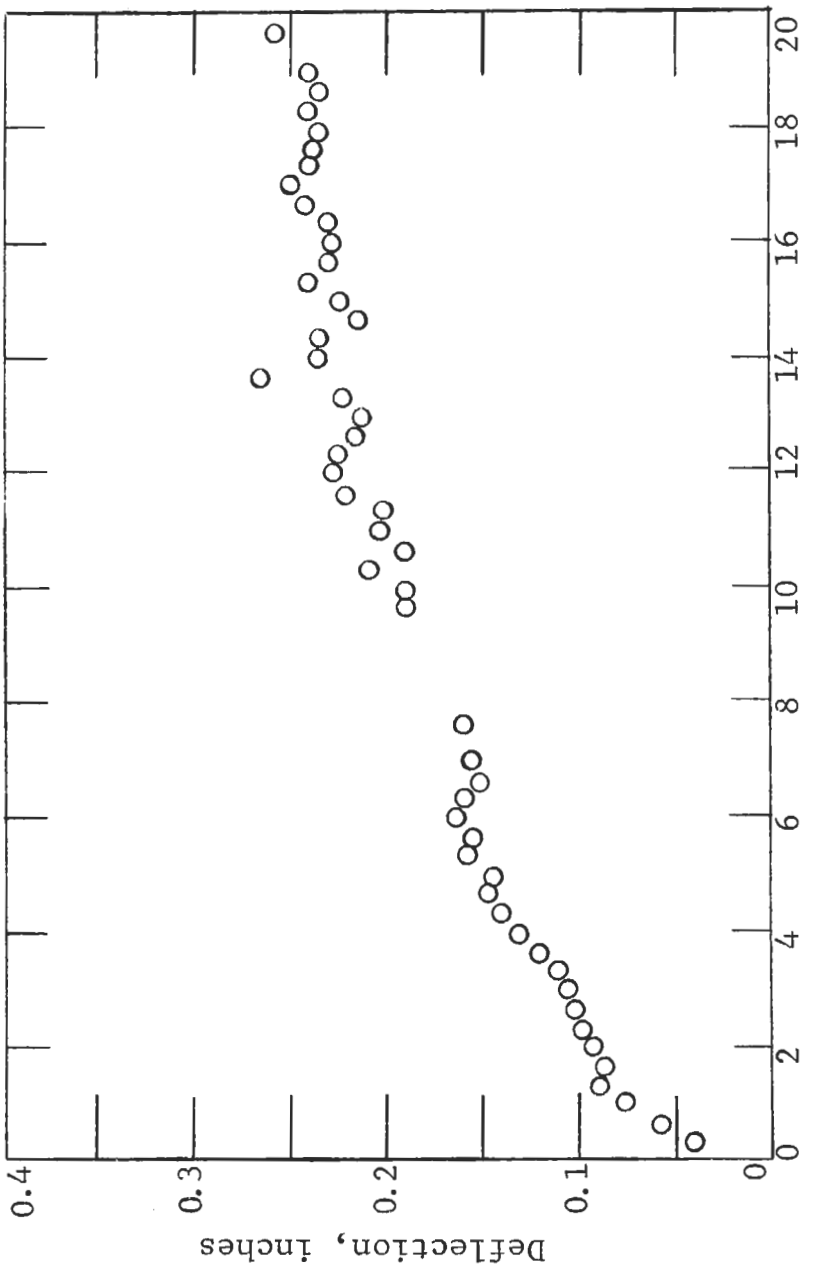

Figure 122. LONG TERM FLEXURAL CREEP FOR JTA (3182°F, 297 psi, A/G)

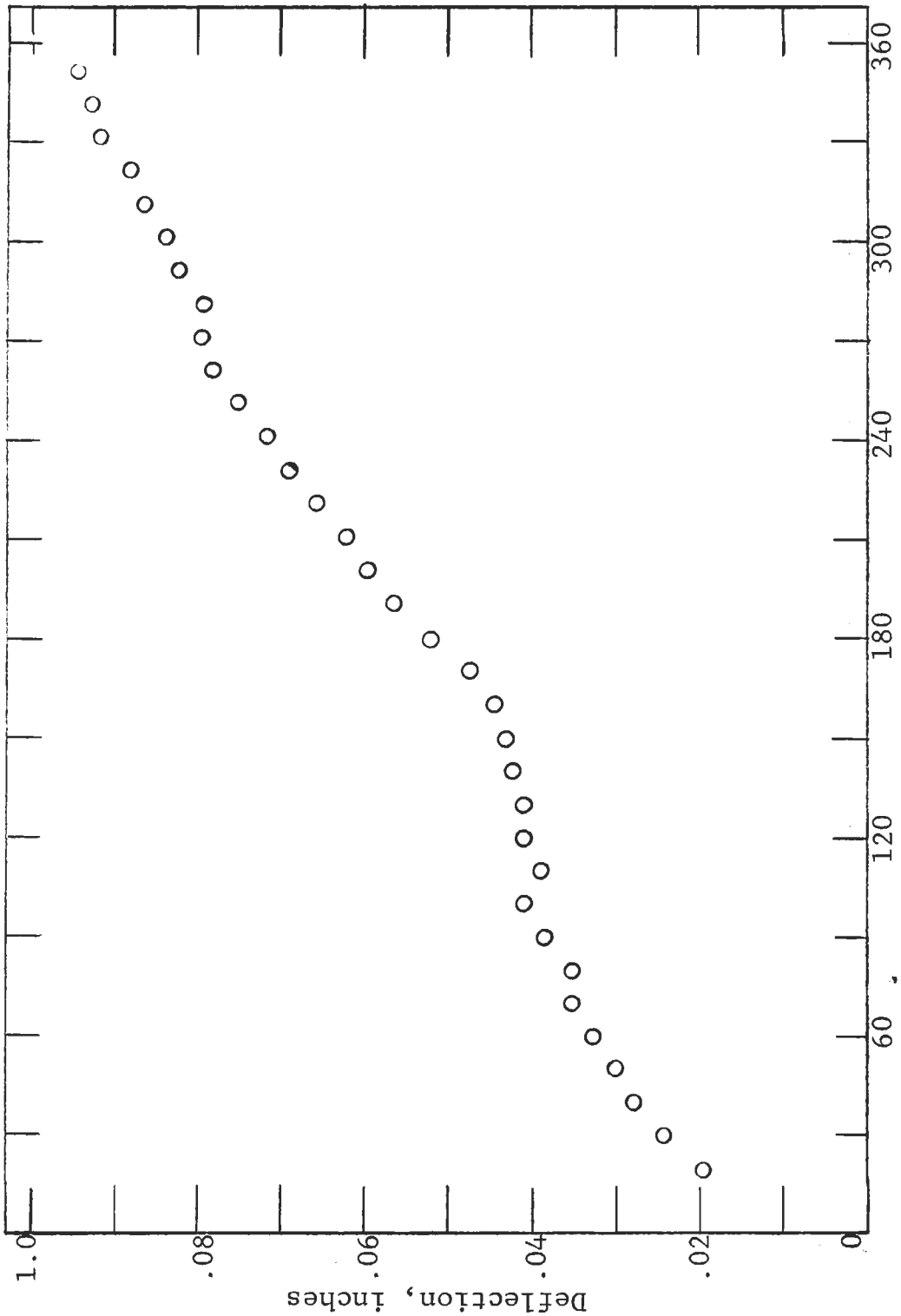

Figure 123. LONG TERM FLEXURAL CREEP FOR JTA (3992°F, 74 psi, A/G)

of data for both long- and short-term creep was good with respect to creep data usually obtained for ceramic materials.

Figure 124 provides a log-log plot of the data for use when extraplating the data for design use. The data used to produce the curves shown in Figure 124 were analyzed for the trends shown, and certain assumptions were made. The data obtained, while limited, appeared to exhibit similar behavior for with- and across-grain orientation. Multiple points for creep rate versus temperature and stress level were only obtained from 3182°F to 4082°F for with- and across-grain orientations. The creep-rate envelopes shown for these data led to the assumption that grain orientation may not be significant with respect to creep rates. After making this assumption, the 3642°F plot was drawn by combining and plating the with- and across-grain creep data. The data shown in Figure 124 should be used with caution, but they at least provide the design with some indication as to what the long-term deformation of JTA graphite will be in steady state creep over a temperature and stress range.

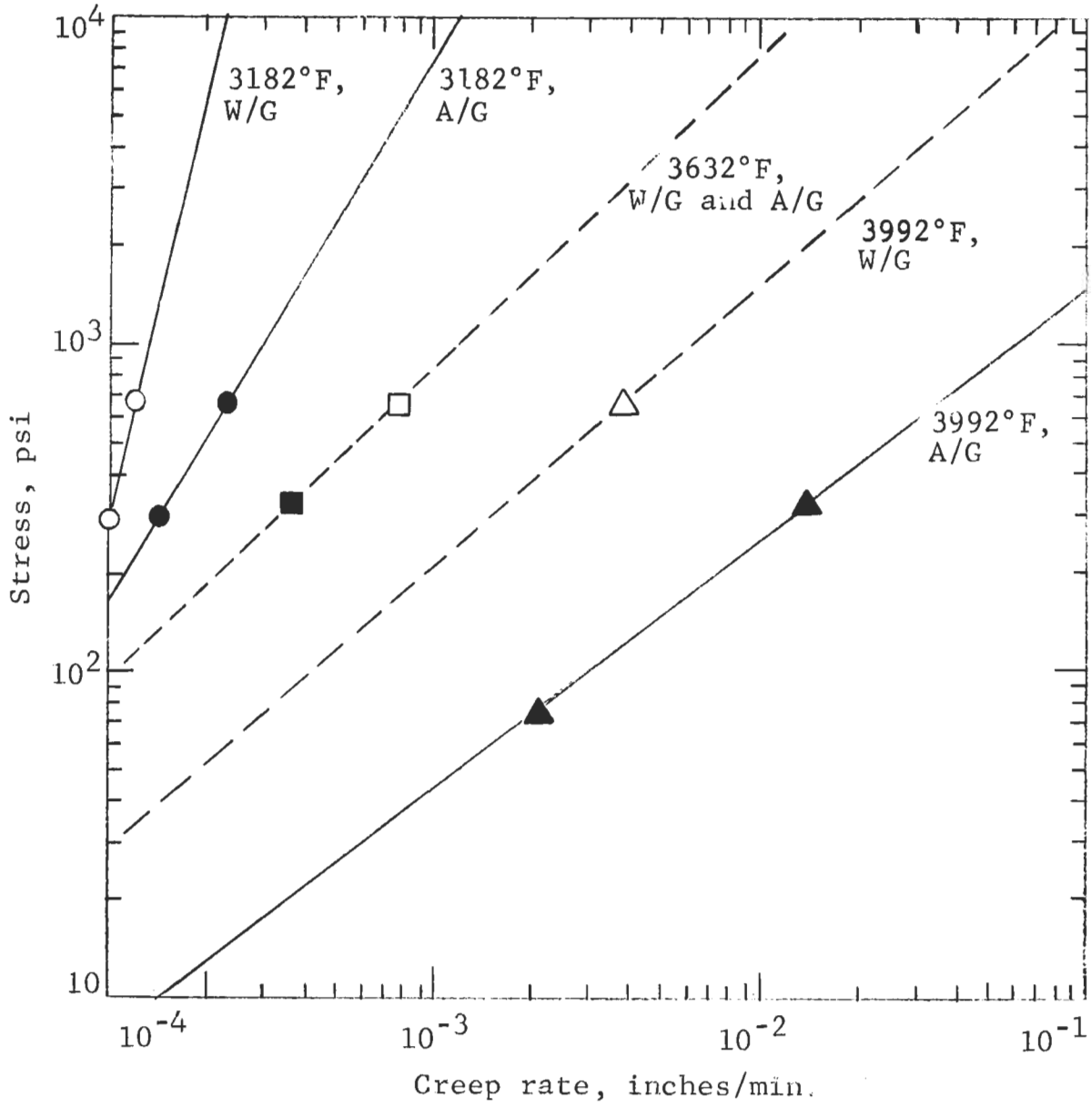

Figure 124. LOG-LOG OF SUMMARIZED CREEP DATA

SECTION V

THERMAL PROPERTIES

Choice of a material for a specific use is based mainly on performance. The expected performance of a material is the principal concern of the designer and one that requires the greatest amount of analytical treatment. Since JTA graphite is specifically designed for high-temperature use in an oxidizing atmosphere, its thermal properties are of utmost concern with respect to thermal stress and heat-transfer characteristics. The material properties that determine the thermal stress resistance of a material are: tensile strength (σ), Young's elastic modulus (E), Poisson's ratio (μ), coefficient of thermal expansion (α), thermal conductivity (K), and emissivity (ρ). Each of these is a function of temperature. The temperature at which thermal friction occurs is a function of these properties:

$$\Delta T = f\left(\sigma, \frac{1}{E}, \frac{1}{\alpha}, K, \mu, c\rho\right) \qquad (24)$$

Material with good thermal-fracture resistance should have high strength, high emissivity, high thermal conductivity, and low values of thermal expansion and modulus of elasticity. The mechanical properties, such as strength, and the elastic properties have been discussed, and the thermal properties such as expansion, conductivity, and emissivity are discussed below.

1. THERMAL EXPANSION

A prime factor in analyzing thermal-stress characteristics is thermal expansion. Thermal-expansion measurements were made on bars 1/4 in. square x 4 in. long. A filar microtelescope was used to make expansion measurements. Five specimens were studied for each grain orientation. Measurements were made at as high as 4082°F.

Thermal-expansion data are presented in Figures 125 and 126. Data from other programs are also shown in these figures for comparison purposes. A comparison of the expansions obtained from the programs show fair agreement, except for the Union Carbide data for across-grain expansion above 3182°F. Above this temperature the Union Carbide thermal-expansion data exhibited a steep rise.

2. THERMAL CONDUCTIVITY

The thermal conductivity of the JTA graphite was determined from room-temperature to 1500°F by the split-block method and from 1500 to approximately 4000°F by determining the thermal diffusivity[15] and then calculating thermal conductivity from the measured values of thermal diffusivity, specific heat, and density.

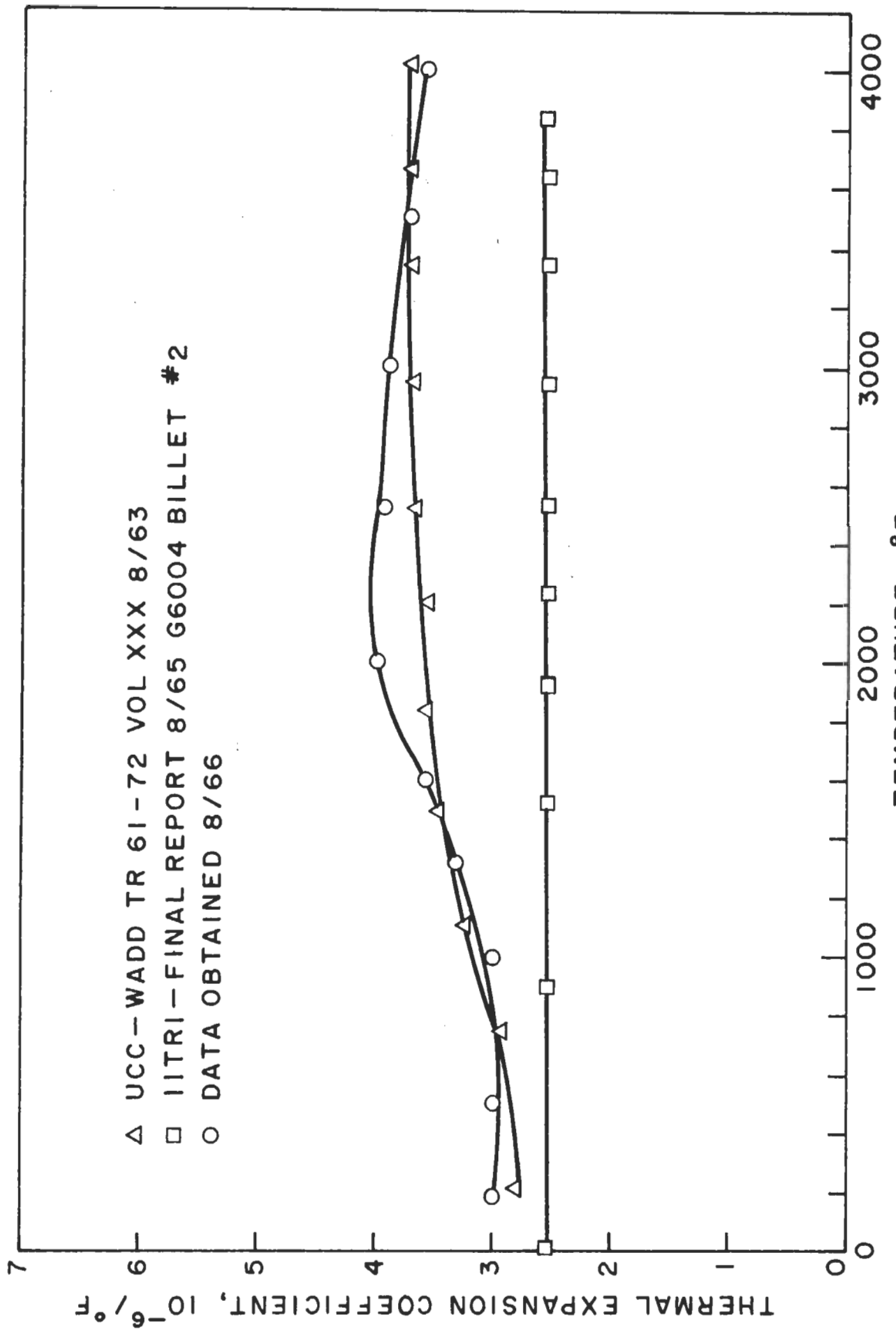

Figure 125. AVERAGE THERMAL EXPANSION COEFFICIENT OF WITH GRAIN JTA GRAPHITE

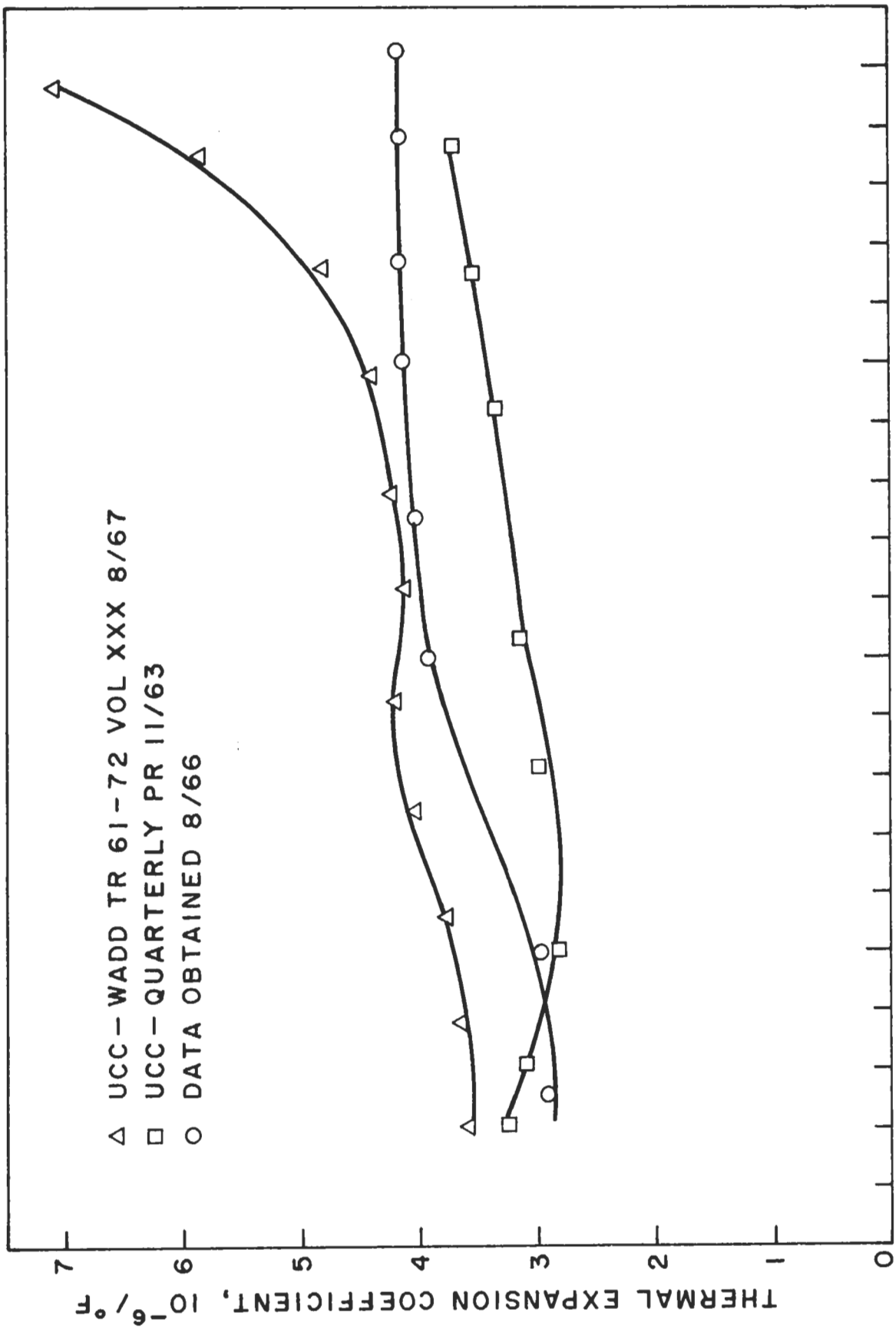

Figure 126. AVERAGE THERMAL EXPANSION COEFFICIENT OF ACROSS GRAIN JTA GRAPHITE

At elevated temperatures, thermal conductivity can be obtained from diffusivity. Thermal diffusivity is defined as:

$$\alpha = \frac{k}{\rho c_p} \qquad (25)$$

where

k is the thermal conductivity
ρ is the density
c_p is the specific heat.

If thermal diffusivity, specific heat, and density are known, thermal conductivity can be calculated from Equation 25. At high temperatures density and specific heat are more easily measured than thermal conductivity. The units of thermal diffusivity are $(\text{length})^2\ (\text{time})^{-1}$; the simplicity of these units suggests that this property may be more easily measured than thermal conductivity. The thermal-diffusivity measurement was obtained by the transient-cooling technique. Values of density and specific heat were obtained by independent measurements. The specific heat apparatus is shown in Figure 127.

Results of determinations of thermal conductivity of materials by the split-block method and by the Powell stacked-disk method, an absolute method, compared very well. Errors in measurement may result from improper guarding, which allows heat loss from the periphery of the cylinders and poor contact between cylinder faces and consequent distortion of the heat-flow pattern. It is believed that the accuracy of results obtained by using this apparatus is ±4%.

The technique used to determine thermal diffusivity at high temperatures can be described as follows. A slab of material is mounted in a furnace and heated to a constant, uniform temperature. A heat sink, which consists of a thin section of material, is mounted outside the furnace and is provided with a mechanical drive capable of rapidly thrusting the heat sink into the furnace. The heat sink remains in the furnace; then the drive mechanism rapidly withdraws it from the furnace. The sink does not physically contact the slab. Since the sink is at room temperature, radiation heat interchange occurs between the slab face and the heat sink, and the slab temperature drops. The temperature-time behavior at a point in the slab is then measured. The thermal-diffusivity furnace is shown in Figure 128.

Thermal-conductivity data for JTA are shown in Table XXII. The measurements at as high as 1400°F were made in a wire-wound resistance furnace, and those from 1500°F to 3600°F were made in a carbon resistance furnace. The results showed that thermal conductivity across the grain is approximately half that of the with-grain orientation. These results verify the expected anisotropy of properties of JTA graphite as 2:1 for the across- and

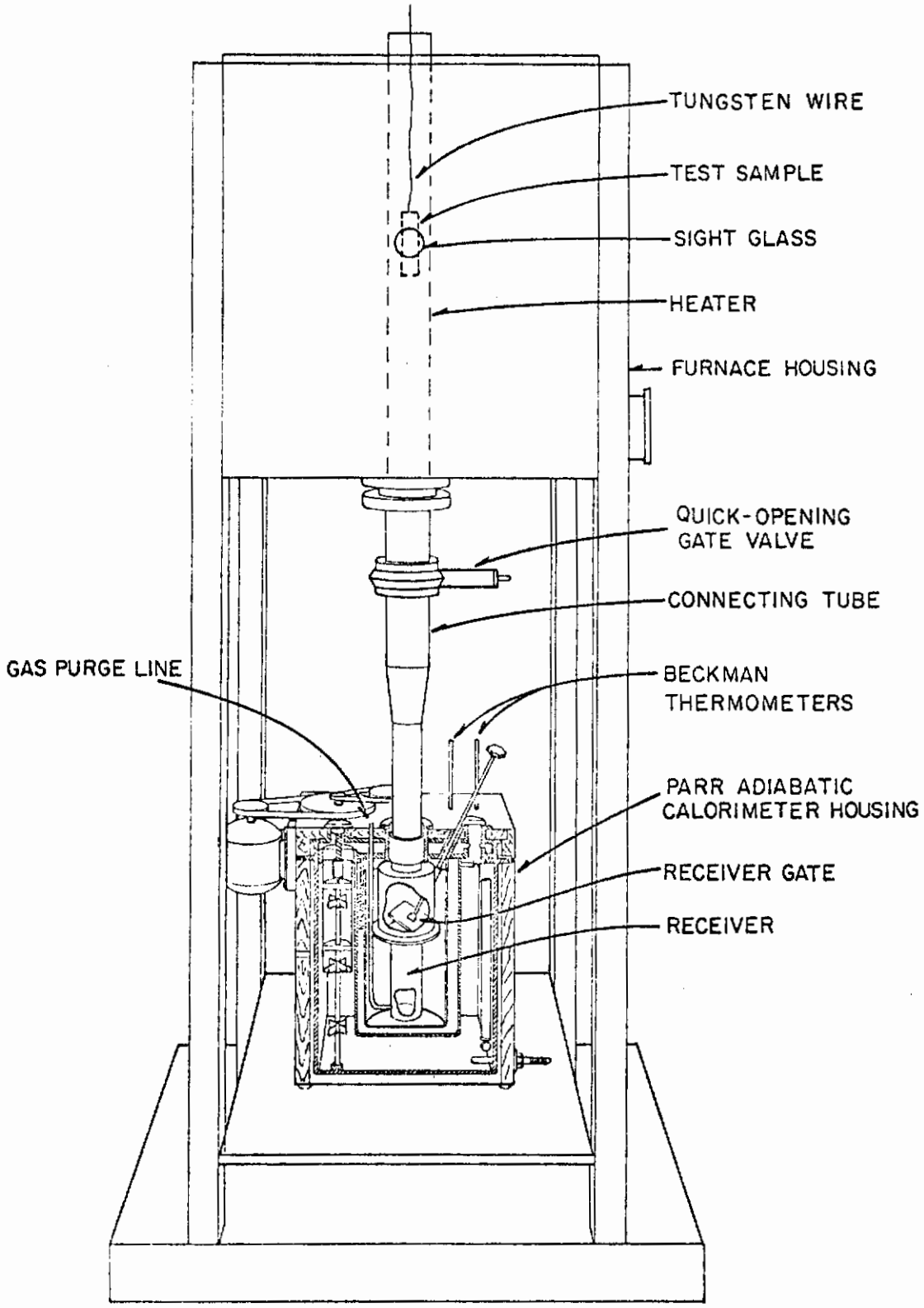

Figure 127. SCHEMATIC DIAGRAM OF APPARATUS FOR MEASURING SPECIFIC HEAT

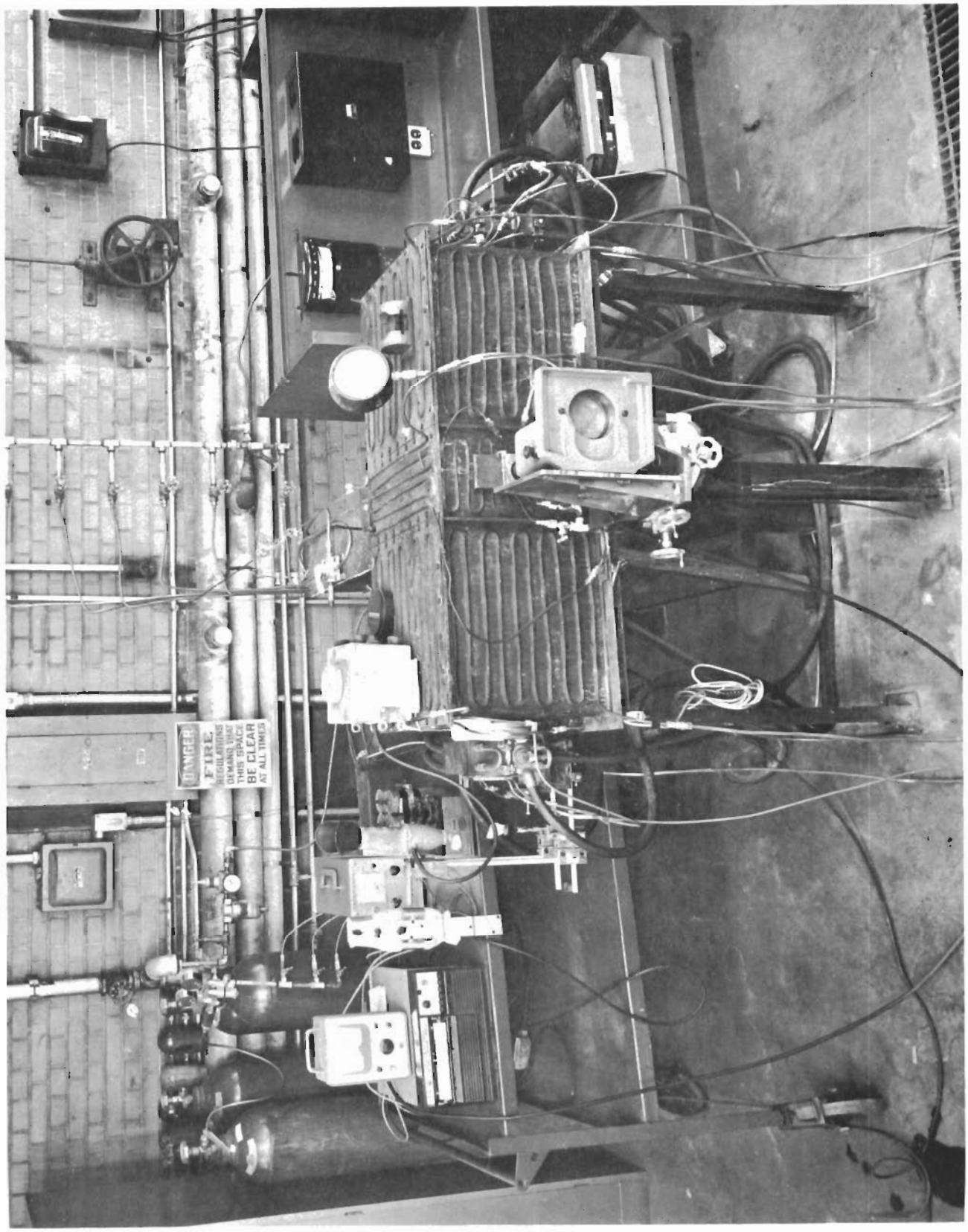

Figure 128. THERMAL DIFFUSIVITY APPARATUS AND ASSOCIATED SYSTEMS

Table XXII. THERMAL CONDUCTIVITY OF JTA GRAPHITE

Sample 7-F-12 (With grain)		Sample 14-G-1 (With grain)		Sample 14-G-1 (Across grain)	
Temp. °F	Thermal conductivity, Btu/hr ft °F	Temp. °F	Thermal conductivity, Btu/hr ft °F	Temp. °F	Thermal conductivity Btu/hr ft °F
196	71.1	209	72.5	178	37.1
230	69.0	215	71.9	178	37.0
537	63.7	427	67.2	510	34.6
535	64.3	431	68.0	493	34.9
932	53.3	909	54.6	696	33.1
925	55.0	894	55.3	708	32.4
1325	49.2	1371	51.2	1392	28.2
1328	51.1	1367	50.5	1385	28.6
2015	45.5	1925	44.5	1905	24.8
2550	41.9	2480	44.0	2450	22.0
3005	42.6	3035	41.1	2980	20.7
3570	40.1	3510	41.0	3540	19.8

with-grain orientations. The data are similar to those previously reported for this material.(15) Measurements were not made at higher than 3600°F because fumes from the JTA prevented accurate sample observation.

3. SPECIFIC HEAT

The enthalpies of three JTA graphites (7-F-14, 7-F-12, and 14-G-1) were measured from room-temperature to 4000°F by using the drop-calorimeter technique. A sample of each material, was heated to a desired temperature in a furnace and then dropped into a modified Parr calorimeter. Three drops were made at each temperature for each material in order to assure the accuracy and the reproducibility of the results. The process was repeated at sucessively higher temperatures at intervals of approximately 200°F.

The enthalpy of the material was calculated from the experimental measurements by using the following equation:

$$\Delta H = \frac{W_e (t_f - t_i)}{M_s} \tag{26}$$

where

W_e is the water equivalent, receiver, and weight water contained in bucket, (Btu/°F)
t_f and t_i are the final and the initial calorimeter temperatures, respectively, as measured by the calorimeter thermometer (°F)
M_s is the mass of the sample (lb)

From the enthalpy values, the enthalpy curve versus temperature was obtained. An equation was fitted to this enthalpy curve, and specific heat was determined by differentiating it with respect to temperature at constant pressure.

$$C_p = \left(\frac{\partial H}{\partial t}\right)_p \tag{27}$$

where

C_p is the specific heat at constant pressure
H^p is enthalpy
t is temperature.

The enthalpies of the three materials as functions of temperature are presented in Tables XXIII through XV and in Figure 129.

Since there was no significant difference among enthalpy values of all three JTA graphites, one function for specific heat versus temperature was developed for all three materials. This is shown in Table XXVI and Figure 130.

Table XXIII. ENTHALPY VALUES FOR JTA GRAPHITE (7-F-14) (Temperature, 80°F)

Temp., °F	ΔH, Btu/lb
80	0
215	21
426	60
630	105
784	145
973	196
1154	245
1342	300
1510	350
1750	425
1912	477
2143	560
2297	605
2510	685
2723	774
2905	845
3120	920
3296	1000
3471	1080
3652	1147
3789	1232
3973	1310

Table XXIV. ENTHALPY VALUES FOR JTA GRAPHITE (7-F-12) (Temperature, 80°F)

Temp., °F	ΔH, Btu/lb
80	0
178	15
362	48
583	95
730	130
912	180
1098	230
1306	293
1470	338
1620	385
1835	452
2057	528
2210	579
2445	665
2681	750
2901	843
3124	925
3305	1003
3497	1086
3670	1162
3809	1230
3962	1315

Table XXV. ENTHALPY VALUES FOR JTA GRAPHITE (14-G-1) (Temperature, 80°F)

Temp., °F	ΔH, Btu/lb
80	0
212	20
415	58
620	103
783	143
963	192
1140	241
1315	290
1508	350
1690	404
1903	475
2160	560
2345	627
2516	690
2749	782
2910	841
3117	922
3315	1005
3491	1080
3663	1154
3796	1221
3971	1312

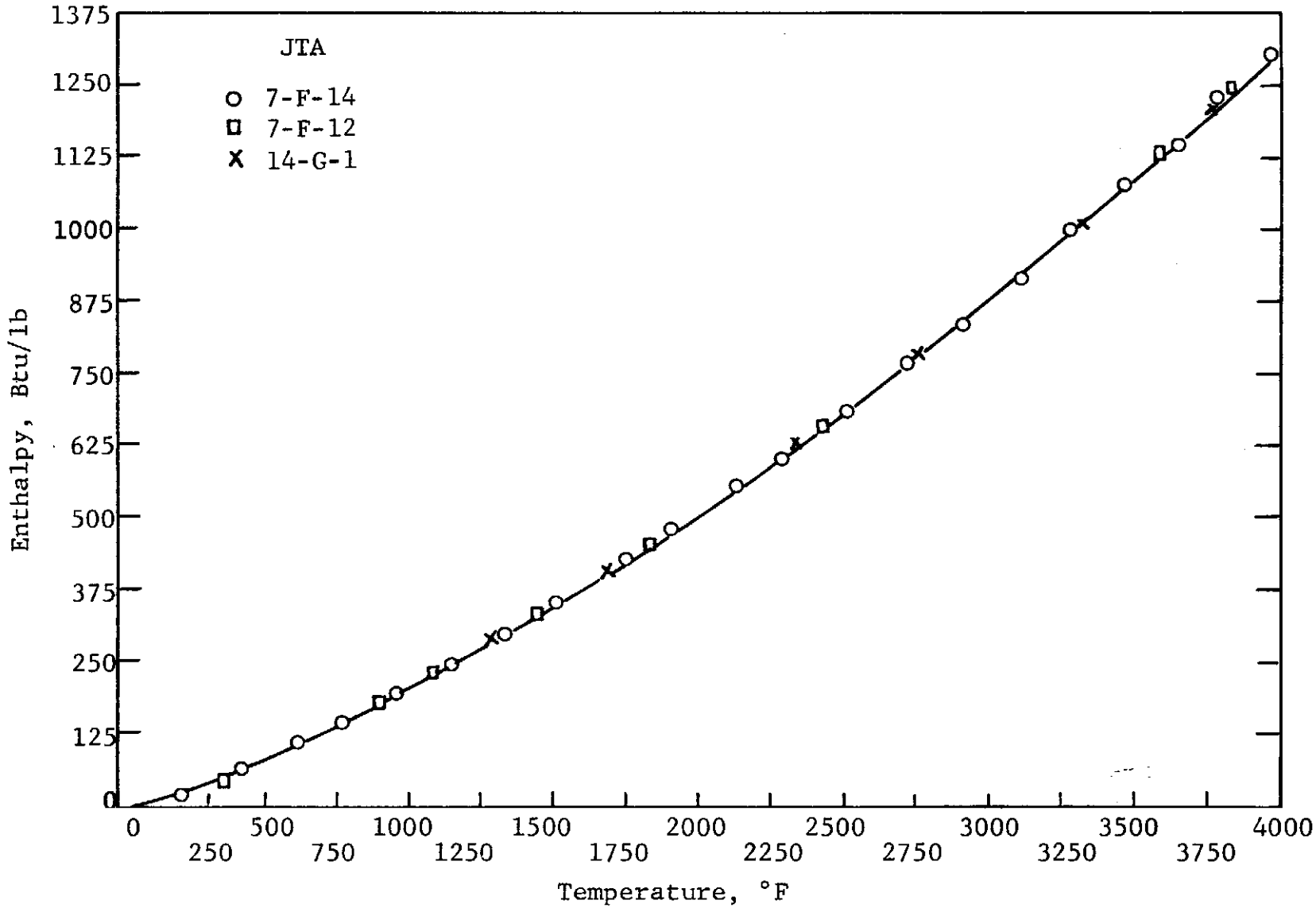

Figure 129. ENTHALPY OF JTA GRAPHITES (7-F-14, 7-F-12, and 14-G-1)

Table XXVI. SPECIFIC HEAT OF JTA GRAPHITES (7-F-12, 7-F-14, and 14-G-1)

Temp., °F	C_p, Btu/lb °F
500	0.220
1000	0.270
1500	0.310
2000	0.325
2500	0.360
3000	0.390
3500	0.430
4000	0.470

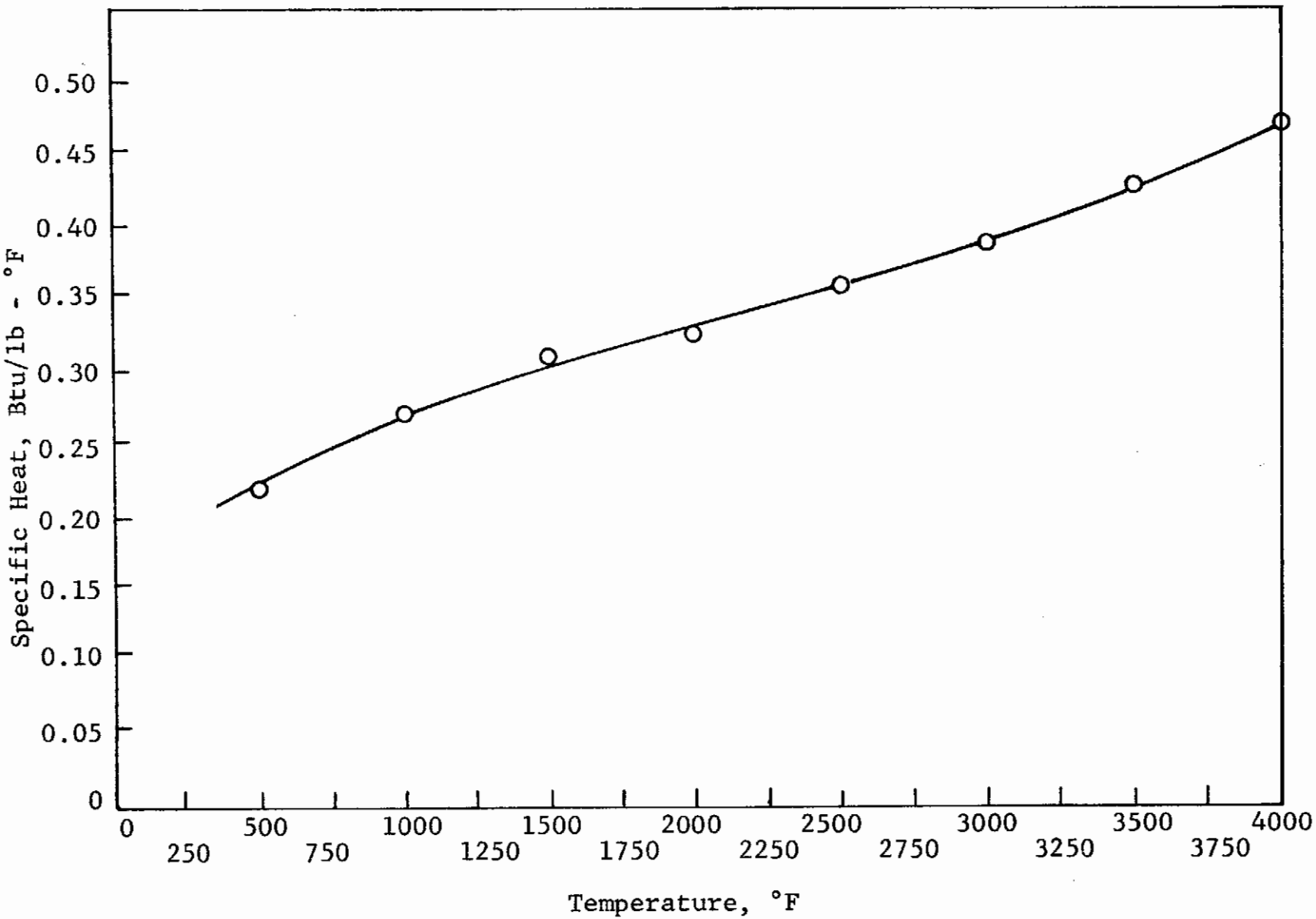

Figure 130. SPECIFIC HEAT OF JTA GRAPHITES (7-F-14, 7-F-12, and 14-G-1)

4. NORMAL EMITTANCE

The total normal emittance of four JTA graphite specimens was determined by the comparative method over the temperature range of 1985°F to 4082°F. The method consists of heating a specimen in a furnace to a desired temperature. After steady-state conditions are reached, the radiant intensity from the surface of the specimen is compared to the radiant intensity from a black-body cavity at the same temperature as the specimen. The ratio of the two intensities is the total normal emittance of the material.

Four specimens of JTA graphite were machined to 1 in. in diameter x 1 in. long. Three of the four specimens were heated 1 hr in air at constant temperatures of 3182°F, 3632°F, and 4082°F, respectively. The fourth specimen was not heated before the emittance measurements were made. The four specimens, as they appeared before the start of the emittance measurements, are shown in the top photograph of Figure 131.

The specimens were heated in a graphite resistance-heated furnace in which an argon atmosphere was maintained throughout the tests. Each specimen was measured at approximately 2012°F, 2552°F, 3002°F, 3452°F and 3992°F. The heating schedule was approximately the same for all specimens, namely, room temperature to 2012°F for 2 hr, 2552°F for 1 hr, 3002°F for 1 hr, 3452°F for 1 hr, and 3992°F for 1 hr.

The emittance instrumentation consists basically of a thermistor bolometer radiation detector. A long water-cooled tube and a bridge circuit are connected to an oscilloscope. The water-cooled tube is open at both ends. Radiation from the sample surface passes through the tube and is detected by the thermistor bolometer mounted at the opposite end of the tube. The cooled tube and the thermistor are mounted so they can move up and down as a unit.

The thermistor bolometer is mounted in one leg of a dc Wheatstone-bridge circuit. An identical thermistor, which is shielded from the incoming radiation, is mounted in another leg of the bridge circuit. The signal from the bridge circuit is read out on an oscilloscope. A more detailed description of the instrumentation was given in an earlier report.(15)

The following operations were performed to make the emittance measurements:

1. The sample, 1 in. in diameter and 1 in. long, was placed in the cavity of a graphite sample holder located in the midsection of the graphite tube heater. The length-to-diameter ratio of the cavity was sufficient to provide an effective emittance nearly equal to unity.

VIRGIN JTA

JTA OXIDIZED 1 HR AT 3182°F

JTA OXIDIZED 1 HR AT 3632°F

JTA OXIDIZED 1 HR AT 3992°F

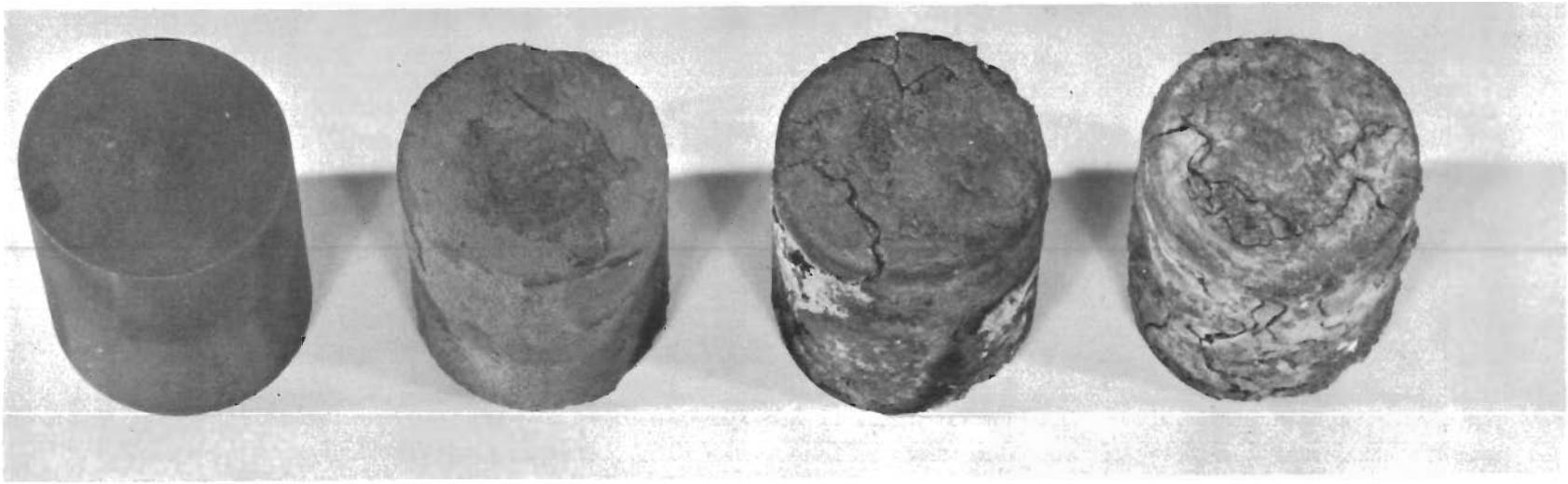

Figure 131. JTA GRAPHITE BEFORE (TOP) AND AFTER (BOTTOM) HEATING DURING EMITTANCE MEASUREMENTS

2. The furnace was heated until steady-state conditions were achieved at the desired temperature. For these conditions, the sample and the sample holder were at the same temperature.

3. The water-cooled tube was rapidly inserted into the furnace until the tip of the tube was within 1/16 in. of the sample surface. The time sweep of the oscilloscope was triggered as the tube was inserted in the furnace. The maximum bolometer output occurred as the tube tip reached the entrance of black-body cavity. The bolometer output was lower when the tube tip was at the sample surface, depending on the total normal emittance of the material surface.

When the cooled tube is near the sample surface, heat is lost from the sample surface, and the sample temperature rapidly drops. However, with a record of the bolometer output versus time, the radiant energy at time zero (when the cooled tube tip first reaches the sample surface) can be easily determined.

The results of the emittance measurements are shown in Figure 132 and Table XXVII. The emittance of all samples ranged from 0.82 to 0.92. It seems apparent that the oxidized coating was adversely affected by heating in an inert atmosphere, as can be seen in Figure 131. The last sample heated during the emittance measurements, which had been oxidized at 3992°F, was not heated above 2912°F in order to determine whether the oxidized coating was affected by heating above 2912°F in the inert atmosphere. However, this sample had an appearance only slightly different from the samples heated to 3992°F. The emittance values for JTA graphite heated in air(12) are also shown in Figure 132 for comparison.

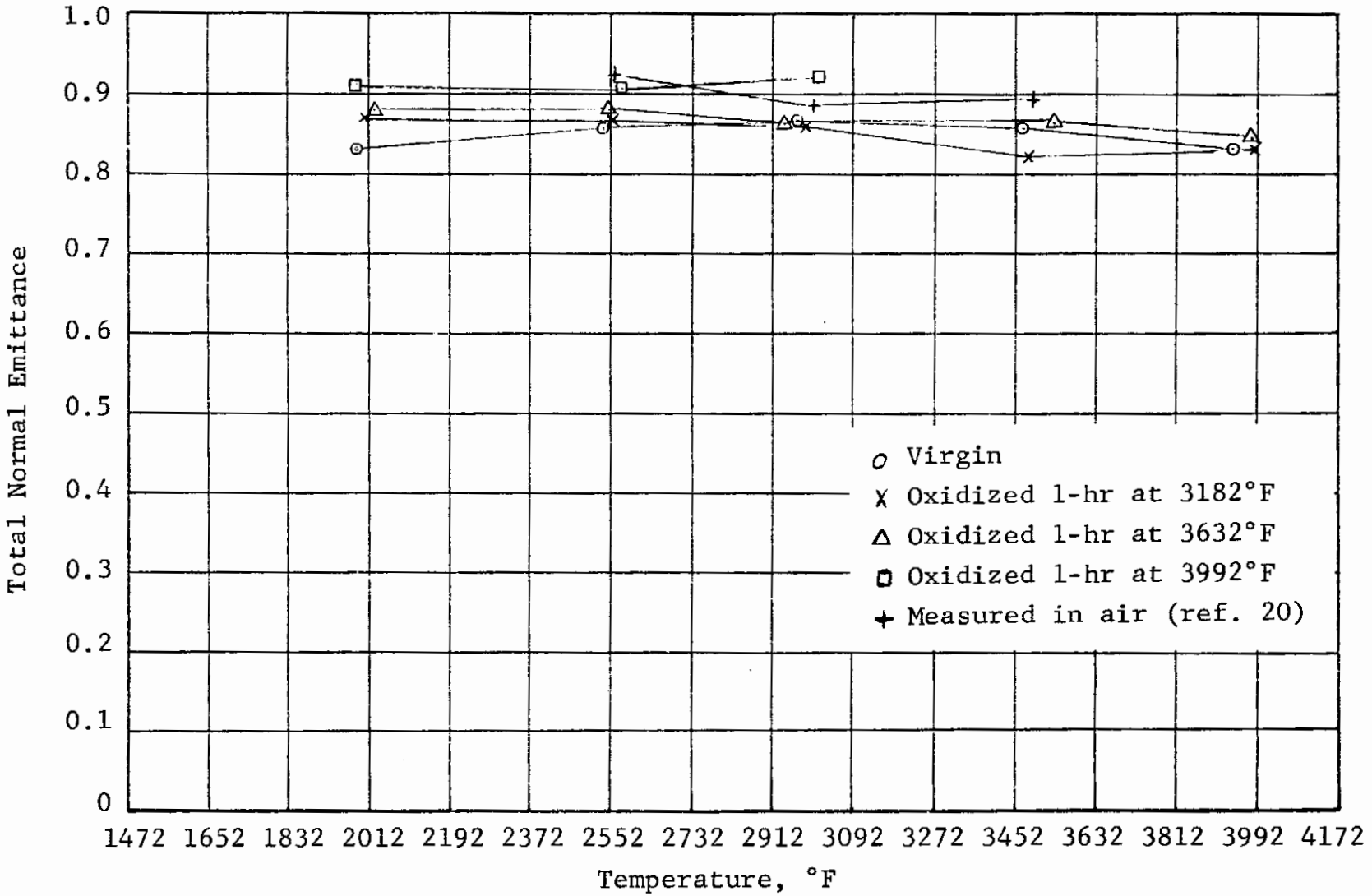

Figure 132. TOTAL NORMAL EMITTANCE OF VIRGIN AND OXIDIZED JTA GRAPHITE

Table XXVII. EMITTANCE OF VIRGIN AND OXIDIZED JTA GRAPHITE

Sample preparation	Temp., °F	Emittance
Virgin	1981	0.83
	1985	0.83
	2534	0.86
	2539	0.85
	2962	0.86
		0.87
	3466	0.86
	3470	0.85
	3938	0.84
		0.82
Oxidized 1 hr at 3182°F	2003	0.87
	2012	0.88
	2561	0.87
	2570	0.86
	2984	0.86
	2989	0.85
	3488	0.81
		0.83
	3982	0.84
		0.82
Oxidized 1 hr at 3632°F	2030	0.89
		0.88
	2552	0.88
		0.89
	2948	0.86
		0.86
	3560	0.87
		0.86
	3974	0.84
	3979	0.85
Oxidized 1 hr at 4092°F	1985	0.92
		0.90
	2588	0.91
		0.90
	3020	0.92
		0.92

SECTION VI

CONCLUSIONS AND RECOMMENDATIONS

JTA graphite is a high strength graphitic material which possesses moderate oxidation resistance up to 2750°F at ambient air pressures and excellent resistance at lower air pressures to above 3650°F. Measured physical and mechanical properties show a 2:1 anisotropy with respect to with-grain and across-grain orientations. Its advantages over other graphitic materials is its relatively high strength and oxidation resistance. Its major disadvantages are its relatively high bulk density, high cost, and apparent difficulty in making suitable billets in large sizes. The observed variability within and between billets studied in this program is similar to that generally observed in graphite. However, this variability is a problem in employing the material for structural applications.

The properties of JTA graphite suggest its consideration as a structural reentry material; its with-grain tensile strength to density ratio is 4000, compared to approximately 800 for standard graphite(16). Its across-grain ratio is 2000 as compared to 600. Since its thermal conductivity and thermal expansion is similar to that for standard graphite, its thermal shock resistance should also be similar. This combination of properties together with its oxidation resistance is indicative of its applicability for nose caps, leading edge surfaces, and other structural hot parts of reentry vehicles.

Standard testing techniques, using an inert atmosphere, were employed for measuring tension, compression, flexure, coefficient of expansion, thermal conductivity, specific heat, and normal emittance, and determining elastic properties and creep resistance. These demonstrated techniques have provided adequate design data for most brittle materials. However, when determining the strength of JTA-type materials under oxidizing conditions, weight loss, alone, presents erroneous data inasmuch as compensating reactions simultaneously occur. Also, ambient strength measurements do not reflect this changing nature of the material. Studies on this program have indicated that testing should be performed under actual temperature and atmospheric service conditions. Results indicated significant differences when obtained under ambient conditions (after oxidation) as compared to under service temperature and atmospheric conditions. Our test results also indicate that indirect methods of obtaining Poisson's ratio do not produce reliable data, and direct measurements are required.

It is recommended that future work be conducted to improve fabrication procedures to insure more reliability in larger billet sizes, and to conduct studies to develop improved high temperature dynamic oxidation test procedures, and improved direct high temperature Poisson ratio measurement procedures.

REFERENCES

1. Bortz, S. A., Wade, T. B., "Analysis of Mechanical Testing Procedure for Brittle Materials," AMRA CR 67-09/1 (September 1967).

2. "Evaluation of Graphite Refractory Composites for High-Temperature Structural Use," IITRI Project G6004 Final Report for Ohio State University Research Foundation (July 15, 1965).

3. Zeitsch, K. V., Criscione, J. M., "Oxidation Resistant Graphite-Base Composites," WADD-TR-61-72, Vol. XXX (August 1963).

4. Shaffer, P. T. B., High-Temperature Materials, Plenum Press, New York (1964).

5. Anthony, F. M., et al, "Selection Techniques for Brittle Materials. The Evaluation of JTA Graphite Composite as a Structural Refractory Ceramic Body," AFML-TR-67-78, (May 1967).

6. "Metal Carbide-Graphite Composites," IITRI Project G6003 Summary Report, NASA Contract No. NASr-65(09) (September 1967).

7. Technical Report AFML-TR-66-310, Part I, Air Force Materials Laboratory, Wright-Patterson Air Force Base, Ohio (October 1966).

8. Nightingale, R. E., Nuclear Graphite, Academic Press, pp. 90-91 (1962).

9. Barnett, R. L., et al, "The Behavior and Design of Brittle Structures," AFFDL-TR-65-165 (September 1966).

10. Evaluation of IITRI Split Spherical Collet Grip for Tensile Testing of Brittle Materials," IITRI Project G6019 for Douglas Aircraft Company, Santa Monica, California (December 1967).

11. Pears, C. D., "Evaluation of Tensile Data for Brittle Material Obtained with Gas Bearing Concentricity," ASD-TDR-63-245 (May 1963).

12. Dally, J. W., "Evaluation of Thermal Protective Systems for Advanced Aerospace Vehicles," ML TDR 64-204, Vol. III, (April 1965).

13. Durelli, A. J., Ferrer, L., "New Methods to Determine Elastic Constants," Materials Research and Standards, pp. 988-991 (December 1963).

14. Faupel, J. H., Engineering Design, John Wiley and Sons, New York (1964).

15. Christian, W. J., et al, "Evaluation of Thermal Protective Systems for Advanced Aerospace Vehicles," ML TDR 64-204, Vol. II (April 1965).

16. "The Industrial Graphite Engineering Handbook," Union Carbide Corporation, New York, New York (1965).

APPENDIX I

JTA SPECIFICATIONS

The following material specifications were agreed upon by the Carbon Products Division of Union Carbide Corporation for the production and supplying of JTA billets as required for this program.

Finished size:	14-in.-diameter x 7-in.-high
Tolerance:	+0.25 -0.00
Material removal:	0.25 min on all surfaces after pressing
Density:	3.00 to 3.10 g/cc
Maximum total impurities in starting powders:	1.5%
X-ray requirements:	4 per billet, to be mutually agreed upon by purchaser and supplier
Composition:	The normal JTA composition is to be used. The supplier shall specify the weight percentages of major constituents, carbon zirconium diboride, silicon used for each billet, and shall supply it to the purchaser along with raw material samples.
Raw Materials:	Each of the raw material powders used for making billets for a particular order shall be obtained from single lots.
Sampling of raw material:	After dividing the raw materials required for each billet, but just prior to blending of constituents, three samples of each constituent shall be taken, suitably identified, and supplied to the purchaser prior to delivery of the billet. Each sample shall be, as a minimum, sufficient to fill a vial 1-in. in diameter by 3-in.-high.

Sampling of blended material:	After the constituents for a billet have been dry blended, two samples shall be taken, suitably identified, and supplied to the purchaser along with the raw material samples. Each sample shall be, as a minimum, sufficient to fill a vial 1-in. in diameter by 3-in.-high.

The following criteria is used to judge the quality of the JTA material and failure to meet any of the requirements shall be cause for rejection and replacement without additional cost to the purchaser.

1. The density of the finished machined billet shall not be less than 3.00 g/cc as determined by either weight and volume measurements or as determined by water displacement measurements.

2. The minimum finished size shall be 14.00-in.-diameter by 7.00-in.-high.

3. The material shall be free from cracks and voids in excess of 9.03-in. in major dimension, as observable visually and with radiographic techniques normally employed for JTA material when large pieces equal to at least one-eighth (1/8) of the billet volume are examined.

4. After the billet has been cut into test samples, at least 90% of the room temperature strength values shall be free of voids and cracks in excess of 0.03-in. in major dimension as observed visually and by radiography.

5. After modulus of rupture samples are tested, at least 90% of the room temperature strength values shall exceed 10,000 psi with the grain and 5000 psi across the grain. Specimen size shall not exceed 1/2 x 1/2-in. cross section.

6. Other considerations which are mutually agreeable. The value of these specifications in improving both characterization and uniformity of structure has been shown by the producer's having revised its manufacturing procedure to make the quality material required for Contract AF 33(615)-3028. The value of uniform, characterizable structures in reducing property variability will be observed when the data obtained on Contract AF 33(615)-3028 and the proposed program are compared with data obtained on other programs.

APPENDIX II

CHEMICAL ANALYSIS

CHEMICAL AND SPECTROGRAPHIC ANALYSES OF STARTING POWDERS, UNCURED JTA BLENDS

Chemical Analysis

(Error < ± 5% of Quantity Measured)

	Blend I*		Blend II*	
Nonvolatile Carbon	36.13%	35.91%	36.09%	35.97%
Volatile Matter	12.13%	12.26%	12.07%	12.17%
Oxygen	1.14%	1.24%	1.13%	1.13%
Zirconium	29.65%	29.59%	29.88%	30.12%
Boron	7.94%	7.54%	7.99%	8.38%
Silicon	9.06%	9.05%	8.88%	8.80%
Nitrogen	265 ppm	280 ppm	468 ppm	482 ppm

Spectrographic Analysis

(Error < ±10% of Quantity Measured)

	Blend I*	Blend II*
Aluminum	0.08%	0.08%
Barium	0.003%	0.003%
Cobalt	0.03%	0.03%
Chromium	0.002%	0.002%
Copper	0.15%	0.08%
Iron	0.2%	0.15%
Hafnium	0.2%	0.2%
Manganese	0.002%	0.005%
Columbium	0.01%	0.01%
Nickel	0.003%	0.003%
Tin	0.001%	0.001%
Titanium	0.04%	0.04%

Note: Other elements not detected

ppm - Parts per million

*Blends were not identified as to the billet produced

CHEMICAL AND SPECTROGRAPHIC ANALYSES
SILICON METAL

Chemical Analysis

(Error < ±10% of Quantity Measured)

Oxygen	0.83%	0.76%
Nitrogen	29 ppm	30 ppm

Spectrographic Analysis

(Error < ±10% of Quantity Measured)

Aluminum	0.7%
Boron	0.005%
Barium	0.005%
Calcium	0.5%
Chromium	0.007%
Copper	0.15%
Iron	0.5%
Magnesium	0.002%
Manganese	0.06%
Nickel	0.003%
Lead	0.007%
Silicon	HIGH
Tin	0.03%
Strontium	0.003%
Titanium	0.04%
Vanadium	0.001%
Zirconium	0.03%

Note: Other elements not detected

ppm - parts per million

CHEMICAL AND SPECTROGRAPHIC ANALYSES
ZIRCONIUM DIBORIDE

Chemical Analysis

(Error < ±5% of Quantity Measured)

Zirconium	76.00%	75.95%
Boron	18.75%	18.66%
Oxygen	1.67%	1.78%
Nitrogen	281 ppm	299 ppm

Spectrographic Analysis

(Error < ±10% of Quantity Measured)

Aluminum	0.04%
Cobalt	0.04%
Chromium	0.005%
Iron	0.2%
Hafnium	0.2%
Manganese	0.001%
Columbium	0.05%
Nickel	0.005%
Silicon	0.6%
Titanium	0.07%

Note: Other elements not detected

ppm - parts per million

SPECTROGRAPHIC ANALYSES OF PITCH AND GRAPHITE POWDERS

(Error < ±10% of Quantity Measured)

PITCH

Aluminum	0.006%
Boron	0.005%
Calcium	0.004%
Iron	0.005%
Magnesium	0.002%
Silicon	0.007%
Zinc	0.007%
Zirconium	0.015%

Note: Other elements not detected

GRAPHITE

Aluminum	0.03%
Boron	0.005%
Calcium	0.05%
Copper	0.001%
Iron	0.1%
Magnesium	0.02%
Silicon	0.1%
Titanium	0.002%
Zirconium	0.07%

Note: Other elements not detected

CHEMICAL AND SPECTROGRAPHIC ANALYSES OF CURED JTA BILLET SAMPLES

Chemical Analysis

(Error < ±5% of Quantity Measured)

	Billet A		Billet B		Billet C	
Free Carbon	42.94%	42.98%	48.24%	48.36%	44.20%	44.40%
Oxygen	0.205%	0.218%	0.148%	0.169%	0.240%	0.242%
Total Carbon	47.95%	48.27%	52.02%	52.45%	49.01%	49.27%
Zirconium	33.13%	33.31%	33.66%	33.42%	33.00%	33.06%
Boron	8.61%	8.51%	8.38%	8.56%	8.60%	8.49%
Silicon	9.00%	8.92%	5.47%	5.32%	8.97%	9.02%
Nitrogen	34 ppm	40 ppm	47 ppm	42 ppm	272 ppm	288 ppm

ppm parts per million

Spectrographic Analysis

(Error < ±10% of Quantity Measured)

	A	B	C
Aluminum	0.1%	0.07%	0.1%
Barium	0.003%	0.003%	0.003%
Cobalt	0.02%	0.02%	0.02%
Chromium	0.001%	0.001%	0.001%
Copper	0.03%	0.03%	0.05%
Iron	0.3%	0.3%	0.3%
Hafnium	0.2%	0.2%	0.2%
Maganese	0.002%	0.002%	0.002%
Columbium	0.01%	0.01%	0.01%
Nickel	0.003%	0.003%	0.003%
Titanium	0.03%	0.03%	0.05%

Note: Other elements not detected.

APPENDIX III

ANALYSIS OF VARIANCE OF FLEXURAL STRENGTH FOR 7-F-12, 7-F-14, and 14-G-1

An analysis of variance is a test, whereby one may determine whether or not several samples are members of the same parent population. The test compares the variation of values between members of the samples with the variation between samples. If all of the samples are from the same population, the ratio of these two variations should be small. A large ratio, on the other hand, is an indication that there are differences between samples either in the material or in the test itself.

The following is an outline of the method of calculation used in the analysis:

N = number of items in all samples

T = grand total of all of the values measured

$\overline{X}$ = grand average T/N

n = number of samples

i = number of items in a given sample

$\overline{x}$ = the average of a given sample

To calculate the variance between samples:

$\sum_{n} (\overline{x}_n - \overline{X})^2 i_n$ = between-samples sum of squares

$n - 1$ = between-samples degrees of freedom, then;

$$\frac{\sum_{n} (\overline{x}_n - \overline{X})^2 i_n}{n - 1} = \text{between-samples estimate of variance}$$

To calculate the variance with the samples,

$\sum_{ni} (x_i - \overline{x}_n)^2$ = within-sample sum of squares

$\sum_{n} (i_n - 1)$ = within-sample degrees of freedom

$$\frac{\sum_{ni} (x_i - \bar{x}_n)^2}{\sum_{n} (i_n - 1)} = \text{within-sample estimate of variance}$$

The largest ratio of these two estimates is then compared with tables which indicate the values of the ratio which will be exceeded with various degrees of probability* (i.e., in the case analyzed, the ratio will exceed a value of 19.5 in 5% of the analyses and will exceed 99 in only 1% of them). Normally, a calculated value which exceeds the 1% value from statistical tables is taken as a very strong indication of real differences between samples and a value exceeding the 5% value is taken as a moderate indication of real differences between samples.

As may be seen from the following tables, in the analysis carried out on JTA specimens, all tests except the sonic modulus test give variance ratios well below the 5% level. The high values of the ratio obtained in the case of sonic modulus, when considered in the light of the low values obtained in the flexure and tangent modulus analyses, seem to indicate a variability in the test rather than in the material.

*Moroney, M. J., Facts From Figures, Penguin Books, Baltimore, Maryland (1954).

ANALYSIS OF VARIANCE FOR FLEXURE STRENGTHS
OF 3 x 1/4 x 1/4 IN. SPECIMENS
FROM BILLETS 7-F-12, 7-F-14, AND 14-G-1

Source of Variation	Sums of Squares	Degrees of Freedom	Variance Estimate	F*
		With Grain		
Between samples	5,338,040	2	2,669,020	2.86
Within samples	206,067,650	27	7,632,135	
Total	211,405,690	29		
		Across Grain		
Between samples	9,271,710	2	4,635,855	9.3
Within samples	13,479,100	27	498,070	
Total	22,750,810	29		

*1% level of F = 99; 5% level of F = 19.5.

ANALYSIS OF VARIANCE FOR TANGENT MODULUS
OF 3 x 1/4 x 1/4 IN. SPECIMENS
FROM BILLETS 7-F-12, 7-F-14, AND 14-G-1

Source of Variation	Sums of Squares, x 10^{12}	Degrees of Freedom	Variance Estimate x 10^{12}	F*
		With Grain		
Between samples	53.789	2	26.8945	6.78
Within samples	107.085	27	3.966	
Total	160.874	29		
		Across Grain		
Between samples	4.561	2	2.2805	1.67
Within samples	36.752	27	1.361	
Total	41.313	29		

*1% level of F = 99; 5% level of F = 19.5.

ANALYSIS OF VARIANCE FOR SONIC MODULUS
OF 3 x 1/4 x 1/4 IN. SPECIMENS
FROM BILLETS 7-F-12, 7-F-14, AND 14-G-1

Source of Variation	Sums of Squares, x 10^{12}	Degrees of Freedom	Variance Estimate x 10^{12}	F*
		With Grain		
Between samples	25.585	2	12.7925	38.9
Within samples	8.904	27	0.329	
Total	34.489	29		
		Across Grain		
Between samples	415.373	2	207.6865	1070
Within samples	5.215	27	0.193	
Total	420.588	29		

*1% level of F = 99; 5% level of F = 19.5.

DISTRIBUTION LIST

AFML (MAA)
Wright-Patterson AFB, Ohio 45433

AFML (MAAM/Library) 5 cys
Wright-Patterson AFB, Ohio 45433

AFML (MAA/D. Shinn) 2 cys
Wright-Patterson AFB, Ohio 45433

AFML (MAC)
Wright-Patterson AFB, Ohio 45433

AFML (MAT) 2 cys
Wright-Patterson AFB, Ohio 45433

AFML (MAN) 2 cys
Wright-Patterson AFB, Ohio 45433

AFML (MAM) 2 cys
Wright-Patterson AFB, Ohio 45433

AFML (MAX/Dr. Tanner)
Wright-Patterson AFB, Ohio 45433

AFML (MAS)
Wright-Patterson AFB, Ohio 45433

AVTM
Wright-Patterson AFB, Ohio 45433

AFML (MAAE) (All extra Copies)
Wright-Patterson AFB, Ohio 45433

AFFPL (APFT)
Wright-Patterson AFB, Ohio 45433

AFFPL (APT)
Wright-Patterson AFB, Ohio 45433

ASD (ASEP)
Wright-Patterson AFB, Ohio 45433

ASD (ASNPI)
Wright-Patterson AFB, Ohio 45433

ASD (ASNPD-30)
Wright-Patterson AFB, Ohio 45433

AFFDL (FDT)
Wright-Patterson AFB, Ohio 45433

SAMSO (SMT/AFML)
Attn: L. Hjelm
AF Unit P. O.
Los Angeles, California

SSD (SSPRE-2)
AF Unit P. O.
Los Angeles, California 90045

US Army Materials Research Agency
Attn: (AMXMR-TMS) Library
Watertown, Massachusetts 02172

INFORMATION CENTERS AS APPLICABLE

AF Machinability Data Center
Metcut Research Assoc., Inc.
Attn: Dr. J. F. Kahles
3980 Rosslyn Drive
Cincinnati, Ohio 45209

Mechanical Properties Data Center
Attn: A. J. Belfour
Belfour Engineering Company
13919 West Bay Shore Drive
Traverse City, Michigan 49684

Defense Ceramic Information Center
Battelle Memorial Institute
505 King Avenue
Columbus, Ohio 43201

Thermophysical Properties Research Ctr.
Purdue University
2595 Yeager Road
West Lafayette, Indiana 47906

AFSC STLO (SCTL-1)
424 Trapelo Road
Waltham Federal Center
Waltham, Massachusetts 02154

AFSC STLO (SCTL-5)
26 Federal Plaza
New York, N. Y. 10007

AFSC STLO (SCTL-9)
Dept of the Navy
Munitions Bldg.
Washington, D. C. 20360

AFSC STLO (SCTL-3)
227 Federal Office Bldg.
1240 East 9th Street
Cleveland, Ohio 44199

AFSC STLO (SCTL-4)
500 Sough Ervoy Street
Dallas, Texas 75201

AFSC STLO (SCTL-2)
O'Hara Office Center
3166 Des Plaines Avenue
Des Plaines, Illinois 60018

AFSC STLO (SCTL-6)
363 S. Taaffe Avenue
Sunnyvale, California 94086

AFSC STLO (SCTL-10)
AF Unit Post Office
Los Angeles, California 90045

AFSC STLO (SCTL-7)
C/O The Boeing Company
Seattle, Washington 98124

AFSC STLO (SCTL-11)
Bldg. No. 390
Aberdeen Proving Ground
Maryland 21005

AFSC STLO (SCTL-12)
Bldg. No. 1501
Edgewood Arsenal, Maryland 21010

AFSC STLO (SCTL-14)
US Army Elec. R&D Lab
Ft. Monmouth, New Jersey 07703

AFSC STLO (SCTL-15)
Hq Army Munitions
Dover, New Jersey 07801

AFSC STLO (SCTL-13)
P. O. Drawer 942
APO New York 09827

AFSC STLO (SCTL-17)
Naval Missile Center
Point Mugu, California 93041

AFSC STLO (SCTL-16)
Naval Air Dev. Center
Johnsville, Warminster, Pa. 18974

AFSC STLO (SCTL-19)
Naval Research Laboratory
Washington, D. C. 20390

AFSC STLO (SCTL-18)
Naval Weapons Center
Code 143
China Lake, California 93555

AFSC STLO (SCTL-20)
Ames Research Center (NASA)
Moffett Field, California 94035

AFSC STLO (SCTL-23)
Lewis Research Center (NASA)
21000 Brookpark Road
Cleveland, Ohio 44135

AFSC STLO (SCTL-21)
Langley Research Center (NASA)
Langley AFB, Virginia 23365

AFSC STLO (SCTL-22)
Manned Spacecraft Center (NASA)
Houston, Texas 77058

AFSC STLO (SCTL-24)
Mass. Institute of Technology
68 Albany Street
Cambridge, Massachusetts 02139

Defense Documentation Center
Cameron Station (20 cys)
Alexandria, Virginia 22314

Federal Aviation Agency
Library Section (MS-112)
Washington, D. C. 20390

Materials Advisory Board
National Academy of Sciences
2101 Constitution Avenue
Washington, D. C. 20418

Department of the Navy
Bureau of Weapons
Attn: N. Promisel
21st & Constitution Avenue
Washington, D. C. 20025

NASA
Attn: George Deutsch, RRM
Washington, D. C. 20546

Army Materials Research Agency
Attn: Norman L. Reid
Watertown, Massachusetts

NASA
Scientific & Tech Info Facility
Attn: RQT-11988 (2 cys)
P. O. Box 5700
Bethesda, Maryland 20014

Aerojet General Corporation
Attn: Tech Library
Downey, California 91703

Aerojet-General Corporation
Attn: Technical Library
P. O. Box 296
Azusa, California 91703

Aerojet-General Corporation
Attn: Technical Library
P. O. Box 1947
Sacramento, California 95809

Aerospace Corporation
Attn: Library Tech Info Group
P. O. Box 95085
Los Angeles, California 90045

American Machine & Foundry
Attn: Library
1025 N. Royal Street
Alexandria, Virginia 22314

Arthur D. Little, Inc.
Attn: Library
15 Acorn Park
Cambridge, Massachusetts 02140

Aerospace Industries Association
Attn: J. P. Reese
1725 DeSales Street, N. W.
Washington, D. C. 20036

U. S. Atomic Energy Commission
Reference Branch
Attn: Margaret Pflugger
Tech Info Service AEC
Attn: Document Control Sec.
P. O. Box 62
Oak Ridge, Tennessee

Avco Corporation
Attn: Technical Library
550 South Main Street
Stratford, Connecticut 06497

Avco Corporation
Research & Advanced Dev. Division
Attn: Research Library
201 Lowell Street
Wilmington, Mass. 01887

Battelle Memorial Institute
Attn: DMIC (2 cys)
505 King Avenue
Columbus, Ohio 43201

Bell Aircraft Corporation
Attn: Tech Library
P. O. Box 1
Buffalo, New York 14205

Boeing Company
Aerospace Division
Attn: Library, 13-84
P. O. Box 3707
Seattle, Wash. 98124

Chance Vought Aeronautics
Attn: Library
P. O. Box 6267
Dallas, Texas 75222

Chrysler Corporation
Missile Div.
P. O. Box 2628
Detroit, Michigan 48231

Curtiss-Wright Corporation
Wright Division
Attn: Library
Woodridge, N. J. 07075

Curtiss-Wright Corporation
Curtiss Division
Attn: Engineering Library
Caldwell, N. J. 07006

Curtiss-Wright Corporation
Attn: Library
Quehanna, Pa.

McDonnell-Douglas Acft Co.
Attn: Library
3855 Lakewood Blvd.
Long Beach, California 90801

McDonnell Douglas Aircraft Corp.
Data & Services Section
3000 Ocean Park Blvd.
Santa Monica, California 90406

The Garrett Corporation
Airesearch Manufacturing Co, Div
Attn: Library
9851-9951 Sepulveda Blvd
Los Angeles, California 90009

General Dynamics/Fort Worth
Attn: Library
P. O. Box 748
Fort Worth, Texas 76101

General Dynamics/General Atomics
Attn: J. F. Watson
P. O. Box 608
San Diego, California 92212

General Dynamics/Pomona
Attn: Structures & Matl's Sec.
Pomona, California 91766

General Dynamics/Astronautics
Attn: Library & Info Services (128-00)
P. O. Box 1128
San Diego, California 92112

General Electric Company
Attn: Library
Matl's Dev. Lab.
Adv. Matl's Evaluation
Cincinnati, Ohio 45215

General Electric Company
Missile & Space Div.
Attn: Library
P. O. Box 8555
Philadelphia, Pennsylvania 19101

General Motors Corporation
Allison Division
Attn: Tech Library
Indianapolis, Indiana 46206

Grumman Aircraft Corporation
Attn: Tech Library
Bethpage, New York 11714

Hughes Aircraft Company
Attn: Tech Document Ctr
Florence & Teale Streets
Culver City, California 90232

ITT Research Institute
Attn: Tech Library
10 West 35th Street
Chicago, Illinois 60616

Institute of the Aerospace Sciences
Tech Info Service
Attn: Library
750 Third Avenue
New York, New York 10017

Jet Propulsion Laboratory
California Institute of Tech.
Attn: V. F. Lardenoit
4800 Oak Grove Drive
Pasadena, California 91103

Ling-Temco-Vought, Inc.
Attn: Library
P. O. Box 5907
Dallas, Texas 75222

Lockheed Missiles & Space Co.
Attn: Library
P. O. Box 504
Sunnyvale, California 94088

Lockheed-California Company
Attn: L. Yates, Matl's & Proc.
Dept 77-11, Bldg. 170
P. O. Box 551
Burbank, California 91503

Lockheed Missiles & Space Co.
Attn: Tech Info Ctr
3251 Hanover Street
Palo Alto, California 94306

Marquardt Corporation
Attn: Tech Library
16555 Saticoy Street
Van Nuys, California 91406

Martin-Marietta Corporation
Attn: Tech Library
Baltimore, Maryland 21203

Martin-Marietta Corporation
Denver Div.
Attn: Libraries Section
P. O. Box 179
Denver, Colorado 80201

McDonnell Douglas Corp.
Attn: ENG. Library Dept 218
P. O. Box 516
St Louis, Missouri 63116

North American-Rockell, Inc.
Attn: Eng. Data Sec.
4300 E. Fifth Avenue
Columbus, Ohio 43216

North American-Rockwell, Inc.
Attn: Tech Library
International Airport
Los Angeles, California 90009

North American-Rockwell, Inc
Rocketdyne Div.
Attn: Tech Library
6633 Canoga Avenue
Canoga Park, California 91304

North American-Rockwell, Inc.
Space & Info Sys Div.
Attn: Tech Info Ctr 09-314
12214 Lakewood Blvd.
Downey, California 90241

Northrop/Norair Division
Supvr. Tech Information
3801 West Broadway
Hawthorne, California 90250

Northrop/Ventura Division
Attn: Library
Matls Engineering
1515 Rancho Conejo Blvd.
Newbury Park, California 91320

Pratt-Whitney Aircraft
Attn: Tech Library
P. O. Box 2691
West Palm Beach, Florida 33402

Pratt-Whitney Aircraft Corp.
Attn: Library
362 S. Main St.
East Hartford, Connecticut 06108

Republic Steel Corporation
Attn: R. Place/Tech Library
Cleveland, Ohio 44117

Fairchild-Hiller Corporation
Attn: Engr. Library
Farmingdale, LI, New York 11735

Solar Aircraft Company
Attn: Library
Main Plant & Offices
2200 Pacific Highway
San Diego, California 92101

Space Technology Labs., Inc.
Attn: Tech Library
P. O. Box 4277
Patrick AFB, Flordia 32925

Space Technology Labs., Inc.
Operations Systems Office
Norton AFB, California 92409

Space Technology Labs., Inc.
Attn: Engr Data Control
One Space Park
Redondo Beach, California 90278

Thompson Ramo Wooldridge, Inc.
Attn: Tech Library
5500 W. El Segundo Blvd.
P. O. Box 90215 Airport Station
Los Angeles, California 90045

Thompson Ramo Wooldridge, Inc.
Attn: Tech Library
23555 Euclid Avenue
Cleveland, Ohio 44117

United Aircraft Corporation
Missiles & Space Sys Div.
Attn: Tech Library
440 Main Street
East Hartford, Connecticut 06108

University of Dayton
Research Institute
300 College Park
Dayton, Ohio 45409

Westinghouse Research Labs
Attn: Tech Library
Beulah Road, Churchill Borough
Pittsburgh, Pennsylvania 15235

ASD (ASRCTC)
Attn: D. C. Harleman
Wright-Patterson AFB, Ohio 45433

ASD (ASRMDS)
Attn: Sgt J. C. Ingram
Wright-Patterson AFB, Ohio 45433

Aerospace Corporation
Attn: Norman N. Au
El Segundo, California

Aerospace Corporation
2400 E. El Sagundo Blvd.
Attn: Dr. B. G. Kendall
El Sagundo, California

AFML (MATC/L. Conlon)
Wright-Patterson AFB, Ohio 45433

Atomics International Div. NAA
Research Dept.
Attn: S. C. Carniglia
Canoga Park, California

Avco R&D
Attn: R. Y. Peterson
Materials Engineering
201 Lowell Street
Wilmington, Massachusetts

Battelle Memorial Institute
505 King Avenue
Columbus, Ohio 43201
Attn: Mr. A. Rudnick

Bell Aerosystems Co.
Attn: Frank M. Anthony
P. O. Box 1
Buffalo, New York 14205

Bell Aerosystems Co.
Attn: Leon Marcus (C-45)
P. O. Box 1
Buffalo, New York 14205

Boeing Airplane Co.
7755 E. Marginal Way
Attn: W. M. Sterry
Seattle 24, Washington

Bureau of Naval Weapons
Attn: N. E. Promisal, Dir.
Dept. of the Navy
Materials Div. RRMA
Washington 25, D. C.

Carborundum Co.
Attn: K. M. Taylor
Research Labs.
Niagra Fall, New York

Corning Glass Works
Attn: M. G. Britton
Ceramic Research Div.
Corning, New York

Ford Motor Company
Aeronautics Div.
Attn: W. M. Fassell
P. O. Box 697
Newport Beach, California

General Electric Co.
Attn: L. R. McCreight, Manager
Materials Studies
Aeroscience Lab.
Philadelphia, Pennsylvania 19101

Georgia Inst. of Technology
Engineering Experiment Station
Attn: J. D. Walton
Atlanta, Georgia

Langley Research Center NASA
Attn: E. Mathauser
Langley, Virginia

Ling-Temco-Vought
Aeronautics Div., Box 5907
Attn: William Aves
Dallas, Texas

Lockheed Missile & Space Co.
3251 Hanover Street
Materials Div. - Bldg. 202
Attn: Clause Goetzel
Palo Alto, California

Joseph Marin
Dept of Mat Sc & Chem
U S Naval Post Graduate School
Monterey, California

The Marquardt Corp.
16555 Saticoy Street
Attn: S. Sklarew
Van Nuys, California 91406

Marshall Space Flight Center
Attn: D. Gates
Research Projects Division
Huntsville, Alabama 35812

The Martin Company
Attn: J. J. Saunders
Advanced Design Div.
Baltimore, Maryland 21203

Melpar, Inc.
Attn: L. K. Eliason
3000 Arlington Blvd.
Falls Church, Virginia

McDonnell Aircraft Co.
Attn: D. Kummer
St Louis, Missouri 63116

NASA Scientific & Tech Info. Facility
P. O. Box 33
Attn: Acquisitions Br. (SQT 35999)
College Park, Maryland 20740

National Carbon Research Lab.
Attn: J. C. Bowman
12900 Snow Road
Parma, Ohio

North American Aviation, Inc.
Attn: J. W. Huffman
International Airport
Los Angeles, California

Norton Company
Attn: Dr. N. N. Ault
Worcester, Massachusetts

Pr. R. Mallory & Co., Inc.
3029 E. Washington St.
Attn: Tech Library
Indianapolis, Indiana 46206

Poco Graphite
Attn: E. Peters
P. O. Box 1524
Garland,Texas

Rand Corporation
Attn: W. Micks'
Santa Monica, California

Space Technology Labs.
Attn: J. Bohn
One Space Park
Redondo Beach, California 90278

Spindletop Research Center
Attn: Dr. W. Lambertson
2224 Yound Drive
Lexington, Kentucky

Solar
Attn: J. Long
2200 Pacific Highway
San Diego, California 92112

Southern Research Institute
2000 9th Avenue. South
Attn: C. D. Pears
Birmingham, Alabama

TRW Systems
Attn: K. King
One Space Park
Redondo Beach, California 90278

University of Dayton
Attn: J. Wurst
300 College Park
Dayton, Ohio 45409

U.S. Naval REsearch Lab.
Attn: E. Chapin
4555 Overlook Avenue, SW
Washington, D.C.

Union Carbine Corporation
Attn: D. L. Hiller
P. O. Box 500
Lawrenceburg, Tennessee

University of California
Lawrence Radiation Lab
P.O. Box 808
Livermore, California

University of Washington
Attn: J. I. Mueller
Ceramic Engineering Division
Seattle, Washington 98105

Jerome C. Schutzler
14034-D Marquesas Way
Marine Del Rey, California 90291

Henry W. Babel
18725 San Fernando Mission Blvd.
Northridge, California 91324

Unclassified
Security Classification

DOCUMENT CONTROL DATA - R&D
(Security classification of title, body of abstract and indexing annotation must be entered when the overall report is classified)

1. ORIGINATING ACTIVITY (Corporate author) IIT Research Institute Chicago, Illinois 60616	2a. REPORT SECURITY CLASSIFICATION Unclassified 2b. GROUP None

3. REPORT TITLE

PROPERTIES OF JTA GRAPHITE

4. DESCRIPTIVE NOTES (Type of report and inclusive dates)

Final Technical Report, May 1965 through December 1967

5. AUTHOR(S) (Last name, first name, initial)

Bortz, Seymour A.

6. REPORT DATE	7a. TOTAL NO. OF PAGES	7b. NO. OF REFS
July 1968	208	16

8a. CONTRACT OR GRANT NO.	9a. ORIGINATOR'S REPORT NUMBER(S)
AF33(615)-3028 b. PROJECT NO. 7381 c. Task No. 738106 d.	IITRI-G6001-F 9b. OTHER REPORT NO(S) (Any other numbers that may be assigned this report) AFML-TR-68-178

10. AVAILABILITY/LIMITATION NOTICES

See Attached Page.

11. SUPPLEMENTARY NOTES	12. SPONSORING MILITARY ACTIVITY
	AFML (MAAE) Wright-Patterson AFB, Ohio 45433

13. ABSTRACT

The purpose of this program was to attempt to test a material that forms its own oxidation resistant protection and to characterize the physical and the mechanical properties of Union Carbide Corporation's JTA graphite in order to determine its usefulness for aerospace applications. Two 7-in.-diameter, 6.5-in.-long and two 14-in.-diameter 7-in.-long JTA billets were examined. They had no gross flaws or density differences and were acceptable within the limitations of the procurement specifications. Their densities were greater than 3.00 g/cc, and they contained graphite, zirconium diboride, and beta-silicon carbide, the distribution of which varied only slightly among the four billets. The zirconium diboride and beta-silicon carbide content at the edge of the billets was less than that in the center. The oxidation resistance varied with temperature and oxygen pressure. Maximal oxidation resistance under ambient conditions occurred at 2750°F. The strength was retained at low pressures (less than 10-1 torr) and at temperatures as high as 3650°F. Oxidation at temperatures of greater than 1750°F produced a protective zirconium coating. Sonic modulus measurements were not sensitive enough to differentiate between flaw distributions of the with- and the across-grain orientations. JTA graphite is anisotropic, and its with-grain orientation is about twice as strong as its across-grain orientation. A minimal 1/4-in. cross section was adequate for determining average (Cont'd)

DD FORM 1 JAN 64 1473

Unclassified

14. KEY WORDS	LINK A		LINK B		LINK C	
	ROLE	WT	ROLE	WT	ROLE	WT
Characterize and correlate physical and mechanical properties Two 7" billets and two 14" billets High temperature testing in inert and oxidizing atmospheres						

INSTRUCTIONS

1. ORIGINATING ACTIVITY: Enter the name and address of the contractor, subcontractor, grantee, Department of Defense activity or other organization *(corporate author)* issuing the report.

2a. REPORT SECURITY CLASSIFICATION: Enter the overall security classification of the report. Indicate whether "Restricted Data" is included. Marking is to be in accordance with appropriate security regulations.

2b. GROUP: Automatic downgrading is specified in DoD Directive 5200.10 and Armed Forces Industrial Manual. Enter the group number. Also, when applicable, show that optional markings have been used for Group 3 and Group 4 as authorized.

3. REPORT TITLE: Enter the complete report title in all capital letters. Titles in all cases should be unclassified. If a meaningful title cannot be selected without classification, show title classification in all capitals in parenthesis immediately following the title.

4. DESCRIPTIVE NOTES: If appropriate, enter the type of report, e.g., interim, progress, summary, annual, or final. Give the inclusive dates when a specific reporting period is covered.

5. AUTHOR(S): Enter the name(s) of author(s) as shown on or in the report. Enter last name, first name, middle initial. If military, show rank and branch of service. The name of the principal author is an absolute minimum requirement.

6. REPORT DATE: Enter the date of the report as day, month, year; or month, year. If more than one date appears on the report, use date of publication.

7a. TOTAL NUMBER OF PAGES: The total page count should follow normal pagination procedures, i.e., enter the number of pages containing information.

7b. NUMBER OF REFERENCES: Enter the total number of references cited in the report.

8a. CONTRACT OR GRANT NUMBER: If appropriate, enter the applicable number of the contract or grant under which the report was written.

8b, 8c, & 8d. PROJECT NUMBER: Enter the appropriate military department identification, such as project number, subproject number, system numbers, task number, etc.

9a. ORIGINATOR'S REPORT NUMBER(S): Enter the official report number by which the document will be identified and controlled by the originating activity. This number must be unique to this report.

9b. OTHER REPORT NUMBER(S): If the report has been assigned any other report numbers *(either by the originator or by the sponsor)*, also enter this number(s).

10. AVAILABILITY/LIMITATION NOTICES: Enter any limitations on further dissemination of the report, other than those imposed by security classification, using standard statements such as:

(1) "Qualified requesters may obtain copies of this report from DDC."

(2) "Foreign announcement and dissemination of this report by DDC is not authorized."

(3) "U. S. Government agencies may obtain copies of this report directly from DDC. Other qualified DDC users shall request through _____."

(4) "U. S. military agencies may obtain copies of this report directly from DDC. Other qualified users shall request through _____."

(5) "All distribution of this report is controlled. Qualified DDC users shall request through _____."

If the report has been furnished to the Office of Technical Services, Department of Commerce, for sale to the public, indicate this fact and enter the price, if known.

11. SUPPLEMENTARY NOTES: Use for additional explanatory notes.

12. SPONSORING MILITARY ACTIVITY: Enter the name of the departmental project office or laboratory sponsoring *(paying for)* the research and development. Include address.

13. ABSTRACT: Enter an abstract giving a brief and factual summary of the document indicative of the report, even though it may also appear elsewhere in the body of the technical report. If additional space is required, a continuation sheet shall be attached.

It is highly desirable that the abstract of classified reports be unclassified. Each paragraph of the abstract shall end with an indication of the military security classification of the information in the paragraph, represented as *(TS), (S), (C), or (U)*.

There is no limitation on the length of the abstract. However, the suggested length is from 150 to 225 words.

14. KEY WORDS: Key words are technically meaningful terms or short phrases that characterize a report and may be used as index entries for cataloging the report. Key words must be selected so that no security classification is required. Identifiers, such as equipment model designation, trade name, military project code name, geographic location, may be used as key words but will be followed by an indication of technical context. The assignment of links, rules, and weights is optional.

Continuation of DD Form 1473:

10. This document is subject to special export controls and each transmittal to foreign governments or foreign nationals may be made only with prior approval of the Materials Engineering Branch, Materials Support Division, Air Force Materials Laboratory, MAAE, Wright-Patterson AFB, Ohio 45433.

13. Abstract

mechanical properties. Its strength did not vary between strain rates of 0.02 and 20 in./min. The ratio of the tensile strength to the flexural strength to the compressive strength is 1:1.45:2.5 for the with-grain orientation (tensile strength, 12,140 psi) and 1:1.23:5.2 for the across-grain orientation (tensile strength, 6300 psi). Under ambient atmospheric conditions and all temperatures tested, strength loss due to oxidation was about one-third to one-half the measured strength. The strength of the interior of oxidized JTA was the same as that of the virgin material. The mechanical properties peaked at 3150°F, at which the strength was higher than at ambient temperatures. The thermal properties, except for thermal expansion, were the same for all four billets. The variability of the mechanical data was within limits generally noted for ceramic materials but greater than that desired by designers of brittle materials. The batch-to-batch differences, primarily due to raw-material impurities and processing variations (e.g., hot-pressing-temperature variation) must be reduced.